Nonlocal models of flow in multi-scale porous and fractured media

Mojdeh Rasoulzadeh

▶ **To cite this version:**

Mojdeh Rasoulzadeh. Nonlocal models of flow in multi-scale porous and fractured media. Other [cond-mat.other]. Institut National Polytechnique de Lorraine, 2011. English. NNT : 2011INPL025N . tel-01749533

HAL Id: tel-01749533
https://hal.univ-lorraine.fr/tel-01749533

Submitted on 29 Mar 2018

HAL is a multi-disciplinary open access archive for the deposit and dissemination of scientific research documents, whether they are published or not. The documents may come from teaching and research institutions in France or abroad, or from public or private research centers.

L'archive ouverte pluridisciplinaire **HAL**, est destinée au dépôt et à la diffusion de documents scientifiques de niveau recherche, publiés ou non, émanant des établissements d'enseignement et de recherche français ou étrangers, des laboratoires publics ou privés.

AVERTISSEMENT

Ce document est le fruit d'un long travail approuvé par le jury de soutenance et mis à disposition de l'ensemble de la communauté universitaire élargie.

Il est soumis à la propriété intellectuelle de l'auteur. Ceci implique une obligation de citation et de référencement lors de l'utilisation de ce document.

D'autre part, toute contrefaçon, plagiat, reproduction illicite encourt une poursuite pénale.

Contact : ddoc-theses-contact@univ-lorraine.fr

LIENS

Code de la Propriété Intellectuelle. articles L 122. 4
Code de la Propriété Intellectuelle. articles L 335.2- L 335.10
http://www.cfcopies.com/V2/leg/leg_droi.php
http://www.culture.gouv.fr/culture/infos-pratiques/droits/protection.htm

INSTITUT NATIONAL POLYTECHNIQUE DE LORRAINE

NANCY – UNIVERSITÉ

Laboratoire d'Energétique et de Mécanique Théorique et Appliquée
École Doctorale EMMA

THÈSE

présentée en vue pour obtention du grade de :

DOCTEUR DE L'I.N.P.L.

spécialité : Mécanique-Énergétique

par :

Mojdeh Rasoulzadeh

MODELES NON LOCAUX DES ECOULEMENTS EN MILIEUX POREUX ET FRACTURES MULTI-ECHELLES

Soutenue publiquement le 20 avril 2011 devant la Commission d'Examen composé de :

Rapporteurs	:	AMAZIANE Brahim
		JOSSERAND Christophe
Examinateur	:	MIKELIC Andro
		PANFILOVA Irina
		PERIERA Antonio
Invité	:	KUCHUK Fikri
		SOUHAR Mohammed
Directeur de thèse	:	PANFILOV Mikhaïl

To my dearest Alireza for supporting me by

his love,

my mother and

the memory of my father

Remerciements

Je tiens à remercier tout particulièrement Monsieur Mikhaïl PANFILOV, Professeur à l'INPL, pour le travail productif et stimulant que nous avons mené ensemble.

Je remercie l'entreprise Schlumberger pour la prise en charge de son financement ainsi que pour l'intérêt qu'ils ont porté pour les progrès des élèves dans les pays qu'ils travaillent.

Je tiens à remercier Monsieur F. LEMOINE, Directeur du Laboratoire d'Énergétique et de Mécanique Théorique et Appliquée (LEMTA-ENSEM-INPL) de m'avoir accueillie dans son laboratoire.

Je remercie également tout les membres de jury d'avoir accepté de juger mon travail en participant au jury.

Je remercie tout mes amis du Laboratoire pour leur accueil et leur soutien durant ces années de travail.

Résumé

Plan de cette thèse

La thèse est composée de six chapitres.

Les chapitres 1 - 3 sont consacrés à l'analyse des modèles macroscopiques de l'écoulement en milieu fracturé. Dans le chapitre 1 on étudie problème de l'écoulement monophasé dans un milieu multi échelles, et on introduit les conditions nécessaires de l'existence d'autosimilarité d'un écoulement. Un modèle général effective s'appuyant sur le concept d'un milieu avec longue mémoire y est proposé. Une fonction de transfert pour un nombre d'échelles quelconque est déduite et son comportement asymptotique lorsque le nombre d'échelles tend vers infini est étudié. Le comportement asymptotique de non localités est trouvé.

Dans le chapitre 2 la technique d'homogénéisation à deux échelles est appliquée aux milieux fracturés de double porosité. Il est démontré que le terme d'échange peut être déterminé à travers le noyau d'Abel.

En suite, dans le chapitre 3 ce résultat est utilisé pour étudier le comportement de fluides dans un milieu fissuré fracturé. Le milieu était considéré comme constituant de blocs et de fractures de deux types: les fractures à l'échelle microscopique ou les fissures et les fractures macroscopiques. Des différentes échelles de temps ont été mises en place afin d'obtenir des modèles non-triviaux du domaine.

Dans les chapitres 4, 5 on examinait le comportement microscopique de l'écoulement à l'intérieur d'une fracture mince pour deux géométries différent: plane parallèle et cylindrique. Les caractéristiques de l'écoulement ont été obtenues. L'effet de la présence d'afflux à travers les parois du canal sur les pertes de pression le long du canal a été étudié. Il

était utilisé une approche asymptotique à la solution du problème de Navier Stokes dans un canal ondulé.
Dans le chapitre 4 on étudie l'écoulement stationnaire d'un fluide incompressible dans une fracture en forme de plane-parallèle avec des limites latérales imperméables et perméables. Une expression analytique (ou une méthode analytique) afin d'obtenir la perte de pression moyenne le long de la fracture est proposée. Les résultats obtenus sont validés avec le logiciel COMSOL.
Dans le chapitre 5 on se sert de la même méthodologie pour étudier un puits horizontal. L'expression analytique (ou une méthode analytique) afin d'obtenir la perte de pression moyenne le long du puits est egalement proposée.
Dans le chapitre 6 on couple méthode de levelset avec le modèle analytique qu'on a obtenu afin de déterminer écoulement diphasique dans le puits. Le champ de vitesses externe nécessaire à savoir pour l'évolution de la fonction levelset est calculé par le modèle analytique du chapitre 5. Après chaque évolution, la nouvelle disposition spatiale des fluides dans le domaine est utilisée pour déterminer le nombre de Reynolds et de la distribution de viscosité.

Modèles macroscopiques d'écoulement dans un milieu poreux hétérogènes multi-échelles

Un ensemble de fractures situé dans un milieu poreux représente un cas typique de réservoirs naturellement hétérogènes qui contient de l'huile, du gaz ou de l'eau, Fig. 1. Le système de fracture typique représente un système hiérarchique de réseaux inclus l'un dans l'autre et ayant des perméabilités et des ouvertures différentes. Respectivement les blocs poreux situés entre les fractures forment aussi un système hiérarchique. Modélisation d'écoulement dans un milieu multi-échelle est l'un des problèmes les plus difficiles de la théorie qui reste ouverte pour le cas général.

Dans la thèse présente, nous allons analyser les problèmes de modélisation des écoulements dans un tel milieu. Nos efforts sont concentrés au premier tour sur la description adéquate d'un milieu hétérogène fracturé où l'hétérogénéité possède est observable à plusieurs échelles spatiales et possède des différentes structures. Les études des écoule-

ments dans un milieu fracturés en fonction des propriétés conductrices du milieu et de la taille des fractures est un problème compliqué, qui nécessite de description de l'écoulement dans des différentes parties du domaine et se compose de plusieurs problèmes couplés qui doivent être formulés indépendamment. Les modèles mathématiques décrivant le comportement du système à l'échelle spatiale de base (la plus petite) peuvent être réduits, par différentes techniques, à un modèle soi-disant effectif (autres termes également employés : macroscopique et homogénéisé) qui gouverne l'écoulement à l'échelle globale en opérant avec les propriétés effectives du domaine.

Concept de double porosité

On commence par le cas le plus simple où il y a que deus échelles. Traditionnellement, on distingue deux échèles spatiales caractéristiques dans un milieu poreux. Le premier est un pore-échelle qui correspond à un assemblage assez grand nombre de pores. Le deuxième est formée par une structure composite du milieu poreux qui peut-être construit de plusieurs types de roches poreuses avec la conductivité hydrodynamique distinctes. La taille d'un bloc forme échelle de bloc. Le modèle consistant en un tel deux types d'échelles est considéré comme un modèle double porosité. Dans les milieux à double porosité ou double perméabilité les caractéristiques conductrices subissent des fortes discontinuités : différentes pour les fractures et les blocs. Dans l'approche de double porosité, les discontinuités présentes partout dans le réservoir sont considérées comme un système d'un point de vue analogique au système des pores à l'échelle microscopique. Ainsi un réservoir fracturé représente une superposition de deux "systèmes de conduits" distincts possédant de différentes propriétés conductrices ainsi que les capacités de stockage (ce qu'on identifie avec la porosité). Les fractures represent des pores "macroscopiques".

On va appeler le système de petits pores la matrice. La matrice contient les pores les plus étroits et possède une grande capacité de stockage, mais une faible capacité laisser passer l'écoulement, c'est interconnecté avec le réseau de fractures, qui possède une faible capacité de stockage, mais une forte capacité de laisser passer l'écoulement. Le modèle de double porosité distingue des différents écoulements dans les parties plus perméable ou moins imperméable du réservoir. Ces deux écoulements sont reliés entre eux par un terme

d'échange. Ainsi les problèmes d'écoulement dans deux réseaux de canaux ne peuvent pas être étudiés séparément.
Il est évident qu'avec une telle définition, le modèle de double porosité est similaire au modèle classique qui opère avec une seule porosité et une seule perméabilité, la différence consiste en nombre d'équation (deux contre une) et en présence du terme d'échange. Ce terme d'échange établit l'interaction entre les fractures et la matrice, ce qui est le facteur essentiel qui contrôle la performance de production d'un réservoir naturellement fracturé. Des différentes formulations existantes du modèle à double porosité se distinguent principalement de la façon dont l'échange de masse est pris en compte. Le modèle de base d'un milieu à double porosité est proposé par Barenblatt [Barenblatt, Entov and Ryzhik, 1990]. Dans ce modèle conceptuel, le milieu poreux fracturé est représenté par deux systèmes distincts, mais en interaction, dont chacun est considéré comme un continu présent dans tout le domaine entier. Les phénomènes d'interaction entre deux continus sont pris en compte comme l'échange de fluide entre les fractures et les blocs poreux. Il est supposé que tout petit volume élémentaire représentatif (VER) comprend de nombreuses fractures aléatoire et des blocs poreux. Le mouvement du fluide dans un tel système est alors décrit par deux équations de bilan, une pour chaque continu (ou milieu), couplées à travers le terme d'échange de fluide. Ce dernier dépend des différences de niveau piézométrique entre deux continus en tout point. L'écoulement d'infiltration dans les blocs, la zone moins perméable, est négligé. Dans ce modèle tous les paramètres de l'écoulement en chaque point sont données par deux valeurs, dont chacune se rapporte à une des parties du milieu.
En général les types suivants de termes de l'échange peut être noté:

Modèle avec échange de masse quasi-équilibre Le modèle classique dérivée de l'approche phénoménologique [Barenblatt, Entov and Ryzhik, 1972], [Barenblatt, Zheltov and Kochina, 1960], [Barenblatt, Entov and Ryzhik, 1990] considère les blocs denses et la fracture très perméable comme deux continuums coexistant avec échange de masse entre les décrite par un terme d'échange.

Dans certaines variantes du processus les blocs ne sont considérées que comme un élément de capacité. Ils jouent le rôle de blocs de la faible perméabilité [Coats and Smith, 1964]. Dans le document original [Barenblatt, Zheltov and Kochina, 1960], un variante est proposé lorsque les blocs correspondent aux éléments de capacité, alors que la capacité de fractures est négligée. Les modèles similaires sont proposées plus tard dans [Böhm and Showalter, 1985],

[Charlaix, Hulin and Plona, 1987], [Duguid and Lee, 1977], [Evans, 1983], [Warren and Root, 1963].

Modèle de quasi-homogène Dans le document [Odeh, 1965], l'échange est montré pour être rapidement mis en place, ainsi que d'être extrêmement insignifiante. La pression dans un milieu très hétérogène est uniforme pour les blocs et les fractures et peut être décrite par une équation de diffusion parabolique, sans conditions de l'échange. Le terme d'échange est démontré à l'ordre ε^2 lorsque la porosité et la champs de perméabilité sont similaires.

Modèle avec terme d'échange non-stationnaire. Dans [De Swaan, 1976] l'échange non-stationnaire est pris en compte par la présentation sous la forme d'une convolution du gradient de pression à la limite de bloc. Dans les documents [Panfilov, 1990], [Panfilov, 1986] un modèle plus général avec la forme étroite du terme d'échange est calculé par homogénéisation pour une classe très hétérogène des milieux (médias type de source).

Modèle avec échange non-stationnaire et le type de 'translation'. Le modèle est dérivé dans [Panfilov, 1993], [Panfilov, 1994], pour les milieux très hétérogène des 'translation-type' de source. Les blocs fonctionnent de deux façons, en tant que source non-stationnaires, ainsi que leur donner une contribution à l'écoulement 'translation' à travers le milieu. Le terme d'échange est décrit par la deuxième dérivé de la pression.

Maintenaient on essaye de étudier les effets de présence de plus d'échelles sur le comportement de milieu.

Milieu multi-échelles

En réalité, des roches naturellement fracturés sont caractérisés par une structure multi-échelle des réseaux de fractures, résultant de l'existence de fractures des différents ordres de perméabilité et des différentes tailles. Le comportement macroscopique d'un milieu à plusieurs porosités est un problème toujours ouvert. Un modèle des milieux fracturés à trois échelles est proposé dans [Amaziane, Goncharenko and Pankratov, 2005] pour le cas particulier de dégénérescence des conditions limites sur le contact de fractures et les blocs. Un arrangement particulier d'un milieu quadruple fracturé est étudié dans [Dreier, Ozkan

et Kazemi, 2004]. Ils ont proposé un modèle analytique pour l'écoulement dans un système de quatre porosités qui consistait en un réseau triple des fractures et un système unique de matrice. Les fractures sont classé, en fonction de leur taille et leur conductivité, des micro fractures (les plus denses plus bas, les fractures de conductivité macro) et les méga fractures (plus grande taille, plus grande conductivité). Ils ont supposé que seulement les méga fractures, transporte de fluide du réservoir au puits. L'écoulement dans les trois fractures est supposé transitoire. L'échange de fluide entre la matrice et la fracture est pris en compte comme pseudo-steady. Différents modèles sont étudiés, en premier lieu lorsque le micro fractures sont interconnectés avec des macros fractures et n'ont aucun rapport avec le système de méga fracture.

Deuxième lorsque micro fractures et macro fractures sont reliées à des méga fractures mais pas directement reliés les uns aux autres. Ce modèle est approprié pour les réservoirs que les deux ensembles de fractures peut coexister, mais ne pas interférer. Un système d'équations de flux interconnectés à travers le terme d'échange proportionnel à la différence de pression entre les domaines interconnectés est résolu par l'aide de la transformation de Laplace. Les fonctions de transfert pour un réservoir limité sont proposées.

Dans [Peszynska 2007] un modèle général multi-échelles est proposé pour les problèmes elliptiques-paraboliques d'écoulement qui peut être utilisé dans les milieux poreux.
À notre avis deux approches principales semblent être applicables à un milieu multi-échelles. En bas on va etudier les deux approches:
(i) *la micro-modélisation*: on résout directement le problème de l'écoulement numériquement ou analytiquement dans le milieu tout en tenant compte de tous les détails de la structure moyenne. Pour les structures périodiques souvent, il est possible d'obtenir des solutions analytiques par la méthode de superposition. Pour les médias irrégulières et non-périodiques, la seule solution possible est la solution numérique. Le problème de la modélisation numérique directe consiste en la nécessité d'utiliser des maillages très fins dont la taille doit être beaucoup plus basse que l'échelle inférieure de la structure hiérarchique moyenne.
(ii) *l'homogénéisation et la macro-modélisation*: on peut développer le modèle moyenne d'écoulement sur des hétérogénéités. Un tel modèle décrit le comportement d'un milieu homogène équivalent, sa solution numérique ne demande pas d'utiliser des maillages très fines.

Micro-modélisation des réseaux de fractures

Comme les méthodes numériques, leur analyse est en dehors de l'objectif de cette thèse. Toutes sont basées sur des très fines maillages numériques, ce qui réduit leur efficacité. Les méthodes d'analyse sont en grande partie basées sur la superposition de solutions élémentaires qui décrivent l'écoulement dans le voisinage de chaque fracture considérée indépendamment de tous les autres. Plus exactement la superposition est réalisée en termes de fonctions de Green. En effet, si on considère une fracture comme une surface en 3D ou en 2D d'une ligne, encastrée dans un réservoir infini, alors la solution du problème de la perturbation du réservoir par cette fracture (en imposant une pression donnée le long de la fracture) représente la fonction de Green de l'opérateur correspondant décrivant l'écoulement.

Utilisation des fonctions de Green dans la modélisation de milieu fracturé multi-echelles

Le concept de fonction de Green est introduit en ingénierie des réservoirs [Gringarten and Ramey, 1973] par Gringarten et al. Ils ont appliqué leur méthode aux réservoirs fracturés [Gringarten and Ramey, 1974] dans le cas de présence d'une fracture vertical avec conductivité infinie. Postérieurement Kuchuk et al ont appliqué la théorie générale des fonctions de Green dans les milieux composites [Carslaw and Jaeger, 1959] aux réservoirs hétérogènes [Kuchuk, Habashy and Torres-Verdin, 1996] et ont obtenu les fonctions de transfert pour les cas particuliers des réservoirs latéralement ou horizontalement composites
[Kuchuk and Habashy, 1997]. Ce modèle est capable d'examiner les réservoirs fracturés dans le cas de la petite ouverture des couches et un contraste élevé des perméabilités entre les couches étroites et les autres couches. Les fractures à conductivité infinie et conductivité finie [Kuchuk and Habusky, 1994] peuvent être traitées dans ce modèle.

Méthode d'homogénéisation appliquée aux milieux multi-echelles

Du point de vue de la théorie de perturbation, le processus d'écoulement dans un milieu hétérogène peut être décrit par une équation différentielle dont les coefficients qui déterminent les propriétés du milieux varient rapidement dans l'espace suite à l'hétérogénéité du milieu. La théorie de l'homogénéisation est connue comme une méthode efficace pour étudier les milieux poreux fortement hétérogènes [Bakhvalov and Panasenko, 1989], [Allaire 1992].

L'idée d'homogénéisation consiste en ce que un média efficace peut être obtenu à partir du média réel, si l'échelle de l'hétérogénéité $\varepsilon = \frac{l}{L}$ tend vers zéro. Vraiment, la plus bas ε, la structure du milieu devient plus fine. A la limite, chaque cellule se transforme en point, et nous obtenon un milieu homogène avec une structure interne de chaque point. Par conséquent, le terme zéro des développements asymptotiques détermine la forme de l'équation moyenne. La convergence faible ne peut être assurée.

Le concept du milieu à double porosité est largement étudié à l'aide de la méthode d'homogénéisation à deux échelles [Hornug, 1997], [Panfilov, 2000], [Arbogast, Douglas and Hornung, 1990].

Mémoire dans les milieux à double porosité

Le modèle de l'échange non-stationnaire est d'abord proposée dans [De Swaan1976]. La relation est obtenu en résolvant analytiquement le problème non stationnaire de l'écoulement dans un seul bloc, causée par une réduction de la pression à la limite de bloc. Le terme d'échange est obtenu en forme de la convolution temporelle du gradient de pression à la frontière avec les fonctions de Green. Cela signifie l'apparition de la mémoire.

Un modèle similaire avec le terme d'échange non-stationnaire est obtenue par la technique d'homogénéisation beaucoup plus tard dans [Arbogast, Douglas et Hornung, 1990] et [Panfilov, 1990]. Le terme d 'échange est obtenu sous la forme d'un opérateur intégro-différentielle appliquée à la dérivée temporelle de la pression dans les fractures. Le noyau de cet opérateur est obtenu sous la forme analytique explicite grâce à l'expansion de Fourier de la fonction de Green décrivant la perturbation d'un seul bloc a partir de sa limite. Ce modèle est obtenu pour une valeur spécifique du rapport entre la perméabilité de bloc et

de la fracture, ω , qui était de l'ordre ε^2, où est la période de l'hétérogénéité de milieu. Ce modèle est appelée modèle ε^2. Pour les autres valeurs de ω, d'autres modèles ont été obtenus dans [Panfilov 1993],[Panfilov, 1994].
Si $\varepsilon << \omega << 1$, les blocs ne sont plus imperméables pour les fluides. Une partie du liquide peut traverser chaque bloc, grâce à laquelle les blocs contribue à la perméabilité effective. Dans le même temps processus de l'échange devient négligeable. Le système est décrit par une seule pression, et le modèle macroscopique garde la même forme à l'échelle microscopique.

Si $\varepsilon^2 << \omega << \varepsilon$, les blocs jouent un double rôle. Tout d'abord, ils sont les sources de fluide par rapport a fractures, qui détermine l'apparition du terme d'échange. Deuxièmement, ils contribuent à la perméabilité effective. L'écoulement dans un bloc représente une superposition de l'écoulement source et un flux de translation dans la direction des gradients de pression macroscopique. Le terme d'échange est différent du cas de milieu ε^2. Le noyau de l'opérateur devient delta-fonction, ce qui signifie que le terme non local se transforme en un local, qui est la dérivée seconde de la pression dans le temps. C'est le cas d'une mémoire à court terme.

Mémoire dans les milieux fracturés

Dans la littérature le modèle à double porosité est souvent surnommé le milieu poreux fracturé. Ce n'est pas trop exact. Si le même ordre de paramètres ε^2 pour le rapport de la perméabilité, et 1 pour le taux de porosité est appliquée pour un milieu avec des fractures minces, puis les effets de mémoire sera entièrement disparaître. L'échange entre les fractures et les blocs devient trop rapide, et l'effet du temps devein négligable. Pour obtenir le modèle avec mémoire, similaire au modèle à double porosité, il est nécessaire de changer les rapports entre les perméabilités. En outre, même dans ce cas le processus d'échange est suffisamment différents de milieu à double porosité, grâce à laquelle, les conditions de la mémoire a suffisamment différentes structure. Par conséquent, le modèle fracturé poreux avec de la mémoire représente un résultat indépendant, identique importante que le modèle de milieu à double porosité.
Le premier modèle d'écoulement en milieu poreux fracturé avec fractures minces qui s'est

avéré les effets de mémoire est obtenu par Pankratov et Rybalko dans [Pankratov et Rybalko, 2002], [Pankratov et Rybalko 2003]. Les auteurs ont montré que la mémoire ne s'affiche que si les blocs poreux (entouré par des fractures) sont très serrés, de sorte qu'ils ne fonctionnent que grâce à partir d'une couche limite dont l'épaisseur est du même ordre que l'ouverture des fractures. Dans ce cas, la contribution des blocs et des fractures dans le processus macroscopique sera du même ordre. Dans les publications consécutives les auteurs ont développé les classes de processus analysés, [Amaziane, Pankratov et Rybalko, 2005], [Amaziane, Pankratov et Piatnitski, 2007].
Le comportement global du milieu fracturé par rapport à différents paramètres tels que l'épaisseur de fracture, la taille des blocs et le rapport de la perméabilité, et des termes sources oscillant est étudiée. Il est démontré que pour les fractures minces qui sont très perméables le terme de mémoire se réduit à un noyau d'Abel. Les auteurs n'ont pas présenté la technique constructive du développement du modèle. Leur objectif était d'étendre les théorèmes de convergence élaboré par le méthode de Khrouslov [Marchenko et Khrouslov, 1974]. En fait, la méthode de Khrouslov est applicable pour les domaines dans les quels les blocs sont entièrement imperméables. Pankratov et Rybalko ont étendu le résultats pour les médias perméables partout. Il est montré que le modèle global homogénéisée est également de type parabolique mais avec les termes non locaux qui pourraient être considérés comme un terme source ou comme un temps de retard [Bourgeat et. al 1999], [Pankratov et Rybalko 2003].

L'accumulation de la mémoire dans un milieu multi-échelle

Supposons que nous avons le milieu ε^2 à toutes les échelles. Tel que mentionné précédemment, une seule étape d'homogénéisation des deux milieux voisins conduit à l'apparition de la mémoire dans terme de l'échange. L'équation macroscopique change de type: au lieu de l'équation de diffusion à l'échelle macroscopique nous obtenons une équation macroscopique intégro-différentielles. La prochaine étape d'homogénéisation conduira à la mémoire supplémentaire, et consécutivement à l'apparition d'une nouvelle équation dont les macro-échelle forme et le type mathématiques sont impossibles à prévoir.

L'homogénéisation sur plusieurs des échelles conduira à l'accumulation des effets de mémoire causé à chaque étape d'homogénéisation. Le modèle limite correspondant à nombre

infini d'échelles représente un grand intérêt scientifique.

D'abord on va etudier les modeles de milieux à plusieurs echelles qui existent deja:

Les médias multi-échelle n'ont pas été suffisamment bien étudiés dans la littérature.

Le milieu fracturé à trios echelles porous est d'abord développée dans [Amaziane, Goncharenko et Pankratov, 2005]. Le milieu consistait ensemble de grande fractures, de petites fractures et les petits blocs serrés. Les auteurs ont analysé le cas ou l'ouverture fracture à chaque échelle est la même en coordonnées locales. Autrement dit, si δ est l'ouverture des grands fractures, alors l'ouverture des petits fractures est $\delta\varepsilon$. Le modèle obtenu prouvé les effets de mémoire. Un tel milieu correspond à la situation quand chaque échelle génère une couche limite, de sorte que le seul filet formé par de minces de grandes fractures voisins et couches limites sera active. Le défaut de ce milieu est constitué de la majeure volume du milieu restera non perturbé. Dans la thèse presente nous considérons une autre classe de milieux fracturés tri-échelle, ce qui assure l'inactivité de la partie centrale de petits blocs. Nous avons obtenu un modèle différent de celui obtenu dans [Amaziane, Goncharenko et Pankratov, 2005].

Un arrangement particulier d'**un milieu fracturé quadruple** est étudiée dans [Dreier, Ozkan et Kazemi, 2004]. Ils ont proposé un modèle analytique pour l'écoulement dans un système de quadruple porosité qui consistait en un réseau triple fracturé d'un système unique matrice.

Les fractures ont classé, en fonction de leur taille et leur conductivité, de fractures micro (les plus denses , moin de conductivité) et les fractures méga (plus grande taille, plus grande conductivité). Ils ont supposé que les méga fractures seulement transport de fluide du réservoir vers le puits.

L'écoulement dans les trois fractures est supposé transitoire quand l'échange de fluide entre matrice et les fractures est pris en compte pseudosteady. Deux modèles différents sont étudiés: Premiere lorsque les micro fractures sont reliées à des fractures macro et n'ont aucun rapport avec les méga fractures. Deuxième lorsque les fractures micro et macro sont reliées à des fractures méga mais pas directement reliés les uns aux autres. Ce modèle est approprié pour les réservoirs que les deux ensembles de fractures peut co-exister, mais pas interférer. Une système d'équation interconnectés à travers de terme l'échange est

proportionnel à la différence de la pression entre les domaines interconnectés est résolu par la l'aide de la transformation de Laplace. Les fonctions de transfert pour un réservoir limitée sont proposés.

Le modèle ε^2 multi-échelles est analysé en [Douglas et al, 1998] où l'existence formelle de le comportement macroscopique est prouvé. En fait, Douglas et al. sont les premiers qui ont introduit une géométrie auto-similaire pour un modèle multi-échelles. Ils ont présenté la modèle moyenne d'un milieux de trois porosité du et ont proposé le modèle homogénéisé pour un système multi-échelles (N +1). Ils ont mis en place un processus hiérarchique d'homogénéisation à partir de l'échelle la plus petite, à l'échelle dernière. À chaque étape, ils ont montré le wellposedness de chacun des modèles. Les termes de mémoire ne sont pas du tout discutés. Aucune des problèmes de la micro-échelle sont résolus.

Dans [Peszynska 2007] une tentative pour développer le modèle multi-échelle est considérée pour les problèmes d'écoulement elliptique et parabolique. Ce modèle formel est formulée par un opérateur qui est déterminé implicitement par des équations fonctionnelles et ne peuvent pas être calculé en pratique. Le problème de comportement macroscopique de l'écoulement dans un milieu multi-échelles ε^2 reste ouverte. Solution de ce problème est l'objectif des chapitres (1) et (2).

Les effets d'accumulation de mémoire n'étaient étudiés pour le cas générale.ö

L'essentielle de ce travaille

Nous considérons l'écoulement monophasique dans un milieu multi-échelle, de sorte que, dans toute partie homogène du milieu, l'écoulement est décrit par une équation de diffusion en termes de pression du réservoir (qui est le modèle classique). L'objectif de cette recherche est d'obtenir le comportement homogénéisé de l'écoulement. Un tel comportement est non-trivial dans le cas général et dépend essentiellement du rapport de perméabilités de chaque deux échelles conséquentes.

Nous avon présenté l'ensemble des domaines $\widetilde{\Omega}^i$ dans R^3 $(1 \leq i \leq n)$ qui se chevauchent entre eux et dont la somme constitue une grande cube $\widetilde{\Omega}^i$. Le système de domaines $\widetilde{\Omega}^i$ est géométriquement auto-similaire, c'est à dire qu'il représente le système de cubes identiques

inséré périodiquement à l'intérieur des cubes plus grande $\widetilde{\Omega}^{n+1}$, comme illustré à la figure (1.1). Dans le cas général, les cubes ne peuvent pas être nécessairement cubes vrai, ainsi nous les appelons "les blocs".
Le milieu $\widetilde{\Omega}^i$ représente la superposition des blocs non-interscetant $\widetilde{\Omega}^{i-1}$ et la fracture Ω^i. À son tour, le milieu $\widetilde{\Omega}^{i-1}$ est la superposition de blocs $\widetilde{\Omega}^{i-2}$ et les fractures Ω^{i-1}, et ainsi de suite. Le milieu $\widetilde{\Omega}^2$ est la superposition de blocs de $\widetilde{\Omega}^1$ et les fractures Ω^2. Les blocs de $\widetilde{\Omega}^1$ sont homogènes. Le rapport entre les dimensions linéaires des périodes de médias $\widetilde{\Omega}^{i-1}$ et $\widetilde{\Omega}^i$ est une valeur constante petite ε.

Pour caractériser la taille absolue de chaque milieu, nous introduisons le système de coordonnées principaux $x = x^{(n)}$ associée au réseau le plus grande de fractures, Ω^n. La notation $x^{(n)}$ désigne une vecteur dans R^3: $x^{(n)} = \{x_1^{(n)}, x_2^{(n)}, x_3^{(n)}\}$. Dans Fig. (1.1), on voit que tout domaine de rupture Ω^i $(i > 1)$ est auto-connecté au correspondant période de la milieu $\widetilde{\Omega}^i$. En outre, il est directement relié pour les fractures de l'échelle plus petite Ω^{i-1}, mais n'a pas connexion directe avec les blocs de $\widetilde{\Omega}^{i-2}$. Le système de fractures connecté Ω^i pour i diverses crée un connecté hiérarchique du réseau multi-échelle, qui sera appelé le réseau de fractures. Physiquement, ces fractures sont les canaux poreux très perméables.

Avec x nous allons introduire les coordonnées locales y^i comme (1.1), et les cellules élargie locales qui sont les périodes de l'hétérogénéité à chaque échelle élargie de telle sorte que leur volumes est égale à 1 dans le système de coordonnées correspondante.
Chaque cellule $\widetilde{Y}^i$ se compose de deux sous-domaines ne se croisent pas appelé "fractures" Y^i et des "blocs" Y^{i-1} qui sont les images des sous-domaines Ω^i et Ω^{i-1}, respectivement. Afin d'éviter de nouvelles notations, nous noterons la cellule correspondant à $\widetilde{\Omega}^i$ que $Y^i \cup \widetilde{Y}^{i-1}$. Ainsi, une cellule est définie strictement comme equation (1.2).

Tous les médias Ω^i correspondent à l'échelle de coordonnée macroscopique x, mais ils peuvent être pris en compte dans différents systèmes de coordonnées. Le lien entre l'original $\widetilde{\Omega}^n$ et sa cellule (de la plus haute échelle) est représenté sur la Fig. (1.2).
Les équations de l'écoulement formulées par la coordonnée macroscopique x peuvent être formulées comme equation(1.5)où la condition d'autosimilarité est donnée dans l'équation (1.6).

Dans le cas d'un rapport modéré des perméabilités entre deux échelles conséquentes, le modèle macroscopique représente une équation de diffusion, mais avec le paramètre de diffusivité effectif déterminée par un nombre infini de problèmes cellulaires à chaque échelle. Dans le cas d'un milieu auto-similaire, ce système de problèmes cellulaires peut être découplé et réduit à une seule équation. Lorsque le rapport des perméabilités est élevé (un milieu à double porosité à chaque échelle), le modèle macroscopique n'est plus gouverné par une équation de diffusion.
En fait, même dans le cas d'un milieu à double porosité de deux échelles, la transition entre les deux échelles conséquentes amène à l'apparition des effets de mémoire et au changement du type de l'équation décrivant l'écoulement. Nous obtenons l'équation de diffusion avec un opérateur intégro-différentiel qui résulte décrivant l'échange de masse entre les structures à deux différentes échelles.

Dans un milieu double porosité à plusieurs échelles, la deuxième transition va transformer l'équation de mémoire vers une autre équation, et ainsi de suite.
Même dans le cas relativement simple de trois échelles, le modèle macroscopique adéquate n'est pas trivial et, pour le moment, n'est pas éclairci dans la littérature.

La condition nécessaire et suffisante pour pouvoir considérer le milieu comme auto-similaire consiste en ce que la structure du milieu à chaque échelle se répète et que le rapport des perméabilités soit fixe et coïncide avec le rapport des échelles spatiales en puissance 2. Le problème pour l'équation de diffusion qui gouverne l'écoulement à chaque échelle est auto-similaire (dans le sens commun).
Dans le cas d'un milieu multi-échelles, le modèle macroscopique peut être déduit pour un nombre quelconque (compris infini) d'échelles spatiales. L'homogénéisation d'un milieu multi-échelles représentera un processus itératif infini de 'upscaling' d'échelle plus bas Ω^{n-1} à échelle grande Ω^n.

À la première étape, on homogénéise le système sur la plus petite cellule $Y^2 \cup Y^1$. $y^{(2)}$ est la variable lente, alors $y^{(1)} = y^{(2)}/\varepsilon$ est la variable rapide. Le milieu $\widetilde{\Omega}^2$ et sa cellule sont présentés sur la Fig. (1.4).
L'homogénéisation de ce système conduit à un modèle bien connu de double porosité [Panfilov, 2000].

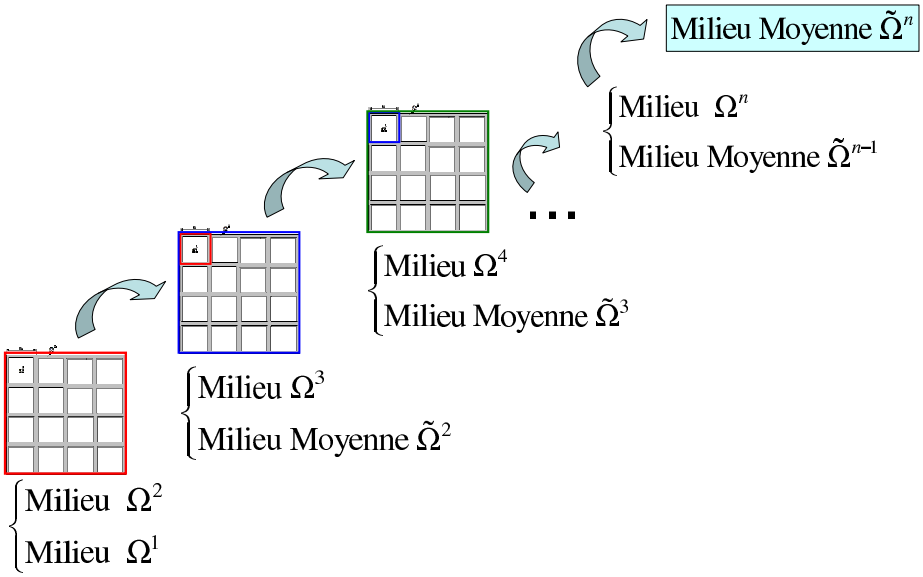

Figure 1: Processus itératif de 'upscaling'

À la deuxième étape, nous considérons le domaine qui se compose de la fracture Ω^3 et le bloc déjà homogénéisé $\widetilde{\Omega}^2$. Variable $y^{(3)}$ est la coordonnées lente, $y^{(2)}$ est la coordonnées rapide. Le milieu Ω^3 en coordonnées $y^{(n-3)}$ et son cellule en coordonnées $y^{(2)}$ est représenté sur la Fig. (1.7).

On a utilisé la méthode induction pour obtenir la modèle effective de transition d'échelle $i-1$ vers échelles i. Dans chaque étape la solution de problème local dans le bloc nous donne noyau effective de cette étape. La solution de problème locale se concerne à résoudre une équation intergo-différentielle avec les conditions limites de continuité de la pression sur les limites. Ce problème peut être résolu en utilisant de fonctions de Green et par la séparation de partie temporaire et spatiale.

L'équation définitive contient un opérateur intégro-différentiel dont le noyau est déterminé comme la solution d'une autre équation intégro-différentielle, et ainsi de suite.

Nous avons trouvé une forme récurrente décrivant le terme noyau dans chaque échelle en fonction du noyau dans l'echelle précédente.

Nous avons développé un modèle général homogénéisé de l'écoulement dans un tel milieu

à l'aide de la méthode de homogénéisation asymptotique.
Nous avons développé une procédure numérique conçue à calculer le noyau effectif pour un certain nombre arbitraire d'échelles. Pour un nombre infini d'échelles, la convergence du noyau effectif est prouvé numériquement. L'existence d'une limite de la série des noyaux est déjà démontré par Douglas et al. [Douglas *et al*, 1998].
Après 7 ou 8 échelles, le noyau tend à limiter son comportement et il n'y a plus besoin de prendre en compte plus de nombre d'échelles. Nous avons trouvé cette limite du noyau analytiquement. Aussi nous avons utilisé un apporch itérative pour trouver cette limite. La limite itératif du noyau coïncide avec la limite du noyau récurrentes.

Pour les milieux non-autosimilaires (qui ne satisfont pas au critère mentionné), nous avons obtenu les modèles homogénéisés pour deux échelles et trois échelles (un milieu à triple-porosité).
La différence principale entre milieux fracturés et les milieux multi echelles est le fait que les fractures sont très mince, ce qui signifie l'apparition d'un nouveau paramètre de petite taille. Il change la structure des développements asymptotiques et, consécutivement, le comportement macroscopique. En particulier, la grande perméabilité interne de chaque fracture n'assure pas son rôle dominant dans le processus de transport . Si l'ouverture de fracture est trop mince, sa perméabilité effective peut être égal ou même inférieure à la perméabilité de blocs.
Il est montré que dans certains cas, chaque bloc sera perturbé qu'au sein d'une couche limite juste en contact avec la fracture. Dans cette couche limite chaque bloc fonctionne comme une source à l'égard de l'écoulement dans les fractures. Cela va changer qualitatif de la structure des fonctions de Green des opérateurs décrivant l'écoulement dans un bloc, et la structure respective des noyaux dans les équations macroscopiques. Il est montré que cette type de modéle correspond à noyau d'Abel qui permet des solutions analytiques des équations intégrale correspondante. L'apparition de couche limite et le modèle macroscopique correspondant à ce cas est obtenue dans [Pankratov].
Pour un milieu fracturé simple l'effet de mémoire dans le modèle homogénéisé se décrit par un opérateur spécial : convolution avec le noyau d'Abel. Ces équations sont faciles à résoudre analytiquement ou peuvent être réduites à des équations différentielles. Ceci fournit un outil efficace multi-échelle pour analyser les milieux fracturés, jusqu'à l'obtention

de la structure des noyaux effectif complètement sous une forme analytique.

Nous avons étudié le problème d'écoulement dans un réservoir limité fracturé à deux échelles, qui a un modèle équivalent d'une équation integro-différentielle de noyau Abel. Ce problème est réduit d'une équation intégrale de Fredhom avec un noyau d'Abel. La solution explicite de ce problème est montrée dans la Fig. (2.4).

En présence de trois niveaux de fractures, en fonction du rapport entre les paramètres, deux modèles différents peuvent être obtenus. Nous avons présenté les deux modèle et on a montré que le cas ou tous les factures dans la deuxièmes échelles participes dans le modèle effective a l'intérêt à être étudie. Les expressions exactes analytiques pour les noyaux effectifs sont déduites.
Nous avons démontré que le comportement multi-échelle des milieux est différent dans les cas des milieux fracturés et du milieu à double porosité classique. Nous supposons que la perméabilité des milieux augmente de façon monotone à partir du milieu Ω^1 à milieu Ω^3. La perméabilité de la plus grande fracture est d'ordre 1, la perméabilité des fractures Ω^2 est $\omega \leq 1$. Le rapport entre la perméabilité de fracture Ω^1 et Ω^2 est $\varepsilon^{2+\alpha}$, similaire au cas analysés pour milieux poreux fracturé à deux échelles (chapitre 3).

Les modèles d'écoulement dans une seule fracture traversant un milieu poreux

L'analyse de l'écoulement dans les réseaux de fracture serait incomplète sans une étude de l'écoulement dans une seule fracture. Le problème principal consiste à obtenir une équation adéquate pour le bilan de quantité de mouvement. Comme ouverture de fracture est très faible, les modèles moyenne sur l'ouverture de fracture sont d'intérêt. Dans la théorie consacrée à la description macroscopique de l'écoulement dans un réseau de fractures traditionnellement la loi de Darcy est utilisée comme l'équation du bilan de quantité de mouvement dans tous les éléments du milieu à l'échelle macroscopique. Ce n'est cependant pas trop exact, car plusieurs phénomènes causent des écarts de la loi de Darcy. Tout d'abord, il s'agit d'un nombre non nul Reynolds pour l'écoulement à l'intérieur de fracture,

ce qui détermine les effets non-linéaires négliger l'inertie. Deuxièmement, il est le flux externes passant la limite de fracture, ce qui influence à la fois le bilan de masse moyenne et le bilan de quantité de mouvement. En troisième, les fractures ont les limites ondulées, qui influent sur les régimes d'écoulement et leur modèle moyenne.

La caractéristique de l'écoulement dans une fracture (ou même dire puits horizontal)est fortement affectée par la présence de ces phénomènes. Plusieurs études qui est fait en se concentrant sur l'une des effets mentionnée, mais un modèle mixte envisage en même temps l'effet de l'écoulement entre les parois ondulées perméable est restée un problème ouvert.

Écoulement plan-parallèle à l'intérieur des murs solides

Le point de départ pour étudier l'écoulement dans une fracture consiste à analyser l'écoulement plan-parallèle Stokes dans un canal régulier avec des murs imperméables. L'équation moyenne sur l'épaisseur du canal représente la loi de Poiseuille: [Bennett et Myres, 1962], [Savage, 1963], [Pfitzner,1976], [Iwai, 1976], [Landau et Lifshitz, 1986], [Sutera et Skalak, 1993], [Zimmerman etBodvarsson1996]. Les équations 2D de Navier-Stokes dans un logement tuyau cylindrique est examinée pour le cas de parois lisses dans [Peube, 1963], où la solution est présentée sous la forme d'une série de puissance par rapport à $1/r$. Le rôle important des effets d'inertie macroscopique pour disque plat en forme de fractures est confirmée dans les documents par [Vatistas, Ghila, et Zitouni, 1995] et [Zitouni et Vatistas, 1997].

Écoulement à l'intérieur des parois perméable

Dans le cas d'une fracture à parois perméables, l'afflux permanent de la fracture de les roches poreuses ambiante produit augmentation progressive de la vitesse d'écoulement (et le nombre de Reynolds) le long des fractures. Donc Re peut atteindre des valeurs suffisamment élevé au cours de laquelle les effets d'inertie doivent être conservés dans le modèle. Il faut fonctionner avec les équations de Navier- stocks complète. L'importance de l'effet de l'afflux dans les parois du canal était connue dans modélisation de l'écoulement dans les puits horizontaux, qui représentent le trou perforé dans des roches poreuses. Berman

est le premier qui a étudié le système de l'équation de Navier-Stokes pour un canal long à parois poreuses. La solution est obtenue grâce à une série de perturbations en fonction du nombre Reynolds de parois comme un paramètre de perturbation [Berman,1953]. Il a proposé une solution similaire, en termes de fonctions de flux, en vertu de laquelle les équations de Navier-Stokes sont réduites à une équation non linéaire du quatrième ordre différentielles ordinaires avec deux conditions aux limites à chaque paroi. Cette équation, appelée le problème de Berman est perturbé par le petit paramètre. Plusieurs auteurs ont étudié l'équation Berman. En particulier, [Sellars, 1955], [Yuan,1956], [White, Barfield et Goglia, 1958], [Proudman, 1960], [Terrill, 1964], [Robinson, 1987], [Zaturska, Drazin et Banks, 1988]. Si le nombre de Reynolds de parois est assez petit, il n'ya qu'une seule solution. L'augmentation de Reynolds de parois, les bifurcations apparient donner lieu à de nouvelles branches de solutions. Dans ce cas, le petit paramètre perturbation est l'inverse de Reynolds. Plusieurs articles sont consacrés à modéliser l'écoulement dans un tuyau à parois perméables [Berman, 1958], [Ihara, Kikuyama et Mizugushi, 1994], [Ouyang, 1998], [Ouyang, Arbabi et Aziz, 1998]avec un en vue d'applications aux puits horizontaux. Les deux approches analytiques et expérimentales sont appliquées. Le modèle moyenne d'écoulement représente la relation algébrique entre la chute de pression globale et la vitesse d'écoulement. Les modèles mécanistique proposés sont pour la plupart liées à des données expérimentales à travers les coefficients empiriques nécessaires. Yuan [Yuan et Finkelstein, 1956] est le premier qui à étudié l'effet de l'injection uniforme et d'aspiration à travers les parois expérimentalement. Une seule perforation est supposé. Le modèle d'Ouyang représente l'élan équilibre l'équation [Ouyang, 1998], [Ouyang, Arbabi et Aziz, 1998], qui contient une modification de facteur de frottement pour le tuyau perforé. Il est montré que l'impact de l'afflux de parois ou la sortie dépend sur le régime d'écoulement: elle augmente le frottement à la paroi pour un écoulement laminaire, et qu'elle diminue pour écoulement turbulent.

Écoulement entre les limites non uniformes

En réalité, ni le puits, ni la fracture ne sont pas complètement lisse et ils peuvent être considérés comme des tuyaux ondulés qui ont des limites irrégulières. Par exemple, une seule fracture dans le modèle idéalisé du milieu à double porosité a ouverture variable

périodique. Variations continue du nombre de Reynolds le long du canal détermine le rôle important des effets non-linéaires d'inertie, qui sont renforcées par les oscillations locales du champ de vitesse provoquée par des ondulations de la limite.
Écoulement dans un canal ondulé avec les parois impermeables est étudié dans le cadre d'une application pour les fractures. Un écoulement de Stokes avec un nombre très petit de Reynolds est étudiée par Adler et al. [Malevich, Mityushev and Adler, 2006]. En plus l'écoulement dans une fracture en forme de disque ondulé avec la condition limite 'no slip' sur les murs a été étudiée par Panfilov et al [Panfilov and Bues, 2004]. L'approche présentée dans leur travail, nous sert de base pour développer un modèle analytique pour l'écoulement dans les tuyaux /canaux ondulés que nous étudions dans la thèse présente.

Nous avons étudié écoulement stationnaire incompressible dans un puits ondulé ou dans une fracture. L'équation stationnaire de Navier Stokes dans le système de coordonnées cylindriques, ce qui représente un puits, ou à l'intérieur de deux plans parallèles ondulées en coordonnées cartésiennes, ce qui représente une fracture, est considéré.
Sur la base de la méthode développée dans [Panfilov and Bues, 2004], un modèle asymptotique est obtenu pour décrire chacun des cas. L'objectif est de trouver la perte de pression le long du tuyau /canal imposées aux différentes conditions aux limites: glissement et pas de glissement. Il est démontré qu'un nouveau terme de frottement résultant de l'afflux change de gradient de pression le long de la direction du flux principal, qui est périodique dans le cas des murs imperméables.
Ce terme de frottement est largement étudiée dans la littérature [Ouyang, Arbabi and Aziz, 1998] pour le cas de l'écoulement dans une géométrie uniforme, où l'effet de la longueur du tube dominante n'a pas été pris en compte.
Dans notre cas les champs de pression et de vitesse sont obtenus en appliquant la technique asymptotique à deux échelles sur équations de Navier-Stokes. Le comportement non linéaire de la vitesse par rapport à la perte de pression est observé. Dont est nominée comme les corrections non linéaires de la loi de Darcy dans nombres de Reynolds élevé, ce qui est le résultat des effets d'inertie dominante ainsi que la présence d'afflux.
Les parameters effectives de l'écoulement sont définis analytiquesment.

Écoulement dans une fracture avec les parois ondulés

Nous supposons que la fracture est entouré par le milieu poreux contenant de l'huile. Un autre fluide (eau) est injecté à travers la section de gauche à débit donné $Q°$. Les parois de la fracture sont perméables à l'eau et autorise le pétrole de les traverser. Ce modèle la peut être appliqué pour le problème de forage en sous sur les puits horizontale. Pour les conditions de forage en sous, la pression à l'intérieur du puits est maintenue à être inférieure à celle dans le réservoir, afin d'huile pénètre dans le puits à travers les murs. L'ordre d'afflux est considéré inférieur à l'ordre de vitesse caractéristique. Evidemment une couche limite le long des murs existe.
Supposons que les oscillations de limites soient périodique de période ℓ, le rayon moyen de puits R_w et la longueur caractéristique du puit soient L. En première approximation, nous supposons que les propriétés physiques de l'huile et l'eau sont à proximité, de sorte que le fluide peut être considéré comme le liquide presque monophasique de la densité ρ et la viscosité dynamique μ. Le fluide est incompressible, le écoulement est stationnaire. L'écoulement est axe-symétrique , de sorte que la composante angulaire est nulle.

En coordonnées cylindriques (R, θ, X) ou l'origine est située à l'axe du puits, la moitié supérieure du puits représente le domaine: $\{0 < R < R_w\tilde{\phi}(X), \quad 0 < X < L, \quad 0 < \theta < 2\pi\}$, où $\tilde{\phi}(X)$ est la fonction périodique de période ℓ et la valeur moyenne 1 . Dans le cas où $\tilde{\phi} = 1$, le puits est le cylindre régulier infini.
En presantant les variables sans dimension (5.2), les équations de Navier Stokes en système de coordonnées cylindriques, décrivant l'écoulement dans le domaine de $\mathcal{W} = \{0 < r < \phi(x), \quad 0 < x < 1\}$ est écrit que (5.3). Expansion asymptotique par rapport a deux paramètres petits $\omega = \dfrac{\ell}{L}$ et $\varepsilon = \dfrac{R_w}{L}$ nous permet à réduire le system des équation Navier Stokes à une system des équation différentielle ordinaire.

La solution obtenue permet de calculer les rotations, les zones stagnantes, la séparation des flux, ainsi que l'apparence d'instabilité. L'afflux à travers les murs influence significativement la structure globale des lignes de courant.

Méthode de solution

Développement asymptotique peut être réalisée en deux étapes consécutives: $\omega \to 0$ et $\varepsilon \to 0$, en supposant que:

$$\lim_{\varepsilon,\omega\to 0} \mathcal{U} = \lim_{\varepsilon\to 0} \left(\lim_{\omega\to 0} \right) \mathcal{U}$$

où $\mathcal{U} \equiv \{u, v, p\}$ est la solution au problème considéré. Dans la première étape, le paramètre ε est considéré comme fixe et la solution au problème (5.3) est construit comme une expansion régulière asymptotique de $\omega \to 0$: le terme de zéro d'un tel développement asymptotique conduit à des fonctions de moyenne sur l'épaisseur des fractures, ou, du moins, à toutes les fonctions dont le comportement le long de x correspond à la solution exacte dans le sens moyenne. On peut dire que la limite de $\omega \to 0$ signifie l'élimination de la variable radiale r, ce qui signifie l'homogénéisation along r. À la limite $\varepsilon \to 0$, nous obtiendrons un système qui est homogénéisé le long de x.

Ainsi, le terme zéro de l'expansion asymptotique est prévu être égale à la valeur moyenne. D'où la méthode asymptotique de solution est proche de la procédure d'homogénéisation. Les équations moyennes de l'écoulement représentent l'intérêt principal de ce chapitre. Dans le même temps, notre objectif est d'obtenir la solution à tous les points du domaine, mais pas seulement les équations moyennées. Nous allons mettre au point plusieurs du développement asymptotique.
En raison de la particularité de la méthode utilisée, les solutions obtenues n'ont pas besoin de fournir un modèle d'écoulement exact détaillée, mais ils sont censés présenter comportement homogénéisé adéquates.

Modèle homogénéisé

La méthode de perturbation régulière est utilisée pour réduire un système d'équations aux dérivées partielles à un système d'équations différentielles ordinaires. La théorie des perturbations est une méthode mathématique générale qui permet de trouver une solution approchée d'une équation mathématique.
La méthode consiste à chercher la solution approchée de l'équation sous la forme d'un développement en série des puissances du paramètre petit, cette solution approchée étant

supposé être une approximation d'autant meilleure de la solution exacte, mais inconnue, que la valeur absolue du paramètre ε est plus "petite". Dans notre cas comme on peut voir le système d'équations différentielles est singulière par rapport à ω. Mais dans le cadre de cette étude cette singularité n'affecte pas le comportement général de la solution obtenue. Les résultats obtenus sont des termes, y compris de ϕ et /ou de ses dérivés et les intégrales des pouvoirs différents. Le petit paramètre ε détermine les fluctuations géométriques entre le problème a travers de cette fonction. Le processus d'homogénéisation sur ε est limitée à une simple moyenne sur une période de perturbations.
Sur la base de définition de méthode à deux échelles, nous définissons une nouvelle variable lent qui représente coordonnée spatiale petite: $y = \dfrac{x}{\varepsilon}$.

Fonctions de courant

Dans le système de coordonnée cylindrique compte tenu de la symétrie par rapport à la coordonnée angulaire, les lignes de courants peuvent être obtenu en termes de composantes de la vitesse radiale et longitudinale respectivement u, v. On a utilisé condition additionnelle de satisfaction de vitesse d'afflux sur les limites.

Comportement de l'écoulement dans un tuyau réguliers

Les résultats presque trivial sont obtenus pour un tuyau regulaire ($\phi = 1, \quad \phi' = 0$) soit avec ou sans afflux,Fig. 5.2, Fig. 5.3, Fig. 5.4.
On voit que dans le cas d'afflux à travers les limites, après certain nombre de Reynolds une instabilité apparaît. Avec l'afflux le gradient de pression augmente linéairement le long du puits.

Comportement de l'écoulement dans un tuyau ondulé

La solution obtenue peut être utilisée pour examiner l'écoulement microscopique d'un tuyau ondulé. Pour une onde sinusoïdale donnée par: $\phi(x) = 1 + a\sin(2\pi x/\varepsilon)$ où a est

un nouveau paramètre sans dimension égale au rapport de l'amplitude d'ondulation à la moitié de l'ouverture moyenne.
Les résultats de $\omega = 0,01$, $\varepsilon = 0,01^{0,75} = 0,0316$ et $a = 0,3$ sont présentés sous la forme de lignes de courant et de champ de la pression et la vitesse. Le flux se déplace de gauche à droite. La moitié supérieure du domaine est présentée.

Apparition de flux secondaire

Flux secondaire ne sont pas visibles jusque'a certains Reynolds, comme on le voit dans la Fig. (5.5-a) flux secondaire n'apparaît pas. Dans la Fig. (5.6) un nombre relativement élevé de Reynolds est choisi en vue d'assurer la formation de flux secondaire. Il est bien vue que flux secondaire ne se présente pas que afin de deuxième approximation de série asymptotique. Dans la Fig. (5.7), la fonction de courant est tracée en utilisant les zeroth, premier et deuxième approximations. La correspondance la plus exacte avec le modèle d'écoulement vrai est obtenu dans la seconde approximation. Le rapprochement de zéro, qui décrit un écoulement sans inertie, produit toujours une trame fine et symétrique de lignes de courants.
On voit que quand il n'ya pas d'afflux à travers des limites, le gradient de la pression au long du puits est périodique.

L'influence d'afflux sur le gradient de la pression et de l'instabilité

En présence d'afflux les lignes de courant se change et instabilité s'apparaisse, en plus le gradient de pression augmente au long de la puits, Fig. (5.5), Fig. (5.8).
L'apparition de l'instabilité peut être noté par la positive perte de pression qui détermine le flux dans le sans contraire. Ce comportement n'est pas visible dans la perte de pression moyenne. Ca signifie que l'instabilité est visible seulement dans le comportement microscopique et la direction générale de l'écoulement est toujours de gauche vers droite malgré de l'existence de vorticités locales.

Comportement de perte de pression moyenne

La procédure d'homogénéisation utilisé précédemment donnera le modèle moyenne si l'on moyenne sur la variable lente y. Cela représente la moyenne sur les ondulations. Un autre type de la moyenne sera également appliquée sur le diamètre du tube ondulé, l'autre paramètre de petite taille. Alors le modèle complet homogénéisé peut être obtenue par une homogénéisation double sur le diamètre du tube et sur les ondulations de limites. La moyenne double est appliqué à la perte de pression le long du tube perforé pour obtenir le comportement macroscopique: Comme on peut voir dans l'équation (5.26), la perte de pression moyenne est déterminée en termes d'une loi cubique de la vitesse. En combinant les effets des variations locales des limites et des entrées et caractéristique générale de puits en forme de tube. La pression moyenne peut s'écrire aussi en termes de paramètres effectifs. Dans ce cas on est capable à définir trois paramètres effectifs décrivant différents aspects de perte de pression dans notre problème.

(1)

Le premier paramètre se correspond aux effets visqueux, qui sont le comportement de quasi-Darcy de la perte de pression. La perméabilité effective du puits peut être présentée par ce terme. Egalement ce terme représente la résistivité effectif de tuyau.
La perméabilité effective comprend également les conséquences des limites irrégulières comme les parties locaux de terme de quasi-Darcy. Ces effets sont pris en compte comme une correction à la perméabilité effective, ici déterminé en termes de coefficients de ω^2/ε^2 dans le paramètre λ, le paramètre d'ondulation.
Dans la Fig. 5.9 ca se voie que la présence d'irrégularités dans la géométrie des limites diminue la perméabilité effective du puits de forage de façon significative, tandis que la présence ou l'absence d'entrée n'a pas un rôle significatif sur la perméabilité effective.

(2)

Le deuxième paramètre est l'effet d'inertie pure qui disparaît en l'absence de afflux à travers les limites Fig. 5.10. Dans le cas sans entrée à travers les murs ce terme disparaît, et la perte de pression réduit au loi de Forchheimer.

(3)

Le troisième terme représente l'effet global et local du couplage entre les effet viscose et les effets inertielle. La moyenne des paramètres effectifs sont tracées vs amplitudes onde différentes. $a = 0$ ce qui concerne tuyau régulière sans ondulations. L'effet global est nul en l'absence d'entrée.
Comme il est indiqué dans la Fig. 5.11, ce terme s'annule pour les limites régulières alors qu'elle est positive pour les limites solides et négatives pour les limites poreuses. Cela signifie que la perte de pression le long de puits augmente lorsque que nous avons afflux, afin des effets visco-inertielle croisées.

Comportement moyen de perte de pression dans un tuyau régulière

Dans le cas particulier, la perte de pression moyenne dans un tuyau réguliers avec afflux serait de notre intérêt. On voit que pour une tuyau avec un flux à travers les murs les effets d'inertie pure et des effets croisée de visco-inertie entre la perte de pression moyenne. Pour une tuyau régulière sans afflux nous réduisons à l'équation de Hagen-Poiseuille pour la perte de pression dans les tuyaux. Aussi, en présence d'afflux à travers les limites, la perméabilité effective augmente, Fig. (5.12).

Les interfaces dans un écoulement diphasique incompressibles

Ecoulement diphasique dans les tuyaux en présence d'afflux à travers les limites est la définition générale de problème d'écoulement diphasique dans la fracture ou dans le puits. En général, écoulement multiphasique a un effet significatif sur la perte de pression, et un fort impact sur la performance du réservoir. C'est ce qui explique une stricte nécessité d'un outil précis capable de modéliser des écoulements multiphasiques en puits avant d'être traités par des simulateurs de réservoir.
En gros en ingénierie de réservoir trois catégories de modèles d'écoulement multiphasique existent: Corrélations empiriques, les modèles homogénéisés et modèles mécanistiques.

Des corrélations empiriques sont basées sur des données expérimentales ajustées avec les corrélations. Il est clair que les modèles empiriques peuvent être appliquées seulement à un ensemble de données expérimentales existantes. Des différents modèles sont proposés pour différents modes d'écoulement (annulaire,'bubble, slug flow etc.'), des modèles indifférents au mode d'écoulement sont proposés également.

Les modèles homogènes sont basés sur l'hypothèse qu'au fluide à deux phases on peut attribuer certaines propriétés du mélange après quoi il peut être traité comme un fluide monophasique. Dans les modèles homogènes on peut même introduire une condition de glissement entre les phases par l'analyse de quelques données empiriques. La prise en compte de la condition de glissement entre les phases dans les modèles homogènes amène à des modèles de 'Drift flux'[Zuber and Findlay, 1969], [Hasan and Kabir, 1988], [Hasan and Kabir, 1992], [Hasan and Kabir, 1994], [Ouyang and Aziz, 2000].

Les modèles mécanistiques sont en général les plus précis puisque introduisent de nombreux détails de différents modèles dans le mode de flux. Mais la difficulté principale d'utilisation de modèles mécanistiques consiste en discontinuités qui apparaissant au cours de la transition d'un modèle d'écoulement à l'autre.

Le défaut principal de toutes les approches mentionnées consiste en une forte dépendance des données empiriques ce qui réduit le domaine d'application de ces modèles jusqu'aux cas où il y a suffisamment de données expérimentales déjà obtenues. De plus, ces modèles ne donnent aucune idée de ce qui se passe exactement dans le tuyau par exemple sur la interphases des deux fluides, et des modèles précis de la condition de glissement sur l'interface résultant la tension superficielle.

Aussi, concernant la modélisation d'écoulement diphasique, on peut citer:

Méthode de suivir l'interface(mèthode de Levelset et VOF) qui est connu comme un outil efficace pour étudier problèmes diphasiques, spécialement comme une méthode capable à déterminer les interfaces. L'idée générale est de traiter le système diphasique comme un système monophasique où les propriétés du système dépendent d'une fonction indicatrice qui détermine à quel point, quelle phase est présente actuellement. La formulation du problème d'écoulement constitue d'une équation d'évolution eulérien pour la fonction indicatrice et les équations de conservation de la masse, de la quantité de mouvement et de l'énergie du système.

Suite à un changement monotone des propriétés du fluide sur l'interface (séparant l'un fluide de l'autre) il n'y a pas de discontinuités au niveau des propriétés d'un tel système entrant dans la formulation des coefficients à travers la fonction indicatrice. La condition de glissement sur l'interface est prise en compte comme au moyen d'une force supplémentaire n'agissant que sur l'interface. Cette force est introduite dans l'équation de conservation de quantité de mouvement. Cette idée est utilisée dans [Unverdi and Tryggvason, 1992] pour la première fois.

Dans la méthode de Level-set, la fonction indicatrice est présentée en termes d'une fonction implicite signifiant la distance minimale de chaque cellule de l'interface [Osher and Sethian, 1988], [Sethian 1999], [Osher, Fedkiw and Ronald, 2002]. Cette méthode permet de suivre l'interface plus facilement, et aussi il y a la possibilité de retracer attacher et détacher des interfaces. Volume of Fluid Method (VOF) conçue à choisir la fonction indicatrice comme le pourcentage de présence de l'une de fluide dans la grille spatiale. Détermination de l'interface s'effectue au moyen d'interprétation géométrique de la valeur VOF dans la cellule actuelle et ses voisines, ce que, en effet, représente un processus un peu compliqué.

Ecoulement diphasique annulaire dans un puits: applicable au problème UBD

En forage sous-pression, UBD('underbalanaced drilling') la pression du fluide de forage est inférieure à la pression des pores dans les roches. Par conséquent, la boue de forage ne plus entre la formation et comme un avantage majeur de la détérioration de la formation est très réduite. L'air, gaz, mousse et eau gazeuse sont les fluides légers généralement utilisé lors applications UBD. Dans cette technologie, la condition de sous-pression est nécessaire pour être maintenue par le contrôle de la pression au fond trous en fonction des conditions spécifiques de fonctionnement et le statut réel de fluides dans les puits. Ainsi, la pression de fond-trou doit être prédite avec précision. Le système hydraulique de sous-pression est généralement caractérisé par le flux de deux ou plusieurs phases (mélange liquide, mélange de gaz et solides boutures). Par conséquent, l'objectif est d'établir un écoulement multi

phasique modèle de prédiction et de contrôle de pression selon conditions du puits.
Alors disons simplement le problème d'écoulement diphasique dans un tube est de notre intérêt.

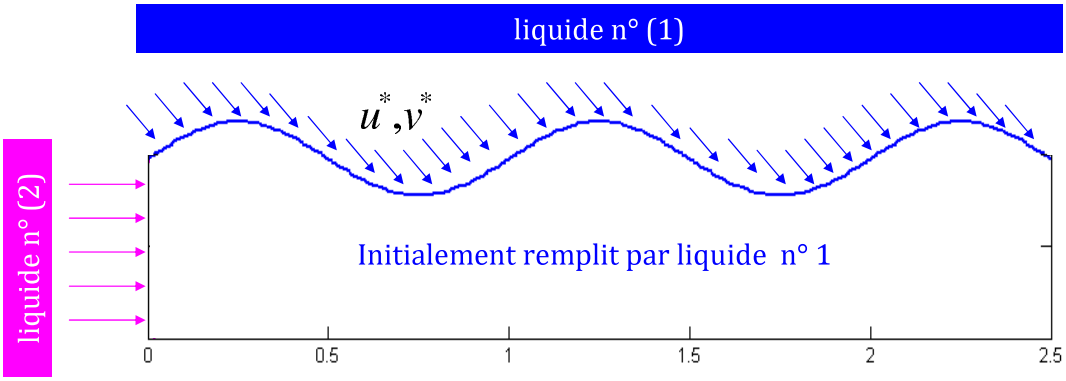

Figure 2: Schema de forage sous-pression

Nous avons étudié l'écoulement diphasique dans un puits horizontal placé dans la strate poreux saturé avec de l'huile, ce qui est observé lorsque la technique de forage sous-pression(UBD) est appliquée. Selon cette technique, l'eau, qui est en permanence injecté dans le puits afin d'enlever la coupe, a la pression inférieure à celle de l'huile dans les roches encaissantes. Pour cette raison, l'huile pénètre dans le puits et circule avec de l'eau. Si la vitesse d'écoulement n'est pas trop élevée, l'huile s'écoule dans une fine couche limite séparé de l'eau par une interface mobile. Une augmentation de la vitesse d'écoulement conduit à l'apparition de l'instabilité.
Ecoulement stationnaire diphasique dans un tube à parois perméables ayant une forme non uniforme est étudié. Les propriétés de chacun des phases ne sont pas trop différents. L'écoulement de chaque phase est décrit par les équations de Navier-Stokes, couplée à une équation de transport convectif a partir d'une fonction indicative qui détermine le type de fluide à chaque point. Pour des raisons de simplement décrire les interfaces, une fonction levelset de distance signée est utilisée. Cette fonction indicative est négative dans l'huile et positif dans l'eau et est nulle sur l'interface de deux liquides.
Méthodes de suivi d'interface comme VOF et Level Set sont des méthodes coûteuses du point de vue de la résolution de système de conservation de la masse et la quantité de

mouvement.
Ici on prend avantage de la solution stationnaire analytique obtenue pour l'écoulement monophasique incompressible dans un canal ondulé, on évolue la fonction de Level-set dans le champ de vitesse résulté, aux petits pas de temps. Une approche de relaxation est utilisée pour adhérer au modèle analytique d'écoulement monophasique et l'équation de transport diphasique sous la condition stationnaire.
Un ENO d'ordre élevé et un schéma numérique de TVD RK est appliquée à l'expansion asymptotique de l'équation levelset d'équation de transport. La perte de pression et de 'liquid hold-up' peut être calculée facilement.
Cette approche asymptotique semi-analytique fournit une technique de suivi de l'interface rapide spécialement en écoulement annulaire à l'intérieur du puits.

Méthode de levelset

Ecoulement incompressibles annulaire diphasique dans un puits horizontal est résolu par le couplage de la méthode levelset et du modèle semi-analytique proposée pour l'écoulement dans les tuyaux ondulés et à parois perméables.
La fonction levelset φ est utilisé comme une fonction d'indicateur pour déterminer l'une des fluides ℓ_1, ℓ_2. La méthode level set est basée sur l'évolution d'une fonction implicite, caractérisant la géométrie de l'interface entre deux fluides, par le champ de vitesse externe. Cette fonction implicite est généralement définie comme une fonction distance signée qui représente la distance minimale de toute position spatiale de l'interface de deux liquides. Le levelset zéro représente l'interface et le levelset positive est représente l'un des fluides et négatifs valeur est pour l'autre fluides. La fonction distance signée a la propriété supplémentaire, $|\nabla\varphi| = 1$. Le gradient de $\nabla\varphi$ est perpendiculaire à la isocontours de φ et des points dans le sens d'augmentation de φ.
Présentation de $|\nabla\varphi| = 1$ simplifie la formulation des vecteurs tangente et normale à l'interface.
L'évolution de la fonction implicite $\varphi(x,t)$ est régie par la formulation eulérienne comme une équation de convection simple, parfois appelé l'équation de levelset:

$$\frac{\partial\varphi}{\partial t} + \overrightarrow{V}.\nabla\varphi = 0$$

Il est clair que, dans cette évolution, la fonction distance signée initialement ne restera pas nécessairement la même fonction. Un processus 'redistancing' [Sussman and Fatemi, 1999] est appliqué après chaque évolution. L'équation 'redistancing' pourrai être résolus pour l'ensemble du domaine, mais pour gagner du temps, on peut réinitialiser φ seulement à des cellules à proximité de l'interface. La redistancing est effectuée pour les cellules à l'intérieur 10 $\triangle x$ de l'interface. La solution se stabilise après environ 10 itération.
Présentant des fonctions levelset, au lieu d'écrire les équations de conservation de la masse et la dynamique de chacun des fluides, nous puissions présenter une équations dont les coefficients sont définis en terme de la fonction de niveau.
La définition (6.4) supprime toutes les discontinuités à travers l'interface, à l'exception du saut de pression due à la tension de surface,

$$[p] = \sigma\kappa$$

où σ est une constante coefficient représente la force de tension entre les deux fluides et κ est la courbure locale de l'interface. Dans le contexte des méthodes de front-tracking soit de la méthode de Volume de fluide ou la méthode de levelset en ajoutant un nouveau terme forçant à le côté droite de équation de navier stokes, on peut appliquer la condition d'absence de saut de pression. Ce nouveau terme forçant prend la forme

$$\frac{Re}{We}\frac{\delta(\varphi)\sigma\kappa\overrightarrow{N}}{\rho}, \qquad We = \frac{\rho_1 L V^2}{\sigma}$$

We est le nombre de Weber, et $\delta(\varphi)$, est la fonction delta modifié determiné par equation (6.12). Dans le cas qu'on a étudié on a négligé les effets de tension de surface car les deux fluides sont considérés au niveau de propriétés très proche.

Evolution asymptotique levelset

Dans le puit de très longue décrits dans la chapitre(5) de ce manuscrit, évolution de la fonction eulérienne levelset en termes de variables non-unidimensionnels présenté dans(5.2) serait comme equation . Où ω est un petit paramètre représentant le rapport de rayon du puits et sa longueur. u, v sont les composantes de la vitesse.
En ce qui concerne l'apparition de petit paramètre, selon la méthode de perturbation

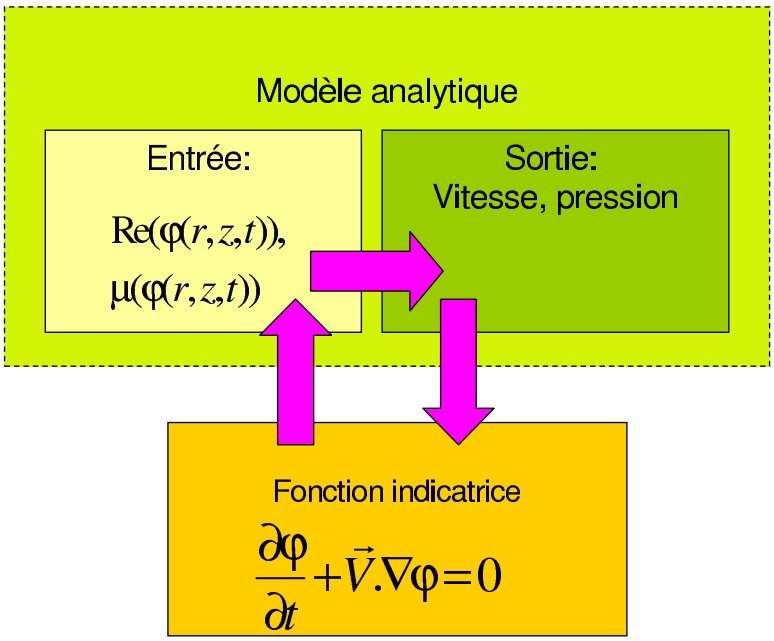

Figure 3: suivi de l'interface par la methode de Levelset

régulière, nous avons développement asymptotique de φ comme système des equations (6.7) que peut être résolu numériquement. La solution est montrée dans Fig. (6.1), ..., (6.3).

La conclusion

La recherche se compose de deux parties: dans la première (chapitres1,2, et 3) nous avons développé des modèles d'écoulement dans les milieux multi-échelles qui prouvent l'effet de mémoire à chaque échelle; dans la seconde partie (chapitres 4,5, et 6) nous avons analysé l'écoulement dans une fracture unique et canal circulaire immergée dans le réservoir poreux à diverses nombres de Reynolds.

Dans la première partie nous avons analysé l'équation de diffusion à chaque échelle en appliquant méthode d'homogénéisation asymptotique avec l'objectif de construire le modèle macroscopique moyenne pour toutes les échelles d'hétérogénéité.

Dans la deuxième partie nous avons étudié les équations de Navier-Stokes et appliqué les méthode asymptotique à deux échelles avec l'objectif d'obtenir l'équation moyenne sur l'ouverture de fracture.

Modèles d'écoulement multi-échelles : milieux ε^2

Tout d'abord, nous avons analysé les médias double porosité (chapitre 1)qui sont ε^2 à que chaque échelle, ce qui signifie que le rapport de la perméabilité entre deux milieux voisins est ε^2. Le petit paramètre ε est la période de l'hétérogénéité à chaque échelle. Les médias à deux échelles de ce type ont étudiées: le modèle obtenu prouvé l'apparition de la non-localité dans le temps. Physiquement, le terme non local décrit l'échange de masse entre les deux milieux, qui est fortement non-stationnaire et dépend de la direction du processus dans le temps. Pour un milieux à deux échelles, le modèle d'homogénéisation se compose de deux équations à deux pressions moyennes. Chacun de ces équation contient les "termes de l'échange": ils sont responsables de l'interaction entre deux pressions.

Les problèmes principaux qui concernent ces médias consistent en les suivantes:

(i) une homogénéisation unique pour deux échelles provoque l'apparition de la non-localité,

qui changent le type des équations. Si nous avons milieu à trois échelles ou plus, quel sera le type de le modèle moyenne?
(ii) L'homogénéisation multi-échelles résulte accumulation de la mémoire. Comment se passe ce processus?
(iii) Est-il possible d'obtenir le modèle générale pour limiter le nombre infini d'échelles?
(iv) Comment on peux calculer les paramètres effectifs du milieu multi-échelles?
Pour les milieux avec une hétérogénéité modérée, l'équation de diffusion garde la forme à chaque étape d'homogénéisation. Grâce à ce la, modèle macroscopique peut être obtenu par la méthode de l'ascension directe: à la première étape, on homogénéise le couple de milieux 1 et 2. A l'étape suivante, on considère le couple de moyenne 3 et la moyenne de 2 moyennes, qui tient déjà de l'interaction avec le milieu précédent. Cette opération est répétée à chaque échelle. De cette manière il est possible de révéler la structure de paramètres effectifs d'équation macroscopique. Ce qui est important dans ce cas, c'est le fait que l'équation moyenne à chaque échelle est connue a priori. Ce n'est pas le cas pour les médias avec la mémoire. En effet, à chaque étape d'homogénéisation l'équation moyenne change du type, de sorte que la forme de l'équation moyenne est inconnue pour n'importe quelle échelle. Pour cette raison, il est impossible d'appliquer la méthode itérative directe hiérarchique décrit ci-dessus.

Nous avons appliqué une autre méthode. Pour un nombre arbitraire d'échelles, nous avons appliqué **la méthode d'induction mathématiques** qui consiste à ce qui suit:
1) on postule la forme générale de l'équation de la moyenne pour tout upscaling i
2) on prouve que cette forme est valable pour i = 1 (la base d'induction);
3) on prouve que, si cette forme est valable pour tout i, alors il sera également valable pour i + 1.

Le point principal de cette méthode est de postuler la forme générale du modèle macroscopique. Afin de suggérer une idée sur cette question, nous avons analysé les caractéristiques communes en deux modèles obtenus pour i = 1 (un milieu à deux échelles) et i = 2 (un milieu à trois échelle). Pour cela nous avons réalisé l'homogénéisation d'un milieu ε^2 à trois échelles. Les résultats obtenus pour i = 1 et i = 2 ont révélé que le modèle macroscopique peut être présenté sous la forme de deux équations à deux pressions conjugués. L'une de ces pressions est en moyenne sur le domaine i et est désigné comme P^i, tandis

que le second est moyenne sur tous les milieux précédents hiérarchique $\tilde{P}^{i-1}$ à partir de $i-1$. Chaque équation contient les termes de l'échange. Selon ces résultats que nous avons supposé que les termes de l'échange peut être présenté comme la convolution avec la dérivée de la la pression conjuguée.

Donc, le problème est réduite afin de déterminer les noyaux de ces opérateurs de convolution, et d'autres paramètres effectifs (perméabilité, la porosité,...). Cette méthode appliquée nous a donné le système fermé d'équations récurrentes pour les noyaux de l'échange du masse. La procédure de solution analytique-numérique de ce système est développé, basé sur la transformation de Laplace. Nous avons montré une convergence des résultats obtenus pour le nombre des différentes échelles d'une limite stable de comportement. Le processus analysé dans ces milieux est auto-similaire. La condition nécessaires et suffisante de l'auto-similaire est proposée afin que chaque échelle le modèle homogénéisé devient auto-similaire. L'avantage d'un milieu auto-similaire est la possibilité d'analyser son comportement pour un certain nombre d'échelles, même pour le nombre infini.

Modèle limite d'écoulement dans un milieu à nombre infini d'échelles

Le problème suivant est retrouvé à la transition i vers la limite $i \to \infty$. Comme l'a dit, la simulation analytico-numérique ont révélé une convergence rapide à un comportement limite stable. En supposant que le processus se stabilise quand $i \to \infty$ nous concluons que les fonctions itératives hiérarchique (la pression et les noyaux effectifs) ont tendance à une limite. Cela nous a permis d'obtenir la limite du modèle macroscopique de l'écoulement, et le problème du délai pour le noyaux efficace à partir des équations récurrentes obtenu pour n'importe quelle échelle i. Le modèle limite est non local, et le noyau de cette équation est la solution d'une équation non-linéaire intégro-différentielle. D'autres paramètres sont également la solution des équations intégro-différentielles. Cette système est réduite à un système fermé non linéaire pour le noyau "local" K sous la forme de la série de Fourier avec les composants en fonction de la fonction K elle-même.

En utilisant de la transformation de Laplace, nous avons développé un code numérique qui résout cette équation numériquement. La solution est obtenue par une méthode itérative: à zéro rapprochement on suppose que le noyau est le delta-fonction, qui donne l'équation explicite pour le noyau. Cette approximation est ensuite remplacé à la droite

de l'équation analysés, et ainsi de suite. Les solutions obtenues sont exactement les mêmes que ceux obtenus que la limite numérique de solutions itératif pour tout i, ce qui prouve la convergence des résultats obtenus. Le résultat principal qualitatifs suivants de cette étude consistent à ce qui suit: nous avons montré que la non-localité peut générer la non-linéarité, qui est un résultat fondamental.

Milieu fracturé à deux-échelle

Le cas du milieu fracturé a un avantage important, et un défaut important. L'avantage est qu'il conduit à des relations analytiques pour les noyaux effectifs, en raison d'une structure simple, mono-dimension de l'écoulement dans une fracture mince. Le défaut consiste en ce que le milieu fracturé qui maintient le non-localité à chaque échelle, n'est pas auto-similaire. Il est donc impossible d'obtenir le modèle limite de nombre infini d'échelles. Alors nous avons analysé les deux-échelle et des médias de trois échelles.

Dans le chapitre 2, nous avons obtenu le modèle moyenne pour milieux fracturé à deux échelles, dans lequel le rapport de la perméabilité est $\omega = \varepsilon^{2+\alpha}$. L'apparition d'un nouveau paramètre petits, l'ouverture de fracture, change la structure des développements asymptotiques et, consécutivement, le comportement macroscopique. Les résultats obtenus dans ce chapitre ne sont pas nouveaux (le modèle du même type a été obtenus d'abord par L. Pankratov), mais sont nécessaires pour développer le modèle suivant de milieu à trois échelle, en utilisant la même méthodologie.

Une caractéristique très importante des milieux fracturés est l'apparition de la couche limite dans le bloc serré qui est seulement perturbé par l' écoulement dans la fracture. Dans cette couche limite chaque bloc fonctionne comme une source à partir de l'écoulement dans les fractures. La partie interne de chaque bloc reste imperturbable. En raison de la géométrie spécial (simplifié) de l'échange entre les fractures et les blocs, le noyau d'échange dans l'operateur de mémoire du modèle moyenne est le noyau Abel. Les équations intégrales avec noyaux d'Abel ont souvent des solutions analytiques ou peuvent être réduites à des équations différentielles. Ceci fournit la outil efficace pour analyser milieux multi fracturés, jusqu'à l'obtention de la structure des noyaux efficace sous une forme complètement analytique. Quelques exemples d'application de ce modèle ont été analysés.

Milieux fracturés à trois échelle

Dans le chapitre 3, un milieu non auto-similaire fracturé à trois échelles est étudiée. Il se compose des petits blocs serrés entouré par les fractures très perméables, mais minces qui sont entourées, à leur tour, par le second système de fractures encore plus perméable et plus grande. Dans l'échelle la plus petite le comportement non locale résulte seulement si la couche limite dans les blocs, décrits ci-dessus, existe. Cela donne la règle pour déterminer l'ouverture des petites fractures et le rapport de perméabilité entre eux et les blocs. Dans le prochain niveau, au contraire, l'apparition de la couche limite dans la superposition de deux milieux précédent est interdit, sinon la majeure partie du milieu sera entièrement exclus du processus. Ceci détermine paramètres optimal de l'ouverture et la perméabilité des fractures importantes. Comme résultat, nous avons montré que le rapport de perméabilité entre les blocs et de petites fractures devrait être inférieur à ε^2, tandis que le rapport de perméabilité entre les deux fracture doit être ε^2. Les ouvertures de fracture ne suivent pas la loi d'échelle comme les périodes de l'hétérogénéité.

Dans ce cas, la première (petite) échelle du milieu se comporte comme le modèle de fracture avec les noyaux d'Abel décrit ci-dessus, alors qu'à l'échelle deuxième le milieu se comporte comme un milieu à double porosité. Le modèle effective moyenne sur toutes les échelles est l'équation intégro-différentielle dont le noyau est déterminée analytiquement. Nous avons comparé les résultats qui fournissent les deux échelles et un modèle à trois échelles, qui sont en bonne correspondance avec une signification physique. En particulier, lors de la récupération de pétrole dans le réservoir de la pression dans un milieu à trois échelle devrait être plus élevée que celle dans un milieu à deux échelles (en raison d'un double système de sources qui l'aliment de grandes fractures), ce qui était exactement obtenus par les modèles obtenus.

Ecoulement dans une fracture et un canal circulaire

Pour compléter l'étude des milieux fracturés, nous avons également analysé l'écoulement dans une seume fracture (chapitre 4). Nous avons étudié le problème de l'écoulement dans une fracture immergé dans un réservoir poreux. Les murs de fracture étaient supposés rogues. L'objectif était de développer le modèle moyenne d'écoulement sur l'ouverture de

fracture tout en tenant compte des flux d'entrée dans la fracture du réservoir a partir de ses parois. L'afflux constitue l'élément principal nouveau de cette étude. Le débit de la fracture est décrit par les équations de Navier- Stokes à divers Re. La solution du problème d'écoulement dans une fracture très long et mince est obtenus sous forme d'analyse par la méthode des développements asymptotiques à l'égard de la fracture l'ouverture et la période des oscillations du mur. Nous avons obtenu l'équation moyenne de quantité de mouvement qui détermine le gradient de pression moyenne à une fonction cubique de la vitesse moyenne d'écoulement. Le terme linéaire correspond à la loi de Darcy, le terme quadratique est provoqué par l'afflux qui réduit l'énergie cinétique, et le terme cubique est les effets visqueux inertiels croisés. Pour les paramètres efficaces, nous avons obtenus des relations analytiques. Le terme quadratique peut être négligé dans toutes les situations. L'afflux qui est supposé d'être faible, en raison de ce qu'elle influence faiblement les termes visqueux et visco-inertiaux. Ainsi, l'afflux influence plus le bilan de masse , mais pas de quantité de mouvement . Les résultats ont été comparés avec des simulations numériques basées sur Comsol Multiphysics. Nous avons montré que même quand il n'y a pas d'entrée de flux à travers les parois après un Reynolds critique, une sorte d'instabilité se pose. L'instabilité est caractérisée par inversion du flux local. Appliquant la même technique, nous avons également obtenu la solution analytique du problème d'écoulement dans un canal circulaire horizontal (chapitre 5). Les résultats obtenus sont qualitativement similaires à ceux obtenus au chapitre 4.

Ecoulement diphasique dans un canal avec les parois permeable

Ecoulement diphasique dans les fractures et les puits horizontaux en présence d'entrées à travers les parois est étudiée dans le chapitre 6, avec un regard à l'application dans le problème de forage sous-équilibré de puits horizontaux. Nous avons développé une méthode analytico-numérique de résoudre le problème pour les fluides ayant propriétés physique à proximité. On calcule analytiquement le champ de vitesse en utilisant les résultats obtenus dans le chapitre 5. Après celui-ci peut calculer la fonction indicateur (levelset fonction) qui est transporté à la vitesse vrai de la fluide. Le niveau zéro de cette fonction est l'interface macroscopiques entre les fluides. Ces opérations peut être répété, ce qui conduit à une méthode itérative de la solution. L'équation pour la fonction levelset

est résolue numériquement. L'exemple de solution est indiqué pour le cas de forage en sous, quand l'eau est injectée dans le canal (le puits horizontal), et l'huile pénètre par les parois du canal à partir du réservoir.La pression dans l'eau est maintenue à moins que ce dans le réservoir. L'évolution de l'interface dans le temps est démontrée.

Contents

Introduction

Methods of modeling heterogeneous fractured and porous media

Fracture net imbedded into a porous medium represents a typical case of natural heterogeneous porous reservoir which contains oil, gas or water Fig. 4.

Figure 4: Example of a fractured-porous rock

The typical fracture system represents a hierarchical system of networks included into one another and having different permeabilities and apertures. Respectively the porous blocks situated between fractures also form a hierarchical system. Thus, one deals with hierarchical, or multiscale media.

Modeling of flow in such media is one of the most difficult problems of the theory which remains open for general case. Only some particular cases were studied in the literature. There exist two general approaches in modeling:

(i) *the micro-modeling*: one resolves directly the problem of flow numerically or analytically in the entire medium while taking into account for all the details of the medium structure. For

periodic structures frequently it is possible to obtain analytical solutions by the method of superposition. For non-periodic irregular media the only numerical solution is possible. The problem of the direct numerical modeling consists of the necessity to use very fine grids whose size should be much lower then the lower scale of the hierarchical medium structure.

(ii) *the homogenization and macro-modeling*: one can develop the flow model averaged over heterogeneities. Such a model describes the behavior of a homogeneous equivalent medium, so its numerical solution does not ask to use very fine grids.

Micro-modeling of fractured networks

As the numerical methods, their analysis is outside the objective of the present thesis. All them are based on very fine numerical grids, which reduces their efficiency. Analytical methods are largely based on the superposition of elementary solutions which describe flow in the vicinity of each fracture considered independently of all other. More exactly the superposition is performed in terms of Green's functions. Indeed, if we consider a fracture as a surface in 3D or a line in 2D, imbedded in an infinite reservoir, then the solution of the problem of perturbation of the reservoir by this fracture (by imposing a given pressure along the fracture) represents the Green's function of the corresponding operator describing flow.

The use of Green's function in reservoir engineering was first suggested by Gringarten et al. [Gringarten and Ramey, 1973]. They applied the established methodology to the fractured reservoirs [Gringarten and Ramey, 1974] to the case of a single vertical fracture with infinite conductivity.

Later Kuchuk et al.[Kuchuk, Habashy and Torres-Verdin, 1996] applied the general theory of Green's functions in composite media [Carslaw and Jaeger, 1959] to the heterogeneous reservoirs and obtained the respective transfer functions for the special cases of laterally or horizontally composite reservoirs [Kuchuk and Habashy, 1997]. This model is capable to examine the fractured reservoir in the case of small aperture of geological strata and high contrast in permeability between the narrowest stratum and all other strata. Both fractures with infinite and finite conductivity can be described through this model [Kuchuk and Habusky, 1994].

While the transfer functions are developed for almost all types of heterogeneity, no limit behavior of a multiscale heterogeneous system is proposed.

Homogenization method applied to heterogeneous media

The second approach consists of using the averaged models of flow in heterogeneous media. They should be constructed before to use them in reservoir simulation.

Flow in a heterogeneous medium can be described by the diffusion-like differential equation with fast oscillating in space coefficients responsible for medium properties. The homogenization theory is an efficient method to study this kind of differential equations.

The idea of homogenization consists in assuming two main properties:

- the medium structure has two very different scales (at least) which correspond to the microscale l and the macroscale L; the high difference between the scales means that the ε=l/L is a small parameter. The lower the value of ε, the more fine-grained becomes the medium structure. In the limit $\varepsilon \to 0$, each heterogeneity cell transforms into a point, so we obtain a homogeneous medium (but with internal structure at each point). So if we construct the solution of our problem for pressure p in the form of an asymptotic expansion: $p = p_0 + \varepsilon p_1 + \varepsilon^2 p_2 + ...$, then the zero term p_0 will correspond to the homogenized pressure. The equation for p_0 will be the homogenized flow equation. Certainly, the only weak convergence may be ensured.

The formalism of the method was developed in [Bakhvalov, 1977], [Bakhvalov and Panasenko, 1989], [Allaire 1992]. The basic convergence theorems can be found in [Sanchez-Palensia, 1980]. Along with this, the mathematical homogenization theory was developing other basic points such as prove of existence and uniqueness of the cell problems, reduction of the periodic cell problem to a boundary-value problem, construction of complete asymptotic expansion, estimations for residual terms of expansions, studying the tensor properties of the effective coefficients, generalization of the theory in case of discontinuous fields close to periodic ones, homogenization of nonlinear equations, e.t.c.

The most full description of the homogenization theory can be found in monographs and reviews [Bensoussan, Lions and Papnicolaou, 1978], [Lions, 1978], [Sanchez-Palensia, 1980], [Crapiste, Rotstein and Whitaker, 1986], [Bakhvalov and Panasenko, 1989], [Adler, 1992]. Basic results has been obtained for periodic fields in [Arbogast, Douglas and Hornung, 1990], [Hornug, 1997], [Panfilov, 2000].

The theory for random media is developed in [Kozlov, 1978a], [Kozlov, 1978b], [Kozlov, 1979a], [Kozlov, 1979b], [Kozlov, 1985], [Kozlov, 1989], [Panasenko, 1988].

Double porosity medium: exchange between blocks and fractures

The media consisting of two rocks having very different permeabilities are called double porosity media. In such media the highly permeable channels form a connected net, while low permeable blocks represent isolated inclusions. Despite the blocks are low permeable they are assumed to contain a large mass of fluid. The permeable channels are usually called "fractures" whereas they are not true fractures. As the permeability of porous blocks is much lower than that of fracture the main flow happens through fractures. Therefore the pressure in fractures varies much faster than in blocks. Due to this a difference between pressure in fracture and block arises, which provokes flow from the block center to the surrounding fractures. As the result, each block works as a source of fluid with respect to fractures and also contributes to the global process. Thus, the macroscopic equations of flow in fractures should contain a source-term which describes the mass exchange with blocks. Depending on the ratio between fracture and block permeability, several different regimes of flow and exchange are possible. They lead to different macroscopic models.

Model with quasi-equilibrium mass exchange. The classical model derived from phenomenological approach [Barenblatt, Entov and Ryzhik, 1972], [Barenblatt, Zheltov and Kochina, 1960], [Barenblatt, Entov and Ryzhik, 1990] considers the tight blocks and the highly permeable connected fractures as two coexisting continua. The mass exchange between them is described by the linear dependence between the flux velocity and the difference of pressures in blocks and fractures. Such a relation represents the steady-state solution of 1D Darcy's law. So the mass exchange is postulated to be steady-state.

In some versions the fluid may flow through blocks but not only through fractures [Coats and Smith, 1964]. In other papers the overall capacity to retain fluid is that of blocks, while the fractures capacity is neglected, [Barenblatt, Zheltov and Kochina, 1960]. Similar models were suggested later in [Böhm and Showalter, 1985], [Charlaix, Hulin and Plona, 1987], [Duguid and Lee, 1977], [Evans, 1983], [Warren and Root, 1963].

The assumption about the quasi-equilibrium exchange flow was checked out in [Kazemi and Thomas, 1969] where it has been shown to be valid after the transient process stabilizes.

However, it has been shown in [Panfilov, 2000] that after the exchange becomes steady-state the averaged pressures in blocks and fractures become identical, and any exchange flow can not be longer detected. Therefore, the assumption of a steady-state exchange is equivalent to the assumption that the block-matrix exchange does not exist.

Such a uniform model without any exchange term was applied in [Odeh, 1965] where it was assumed that the exchange flow was rapidly established and absolutely insignificant.

Memory in double-porosity media

The model with non-stationary exchange was first suggested in [De Swaan, 1976]. The relation for it was obtained by solving analytically the non stationary problem of flow within a single block, caused by a pressure reduction at the block boundary. The exchange term was obtained in the form of the time convolution of the pressure gradient at the block boundary with the Green's function. This meant the appearance of the memory.

The similar model with non-stationary exchange was obtained by homogenization technique much later in [Arbogast, Douglas and Hornung, 1990] and [Panfilov, 1990]. The exchange term was obtained in the form of an integro-differential operator applied to the time derivative of the pressure in fractures. The kernel of this operator was obtained in the explicit analytical form through the Fourier expansion of the Green's function describing the perturbation of a single block from its boundary.

This model was obtained for a specific value of the ratio between block and fracture permeabilities, ω, which was of order ε^2 where ε is the period of medium heterogeneity. This model is called ε^2-model.

For other values of ω, other models have been obtained in [Panfilov, 1993], [Panfilov, 1994]. If $\varepsilon << \omega << 1$, the blocks are no longer impermeable for fluid. A part of fluid can cross each block, due to which the blocks contributes to the effective permeability. At the same time the exchange process becomes neglecting. The system is described by a single pressure, and the macroscopic model keeps the same form as the microscale equations.

If $\varepsilon^2 << \omega << \varepsilon$, the blocks play a double role. First of all, they are the sources of fluid with respect to fracture, which determines the appearance of exchange term. Secondly, they contribute to the the effective permeability. The flow in a block represents a superposition of the source flow and a translational flow in the direction of the macroscopic pressure gradients. The exchange term is different from the case of ε^2-media. The kernel of the integral operator becomes delta-function, which means that the nonlocal term transforms into a local one, which is the second derivative of pressure in time. This is the case of a short-term memory.

Memory in fractured media

In the literature the double porosity model is frequently called the fractured-porous medium. This is not too exact.

If the same order of parameters (ε^2 for the permeability ratio, and 1 for the porosity ratio) is applied for a medium with thin fractures, then the memory effects will entirely disappear. The exchange between fractures and blocks becomes too fast, and the time effect become neglecting.

To obtain the model with memory, similar to double porosity medium, it is necessary to change the ratios between permeabilities. Moreover, even in this case the exchange process is sufficiently different from double porosity medium, due to which the memory terms has sufficiently different structure. Therefore, the fractured-porous model with memory represents an independent result, identically significant as the model of double -porosity medium.

The first model of flow in fractured-porous medium with thin fractures which proved the memory effects was obtained by Pankratov and Rybalko in [Pankratov and Rybalko, 2002], [Pankratov and Rybalko, 2003]. The authors have shown that the memory appears only if the porous blocks (surrounded by fractures) are very tight, so that they work only through a thin boundary layer whose thickness is of the same order as the fracture aperture. In this case the contribution of blocks and fractures into the macroscopic process will be of the same order. In the consecutive publications the authors developed the classes of analyzed processes, [Amaziane, Pankratov and Rybalko, 2005], [Amaziane, Pankratov and Piatnitski, 2007].
The global behavior of fractured media versus different parameters such as the fracture thickness, the size of blocks and the ratio of the permeabilities, and oscillating source terms has been studied. There has been shown that for the thin fractures which are highly permeable the memory term reduces to an Abel kernel. The authors have not presented the constructive technique of development of the model. Their objective was to extend the convergence theorems developed by the method of Khrouslov [Marchenko and Khrouslov, 1974]. In fact, Khrouslov's method is applicable for domains in which the blocks are entirely impermeable. Pankratov and Rybalko extended the results for media permeable everywhere.

It has been shown that the homogenized global model is also of parabolic type but with non-local terms which could be seen like a source term or like a time delay [Bourgeat et. al, 1999], [Pankratov and Rybalko, 2003].

Multiscale media

Various multiscale media can exist, as shown in Fig. 5.

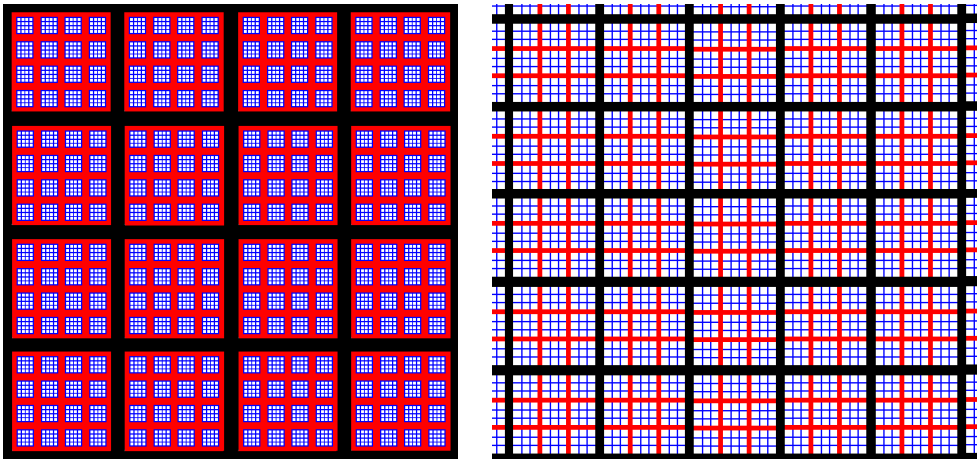

Figure 5: Example of a multiscale media with three hierarchical systems of fractures: black, red and blue

Both media are multiscale hierarchical: the highest level of hierarchy is presented by large black fractures, the second level corresponds to the intermediate red fractures, the third level is presented by the small blue fractures, and the last level corresponds to the white blocks. The difference between these tow examples consists only of the connection between various classes of fractures. In the left-hand medium the black fractures are in contact only with the red fractures, and the red fracture are in contact only with blue fracture. Only the blue fractures are in contact with the blocks. So the system of connections is also hierarchical and follows the same hierarchy. Due to this the behavior of all elements of the same class is similar, and the system is self-similar at all scales.

In the right-hand medium, any classes of fracture are in contact between them and any fractures are in contact with blocks. So the system of connections is not hierarchical. Various elements of the same class are non similar between them. So the medium is multiscale but its geometry is not self-similar.

The advantage of a self-similar medium is the possibility to analyze its behavior for any number of scales, even for the infinite number. This is why in the present thesis we will analyze preferably the structures similar to the left-hand picture in Fig. 5.

Memory accumulation in multiscale medium

Let us assume that we have the ε^2 medium at all scales. As mentioned previously, a single step of homogenization of two neighboring media leads to the appearance of memory in the exchange term. The macroscopic equation changes its type: instead of diffusion equation at the macroscale we obtain an integro-differential macroscale equation. The next step of homogenization will lead to the additional memory, and consecutively to the appearance of a new macroscale equation whose form and mathematical type are impossible to predict.

The homogenization over several scales will lead to the accumulation of the memory effects caused at each step of homogenization. The limit model corresponding to infinite number of scales represents a high scientific interest.

The multi-scale media were not sufficiently well studied in the literature. The tri-scale fractured-porous medium was developed first in [Amaziane, Goncharenko and Pankratov, 2005]. The medium consisted of large fracture net, the net of small fractures ad the small tight blocks. The authors analyzed the case when the fracture aperture at each scale is the same in local coordinates. In other words, if δ is the aperture of the large fractures, then the aperture of the small fractures is $\delta\varepsilon$. The model obtained proved the memory effects. Such a medium corresponds to the situation when each scale generates a boundary layer, so that the only the net formed by thin large fractures and neighboring boundary layers will be active. This net has the internal heterogeneity in the form of small fractures and tight blocks. The defect of this medium consists of that the major volume of the medium will remain non perturbed.

In the present the present thesis we consider another class of tri-scale fractured media, which ensure the inactivity of the central parts of small blocks only. We obtained model which is very different from that obtained in [Amaziane, Goncharenko and Pankratov, 2005].

A special arrangement of a quadruple fractured medium was studied in [Dreier, Ozkan and Kazemi, 2004]. They have proposed an analytical model for flow in a quadruple-porosity system that consisted of a triple-fractured network with a single matrix system. The fractures has been categorized, based on their size and their conductivity, to micro fractures (the most dense,lowest conductivity) macro fractures and mega fractures(largest size, highest conductivity). They have assumed that only the mega fractures transport the reservoir's fluid to the well. Flow in all three fractures is assumed transient whereas the matrix-fracture fluid exchange is taken into account as pseudosteady. Two different models has been studied, first when the micro fractures are interconnected with macro fractures and have no connections with mega fracture

system. Second when micro and macro fractures are connected to mega fractures but not directly connected to each other. This model is appropriate for the reservoirs that the two sets of fractures may co-exist but not interfere. A system of flow equation interconnected through the exchange term proportional to the pressure difference between the interconnected domains is solved by the aid of Laplace transform. The transfer functions for a bounded slab shaped reservoir are proposed.

The ε^2 multiscale media were analyzed in [Douglas *et al*, 1998] where the formal existence of the regular macroscopic behavior was proved. In fact Douglas et al. were the first who introduced a similar geometry for multiporosity or multiscale model. They have presented the triple porosity averaged model and proposed the $(N+1)$ homogenized model for a multiscale system. They have introduced a hierarchical process of homogenization starting from the smallest scale , upscaling to the last scale. In each step they have shown the well-posedness of each of the models. In the proposed averaged model the memory terms are not at all discussed. Neither of the micro-scale problems are solved.

In [Peszynska 2007] an attempt to develop the multiscale model was undertaken for the elliptic-parabolic problems of flow. This formal model was formulated through an operator which is determined implicitly through functional equations and practically cannot be calculated.

The problem of macroscopic behavior of the flow in a ε^2 multiscale medium remains open. The solution of this problem is the objective of chapters (1) and (2).

Models of flow in a single fracture crossing porous medium

The analysis of flow in fracture networks would be incomplete without studying flow in a single fracture. The main problem consists in obtaining an adequate momentum balance equation. As fracture aperture is very small, only the models averaged over the fracture aperture are of interest.

In the theory devoted to the macroscale description of flow in a fracture network traditionally the Darcy law is used as the momentum balance equation in any elements of the medium at the macroscale. This is however not too exact, because several phenomena cause deviations from Darcy's law. First of all, this is a nonzero Reynolds number for flow inside fracture, which determines the non-neglecting nonlinear inertia effects. Secondly, there is the external flux crossing the fracture boundary, which influences both the average mass balance and momentum balance. In third, the real fractures are wavy boundary, which influences flow regimes and their averaged model.

The characteristic of flow in a fracture (or even say horizontal well) is highly affected by the

presence of these phenomena. Several studies has been done focusing on either of the mentioned effects but a mixed model considering at the same time the effect of flow within wavy permeable walls is remained an open problem.

Plane-parallel flow within solid walls

The starting point to study flow in a fracture consists of analyzing the plane-parallel Stokes flow in a regular channel with impermeable walls. The flow equation averaged over the channel thickness represents the Poiseuille law: [Bennett and Myres, 1962], [Savage, 1963], [Pfitzner, 1976], [Iwai, 1976], [Landau and Lifshitz, 1986], [Sutera and Skalak, 1993], [Zimmerman and Bodvarsson1996].

Two-dimensional Navier-Stokes equations in a cylindrical slot was examined for the case of smooth walls in [Peube, 1963], where the solution has been presented in the form of a power series with respect to $1/r$. The important role of the macroscale inertia effects for flat disc shaped fractures was confirmed in papers by [Vatistas, Ghila, and Zitouni, 1995] and [Zitouni and Vatistas, 1997].

Flow within permeable smooth walls

In the case of a fracture/channel with permeable walls, the permanent inflow to the fracture from the ambient porous rocks produces progressive increase of the flow velocity (and the Reynolds number Re) along the fracture length. So Re can reach sufficiently high values at which the inertia effects should be conserved in the model. One has to operate with the complete Navier-Stocks equations. The importance of the effect of inflow across the channel walls was known in modeling the flow in horizontal wells, which represent the hole perforated in porous rocks.

Berman was the first who has studied the system of the Navier-Stokes equation for a rectangular long channel with porous walls. The solution was obtained through a perturbation series in terms of the wall Reynolds parameter as a perturbation parameter [Berman, 1953]. He proposed a similarity solution, in terms of stream functions, under which the Navier-Stokes equations are reduced to a nonlinear fourth order ordinary differential equation with two boundary conditions at each wall. This equation, called the Berman's problem is perturbed by the small parameter. Several authors have studied Berman's equation. In particular,[Sellars, 1955] , [Yuan, 1956], [White, Barfield and Goglia, 1958], [Proudman, 1960] , [Terrill, 1964], [Robinson, 1987], [Zaturska, Drazin and Banks, 1988].

If the wall Reynolds number is small enough, there is only one solution. Increasing wall Reynolds, several bifurcations appear giving rise to new branches of solutions. In this case the small pertur-

bation parameter is the inverse of Reynolds.

Several papers were devoted to model the flow in a pipe with permeable walls [Berman, 1958], [Ihara, Kikuyama and Mizugushi, 1994], [Ouyang, 1998], [Ouyang, Arbabi and Aziz, 1998] with a view to the applications to horizontal wells.

Both analytical and experimental approaches were applied. The averaged flow model represents the algebraic relation between the overall pressure drop and the flow velocity. The mechanistic models proposed are mostly connected to the experimental data through the required empirical coefficients. Yuan [Yuan and Finkelstein, 1956] was the first to investigate the effect of the uniform injection and suction through the wall experimentally. The flow is two-dimensional, steady-state and laminar. One single perforation was assumed to exist. Ouyang's model represents the momentum balance equation [Ouyang, 1998], [Ouyang, Arbabi and Aziz, 1998] which contains a modified friction factor for the perforated pipe. It was shown that the impact of wall inflow or outflow depends on the flow regime: it increases the wall friction for laminar flow, and decreases it for turbulent flow.

Flow within wavy solid walls

The influence of roughness/corrugation in a thin fracture was examined in [Adler and Thovert, 1999] based on the Stokes equations for plane-parallel flow.
In [Chen, 1966] and [Cronsnier, Chevalier and Buès, 2000] experimental data were obtained on pressure drop for divergent confined radial flows between two parallel disc shaped fracture with rough surfaces. It was shown experimentally and numerically that the quadratic deviation appears within the laminar flow regime. Another common approach to study rough fractures consists in detecting empirical corrections to the mean fracture aperture ([Iwai, 1976], [Renshaw, 1995]).

The effect of inertia upon the flow in a thin rough fracture was examined in [Skjetne, Hansen 1999] based on numerical analysis.

Several analytical models addressed channels with sinusoidal walls. The main difference can be said in the way of definition of sinusoidal geometry: either the amplitude of the oscillations is much more smaller than the aperture of the channel or not. A two-dimensional stokes flow through axially symmetric pipe and symmetrical channel bounded by the surfaces $z = b\,(1 + \varepsilon \cos x)$ has been studied in [Burns and Parkes, 1967], where ε is the wall perturbation parameter. The problem was solved by expanding the stream function in a Fourier series involving an infinite set of unknown coefficients. Burns and Parkes obtained a perturbation solution in which these Fourier

coefficients were calculated up to $O(\varepsilon^6)$.

The case of a curvilinear tube with a radius which varies sinusoidally in the axial direction, was studied in [Deiber and Schowalter, 1979] by the method of separated variables. The corresponding ordinary differential equations were solved by a finite difference method.

Stokes flow between two wavy planes [Malevich, Mityushev and Adler, 2006] has been studied by Adler et al. Former to this a complete system of Navier Stokes equations of flow in a disc shaped corrugated fracture with no slip boundary condition on the walls, has been studied by Panfilov et al [Panfilov and Bues, 2004]. The asymptotic technique developed in their paper will be used in the present thesis.

No model for flow within wavy permeable boundaries is proposed.

Our objective is to develop analytical models of flow at various Re in a wavy channel with inflow across the channel boundary. We will show that the model obtained is different from all other models already developed in literature.

Two phase flow in a wavy channel

Two phase flow in fractures and horizontal holes in the presence of inflow through the walls is practically not studied. Such a kind of flow is observed in any oil reservoir exploited by water or gas injection, but also is typical for drilling horizontal wells. Drilling is accompanied with the permanent circulation of water whose pressure can be higher or lower than the pressure of oil in geological formation. Respectively one distinguishes the classical drilling when water prevents oil gush, and underbalanced drilling which prevents the penetration of water in oil reservoir.

In reservoir engineering three categories of models are used to describe the two-phase flow in pipes: the empirical correlations, the homogenized models and the mechanistic models.

The empirical models are based on experimental data matched by some statistical correlations. There exist the models which are devoted to different flow patterns or which are pattern independent.

Homogenous models are based on the assumption that the two phase fluid can be represented by a homogeneous mixture which may be treated as a single phase fluid having some effective properties. They also largely use empirical data. Several versions are capable to take into account some sufficiently fine effects as the slip between the phases, which is done in Drift-flux models [Zuber and Findlay, 1969], [Hasan and Kabir, 1988], [Hasan and Kabir, 1992], [Hasan and Kabir, 1994], [Ouyang and Aziz, 2000].

Mechanistic models are the most accurate as they take into account many details concerning various flow patterns. However the transition from one pattern to another one remains an open problem.

The main defeat of all empirical and semi-empirical approaches consists of their high dependence on empirical data, which reduces the domain of their application. In addition, they ignore the true physics of processes happening at the interphases between phases.

Numerical models deal with the exact Navier-Stokes equations. The main problem of any numerical simulation consists of modeling the behavior of the interfaces which can change their form (bubbles, films, ...), can collides between them and create new interfaces which are singular mathematical phenomena. One of the effective numerical tools is the *Levelset method* ([Osher, Fedkiw and Ronald, 2002]). It is based on the assumption that the fluid is single-phase but with different properties in different zones separated by true interfaces. This enables to apply the direct numerical simulation (DNS) without using the special method of tracking the interfaces. To detect interfaces an indicator function is introduced which is controlled by the Eulerian evolution equation with the true velocity of fluid. The zero isoline of this function corresponds to the interface. The geometrical meaning of the indicator function is the distance between each point and the interface [Osher and Sethian, 1988], [Sethian 1999], [Osher, Fedkiw and Ronald, 2002]. The slip condition on the interface is taken into account as an additional force just acting on the interface added to the the momentum conservation equation. This idea was first introduced in [Unverdi and Tryggvason, 1992].

Another method is known as the Volume of Fluid Method (VOF). It uses the indicator function as the percentage of presence of a given fluid (fluid saturation). The interface corresponds to the the zero value of the saturation.

In the present thesis we will apply the Levelset method to solve the problem of two-phase flow in a fracture and a horizontal hole. We will combine this method with analytical solutions we obtained for single-phase flow.

Outline of this thesis

The objective of the thesis consists of developing the closed model of flow in fractured and porous media with finite and infinite number of scales. The main scientific interest is focused on the problem to what limit leads the process of memory accumulation in media generating the memory at each scale. We will show that the limit exists and leads to the appearance of nonlinearity. We

develop the analysis of the process of the memory accumulation for double-porosity and fractured media. We also analyze the flow through a single fracture with an open boundary, while taking into account the mass inflow from surrounding rocks.

In chapters (1) to (3) we study the macroscale models of flow in multiscale media. Chapters (1) is devoted to study problem of single phase flow in a multiscale self-similar heterogeneous medium which is ε^2 at each scale (which means that each scale generates long-term memory in the averaged equation). The accumulation of the memory is nontrivial process. For instance, the two-scale medium leads to the appearance of the integral operator. The transition to the third scale leads to the model with integral operator whose kernel, in turn, is the solution of another integral equation, and so on. The necessary conditions of self-similarity is introduced. The general effective model for the long-memory case is obtained. The effective kernel of the integral operator is determined through a system of recurrent problems formulated in terms of the integral equations. The numerical algorithm based on the Laplace transform is developed to solve this problem. For the infinite number of scales, we have shown that the limit kernel is determined as the solution of a nonlinear integro-differential equation. The explicit solution of this equation is obtained in terms of the Laplace transform. The convergence of the results is proved numerically.

Multiscale fractured media, is similar to double porosity media, but the thickness of fractures h is very thin, so the system contains an additional small parameter which influences the solution. In particular, if h is very small, the flow through fractures can become event more difficult than through the tight blocks. In chapter (2) we analyze the two-scale fractured medium. Its macroscopic model proves the nonlocal behavior, similar to double porosity media, but not in the case ε^2. To observe the nonlocality, it is necessary that the ratio between the block permeability and that of fracture be lower than ε^2. Such a block is so tight that it remains practically unperturbed, except the thin boundary layer which is in contact with fractures. The Green's function of such a flow through the boundary layer corresponds to a mono-dimensional flow in a domain without boundary, which has analytical representation in which the fractional powers of time appear (square-root of time). Consecutively, the kernel of integral operators arising in macroscopic equations, which is the homogenized Green's function, becomes the Abel kernel. This is qualitatively different from the case of double porosity media. As the Abel integral equations allows for the analytical solutions, the effective kernel, responsible for the memory, may be obtained in the analytical form.

In chapter (3) the three-scale fractured media are studied. It consists of two hierarchical

networks of fractures and tight blocks. The permeability of blocks is lower than that of small-scale fracture, which is, in turn, lower than that of large-scale fractures. It is shown that the nontrivial behavior which ensures the memory effects at each scale is possible if some constraints are imposed on the fracture apertures and permeability ratios. In particular, the permeability ratio between the blocks and small-scale fractures should be lower than ε^2, while the permeability ratio between two nets of fractures should be ε^2. Than at the first (small) scale the medium will behave as the fractured model with Abel kernels described above, while at the second scale the medium behaves as a double porosity medium. The effective model averaged over all scales is the integro-differential equation whose kernel is determined analytically. Some examples of application of this model are analyzed.

In chapters (4), (5), and (6) we studied the flow in a single fracture (chapter 4) and in a single horizontal cylindrical channel (chapters 5 and 6) with open boundaries. The Navier-Stokes equations were resolved analytically by applying the two-scale asymptotic method: the expansion of the solution was searched in the form of a double asymptotic series with respect to the small fracture aperture and the small period of wall corrugation. The model averaged over the crosse-section is obtained. It contains the significant correction to the Darcy law which is related with the inflow through the walls.

In chapter (6) we couple the level set method with the analytical model obtained to determine the two phase flow in the wellbore. The external velocity field necessary for evolution of level set function is calculated by the analytical model of chapter(5). After each evolution the new arrangement of fluids in spatial domain is used to determine the Reynolds and viscosity distribution.

Chapter 1

The model of flow in multi-scale highly heterogeneous media

1.1 Self-similarity of flow in multi-scale media

1.1.1 Medium geometry

Let us introduce the set of domains $\widetilde{\Omega}^i$ in R^3 $(1 \leq i < n)$ which are overlapping between them. The medium $\widetilde{\Omega}^i$ represents the superposition of non-intersecting blocks $\widetilde{\Omega}^{i-1}$ and the fracture Ω^i. In turn, the medium $\widetilde{\Omega}^{i-1}$ is the superposition of blocks $\widetilde{\Omega}^{i-2}$ and fractures Ω^{i-1}, and so on. The medium $\widetilde{\Omega}^2$ is the superposition of blocks $\widetilde{\Omega}^1$ and fractures Ω^2. The blocks $\widetilde{\Omega}^1$ are homogeneous. The system of domains $\widetilde{\Omega}^i$ is geometrically self-similar, i.e. it represents the system of identical cubes $\widetilde{\Omega}^{i-1}$ inserted periodically inside the larger cubes, as shown in Fig. 1.1. In general case the cubes can not be necessarily true cubes, so we will call them "the blocks".

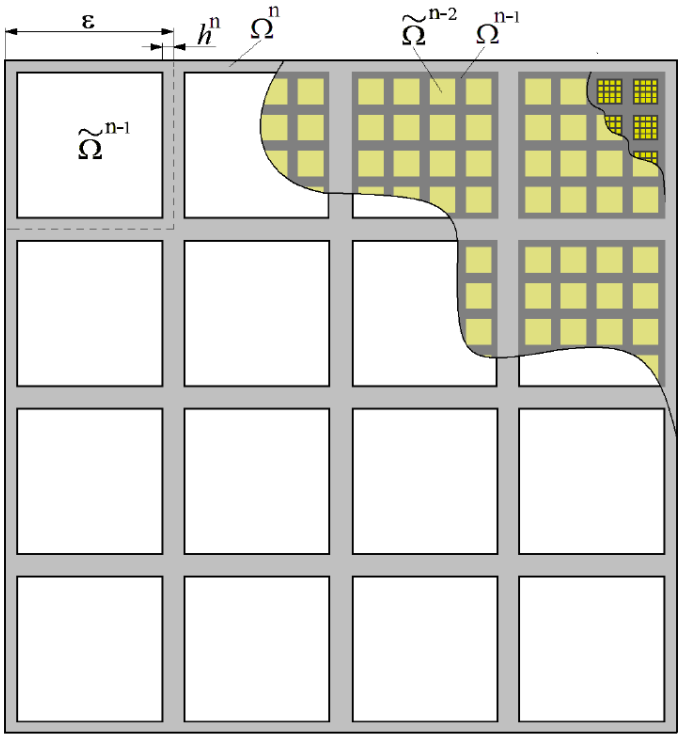

Figure 1.1: Heterogenous medium with n scales

The ratio between the linear sizes of the periods of media $\widetilde{\Omega}^{i-1}$ and $\widetilde{\Omega}^i$ is a constant small value ε.

To characterize the absolute sizes of each medium, we introduce the main coordinate system $x = x^{(n)}$ associated with the largest network of fractures, Ω^n. The notation $x^{(n)}$ means a vector in R^3: $x^{(n)} = \{x_1^{(n)}, x_2^{(n)}, x_3^{(n)}\}$.

In Fig. 1.1 it is seen that any fracture domain Ω^i $(i > 1)$ is self-connected within the corresponding period of the medium $\widetilde{\Omega}^i$. Moreover it is directly connected to the fractures of the smaller scale Ω^{i-1}, but has no direct connection with the blocks $\widetilde{\Omega}^{i-2}$. The system of connected fractures Ω^i for various i creates a connected hierarchical multi-scale network, which will be called the fracture network. Physically these fractures are highly permeable porous channels.

In this chapter the "fractures" are not thin.

Along with x we will introduce the local coordinates:

$$y^{n-1} = \frac{x}{\varepsilon}, \qquad y^{n-2} = \frac{x}{\varepsilon^2}, \quad \ldots \quad y^i = \frac{x}{\varepsilon^{n-i}} = \frac{y^{i+1}}{\varepsilon}, \quad \ldots \quad y^1 = \frac{x}{\varepsilon^{n-1}} \tag{1.1}$$

and the extended local cells which are the periods of heterogeneity at each scale extended in such a way that their volumes are equal to 1 in the corresponding coordinate system. Each cell $\widetilde{Y}^i$ consists of two non-intersecting subdomains called "fractures" Y^i and "blocks" $\widetilde{Y}^{i-1}$ which are the images of the subdomains Ω^i and $\widetilde{\Omega}^{i-1}$ respectively. In order to avoid new notations, we will denote the cell corresponding to medium $\widetilde{\Omega}^i$ as $Y^i \cup \widetilde{Y}^{i-1}$. So a cell is defined strictly as

$$Y^i \cup \widetilde{Y}^{i-1} = \left\{ -\frac{1}{2} < y^{(i-1)} < \frac{1}{2} \right\} \tag{1.2}$$

All media Ω^i correspond to the macroscale coordinate x, but it may be considered in various coordinate systems. In coordinates $y^{(n-1)}$ medium Ω^i extends by $1/\varepsilon$. In coordinates y^k medium Ω^i extends by $1/\varepsilon^{n-k}$. Medium Ω^i extended by $1/\varepsilon^{n-k}$ will be designated as $\Omega^i/\varepsilon^{n-k}$.

The link between the original medium $\widetilde{\Omega}^n$ and its cell (of the highest scale) is shown in Fig. 1.2.

The correspondence between the medium $\widetilde{Y}^{n-1}$ and its cell is presented in Fig. 1.3.

Then, for any medium $\widetilde{Y}^i = \widetilde{\Omega}^i \varepsilon^{n-i}$, the variable y^i is macroscopic ("slow"), while the variable y^{i-1} is microscopic ("fast").

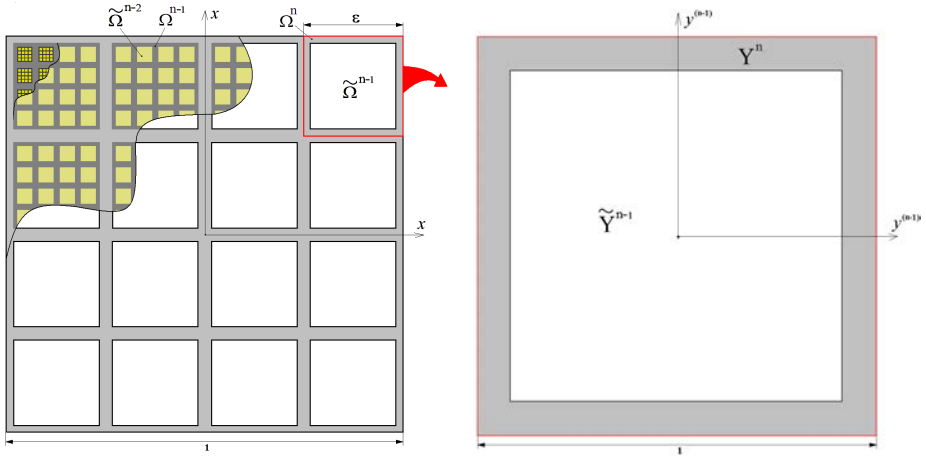

(a) (b)

Figure 1.2: The medium $\widetilde{\Omega}^n$ in coordinates x (a), and its extended cell $Y^n \cup \widetilde{Y}^{n-1}$ in coordinates y^{n-1} (b)

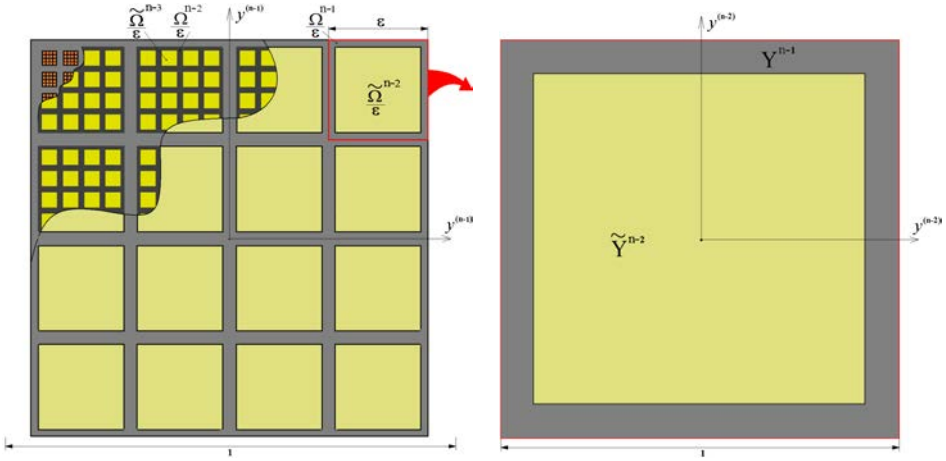

(a) (b)

Figure 1.3: Medium $\widetilde{Y}^{n-1} = \widetilde{\Omega}^{n-1}\varepsilon$ in coordinates y^{n-1} (a), and its extended cell $Y^{n-1} \cup \widetilde{Y}^{n-2}$ in coordinates y^{n-2} (b)

1.1.2 Flow equations

The porosity and permeability of medium Ω^i can be presented in the form:

$$\beta_i b^{(i)}(x), \qquad \alpha_i a^{(i)}(x)$$

where $a^{(i)}, b^{(i)} \sim 1$, while β_i and α_i are constant values.

For the macroscopic medium Ω^n we have:

$$\beta_n = \alpha_n = 1 \tag{1.3}$$

The flow equations formulated through the macroscopic coordinate x will be:

$$\begin{gathered}\beta_i b^{(i)} \frac{\partial p}{\partial t} = \alpha_i \nabla \cdot \left(a^{(i)} \nabla p \right), \qquad x \in \Omega^i \\ \alpha_i a^{(i)} \frac{\partial p}{\partial \nu}|_{\Gamma_-^{i+1,i}} = \alpha_{i+1} a^{(i+1)} \frac{\partial p}{\partial \nu}|_{\Gamma_+^{n+1,n}}\end{gathered} \tag{1.4}$$

where $i = 1, ..., n$, ∇ is the gradient in terms of variables x; $\Gamma^{i+1,i}$ is the interface between Ω^{i+1} and Ω^i; ν is the vector normal to $\Gamma^{i+1,i}$; $\Gamma_+^{i+1,i}$ means that side of the interface which touches the domain Ω^{i+1}.

The same model reformulated through local slow variables for each subdomain $\Omega^i/\varepsilon^{n-i}$ is:

$$\begin{gathered}b^{(i)} \frac{\partial p}{\partial t} = \sigma_i \nabla_i \cdot \left(a^{(i)} \nabla_i p \right), \qquad y^{(i)} \in \Omega^i/\varepsilon^{n-i}; \\ \omega_i a^{(i)} \frac{\partial p}{\partial \nu}|_{\Gamma_-^{i+1,i}} = a^{(i+1)} \frac{\partial p}{\partial \nu}|_{\Gamma_+^{i+1,i}}\end{gathered} \tag{1.5}$$

where

$$\sigma_i \equiv \frac{\alpha_i}{\beta_i \varepsilon^{2(n-i)}}, \qquad \omega_i = \frac{\alpha_i}{\alpha_{i+1}}$$

Operator ∇_i is the gradient in terms of variables $y^{(i)}$.

1.1.3 Definition of the flow self-similarity

The process described by the model (1.5) is self-similar at all scales if :

$$\sigma_i \equiv \frac{\alpha_i}{\beta_i \varepsilon^{2(n-i)}} = const, \qquad \omega_i = \frac{\alpha_i}{\alpha_{i+1}} = const$$

Then we obtain: for α_i:

$$\alpha_i = \alpha_{i+1}\omega, \qquad \alpha_n = 1$$

(according to (1.3)).

This is the geometrical progression, so that: $\alpha_i = \omega^{n-i}$.

For β_i, we obtain:

$$\beta_i = \frac{\alpha_i}{\sigma\varepsilon^{2(n-i)}} = \frac{\omega^{n-i}}{\sigma\varepsilon^{2(n-i)}}$$

Taking into account (1.3), we obtain for i=n: $\sigma = 1$. Then definitely:

$$\alpha_i = \omega^{n-i}, \qquad \beta_i = \left(\frac{\omega}{\varepsilon^2}\right)^{n-i} \tag{1.6}$$

1.1.4 General self-similar model

The model (1.5) formulated now in terms of the local slow coordinate $y^{(i)}$ becomes:

$$\begin{gathered} b^{(i)}\frac{\partial p}{\partial t} = \nabla_i \cdot \left(a^{(i)}\nabla_i p\right), \qquad y^{(i)} \in \Omega^i/\varepsilon^{n-i} \\ \omega a^{(i)}\frac{\partial p}{\partial \nu}|_{\Gamma_-^{i+1,i}} = a^{(i+1)}\frac{\partial p}{\partial \nu}|_{\Gamma_+^{i+1,i}} \end{gathered} \tag{1.7}$$

Two parameters ε^2 and ω determine all the process. For various ratios between them we will obtain qualitatively different models.

For two scales i and $i+1$, we can associate a couple of equations for the corresponding neighboring media $\Omega^i/\varepsilon^{n-i-1}$ and $\Omega^{i+1}/\varepsilon^{n-i-1}$, formulated through the slow variable $y^{(i+1)}$:

$$b^{(i)}\frac{\partial p}{\partial t} = \varepsilon^2\nabla_{i+1}\cdot\left(a^{(i)}\nabla_{i+1}p\right), \qquad y^{(i+1)} \in \Omega^i/\varepsilon^{n-i-1} \tag{1.8a}$$

$$b^{(i+1)}\frac{\partial p}{\partial t} = \nabla_{i+1}\cdot\left(a^{(i+1)}\nabla_{i+1}p\right), \qquad y^{(i+1)} \in \Omega^{i+1}/\varepsilon^{n-i-1} \tag{1.8b}$$

$$\omega a^{(i)}\frac{\partial p}{\partial \nu}|_{\Gamma_-^{i+1,i}} = a^{(i+1)}\frac{\partial p}{\partial \nu}|_{\Gamma_+^{i+1,i}} \tag{1.8c}$$

1.1.5 Multiscale long-memory medium

Let $\omega = \varepsilon^2$.

Then at each scale we will obtain the classical ε^2-medium, of the double-porosity medium.

The behavior of this system is so that the contribution to the macroscale permeability will be significant only for the largest scale Ω^i , as all the other scales have permeability much smaller

$(\varepsilon^2, \varepsilon^4, ...)$. Indeed the condition at the interface means that the normal flow through the interface from larger medium Ω^i to smaller medium Ω^{i-1} will be practically impossible (of order ε^2). So the medium Ω^{i-1} will be excluded from the translational flow happening in the larger medium Ω^i. In other words all the media will be excluded except the largest one Ω^n.

At the same time, the contribution of each medium in the global exchange process will be significant. Despite the small size of each medium with respect to the previous one, the characteristic time of fluid evacuation (in the form of the Source-flow) to the neighboring medium is high and the same on all scales: ε^{-2}.

Due to this, it is expected that the effective permeability will be determined entirely by the last level, while the effective exchange process will be equivalently influenced by all media.

1.1.6 Multi-scale source-translation medium

Let $\omega = \varepsilon^{1-\alpha}, 0 < \alpha < 1$ $(i.e \quad \varepsilon < \omega < 1)$, then for a fixed step of the homogenization process from scale i to $i+1$ we will have a couple of diffusion equations for two corresponding media formulated both in terms of the same larger space variable $x^{(i+1)}$, obtained from (1.8):

$$\begin{cases} b^{(i)}\dfrac{\partial p}{\partial t} = \varepsilon^2 \nabla_{i+1}\cdot\left(a^{(i)}\nabla_{i+1}p\right), & y^{(i+1)} \in \Omega^i/\varepsilon^{n-i-1} \\ b^{(i+1)}\dfrac{\partial p}{\partial t} = \nabla_{i+1}\cdot\left(a^{(i+1)}\nabla_{i+1}p\right), & y^{(i+1)} \in \Omega^{i+1}/\varepsilon^{n-i-1} \\ \varepsilon^{1-\alpha}a^{(i)}\dfrac{\partial p}{\partial \nu}|_{\Gamma_-^{i+1,i}} = a^{(i+1)}\dfrac{\partial p}{\partial \nu}|_{\Gamma_+^{i+1,i}} \end{cases} \tag{1.9}$$

This is the model which possesses also a long-memory at each scale of homogenization due to the exchange process, and whose effective permeability will be influenced by all the media. So we will have a superposition of the source flows and the translational flows on each scale.

1.1.7 Impossibility to exist for self-similar short-memory media

A typical short-memory medium might be presented by the following hypothetical model:

$$\begin{cases} b^{(i)}\dfrac{\partial p}{\partial t} = \varepsilon \nabla_{i+1}\cdot\left(a^{(i)}\nabla_{i+1}p\right), & y^{(i+1)} \in \Omega^i/\varepsilon^{n-i-1} \\ b^{(i+1)}\dfrac{\partial p}{\partial t} = \nabla_{i+1}\cdot\left(a^{(i+1)}\nabla_{i+1}p\right), & y^{(i+1)} \in \Omega^{i+1}/\varepsilon^{n-i-1} \\ \omega a^{(i)}\dfrac{\partial p}{\partial \nu}|_{\Gamma_-^{i+1,i}} = a^{(i+1)}\dfrac{\partial p}{\partial \nu}|_{\Gamma_+^{i+1,i}} \end{cases} \tag{1.10}$$

It is clear that this situation is impossible within the framework of the general self-similar model (1.6).

1.2 Transition between scales 1 and 2

We will analyze the case when $\omega = \varepsilon^2$.

1.2.1 Problem at the first level

The homogenization of a multilevel source medium will represent an iterative infinite process of scaling up from low-scale medium Ω^{i-1} to large-scale medium Ω^i.

At the first step we homogenize the system over the smallest cell $Y^2 \cup Y^1$.

The slow variable is $y^{(2)}$, while $y^{(1)} = y^{(2)}/\varepsilon$ is the fast variable. Extended medium $\widetilde{\Omega}^2$ and its extended cell are shown in Fig. 1.4:

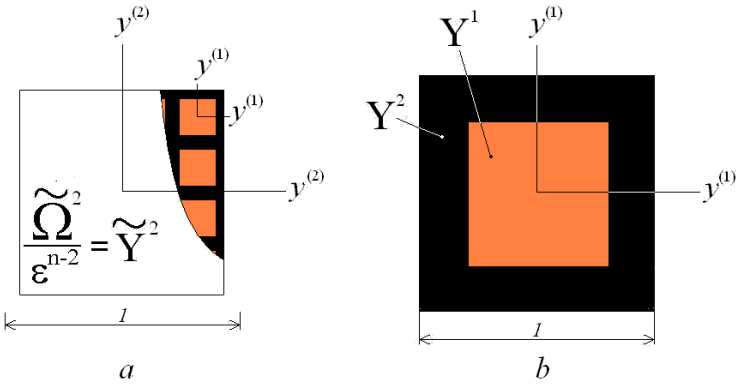

Figure 1.4: Medium $\widetilde{Y}^2 = \widetilde{\Omega}^2/\varepsilon^{n-2}$ (a) and its cell $Y^1 \cup Y^2$ (b)

The original problem formulated through the slow variable is:

$$b^{(1)}\frac{\partial p}{\partial t} = \varepsilon^2 \nabla_2 \cdot \left(a^{(1)} \nabla_2 p\right), \qquad y^{(2)} \in \Omega^1/\varepsilon^{n-2}$$

$$b^{(2)}\frac{\partial p}{\partial t} = \nabla_2 \cdot \left(a^{(2)} \nabla_2 p\right), \qquad y^{(2)} \in \Omega^2/\varepsilon^{n-2} \tag{1.11}$$

$$\varepsilon^2 a^{(1)} \nabla_2 p \cdot \vec{n}\Big|_{\Gamma^{2,1}_-} = a^{(2)} \nabla_2 p \cdot \vec{n}\Big|_{\Gamma^{2,1}_+}$$

1.2.2 Homogenized equations of the first level

The homogenization of this system leads to a well-known double-porosity model [De Swaan, 1976], [Arbogast, Douglas and Hornung, 1990], [Panfilov, 1990] with two pressures P^1 and P^2 averaged

respectively over Y^1 and Y^2:

$$P^1 = P^2 - \int_0^t \frac{\partial P^2}{\partial \tau} K^{(1)}(t-\tau)\, d\tau,$$
$$B^{(2)} \frac{\partial P^2}{\partial t} = \nabla_2 \cdot \left(A^{(2)} \nabla_2 P^2 \right) - B^{(1)} \frac{\partial P^1}{\partial t} \qquad , \qquad y^{(2)} \in \widetilde{\Omega}^2/\varepsilon^{n-2} \tag{1.12}$$

with

$$B^{(2)} = \int_{Y^2} b^{(2)} dy^{(1)} = b^{(2)}(1-\theta), \quad B^{(1)} = \int_{Y^1} b^{(1)} dy^{(1)} = b^{(1)}\theta,$$
$$A^{(2)} = \text{is the effective permeability which is defined in section 1.2.4}$$

symbol θ is the ratio between the volume of medium Y^1 to the volume of the overall cell $Y^1 \cup Y^2$.

The kernel $K^{(1)}(t)$ is of order 1 and is determined in the next section.

System (1.12) can be reduced to one equation:

$$B^{(2)} \frac{\partial P^2}{\partial t} = \nabla_2 \cdot \left(A^{(2)} \nabla_2 P^2 \right) + B^{(1)} \int_0^t \frac{\partial P^2}{\partial \tau} K^{(1)\prime}(t-\tau) d\tau, \qquad y^{(2)} \in \widetilde{\Omega}^2/\varepsilon^{n-2} \tag{1.13}$$

where $K^{(1)\prime} \equiv \dfrac{dK^{(1)}}{dt}$, and we take into account that $K^{(1)}(0) = 1$ (see the next section).

1.2.3 Structure of kernel: $K^{(1)}$

The kernel $K^{(1)}(t)$ is determined through the cell problem formulated in Y^1 [Panfilov, 2000]:

$$K^{(1)}(t) = \frac{1}{\theta} \iint_{Y^{(1)}} G(y^{(1)}, \xi, t) d\xi dy^{(1)} \tag{1.14}$$

where G is the Green function of the operator $b^{(1)} \dfrac{\partial}{\partial t} - \nabla_1 (a^{(1)} \nabla_1)$ in $Y^{(1)}$ with satisfies the zero Dirichlet condition at $\Gamma^{2,1}$

It may be represented in the explicit form through the Fourier expansion of the Green function:

$$K^{(1)}(t) = \sum_{k=1}^{\infty} \frac{\langle R_k \rangle_{Y^1}^2}{\langle R_k^2 \rangle_{Y^1}} \exp\left(\frac{-\mu_k a^{(1)} t}{b^{(1)}} \right) \tag{1.15}$$

where we used the notation:

$$\langle \cdot \rangle_{Y^1} = \int_{Y^1} (\cdot) dy^{(1)}$$

Herein μ_k and $R_k\left(y^{(1)}\right)$, $k \geq 1$ are the series of eigenvalues and eigenfunctions of the Laplace operator ∇_1^2 in Y^1, so that:

$$\nabla_1^2 R_k = -\mu_k R_k, \quad y^{(1)} \in Y^1; \qquad R_k|_{\Gamma^{(2,1)}} = 0 \tag{1.16}$$

These relations have the simplest form if we approximate block Y^1 by a sphere of the equivalent volume $|Y^1| = \theta$. Then the radius of this sphere will be $\rho = \left(\frac{4\theta}{3\pi}\right)^{1/3}$. For sphere, it is easy to obtain:

$$R_k = \frac{\sin\left(r\sqrt{\mu_k}\right)}{r}, \qquad \mu_k = \left(\frac{\pi k}{\rho}\right)^2, \tag{1.17}$$

where $r = \sqrt{\left(y_1^{(1)}\right)^2 + \left(y_2^{(1)}\right)^2 + \left(y_3^{(1)}\right)^2}$ is the radial coordinate within Y^1.

Then

$$\begin{aligned}
\left\langle R_k \right\rangle_{Y^1} &= 4\pi \int_0^\rho r \sin\left(r\sqrt{\mu_k}\right) dr = \frac{4\rho^2}{k}(-1)^{k+1}, \\
\left\langle R_k^2 \right\rangle_{Y^1} &= 4\pi \int_0^\rho \sin^2\left(r\sqrt{\mu_k}\right) dr = 2\pi\rho \\
\frac{1}{\theta}\frac{\left\langle R_k \right\rangle_{Y^1}^2}{\left\langle R_k^2 \right\rangle_{Y^1}} &= \frac{6}{\pi^2 k^2}
\end{aligned} \tag{1.18}$$

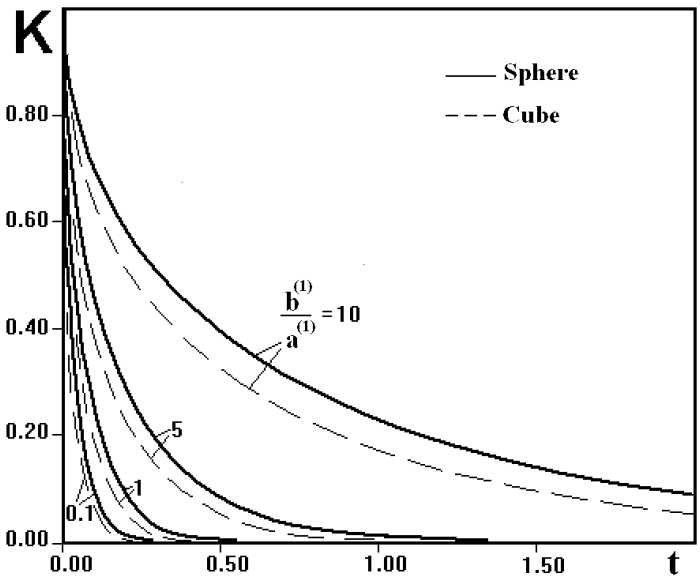

Figure 1.5: Structure of the exchange kernel $K^1(t)$ for spherical and cubic shape of the block Y^1

Therefore, we obtain for $K^{(1)}$:

$$K^{(1)}(t) = \frac{6}{\pi^2} \sum_{k=1}^{\infty} \frac{1}{k^2} \exp\left\{ -\frac{\pi^2 k^2 a^{(1)}}{\rho^2 \, b^{(1)}} \, t \right\} \tag{1.19}$$

The dependence of this function on the volume fraction of blocks θ is shown in Fig. 1.6. The property of this function is: $K^{(1)}(0)$=1.

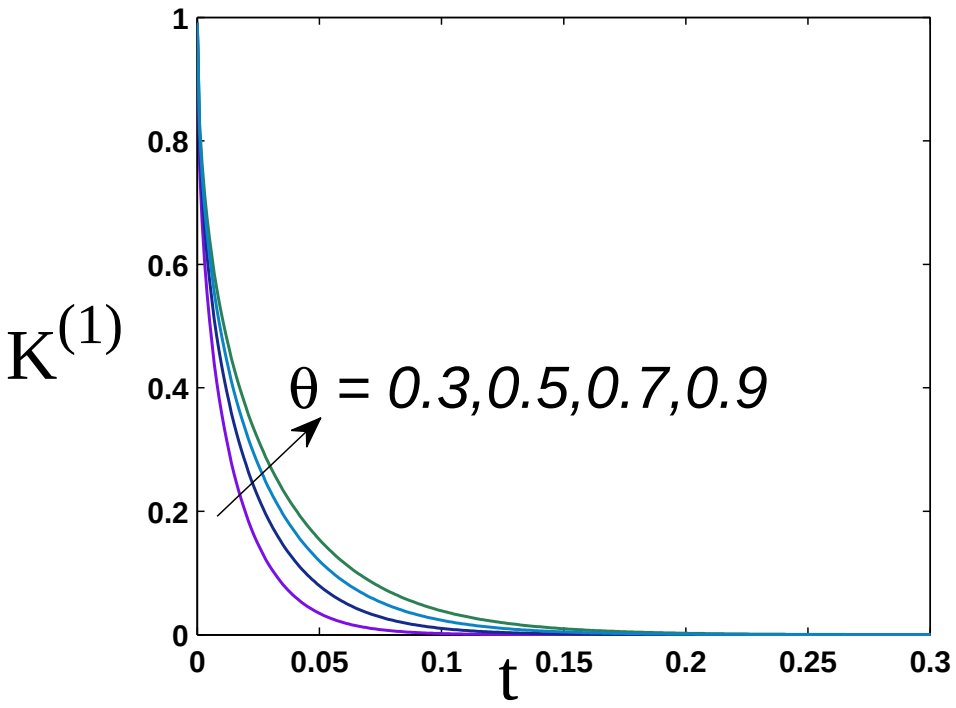

Figure 1.6: Exchange kernel $K^1(t)$ variation w.r.t the fractional volume of block Y^1

1.2.4 Effective permeability

The effective permeability is a tensor in general case, which is defined through three auxiliary functions $\psi_k^{(1)}$:

$$A_{ik}^{(2)} = \int_{Y^2} a^{(2)} \left(\delta_{ik} + \frac{\partial \psi_k^{(1)}}{\partial y_i^{(1)}} \right) dy^{(1)} \tag{1.20}$$

where the cell functions $\psi_k^{(1)}\left(y^{(1)}\right)$, $k=1,2,3$, are the solution of the cell problem:

$$\begin{cases} \nabla_1 \cdot \left(a^{(2)} \nabla_1 \psi_k^{(1)}\right) = -\nabla_1 a^{(2)} \cdot \vec{e}_k, & y^{(1)} \in Y^2 \\ \psi_k^{(1)} \text{ is } y^{(1)} - \text{periodic} \\ \left\langle \psi_k^{(1)} \right\rangle_{Y^2} = 0 \end{cases}$$

where $\vec{e}_k$ is the unit vector along the axis $y_k^{(1)}$.

We consider the symmetrical case, so that all functions $\psi_k^{(1)}$ will be symmetrical. In this case the tensor A becomes a scalar, and it is sufficient to resolve a single cell problem for a fixed k for determine the scalar A:

$$A^{(2)} = \int\limits_{Y^2} a^{(2)} \left(1 + \frac{\partial \psi_1^{(1)}}{\partial y_1^{(1)}}\right) dy^{(1)} \tag{1.21}$$

$$\begin{cases} \nabla_1 \cdot \left(a^{(2)} \nabla_1 \psi_1^{(1)}\right) = -\nabla_1 a^{(2)} \cdot \vec{e}_1, & y^{(1)} \in Y^2 \\ \psi_1^{(1)} \text{ is } y^{(1)} - \text{periodic} \\ \left\langle \psi_1^{(1)} \right\rangle_{Y^2} = 0 \end{cases} \tag{1.22}$$

1.3 Transition between scales 2 and 3

1.3.1 Problem formulation

At the second step we will consider the domain which consists of the connected fracture Ω^3 and an already homogenized "block" $\widetilde{\Omega}^2$. Variable $y^{(3)}$ is the slow coordinates, while $y^{(2)}$ is the fast one. The extended medium Ω^3 in coordinates $y^{(n-3)}$ and its unit cell in coordinates $y^{(2)}$ is shown in Fig. 1.7.

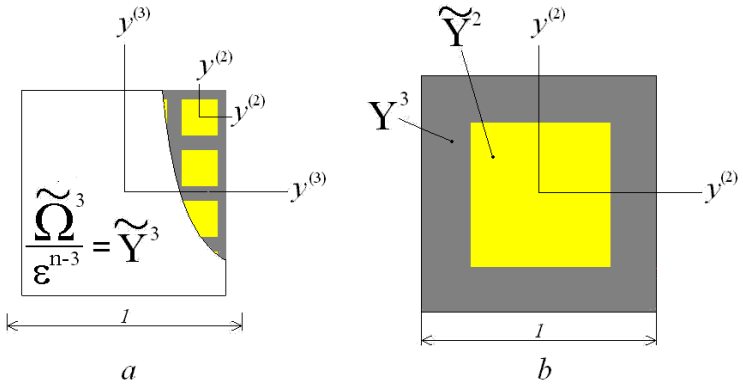

Figure 1.7: Medium $Y^3 = \widetilde{\Omega}^3/\varepsilon^{n-3}$ (a) and its unit cell $\widetilde{Y}^2 \cup Y^3$ (b)

In slow coordinates the problem of flow in $\Omega^3/\varepsilon^{n-3}$ and $\widetilde{\Omega}^2/\varepsilon^{n-3}$ has the form of (1.23a) and (1.23b):

$$B^{(2)}\frac{\partial P^2}{\partial t} = \varepsilon^2\nabla_3\cdot\left(A^{(2)}\nabla_3 P^2\right) + B^{(1)}\int\limits_0^t \frac{\partial P^2}{\partial \tau}K^{(1)\prime}(t-\tau)d\tau, \quad y^{(3)} \in \widetilde{\Omega}^2/\varepsilon^{n-3} \tag{1.23a}$$

$$b^{(3)}\frac{\partial p}{\partial t} = \nabla_3\cdot\left(a^{(3)}\nabla_3 p\right), \qquad y^{(3)} \in \Omega^3/\varepsilon^{n-3} \tag{1.23b}$$

$$\varepsilon^2 A^{(2)}\nabla_3 P^2\cdot\vec{n}\Big|_{\Gamma_-^{3,2}} = a^{(3)}\nabla p\cdot\vec{n}\Big|_{\Gamma_+^{3,2}}, \qquad P^2|_{\Gamma_-^{3,2}} = p|_{\Gamma_+^{3,2}} \tag{1.23c}$$

1.3.2 Two-scale formulation

According to the technique of homogenization we introduce the two-scale functions $P^2\left(y^{(3)}, y^{(2)}, t\right)$ and $p\left(y^{(3)}, y^{(2)}, t\right)$ which are equal to the true functions $P^2\left(y^{(3)}, t\right)$ and $p\left(y^{(3)}, t\right)$ when $y^{(2)} = y^{(3)}/\varepsilon$. Respectively we introduce the two-scale operator $\tilde{\nabla}_3 = \nabla_3 + \varepsilon^{-1}\nabla_2$. Further the symbol

"tilde" will be omitted. The equations (1.23) become:

$$B^{(2)}\frac{\partial P^2}{\partial t} = \nabla_2\cdot\left(A^{(2)}\nabla_2 P^2\right) + \varepsilon\left[\nabla_2\cdot\left(A^{(2)}\nabla_3 P^2\right) + \nabla_3\cdot\left(A^{(2)}\nabla_2 P^2\right)\right] +$$
$$+\varepsilon^2\nabla_3\cdot\left(A^{(2)}\nabla_3 P^2\right) + B^{(1)}\int\limits_0^t \frac{\partial P^2}{\partial\tau}K^{(1)\prime}(t-\tau)d\tau, \qquad y^{(3)}\in\widetilde{\Omega}^3/\varepsilon^{n-3}, \quad y^{(2)}\in\widetilde{Y}^2 \tag{1.24a}$$

$$b^{(3)}\frac{\partial p}{\partial t} = \frac{1}{\varepsilon^2}\nabla_2\cdot\left(a^{(3)}\nabla_2 p\right) + \frac{1}{\varepsilon}\left[\nabla_2\cdot\left(a^{(3)}\nabla_3 p\right) + \nabla_3\cdot\left(a^{(3)}\nabla_2 p\right)\right] +$$
$$+\nabla_3\cdot\left(a^{(3)}\nabla_3 p\right), \qquad y^{(3)}\in\widetilde{\Omega}^3/\varepsilon^{n-3}, \quad y^{(2)}\in Y^3 \tag{1.24b}$$

$$\varepsilon^2 A^{(2)}\left(\nabla_2 P^2 + \varepsilon\nabla_3 P^2\right).\vec{n}\Big|_{\Gamma^{3,2}_-} = a^{(3)}\left(\nabla_2 p + \varepsilon\nabla_3 p\right).\vec{n}\Big|_{\Gamma^{3,2}_+}, \qquad P^2|_{\Gamma^{3,2}_-} = p|_{\Gamma^{3,2}_+} \tag{1.24c}$$

The additional condition is the periodicity with respect to the fast variable $y^{(2)}$.

1.3.3 Necessary condition of existence for periodic solution

Along with system (1.24) it is useful to introduce an integral relation which will enable us to derive the form of the averaged equations.

Let us integrate the first equation (1.24a) over $\widetilde{Y}^2$, the second equation (1.24b) over Y^3, and sum up the results:

$$\left\langle B^{(2)}\frac{\partial P^2}{\partial t}\right\rangle_{\widetilde{Y}^2} + \left\langle b^{(3)}\frac{\partial p}{\partial t}\right\rangle_{Y^3} - B^{(1)}\int\limits_0^t\left\langle\frac{\partial P^2}{\partial\tau}\right\rangle_{\widetilde{Y}^2}K^{(1)\prime}(t-\tau)d\tau =$$
$$= \int\limits_{\Gamma^{3,2}} A^{(2)}\left(\nabla_2 P^2 + \varepsilon\nabla_3 P^2\right).\vec{n}dy^{(2)} + \varepsilon\nabla_3\cdot\left\langle A^{(2)}\left(\nabla_2 P^2 + \varepsilon\nabla_3 P^2\right)\right\rangle_{\widetilde{Y}^2}$$
$$-\frac{1}{\varepsilon^2}\int\limits_{\Gamma^{3,2}} a^{(3)}\left(\nabla_2 p + \varepsilon\nabla_3 p\right).\vec{n}dy^{(2)} + \frac{1}{\varepsilon}\nabla_3\cdot\left\langle a^{(3)}\left(\nabla_2 p + \varepsilon\nabla_3 p\right)\right\rangle_{Y^3}$$

Herein the Gauss theorem was used, as well as the property of a periodic function f with respect to $y^{(2)}$:

$$\int\limits_{\partial_{\text{ext}}Y^3} a\nabla_2 f\cdot\vec{n}\,dy^{(2)} \equiv 0$$

where $\partial_{\text{ext}}Y^3$ means the external boundary of the domain Y^3, and a is a periodic function.

Taking into account the condition (1.24c), we obtain:

$$B^{(2)}\frac{\partial}{\partial t}\left\langle P^2\right\rangle_{\widetilde{Y}^2}+\left\langle b^{(3)}\frac{\partial p}{\partial t}\right\rangle_{Y^3}-B^{(1)}\int\limits_0^t\left\langle\frac{\partial P^2}{\partial\tau}\right\rangle_{\widetilde{Y}^2}K^{(1)'}(t-\tau)d\tau=$$

$$=\varepsilon\nabla_3\cdot\left\langle A^{(2)}\left(\nabla_2P^2+\varepsilon\nabla_3P^2\right)\right\rangle_{\widetilde{Y}^2}+\frac{1}{\varepsilon}\nabla_3\cdot\left\langle a^{(3)}\left(\nabla_2p+\varepsilon\nabla_3p\right)\right\rangle_{Y^3}\qquad(1.25)$$

where we used the notation:

$$\left\langle\cdot\right\rangle_{Y^i}\equiv\int\limits_{Y^i}(\cdot)dy^{(i-1)},\qquad\left\langle\cdot\right\rangle_{\widetilde{Y}^{i-1}}\equiv\int\limits_{\widetilde{Y}^{i-1}}(\cdot)dy^{(i-1)}\qquad(1.26)$$

Physically this relation represents the averaged equation of flow. Mathematically it is the necessary condition of periodicity of the solution. Indeed, we can represent equation (1.24b) in the explicit form with respect to the leading microscale derivatives:

$$\nabla_2\cdot\left(a\nabla_2p\right)=f\left(y^{(2)}\right)\qquad(1.27)$$

where $a=A^{(2)}$ when $y^{(2)}\in\widetilde{Y}^2$; $a=a^{(3)}$ when $y^{(2)}\in Y^3$; and

$$f\left(y^{(2)}\right)\equiv\begin{cases}\varepsilon^2b^{(3)}\dfrac{\partial p}{\partial t}-\varepsilon\left[\nabla_2\cdot\left(a^{(3)}\nabla_3p\right)+\nabla_3\cdot\left(a^{(3)}\nabla_2p\right)\right]-\varepsilon^2\nabla_3\cdot\left(a^{(3)}\nabla_3p\right), & y^{(2)}\in Y^3\\[2ex] B^{(2)}\dfrac{\partial P^2}{\partial t}-\varepsilon\left[\nabla_2\cdot\left(A^{(2)}\nabla_3P^2\right)+\nabla_3\cdot\left(A^{(2)}\nabla_2P^2\right)\right]- & \\ \quad-\varepsilon^2\nabla_3\cdot\left(A^{(2)}\nabla_3P^2\right)-B^{(1)}\displaystyle\int\limits_0^t\frac{\partial P^2}{\partial\tau}K^{(1)'}(t-\tau)d\tau, & y^{(2)}\in\widetilde{Y}^2\end{cases}$$

The solution of this equation should be periodic in $\tilde{Y}^2\cup Y^3$.

According to the Fredholm theorem, the necessary and sufficient condition for the existence of a periodic solution of the equation (1.27) is:

$$\left\langle f\right\rangle_{\widetilde{Y}^2\cup Y^3}=0$$

which yields the relation (1.25).

1.3.4 Asymptotic expansion

We search for the solution of (1.24) in the form of the asymptotic expansion:

$$p\left(y^{(3)},y^{(2)},t;\varepsilon\right)=\sum_{k=0}^{\infty}\varepsilon^k p_k\left(y^{(3)},y^{(2)},t\right),\qquad P^2\left(y^{(3)},y^{(2)},t;\varepsilon\right)=\sum_{k=0}^{\infty}\varepsilon^k P_k^2\left(y^{(3)},y^{(2)},t\right) \tag{1.28}$$

By direct substitution of this expansion into equations (1.24) and (1.25), for three first terms of this expansion it is possible to obtain the closed system of problems:

For P_0^2: it depends on slow and fast variables: $P_0^2=P_0^2\left(y^{(3)},y^{(2)},t\right)$, and is defined as the solution of the problem in the block $\widetilde{Y}^2$:

$$\begin{cases} B^{(2)}\dfrac{\partial P_0^2}{\partial t}=\nabla_2\cdot\left(A^{(2)}\nabla_2 P_0^2\right)+B^{(1)}\displaystyle\int_0^t\frac{\partial P_0^2}{\partial\tau}K^{(1)'}(t-\tau)d\tau, & y^{(2)}\in\widetilde{Y}^2\\ P_0^2|_{\Gamma_-^{3,2}}=p_0|_{\Gamma_+^{3,2}},\\ P_0^2|_{t=0}=p^0 \end{cases} \tag{1.29}$$

For p_0: it depends only on the slow variable: $p_0=p_0\left(y^{(3)},t\right)$, and is defined by the averaged equation resulting from (1.25):

$$\left\langle b^{(3)}\right\rangle_{Y^3}\frac{\partial p_0}{\partial t}-\nabla_3\cdot\left(\left\langle a^{(3)}\right\rangle_{Y^3}\nabla_3 p_0+\left\langle a^{(3)}\nabla_2 p_1\right\rangle_{Y^3}\right)=$$
$$=-B^{(2)}\frac{\partial}{\partial t}\left\langle P_0^2\right\rangle_{\widetilde{Y}^2}+B^{(1)}\int_0^t\frac{\partial}{\partial\tau}\left\langle P_0^2\right\rangle_{\widetilde{Y}^2}K^{(1)'}(t-\tau)d\tau \tag{1.30}$$

For p_1: it depends on the slow and fast variables and is the solution of the problem:

$$\begin{cases} \nabla_2\cdot\left(a^{(3)}\nabla_2 p_1\right)+\nabla_2\cdot\left(a^{(3)}\nabla_3 p_0\right)=0, & y^{(2)}\in Y^3\\ p_1\ \text{ is } y^{(2)}-\text{periodic}\\ \langle p_1\rangle_{Y^3}=0 \end{cases} \tag{1.31}$$

The last condition is needed in order to define the unique solution of this problem. Without this condition we would obtain the problem with infinite number of solutions defined up to an additive constant (similar to the Neumann problem).

Due to this condition, we can obtain the following result for p_0, returning back to the asymptotic expansion (1.28):

$$\langle p\rangle_{Y^3}\equiv P^3=p_0+O\left(\varepsilon^2\right) \tag{1.32}$$

which determines the physical meaning of the function p_0: it is the pressure averaged over Y^3.

The next step consist of solving problems (1.29) and (1.31), which will yield the closed averaged equation (1.30).

1.3.5 Solution of the problem in Y^3

Problem (1.31) is classical and can be solved explicitly through the Fourier series. Indeed, by representing the differential equation in the form:

$$\nabla_2 \cdot \left(a^{(3)} \nabla_2 p_1 \right) = - \underbrace{\nabla_3 p_0}_{\substack{\text{depends on} \\ y^{(3)},t}} \cdot \underbrace{\nabla_2 \left(a^{(3)} \right)}_{\substack{\text{depends on} \\ y^{(2)}}}$$

we can search it in the form of the Fourier series: $p_1 \left(y^{(3)}, y^{(2)}, t \right) = \sum\limits_{k \geq 1} \psi_k \left(y^{(2)} \right) f_k \left(y^{(3)}, t \right)$ with splitting slow and fast variables. Substituting in (1.31) one can show that it is finite, so that:

$$p_1 \left(y^{(3)}, y^{(2)}, t \right) = \sum_{k=1}^{3} \psi_k \left(y^{(2)} \right) \frac{\partial p_0}{\partial y_k^{(3)}} + p_{10} \left(y^{(3)}, t \right) \tag{1.33}$$

where the functions $\psi_k \left(y^{(2)} \right)$, $k = 1, 2, 3$, are the solution of the cell problem:

$$\begin{cases} \nabla_2 \cdot \left(a^{(3)} \nabla_2 \psi_k \right) = -\nabla_2 a^{(3)} \cdot \vec{e}_k, \qquad y^{(2)} \in Y^3 \\ \psi_k \ \text{ is } y^{(2)} - \text{periodic} \\ \langle \psi_k \rangle_{Y^3} = 0 \end{cases} \tag{1.34}$$

where $\vec{e}_k$ is the unit vector along the axis $y_k^{(2)}$.

We consider the symmetrical case, so that all functions ψ_k will be identical. It is then sufficient to resolve a single cell problem for a fixed k.

1.3.6 Solution of the problem in $\widetilde{Y}^2$

Consider the problem (1.29). Let us introduce the new variable: $U \equiv P_0^2 - p_0$. Taking into account the fact that p_0 does not depend on the fast variables, the problem (1.29) becomes:

$$\begin{cases} \mathcal{L}U \equiv \dfrac{\partial U}{\partial t} - \dfrac{A^{(2)}}{B^{(2)}}\nabla_2^2 U - \dfrac{B^{(1)}}{B^{(2)}}\displaystyle\int_0^t \frac{\partial U}{\partial \tau}K^{(1)'}(t-\tau)d\tau = \\ \qquad\qquad -\dfrac{\partial p_0}{\partial t} + \dfrac{B^{(1)}}{B^{(2)}}\displaystyle\int_0^t \frac{\partial p_0}{\partial \tau}K^{(1)'}(t-\tau)d\tau, \qquad y^{(2)} \in \widetilde{Y}^2 \\ U|_{\Gamma_-^{3,2}} = 0, \\ U|_{t=0} = 0 \end{cases} \tag{1.35}$$

where we taken into account that $p_0|_{t=0} = p^0$.

We obtain the problem with homogeneous conditions for non-homogeneous linear integro-differential equation. Its solution is the convolution of the Green function of the operator $\mathcal{L}$ with the right-hand side of equation (1.35):

$$U = -\int\limits_{\widetilde{Y}^{(2)}}\int_0^t G\left(y^{(2)},\xi,t-\tau\right)\left[\frac{\partial p_0}{\partial \tau} - \frac{B^{(1)}}{B^{(2)}}\int_0^\tau \frac{\partial p_0}{\partial \theta}K^{(1)'}(\tau-\theta)\,d\theta\right]d\xi d\tau$$

Then the pressure in block $\widetilde{Y}^{(2)}$ is:

$$P_0^{(2)} = p_0 - \int\limits_{\widetilde{Y}^{(2)}}\int_0^t G\left(y^{(2)},\xi,t-\tau\right)\left[\frac{\partial p_0}{\partial \tau} - \frac{B^{(1)}}{B^{(2)}}\int_0^\tau \frac{\partial p_0}{\partial \theta}K^{(1)'}(\tau-\theta)\,d\theta\right]d\xi d\tau \tag{1.36}$$

where the Green function $G\left(y^{(2)},\xi,t-\tau\right)$ is determined as the solution of equation (1.37) with homogeneous boundary conditions at $\Gamma^{(3,2)}$ and the initial condition:

$$\frac{\partial G}{\partial t} - \frac{A^{(2)}}{B^{(2)}}\nabla_2^2 G - \frac{B^{(1)}}{B^{(2)}}\int_0^t \frac{\partial G}{\partial \tau}K^{(1)'}(t-\tau)\,d\tau = \delta\left(y^{(2)}-\xi\right)\delta(t-\tau), \tag{1.37a}$$

$$G\left(y^{(2)},\xi,t\right)\Big|_{t=0} = \delta\left(y^{(2)}-\xi\right), \tag{1.37b}$$

$$G\left(y^{(2)},\xi,t\right)\Big|_{y^{(2)},\xi\in\Gamma^{3,2}} = 0 \tag{1.37c}$$

Now we get down to the construction of the Green function.

1.3.7 Spectral expansion of the Green's function G

The Green function may be presented through the Fourier series with respect to a complete orthogonal system of functions. Such a system may be presented by the eigenfunctions of the Laplace operator ∇_2^2 which is the spatial part of the operator $\mathcal{L}$.

Let us introduce the Hilbert space of functions $\mathcal{H}$ which have the following properties:

- they are determined in the domain $\widetilde{Y}^{(2)} \times (0 < t < \mathcal{T})$;

- they satisfy the homogeneous Dirichlet boundary condition at $\Gamma^{3,2}$;

- the norm in $\mathcal{H}$ is determined through the scalar product:

$$||f|| = \left(\int\limits_{\widetilde{Y}^{(2)}} f^2 dx \right)^{1/2} = \sqrt{\left\langle f^2 \right\rangle_{\widetilde{Y}^{(2)}}} \tag{1.38}$$

Then the Green's function (1.37) may be presented in the form of the following Fourier series over the orthonormal functions: :

$$G\left(y^{(2)}, \xi, t\right) = \sum_{k=1}^{\infty} \frac{1}{||R_k||^2} T_k(t) R_k(y^{(2)}) R_k(\xi) \tag{1.39}$$

where μ_k and $R_k\left(y^{(2)}\right)$, $k \geq 1$ are the series of eigenvalues and eigenfunctions of the Laplace operator ∇_2^2 in $\mathcal{H}$, so that:

$$\nabla_2^2 R_k = -\mu_k R_k, \quad y^{(2)} \in \widetilde{Y}^{(2)}; \qquad R_k|_{\Gamma^{(3,2)}} = 0 \tag{1.40}$$

while $T_k(t)$ are determined as the solutions of the problem:

$$T_k' - \frac{B^{(1)}}{B^{(2)}} \int\limits_0^t T_k'(\tau) K^{(1)'}(t-\tau)\, d\tau = -\mu_k \frac{A^{(2)}}{B^{(2)}} T_k, \qquad (0 < t < \mathcal{T}), \tag{1.41a}$$

$$T_k|_{t=0} = 1, \quad \forall k \tag{1.41b}$$

where $T_k'(t) \equiv dT_k/dt$.

Proof:

1. It is known that the system $\{R_k\}$ is complete and orthogonal in $\mathcal{H}$. The completeness and

orthonormality means that:

$$\sum_{k\geq 1}\frac{1}{||R_k||^2}R_k(y^{(2)})R_k(\xi)=\delta\left(y^{(2)}-\xi\right) \tag{1.42}$$

2. The form of the expansion (1.39) is determined by the symmetry of the Green function with respect to $y^{(2)}$ and ξ.

3. Substituting this series and (1.40) in (1.37) we obtain (1.41a) for functions $T_k(t)$.

4. Using the initial condition (1.37b) we obtain:

$$\sum_{k\geq 0}\frac{1}{||R_k||^2}T_k(0)R_k(y^{(2)})R_k(\xi)=\delta\left(y^{(2)}-\xi\right)$$

Using this relation and the property (1.42) we obtain the initial condition (1.41b) for functions T_k.

Now we should determine the structure of the functions $T_k(t)$.

1.3.8 Spectral representation of the solution in Y^3

Using all results we obtain for pressure P_0^2 from (1.36):

$$P_0^{(2)}=p_0-\int\limits_0^t\sum_{k\geq 1}\frac{R_k(y^{(2)})\left\langle R_k\right\rangle_{\widetilde{Y}^{(2)}}}{\left\langle R_k^2\right\rangle_{\widetilde{Y}^{(2)}}}T_k(t-\tau)\left[\frac{\partial p_0}{\partial\tau}-\frac{B^{(1)}}{B^{(2)}}\int\limits_0^\tau\frac{\partial p_0}{\partial\theta}K^{(1)\prime}(\tau-\theta)\,d\theta\right]d\tau \tag{1.43}$$

The eigenfunctions R_k and eigenvalues μ_k can be obtained in the explicit way for cubic form of the domain $\widetilde{Y}^2$ [Panfilov, 2000]. These relations have the simplest form if we approximate $\widetilde{Y}^2$ by a sphere of the same volume $|\widetilde{Y}^2|=\theta$. Then the radius of this sphere will be $\rho=\left(\frac{4\theta}{3\pi}\right)^{1/3}$. For sphere, it is easy to obtain:

$$R_k=\frac{\sin\left(r\sqrt{\mu_k}\right)}{r},\qquad \mu_k=\left(\frac{\pi k}{\rho}\right)^2, \tag{1.44}$$

where $r=\sqrt{\left(y_1^{(2)}\right)^2+\left(y_2^{(2)}\right)^2+\left(y_3^{(2)}\right)^2}$ is the radial coordinate within $\widetilde{Y}^2$.

Then

$$\left\langle R_k \right\rangle_{\widetilde{Y}^{(2)}} = 4\pi \int\limits_0^\rho r \sin\left(r\sqrt{\mu_k}\right) dr = \frac{4\rho^2}{k}(-1)^{k+1},$$
$$\left\langle R_k^2 \right\rangle_{\widetilde{Y}^{(2)}} = 4\pi \int\limits_0^\rho \sin^2\left(r\sqrt{\mu_k}\right) dr = 2\pi\rho$$

Then a useful result follows, which will be used further:

$$\frac{1}{\theta}\frac{\left\langle R_k \right\rangle^2_{\widetilde{Y}^{(2)}}}{\left\langle R_k^2 \right\rangle_{\widetilde{Y}^{(2)}}} = \frac{6}{\pi^2 k^2} \tag{1.45}$$

1.3.9 Averaged equations

Let us introduce the pressures, averaged over subdomains Y^3 and $\widetilde{Y}^2$ of a cell:

$$\tilde{P}^2 = \frac{1}{\theta}\left\langle P^2 \right\rangle_{\widetilde{Y}^2}, \qquad P^3 = \frac{1}{1-\theta}\left\langle p \right\rangle_{Y^3}$$

where θ is the volume fraction of blocks $\widetilde{Y}^2$ in a cell $\widetilde{Y}^2 \cup Y^3$.

It follows from the results of the previous section, that:

$$\tilde{P}^2 = \frac{1}{\theta}\left\langle P_0^2 \right\rangle_{\widetilde{Y}^2} + O(\varepsilon), \qquad P^3 = p_0 + O\left(\varepsilon^2\right)$$

Using (1.30) for p_0 and (1.43) for P_0^2 we obtain for the average values:

$$\begin{cases} B^{(3)}\dfrac{\partial P^3}{\partial t} - \nabla_3 \cdot \left(A^{(3)}\nabla_3 P^3\right) = -B^{(2)}\theta\dfrac{\partial \tilde{P}^2}{\partial t} + B^{(1)}\theta \displaystyle\int\limits_0^t \frac{\partial \tilde{P}^2}{\partial \tau} K^{(1)\prime}(t-\tau)\, d\tau \\ \\ \tilde{P}^2 = P^3 - \displaystyle\int\limits_0^t K^{(2)}(t-\tau)\left(\frac{\partial P^3}{\partial \tau} - \frac{B^{(1)}}{B^{(2)}}\int\limits_0^\tau \frac{\partial P^3}{\partial \theta} K^{(1)\prime}(\tau-\theta)\, d\theta\right) d\tau \end{cases} \tag{1.46}$$

where the second-order kernel is defined as:

$$K^{(2)}(t) \equiv \frac{1}{\theta}\sum_{k=1}^{\infty} \frac{\left\langle R_k \right\rangle^2_{\widetilde{Y}^{(2)}}}{\left\langle R_k^2 \right\rangle_{\widetilde{Y}^{(2)}}} T_k(t) \tag{1.47}$$

For spherical forme of the block $\widetilde{Y}^2$ we may use (1.45):

$$K^{(2)}(t) \equiv \frac{6}{\pi^2} \sum_{k=1}^{\infty} \frac{1}{k^2} T_k(t) \tag{1.48}$$

The property of the kernel is: $K^{(2)}(0) = 1$. The dependence of this kernel on θ and the ratio $b^{(2)}/a^{(2)}$ is shown in Fig. 1.8.

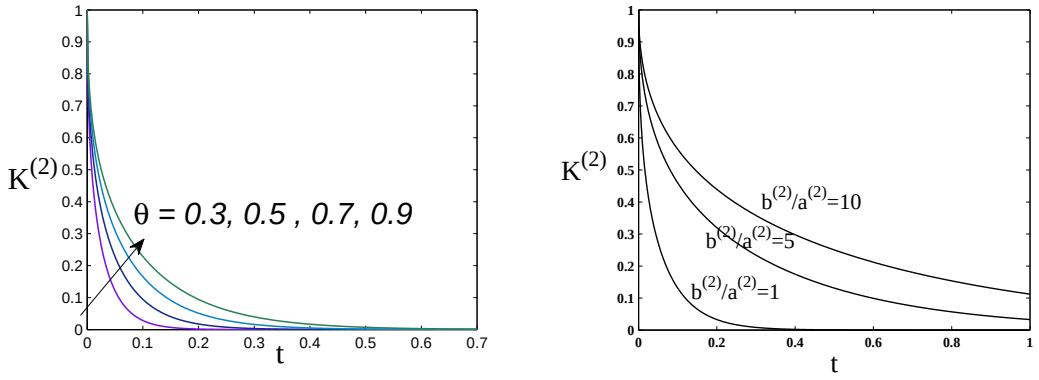

Figure 1.8: Dependence of the exchange kernel $K^{(2)}(t)$ on the fractional volume of block $\widetilde{Y}^2$ (a), and on the block property $b^{(2)}/a^{(2)}$ (b)

1.3.10 Effective permeability for the second level

The effective permeability is defined in the similar way as in section 1.2.4 through three auxiliary functions $\psi_k^{(2)}$:

We consider the symmetrical case, so that all functions $\psi_k^{(2)}$ are symmetrical, and the effective permeability becomes a scalar:

$$A^{(3)} = \int\limits_{Y^3} a^{(3)} \left(1 + \frac{\partial \psi_1^{(2)}}{\partial y_1^{(2)}}\right) dy^{(2)} \tag{1.49}$$

$$\begin{cases} \nabla_2 \cdot \left(a^{(3)} \nabla_2 \psi_1^{(2)}\right) = -\nabla_2 a^{(3)} \cdot \vec{e}_1, \qquad y^{(2)} \in Y^3 \\ \psi_1^{(2)} \ \text{ is } y^{(2)} - \text{periodic} \\ \left\langle \psi_1^{(2)} \right\rangle_{Y^3} = 0 \end{cases} \tag{1.50}$$

where $\vec{e}_k$ is the unit vector along the axis $y_k^{(2)}$.

1.3.11 Equivalent forms of the averaged model

The system (1.46) may be presented in the following equivalent form:

$$\begin{cases} B^{(3)}\dfrac{\partial P^3}{\partial t} - \nabla_3 \cdot \left(A^{(3)}\nabla_3 P^3\right) = -B^{(2)}\theta\dfrac{\partial \tilde{P}^2}{\partial t} + B^{(1)}\theta\dfrac{\partial \tilde{P}^2}{\partial t} * K^{(1)\prime} \\ \\ \tilde{P}^2 = P^3 - K^{(2)} * \left(\dfrac{\partial P^3}{\partial t} - \dfrac{B^{(1)}}{B^{(2)}}\dfrac{\partial P^3}{\partial t} * K^{(1)\prime}\right) \end{cases} \tag{1.51}$$

where we used the operator of convolution: $f(t) * g(t) = \int\limits_0^t f(\tau)\, g(t-\tau)\, d\tau$ and its properties:

$$f(t) * g(t) = g(t) * f(t) \tag{1.52}$$

$$\frac{\partial}{\partial t}(f * g) = f(t) * \frac{\partial g(t)}{\partial t} + f(t)g(0) \tag{1.53}$$

1.4 Transition between two arbitrary scales $i-1$ and i

1.4.1 Analogy between transitions $1 \to 2$ and $2 \to 3$

Transition $1 \to 2$ leads to the averaged model (1.12) :

$$\left\{ \begin{array}{l} P^1 = P^2 - K^{(1)} * \dfrac{\partial P^2}{\partial t}, \\ \\ B^{(2)} \dfrac{\partial P^2}{\partial t} - \nabla_2 \cdot \left(A^{(2)} \nabla_2 P^2 \right) = -B^1 \dfrac{\partial P^1}{\partial t} \end{array} \right. , \qquad y^{(2)} \in \widetilde{\Omega}^2 / \varepsilon^{n-2} \tag{1.54}$$

Transition $2 \to 3$ leads to the averaged model (1.51) :

$$\left\{ \begin{array}{l} \tilde{P}^2 = P^3 - K^{(2)} * \left(\dfrac{\partial P^3}{\partial t} - \dfrac{B^{(1)}}{B^{(2)}} \dfrac{\partial P^3}{\partial t} * K^{(1)'} \right), \\ \\ B^{(3)} \dfrac{\partial P^3}{\partial t} - \nabla_3 \cdot \left(A^{(3)} \nabla_3 P^3 \right) = -B^{(2)} \theta \dfrac{\partial \tilde{P}^2}{\partial t} + B^{(1)} \theta \dfrac{\partial \tilde{P}^2}{\partial t} * K^{(1)'} \\ \\ \end{array} \right. , \qquad y^{(3)} \in \widetilde{\Omega}^3 / \varepsilon^{n-3}$$

(1.55)

where

$$B^{(i)} = \int\limits_{Y^i} b^{(i)} dy^{(i-1)} = \left\{ \begin{array}{ll} b^{(i)} (1-\theta), & i > 1 \\ b^{(1)} \theta, & i = 1 \end{array} \right. , \qquad A^{(i)} = \int\limits_{Y^i} a^{(i)} \left(1 + \frac{\partial \psi_k^{(i-1)}}{\partial y_k^{(i-1)}} \right) dy^{(i-1)}$$

where the functions $\psi_k^{(2)}$, $k = 1, 2, 3$ are defined in the similar was as (1.22) and (1.50).

P^2 is the pressure averaged over fractures Y^2 only, while $\tilde{P}^2$ is the pressure averaged over the entire domain $\tilde{Y}^2$ which includes fracture Y^2 and internal block Y^1.

1.4.2 Case of constant parameters $a^{(i)}$ and $b^{(i)}$

In a self-similar medium the coefficients $b^{(i)}$ and $a^{(i)}$ should be independent of i:

$$b^{(i)} = b, \qquad a^{(i)} = a, \quad \forall i$$

Then all functions $\psi^{(i)}$ defined through (1.22), (1.50) and so on, become identical and defined as:

$$\begin{cases} \nabla_i \cdot (a \nabla_i \psi_1) = -\nabla_i a \cdot \vec{e}_1, & y^{(i)} \in Y^{i+1} \\ \psi_1 \ \text{ is } y^{(i)} - \text{periodic} \\ \langle \psi_1 \rangle_{Y^{i+1}} = 0 \end{cases} \tag{1.56}$$

independently of i, because all domains Y^i become identical. Herein $\vec{e}_k$ is the unit vector along the axis $y_k^{(i)}$.

The the effective permeability at each level becomes also identical:

$$A^{(i)} = A = \int\limits_{Y^i} a \left(1 + \frac{\partial \psi_1}{\partial y_1^{(i-1)}} \right) dy^{(i-1)}, \qquad \forall i \tag{1.57}$$

The effective porosities become:

$$B^{(1)} + B^{(2)} = \theta b + (1-\theta) b = b; \qquad \frac{B^{(1)}}{B^{(2)}} = \frac{\theta}{1-\theta} \equiv \alpha$$

Then equations (1.54) and (1.55) become

$$\begin{cases} P^1 = P^2 - K^{(1)} * \dfrac{\partial P^2}{\partial t}, \\ \\ b\,(1-\theta)\,\dfrac{\partial P^2}{\partial t} - \nabla_2 \cdot \left(A \nabla_2 P^2 \right) = -b\theta \dfrac{\partial P^1}{\partial t} \end{cases} \tag{1.58}$$

$$\begin{cases} \tilde{P}^2 = P^3 - K^{(2)} * \left[\dfrac{\partial P^3}{\partial t} - \alpha \dfrac{\partial P^3}{\partial t} * K^{(1)\prime} \right], \\ \\ b\,(1-\theta)\,\dfrac{\partial P^3}{\partial t} - \nabla_3 \cdot \left(A \nabla_3 P^3 \right) = -b\theta(1-\theta) \dfrac{\partial \tilde{P}^2}{\partial t} + b\theta^2 \dfrac{\partial \tilde{P}^2}{\partial t} * K^{(1)\prime} \end{cases} \tag{1.59}$$

1.4.3 General form of the averaged equations for an arbitrary scale-up $i-1 \to i$

The last relations may be reduced to the common general form for $i \geq 2$:

$$\begin{cases} \tilde{P}^{i-1} = P^i - \dfrac{\partial P^i}{\partial t} * \mathbb{K}^{(i-1)}, \\ \\ b\,(1-\theta)\,\dfrac{\partial P^i}{\partial t} - \nabla_i \cdot \left(A \nabla_i P^i \right) = -b\theta \dfrac{\partial \tilde{P}^{i-1}}{\partial t} * \mathbb{L}^{(i-1)} \end{cases}, \qquad y^{(i)} \in \widetilde{\Omega}^i / \varepsilon^{n-i} \tag{1.60}$$

where $B^{(0)}=0$, and new functions $\mathbb{K}^{(i)}$ and $\mathbb{L}^{(i)}$ are defined as:

$$\mathbb{L}^{(i)}=\begin{cases}\delta(t), & i=1\\ (1-\theta)\delta(t)-\theta K^{(1)\prime}, & i=2\end{cases},\qquad \mathbb{K}^{(i)}=\begin{cases}K^{(1)}, & i=1\\ K^{(2)}*\left(\delta(t)-\alpha K^{(1)\prime}\right), & i=2\end{cases} \tag{1.61}$$

Model (1.60) can be converted to a single equation:

$$b\,(1-\theta)\,\frac{\partial P^i}{\partial t}-\nabla_i\cdot\left(A\nabla_i P^i\right)=-b\theta\frac{\partial}{\partial t}\left(P^i-\frac{\partial P^i}{\partial t}*\mathbb{K}^{(i-1)}\right)*\mathbb{L}^{(i-1)},\qquad y^{(i)}\in\widetilde{\Omega}^i/\varepsilon^{n-i} \tag{1.62}$$

We will search for the averaged model at any scale in the same general form (1.62). The problem consists then in obtaining the iterative relations for operators $\mathbb{K}^i$ and $\mathbb{L}^i$.

1.4.4 Problem formulation

To analyze the transition between scales $i-1$ and i, we should consider the domain which consists of the connected fracture Ω^i and an already homogenized "block" $\widetilde{\Omega}^{i-1}$. Variable $y^{(i)}$ is the slow coordinates, while $y^{(i-1)}$ is the fast one. The extended medium Ω^i in coordinates $y^{(n-i)}$ and its unit cell in coordinates $y^{(i-1)}$ is shown in Fig. 1.7.

In slow coordinates the problem of flow in $\Omega^i/\varepsilon^{n-i}$ and $\widetilde{\Omega}^{i-1}/\varepsilon^{n-i}$ has the form of (1.62) and (1.8b):

$$b\,(1-\theta)\,\frac{\partial P^{i-1}}{\partial t}-\varepsilon^2\nabla_i\cdot\left(A\nabla_i P^{i-1}\right)=-b\theta\frac{\partial}{\partial t}\left(P^{i-1}-\frac{\partial P^{i-1}}{\partial t}*\mathbb{K}^{(i-2)}\right)*\mathbb{L}^{(i-2)},\quad y^{(i)}\in\widetilde{\Omega}^{i-1}/\varepsilon^{n-i} \tag{1.63a}$$

$$b\frac{\partial p^i}{\partial t}=\nabla_i\cdot\left(a\nabla_i p^i\right),\quad y^{(i)}\in\Omega^i/\varepsilon^{n-i} \tag{1.63b}$$

$$\varepsilon^2 A\nabla_i P^{i-1}\cdot\vec{n}\big|_{\Gamma^{i,i-1}_-}=a\nabla p^i\cdot\vec{n}\big|_{\Gamma^{i,i-1}_+},\qquad P^{i-1}|_{\Gamma^{i,i-1}_-}=p^i|_{\Gamma^{i,i-1}_+} \tag{1.63c}$$

1.4.5 Two-scale formulation

According to the technique of homogenization we introduce the two-scale functions $P^{i-1}\left(y^{(i)},y^{(i-1)},t\right)$ and $p^i\left(y^{(i)},y^{(i-1)},t\right)$ which are equal to the true functions $P^{i-1}\left(y^{(i)},t\right)$ and $p^i\left(y^{(i)},t\right)$ when $y^{(i-1)}=y^{(i)}/\varepsilon$. Respectively we introduce the two-scale operator $\tilde{\nabla}_i=\nabla_i+\varepsilon^{-1}\nabla_{i-1}$. Further the symbol "tilde" will be omitted. The equations (1.63) become:

$$b\left(1-\theta\right)\frac{\partial P^{i-1}}{\partial t}+b\theta\,\mathbb{L}^{(i-2)}*\frac{\partial}{\partial t}\left(P^{i-1}-\frac{\partial P^{i-1}}{\partial t}*\mathbb{K}^{(i-2)}\right)=$$
$$=\nabla_{i-1}\cdot\left(A\nabla_{i-1}P^{i-1}\right)+\varepsilon\left[\nabla_{i-1}\cdot\left(A\nabla_{i}P^{i-1}\right)+\nabla_{i}\cdot\left(A\nabla_{i-1}P^{i-1}\right)\right]+$$
$$+\varepsilon^{2}\nabla_{i}\cdot\left(A\nabla_{i}P^{i-1}\right),\qquad y^{(i)}\in\widetilde{\Omega}^{i}/\varepsilon^{n-i},\quad y^{(i-1)}\in\widetilde{Y}^{i-1}\tag{1.64a}$$

$$b\frac{\partial p^{i}}{\partial t}=\frac{1}{\varepsilon^{2}}\nabla_{i-1}\cdot\left(a\nabla_{i-1}p^{i}\right)+\frac{1}{\varepsilon}\left[\nabla_{i-1}\cdot\left(a\nabla_{i}p^{i}\right)+\nabla_{i}\cdot\left(a\nabla_{i-1}p^{i}\right)\right]+$$
$$+\nabla_{i}\cdot\left(a\nabla_{i}p^{i}\right),\qquad y^{(i)}\in\widetilde{\Omega}^{i}/\varepsilon^{n-i},\quad y^{(i-1)}\in Y^{i}\tag{1.64b}$$

$$\varepsilon^{2}A\left(\nabla_{i-1}P^{i-1}+\varepsilon\nabla_{i}P^{i-1}\right).\vec{n}\big|_{\Gamma_{-}^{i,i-1}}=a\left(\nabla_{i-1}p^{i}+\varepsilon\nabla_{i}p^{i}\right).\vec{n}\big|_{\Gamma_{+}^{i,i-1}},$$
$$P^{i-1}|_{\Gamma_{-}^{i,i-1}}=p^{i}|_{\Gamma_{+}^{i,i-1}}\tag{1.64c}$$

The additional condition is the periodicity with respect to the fast variable $y^{(i-1)}$.

The necessary condition of existence for periodic solution is obtained as previously. Let us integrated the first equation (1.64a) over $\widetilde{Y}^{i-1}$, the second equation (1.64b) over Y^{i}, and sum up the results, by using the Gauss theorem, the property of a periodic function with respect to $y^{(i-1)}$ and condition (1.64c):

$$b\left(1-\theta\right)\frac{\partial}{\partial t}\left\langle P^{i-1}\right\rangle_{\widetilde{Y}^{i-1}}+b\theta\left\langle\mathbb{L}^{(i-2)}*\frac{\partial}{\partial t}\left(P^{i-1}-\frac{\partial P^{i-1}}{\partial t}*\mathbb{K}^{(i-2)}\right)\right\rangle_{\widetilde{Y}^{i-1}}+\left\langle b\frac{\partial p^{i}}{\partial t}\right\rangle_{Y^{i}}=$$
$$=\varepsilon\nabla_{i}\cdot\left\langle A\left(\nabla_{i-1}P^{i-1}+\varepsilon\nabla_{i}P^{i-1}\right)\right\rangle_{\widetilde{Y}^{i-1}}+\frac{1}{\varepsilon}\nabla_{i}\cdot\left\langle a\left(\nabla_{i-1}p^{i}+\varepsilon\nabla_{i}p^{i}\right)\right\rangle_{Y^{i}}\tag{1.65}$$

where we used the notation (1.26).

1.4.6 Asymptotic expansion

We search for the solution of (1.64) in the form of the asymptotic expansion:

$$p^{i}\left(y^{(i)},y^{(i-1)},t;\varepsilon\right)=\sum_{k=0}^{\infty}\varepsilon^{k}p_{k}^{i}\left(y^{(i)},y^{(i-1)},t\right),\qquad P^{i-1}\left(y^{(i)},y^{(i-1)},t;\varepsilon\right)=\sum_{k=0}^{\infty}\varepsilon^{k}P_{k}^{i-1}\left(y^{(i)},y^{(i-1)},t\right)\tag{1.66}$$

By direct substitution of this expansion into equations (1.63) and (1.65), for three first terms of this expansion it is possible to obtain the closed system of problems:

For P_{0}^{i-1}: it depends on slow and fast variables: $P_{0}^{i-1}=P_{0}^{i-1}\left(y^{(i)},y^{(i-1)},t\right)$, and is defined as

the solution of the problem in the block $\widetilde{Y}^{i-1}$:

$$\begin{cases} b\left(1-\theta\right)\dfrac{\partial P_0^{i-1}}{\partial t}+b\theta\,\mathbb{L}^{(i-2)}*\dfrac{\partial}{\partial t}\left(P_0^{i-1}-\dfrac{\partial P_0^{i-1}}{\partial t}*\mathbb{K}^{(i-2)}\right)= \\ \qquad\qquad =\nabla_{i-1}\cdot\left(A\nabla_{i-1}P_0^{i-1}\right), \qquad y^{(i-1)}\in\widetilde{Y}^{i-1} \\ P_0^{i-1}|_{\Gamma_-^{i,i-1}}=p_0^i|_{\Gamma_+^{i,i-1}}, \\ P_0^{i-1}|_{t=0}=p^0 \end{cases} \tag{1.67}$$

For p_0^i: it depends only on the slow variable: $p_0^i=p_0^i\left(y^{(i)},t\right)$, and is defined by the averaged equation resulting from (1.65):

$$\begin{aligned} b\left(1-\theta\right)\frac{\partial}{\partial t}\left\langle P_0^{i-1}\right\rangle_{\widetilde{Y}^{i-1}}+b\theta\left\langle\mathbb{L}^{(i-2)}*\frac{\partial}{\partial t}\left(P_0^{i-1}-\frac{\partial P_0^{i-1}}{\partial t}*\mathbb{K}^{(i-2)}\right)\right\rangle_{\widetilde{Y}^{i-1}}= \\ =-\left\langle b\right\rangle_{Y^i}\frac{\partial p_0^i}{\partial t}+\nabla_i\cdot\left\langle a\left(\nabla_{i-1}p_1^i+\varepsilon\nabla_i p_0^i\right)\right\rangle_{Y^i} \end{aligned} \tag{1.68}$$

For p_1^i we obtain the same problem as for p_1 (1.33) and (1.34).

1.4.7 Solution of the problem in $\widetilde{Y}^{i-1}$

Similar to what was done in section 1.3.6, we obtain the following results.

Let us introduce the new variable: $U\equiv P_0^{i-1}-p_0^i$. Taking into account the fact that p_0 does not depend on the fast variables, the problem (1.67) becomes:

$$\begin{cases} \mathcal{L}U\equiv\dfrac{\partial U}{\partial t}+\alpha\mathbb{L}^{(i-2)}*\dfrac{\partial}{\partial t}\left(U-\dfrac{\partial U}{\partial t}*\mathbb{K}^{(i-2)}\right)-\dfrac{A}{b\left(1-\theta\right)}\nabla_{i-1}^2U= \\ \qquad\qquad =-\dfrac{\partial p_0^i}{\partial t}-\alpha\mathbb{L}^{(i-2)}*\dfrac{\partial}{\partial t}\left(p_0^i-\dfrac{\partial p_0^i}{\partial t}*\mathbb{K}^{(i-2)}\right), \qquad y^{(i-1)}\in\widetilde{Y}^{i-1} \\ U|_{\Gamma_-^{i,i-1}}=0, \\ U|_{t=0}=0 \end{cases} \tag{1.69}$$

where we taken into account that $p_0^i|_{t=0}=p^0$.

We obtain the problem with homogeneous conditions for non-homogeneous linear integro-differential equation. Its solution is the convolution of the Green function of the operator $\mathcal{L}$ with the right-hand side of equation (1.69). As the result, the solution is:

$$P_0^{i-1}=p_0^i-\int_0^t\int_{\tilde{Y}^{i-1}}G\left(y^{(i-1)},\xi,t-\tau\right)\left[\frac{\partial p_0^i}{\partial t}+\alpha\,\mathbb{L}^{(i-2)}*\frac{\partial}{\partial t}\left(p_0^i-\frac{\partial p_0^i}{\partial t}*\mathbb{K}^{(i-2)}\right)\right]d\xi d\tau \tag{1.70}$$

where the Green's function $G\left(y^{(i-1)},\xi,t-\tau\right)$ is determined as the solution of the homogeneous equation with homogeneous boundary conditions at $\Gamma^{(i,i-1)}$ and the initial condition:

$$\frac{\partial G}{\partial t}-\frac{A}{b\left(1-\theta\right)}\nabla_{i-1}^{2}G+\alpha\,\mathbb{L}^{(i-2)}*\frac{\partial}{\partial t}\left(G-\frac{\partial G}{\partial t}*\mathbb{K}^{(i-2)}\right)=\delta\left(y^{(i-1)}-\xi\right)\delta\left(t-\tau\right),$$
$$G\left(y^{(i-1)},\xi,t\right)\Big|_{t=0}=\delta\left(y^{(i-1)}-\xi\right),$$
$$G\left(y^{(i-1)},\xi,t\right)\Big|_{y^{(i-1)},\xi\in\Gamma^{i,i-1}}=0$$

The spectral expansion of the Green's function has the form:

$$G\left(y^{(i-1)},\xi,t\right)=\sum_{k=1}^{\infty}\frac{1}{||R_k||^2}T_k^{(i-1)}(t)R_k\left(y^{(i-1)}\right)R_k(\xi) \tag{1.72}$$

where μ_k and $R_k\left(y^{(i-1)}\right),\ k\geq 1$ are the series of eigenvalues and eigenfunctions of the Laplace operator ∇_{i-1}^2 in $\mathcal{H}$.

Functions $T_k^{(i-1)}(t)$ are determined as the solutions of the problem:

$$T_k^{(i-1)\prime}+\alpha\,\mathbb{L}^{(i-2)}*\frac{d}{dt}\left(T_k^{(i-1)}-T_k^{\prime(i-1)}*\mathbb{K}^{(i-2)}\right)=-T_k^{(i-1)}\mu_k\frac{A}{b\left(1-\theta\right)} \tag{1.73}$$
$$T_k^{(i-1)}\Big|_{t=0}=1$$

where $T_k^{(i-1)\prime}(t)\equiv dT_k^{(i-1)}/dt$.

1.4.8 Averaged equations

Let us introduce the pressures, averaged over subdomains Y^i and $\widetilde{Y}^{i-1}$ of a cell:

$$\tilde{P}^{i-1}=\frac{1}{\theta}\left\langle P^{i-1}\right\rangle_{\widetilde{Y}^{i-1}},\qquad P^i=\frac{1}{1-\theta}\left\langle p^i\right\rangle_{Y^i}$$

where θ is the volume fraction of blocks $\widetilde{Y}^{i-1}$ in a cell $\widetilde{Y}^{i-1}\cup Y^i$.

It follows from the results of the previous section, that:

$$\tilde{P}^{i-1}=\frac{1}{\theta}\left\langle P_0^{i-1}\right\rangle_{\widetilde{Y}^{(i-1)}}+O\left(\varepsilon\right),\qquad P^i=p_0^i+O\left(\varepsilon^2\right)$$

So we obtain for the average pressures:

$$b\,(1-\theta)\,\frac{\partial P^i}{\partial t} - \nabla_i\cdot\left(A\nabla_i P^i\right) = -b\theta\,(1-\theta)\,\frac{\partial \tilde{P}^{i-1}}{\partial t} - b\theta^2\,\mathbb{L}^{(i-2)} * \frac{\partial}{\partial t}\left(\tilde{P}^{i-1} - \frac{\partial \tilde{P}^{i-1}}{\partial t} * \mathbb{K}^{(i-2)}\right),$$

$$\tilde{P}^{i-1} = P^i - K^{(i-1)} * \left[\frac{\partial P^i}{\partial t} + \alpha\,\mathbb{L}^{(i-2)} * \frac{\partial}{\partial t}\left(P^i - \frac{\partial P^i}{\partial t} * \mathbb{K}^{(i-2)}\right)\right]$$

The right-hand side of these equations may be presented as the convolution with the pressure derivative, if we take into account that

$$\frac{\partial}{\partial t}\left(\frac{\partial P}{\partial t} * \mathbb{K}(t)\right) = \frac{\partial P}{\partial t}\mathbb{K}(0) + \frac{\partial P}{\partial t} * \mathbb{K}'(t) = \frac{\partial P}{\partial t} * \Big(\mathbb{K}(0)\delta(t) + \mathbb{K}'(t)\Big)$$

and

$$\frac{\partial}{\partial t}\left(P - \frac{\partial P}{\partial t} * \mathbb{K}(t)\right) = \frac{\partial P}{\partial t} * \Big(\,(1-\mathbb{K}(0))\,\delta(t) - \mathbb{K}'(t)\Big)$$

According to (1.61), $\mathbb{K}^{(1)}(0) = \mathbb{K}^{(2)}(0) = 1$. We will assume that this law is valid for all i:

$$\mathbb{K}^{(i)}(0) = 1, \qquad \forall i \tag{1.74}$$

which will be proved further.

Then:

$$\frac{\partial}{\partial t}\left(P - \frac{\partial P}{\partial t} * \mathbb{K}(t)\right) = -\frac{\partial P}{\partial t} * \mathbb{K}'(t)$$

The definite form of the averaged equations becomes:

$$\begin{cases} b\,(1-\theta)\,\dfrac{\partial P^i}{\partial t} - \nabla_i\cdot\left(A\nabla_i P^i\right) = -b\theta\,(1-\theta)\,\dfrac{\partial \tilde{P}^{i-1}}{\partial t} + b\theta^2\,\mathbb{L}^{(i-2)} * \mathbb{K}^{(i-2)'} * \dfrac{\partial \tilde{P}^{i-1}}{\partial t}, \\ \\ \tilde{P}^{i-1} = P^i - K^{(i-1)} * \left[\dfrac{\partial P^i}{\partial t} - \alpha\,\mathbb{L}^{(i-2)} * \mathbb{K}^{(i-2)'} * \dfrac{\partial P^i}{\partial t}\right] \end{cases} \tag{1.75}$$

1.4.9 Determination of the kernels $\mathbb{K}^{(i)}$ and $\mathbb{L}^{(i)}$

Comparing (1.75) and (1.60), and taking into account for (1.61), we obtain:

$$\mathbb{K}^{(i)} = \begin{cases} K^{(i)} * \left(\delta(t) - \alpha \mathbb{L}^{(i-1)} * \mathbb{K}^{(i-1)\prime}\right), & i \geq 2 \\ K^{(i)}, & i = 1 \end{cases} \tag{1.76}$$

$$\mathbb{L}^{(i)} = \begin{cases} (1-\theta)\delta(t) - \theta\, \mathbb{L}^{(i-1)} * \mathbb{K}^{(i-1)\prime}, & i \geq 2 \\ \delta(t), & i = 1 \end{cases} \tag{1.77}$$

The iterative kernels $K^{(i)}$ are determined similar to (1.72) and (1.73), for any $i \geq 1$:

$$K^{(i)}(t) \equiv \frac{6}{\pi^2} \sum_{k=1}^{\infty} \frac{1}{k^2} T_k^{(i)}(t), \tag{1.78}$$

$$T_k^{(i)\prime} - \alpha\, T_k^{(i)\prime} * \mathbb{L}^{(i-1)} * \mathbb{K}^{(i-1)\prime} = -T_k^{(i)} \mu_k \frac{A}{b\,(1-\theta)}, \qquad T_k^{(i)}\Big|_{t=0} = 1 \tag{1.79}$$

with $\mathbb{L}^{(0)} = \mathbb{K}^{(0)} \equiv 0$.

System (1.76), (1.77), (1.78) and (1.79) of four coupled recurrent equations is closed. It determines four sets of functions $\mathbb{K}^{(i)}$, $\mathbb{L}^{(i)}$, $K^{(i)}$ and $T^{(i)}$.

Using these equations it is easy to prove the validity of the condition (1.74). Any kernel $K^{(i)}(t)$ is so that $K^{(i)}(0) = 1$, according to their construction. Any kernel $K^{(i)}(t)$ has the integrable singularity $\sim t^{-1/2}$ when $t \to 0$. Assuming that the behavior of kernels $\mathbb{K}^{(i)}(t)$ and $K^{(i)}(t)$ has no stronger singularity, we obtain that all operators of convolution operators will tend to zero as $t \to 0$.

1.4.10 Physical meaning of functions $\mathbb{K}^{(i)}$ and $\mathbb{L}^{(i)}$, $K^{(i)}$ and $T^{(i)}$

All these four functions have clear physical meaning:

- **"local exchange kernels"** $K^{(i)}$ are responsible for the local mass exchange process between two media i and $i-1$;

- **"effective exchange kernels"** $\mathbb{K}^{(i)}$ are responsible for the cumulated history of the exchange process between all the preceding couples of media;

- **"Fourier spectrum of local kernels"** $T_k^{(i)}$ the Fourier-components of the kernel $K^{(i)}$.

Functions $\mathbb{L}^{(i)}$ are not independent. In the next section it will be shown that they are liner functions of the effective kernels $\mathbb{K}^{(i)}$.

1.4.11 Reduction of the system of recurrent equation

It is possible to show that these two sets of recurrent equations may be reduced to a single one, due to a linear link which exist between $\mathbb{K}^{(i)}$ and $\mathbb{L}^{(i)}$:

$$\mathbb{L}^{(i)} * K^{(i)} = (1-\theta)\mathbb{K}^{(i)}, \qquad i \geq 2 \tag{1.80}$$

Proof: 1. Equation (1.76) and equation (1.77) converted with $K^{(i)}$ has the following form for $i \geq 2$:

$$\begin{cases} \mathbb{L}^{(i)} * K^{(i)} = (1-\theta)K^{(i)} - \theta\, \mathbb{L}^{(i-1)} * \mathbb{K}^{(i-1)\prime} * K^{(i)}, \\ \mathbb{K}^{(i)} = K^{(i)} - \alpha \mathbb{L}^{(i-1)} * \mathbb{K}^{(i-1)\prime} * K^{(i)} \end{cases}$$

Eliminating the double convolution operator by subtracting one equation from another one, we easily obtain (1.80), if we take into account that:

$$\alpha\,(1-\theta) = \theta \tag{1.81}$$

Then we can reduce the number of equations in the coupled system (1.76), (1.77) , (1.78) and (1.79):

$$\mathbb{K}^{(i)} * K^{(i-1)} = K^{(i)} * K^{(i-1)} - \theta\, K^{(i)} * \mathbb{K}^{(i-1)} * \mathbb{K}^{(i-1)\prime}, \quad i \geq 2 \tag{1.82a}$$

$$K^{(i)}(t) \equiv \frac{6}{\pi^2} \sum_{k=1}^{\infty} \frac{1}{k^2} T_k^{(i)}(t), \quad i \geq 1 \tag{1.82b}$$

$$T_k^{(i)\prime} * K^{(i-1)} - \theta\, T_k^{(i)\prime} * \mathbb{K}^{(i-1)} * \mathbb{K}^{(i-1)\prime} = -T_k^{(i)} * K^{(i-1)} \frac{A\mu_k}{b\,(1-\theta)}, \qquad T_k^{(i)}\Big|_{t=0} = 1 \tag{1.82c}$$

Once this system is solved, we can find the functions $\mathbb{L}^{(i)}$:

$$\mathbb{L}^{(i)} * K^{(i)} = \begin{cases} (1-\theta)\mathbb{K}^{(i)}, & i \geq 2 \\ K^{(i)}, \quad i = 1 \end{cases} \tag{1.83}$$

1.4.12 Solution of the problem for hierarchical kernels by Laplace transform

To solve system (1.82), we applied the Laplace transform. Let $\overline{f}(s)$ be the Laplace transformation of function $f(t)$ with parameter s. Then we have:

$$\overline{\mathbb{K}}^{(i)} = \begin{cases} \overline{K}^{(i)} - \theta \dfrac{\overline{K}^{(i)}}{\overline{K}^{(i-1)}} \overline{\mathbb{K}}^{(i-1)} \left(s\,\overline{\mathbb{K}}^{(i-1)} - 1 \right), & i \geq 2 \\ \overline{K}^{(i)}, & i = 1 \end{cases} \tag{1.84}$$

$$\overline{K}^{(i)}(s) = \frac{6}{\pi^2} \sum_{k=1}^{\infty} \frac{1}{k^2} \overline{T}_k^{(i)}(s), \quad i \geq 1 \tag{1.85}$$

$$\left(s\overline{T}_k^{(i)} - 1 \right) \left[\overline{K}^{(i-1)} - \theta\, \overline{\mathbb{K}}^{(i-1)} \left(s\overline{\mathbb{K}}^{(i-1)} - 1 \right) \right] = -\overline{T}_k^{(i)} \overline{K}^{(i-1)} \frac{A\mu_k}{b\,(1-\theta)}, \quad i,k \geq 1$$

So we have for $\overline{T}_k^{(i)}$:

$$\overline{T}_k^{(i)} = \begin{cases} \dfrac{\overline{K}^{(i-1)} - \theta \overline{\mathbb{K}}^{(i-1)} \left(s\overline{\mathbb{K}}^{(i-1)} - 1 \right)}{s\overline{K}^{(i-1)} - s\theta \overline{\mathbb{K}}^{(i-1)} \left(s\overline{\mathbb{K}}^{(i-1)} - 1 \right) + \overline{K}^{(i-1)} \dfrac{A\mu_k}{b\,(1-\theta)}}, & i \geq 2 \\ \dfrac{1}{s + \mu_k a/b}, & i = 1 \end{cases} \tag{1.86}$$

where we have taken into account that $T_k^{(i)}(0) = 1$, $K^{(i)}(0) = 1$, $\mathbb{K}^{(i)}(0) = 1$.

Proof:

$T_k^{(i)}(0) = 1$ is automatically given by the imposed initial condition.

Directly we have $K^{(i)}(0) = 1$ from (1.85).

When $t \to 0$ or $s \to \infty$

$$\lim_{s\to\infty} \overline{\mathbb{K}}^{(2)} = \frac{1}{s} - \theta \frac{1}{s} \left(s \frac{1}{s} - 1 \right) = \frac{1}{s}$$

$\mathbb{K}^{(2)}(0) = 1$ respectively gives $\mathbb{K}^{(3)}(0) = 1$, and so on $\mathbb{K}^{(i)}(0) = 1$.

Also for $t \to \infty$, $s \to 0$:

$$\lim_{s\to 0} \overline{T}_k^{(1)} = \lim_{s\to 0} \frac{1}{s + \mu_k a/b} = \frac{b}{\mu_k a} = \text{cte}$$

then $\lim\limits_{t\to\infty} T_k^{(1)} = 0$ and respectively $\lim\limits_{t\to\infty} K^{(1)} = 0$

For $T_k^{(2)}$ at $t \to \infty$ we can say:

$$\lim_{s\to 0} \overline{T}_k^{(2)} = \lim_{s\to 0} \frac{1 - \theta \left(s\overline{\mathbb{K}}^{(i-1)} - 1 \right)}{s - s\theta \left(s\overline{\mathbb{K}}^{(i-1)} - 1 \right) + \dfrac{A\mu_k}{b\,(1-\theta)}} = \text{cte}$$

Respectively we can say:

$$\lim_{s\to 0} \overline{T_k}^{(i)} = \text{cte}, \qquad \lim_{s\to 0} \overline{K}^{(i)} = \text{cte}, \qquad \lim_{s\to 0} \overline{\mathbb{K}}^{(i)} = \text{cte}$$

whenever:

$$\lim_{s\to 0} \overline{T_k}^{(i-1)} = \text{cte}, \qquad \lim_{s\to 0} \overline{K}^{(i-1)} = \text{cte}, \qquad \lim_{s\to 0} \overline{\mathbb{K}}^{(i-1)} = \text{cte}$$

So we have:

$$\lim_{t\to\infty} T_k{}^{(i)} = 0, \qquad \lim_{t\to\infty} K^{(i)} = 0, \qquad \lim_{t\to\infty} \mathbb{K}^{(i)} = 0$$

The iterative algorithm of solution is the following:

One calculates:

1* $\overline{T}_k^{(1)}$ by using (1.86), for all k.

2* $\overline{K}^{(1)}$ by using (1.85).

3* $\overline{\mathbb{K}}^{(1)}$ by using (1.84).

4* $\overline{T}_k^{(2)}$ by using (1.86), for all k.

5* $\overline{K}^{(2)}$ by using (1.85).

6* $\overline{\mathbb{K}}^{(2)}$ by using (1.84), and so on.

The results of solution are shown in Fig. 1.9, 1.10.

4 - 6 scales are sufficient to represent a medium having more than 6 scales.

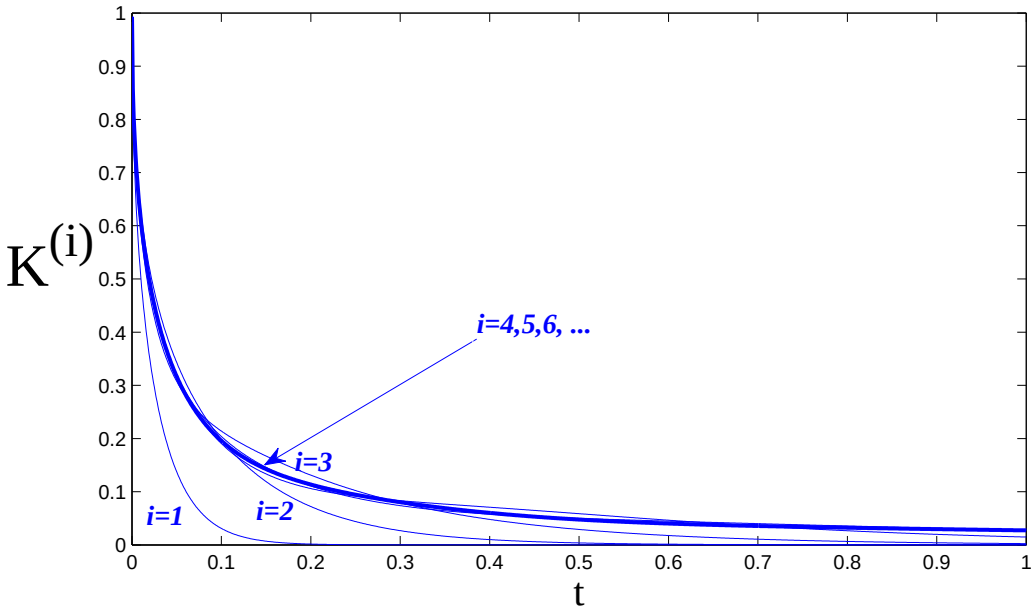

Figure 1.9: Hierarchical local kernels $K^{(i)}$, for $\theta = 0.8$

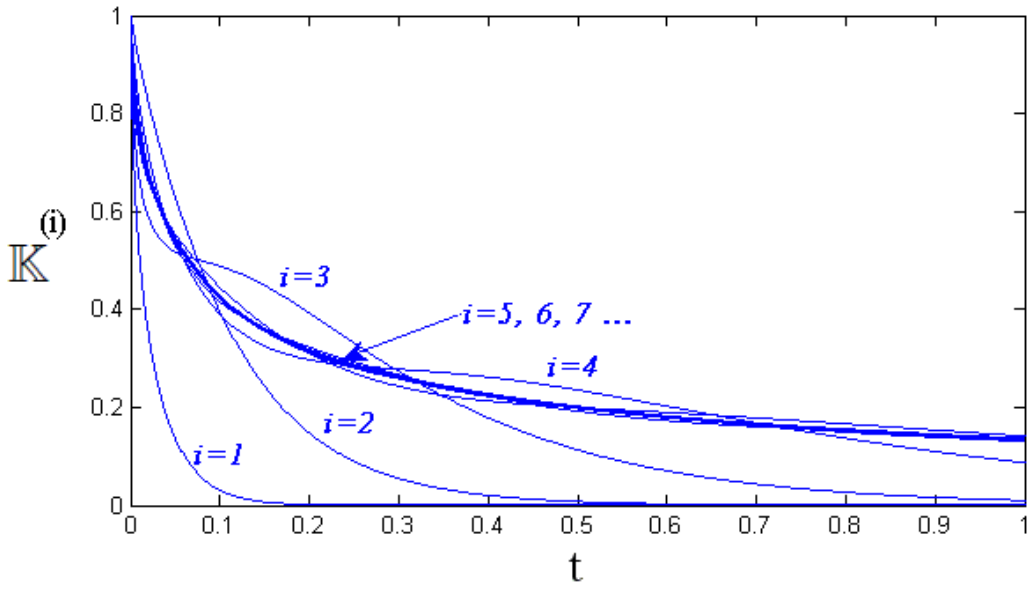

Figure 1.10: Hierarchical effective kernels $\mathbb{K}^{(i)}$, for $\theta = 0.8$

1.5 Limit behavior for infinite number of scales

1.5.1 Limit averaged equation for infinite number of scales

For a medium consisting of infinite number of scales, if the limit behavior exists then the iterative system of averaged models should prove a stabilization with respect to the index i: for high values of i, the the basic functions determining the averaged operators, $\mathbb{K}^{(i-1)}$, $\mathbb{L}^{(i-1)}$, $K^{(i-1)}$ and $T_k^{(i-1)}$, should tend respectively to the functions $\mathbb{K}^{(i)}$, $\mathbb{L}^{(i)}$, $K^{(i)}$ and $T_k^{(i)}$. More generally, all these functions should have the limit $\mathbb{K}$, $\mathbb{L}$, K and T_k, corresponding to $i \to \infty$.

Then for the infinite sequence of transitions, we will obtain the couple of pressures P and $\tilde{P}$ which will be related by the following system of limit average equations resulting from (1.75):

$$\begin{cases} b\,(1-\theta)\,\dfrac{\partial P}{\partial t} - \nabla_i \cdot (A \nabla_i P) = -b\,\theta\,\mathbb{L} * \dfrac{\partial \tilde{P}}{\partial t}, \\ \\ \tilde{P} = P - \mathbb{K} * \dfrac{\partial P}{\partial t} \end{cases} \tag{1.87}$$

The determination of the limit local and effective kernels K and $\mathbb{K}$ represents a new problem.

1.5.2 Nonlinear integral equation for the limit effective kernel

Then we obtain from (1.82a):

$$\mathbb{K} * K = K * K - \theta\, K * \mathbb{K} * \mathbb{K}'$$

or

$$\mathbb{K} = K - \theta\, \mathbb{K} * \mathbb{K}' \tag{1.88}$$

This is the nonlinear integral equation :

$$\mathbb{K} + \theta \int_0^t \mathbb{K}(\tau)\mathbb{K}'(t-\tau)d\tau = K \tag{1.89}$$

Its solution may be obtained in the explicit analytical form by Laplace transform: $\mathbb{K}(t) \to \overline{\mathbb{K}}(s)$:

$$\overline{\mathbb{K}} + \theta\,\overline{\mathbb{K}}\,\left(s\,\overline{\mathbb{K}} - 1\right) = \overline{K}$$

Then

$$\overline{\mathbb{K}} = \frac{1}{2s\,\theta}\left(\theta - 1 + \sqrt{(1-\theta)^2 + 4s\,\theta\,\overline{K}}\right) \tag{1.90}$$

This equations relates $\mathbb{K}$ with the function K, which should be determined.

1.5.3 Nonlinear equation for the limit local kernel K

From (1.82c) it follows for $k \geq 1$:

$$T_k' * K - \theta\, T_k' * \mathbb{K} * \mathbb{K}' = -T_k * K \frac{A\mu_k}{b\,(1-\theta)}, \qquad T_k|_{t=0} = 1$$

Using (1.88), we obtain:

$$T_k' * K - T_k' * (K - \mathbb{K}) = -T_k * K \frac{A\mu_k}{b\,(1-\theta)}, \qquad T_k|_{t=0} = 1$$

or

$$T_k' * \mathbb{K} = -T_k * K \frac{A\mu_k}{b\,(1-\theta)}, \qquad T_k|_{t=0} = 1$$

Applying the Laplace transform (with the parameter s) and using (1.90), we obtain the following explicit result for the spectral functions:

$$(s\overline{T}_k - 1)\frac{1}{2s\,\theta}\left(\theta - 1 + \sqrt{(1-\theta)^2 + 4s\,\theta\,\overline{K}}\right) = -\overline{T}_k\overline{K}\frac{A\mu_k}{b\,(1-\theta)}$$

or

$$\overline{T}_k\left[\frac{1}{2\theta}\left(\theta - 1 + \sqrt{(1-\theta)^2 + 4s\,\theta\,\overline{K}}\right) + \frac{A\mu_k\overline{K}}{b\,(1-\theta)}\right] = \frac{1}{2s\,\theta}\left(\theta - 1 + \sqrt{(1-\theta)^2 + 4s\,\theta\,\overline{K}}\right)$$

$$\overline{T}_k(s) = \frac{\theta - 1 + \sqrt{(1-\theta)^2 + 4s\,\theta\,\overline{K}}}{s\left(\theta - 1 + \dfrac{2\alpha A\mu_k\overline{K}}{b} + \sqrt{(1-\theta)^2 + 4s\,\theta\,\overline{K}}\right)}$$

This is the equation with respect to the Fourier-components T_k of the function K which contains the function K it-self. This proves the nonlinear character of the system equation for K.

Substituting this relation in (1.82b), one obtain the closed nonlinear equation for kernel K:

$$\overline{K}(s) = \frac{6}{\pi^2}\sum_{k=1}^{\infty}\frac{\theta - 1 + \sqrt{(1-\theta)^2 + 4s\,\theta\,\overline{K}}}{sk^2\left(\theta - 1 + \dfrac{2\alpha A\mu_k\overline{K}}{b} + \sqrt{(1-\theta)^2 + 4s\,\theta\,\overline{K}}\right)} \tag{1.91}$$

Once this equation is solved, we can solve the effective kernel by using (1.90).

1.5.4 Iterative method of solving the nonlinear equation for K

The kernel $K(t)$ represents a decreasing function located between 0 and 1. In the zero approximation we can assume that $K(t) \approx \delta(t)$, then $\overline{K} = 1$. Substituting this function in the right-hand side of (1.91) we

will obtain the first approximation for $\overline{K}$:

$$\overline{K}(s) \approx \frac{6}{\pi^2} \sum_{k=1}^{\infty} \frac{\theta - 1 + \sqrt{(1-\theta)^2 + 4s\,\theta}}{sk^2 \left(\theta - 1 + \dfrac{2\alpha A \mu_k}{b} + \sqrt{(1-\theta)^2 + 4s\,\theta} \right)} \tag{1.92}$$

Substituting this function in the right-hand side of (1.91), we obtain the second approximation and so on.

The solution was obtained numerically. The convergence of successive approximations is shown in Fig. 1.11.

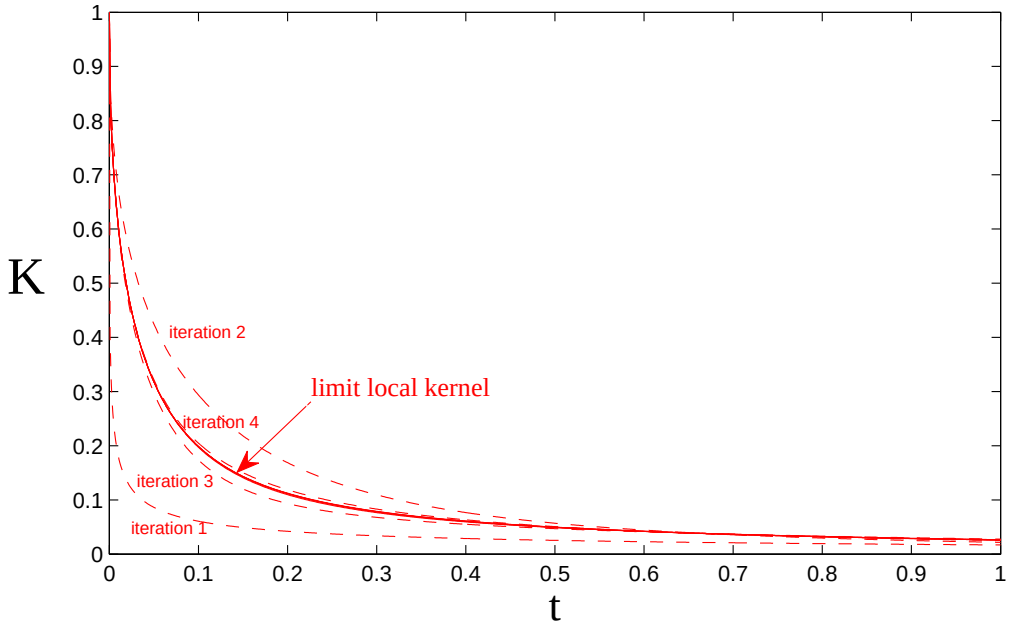

Figure 1.11: Convergence of the iterative method of solving the nonlinear equation (1.91)

After obtaining the local kernel $K(t)$ it is possible to calculate the effective kernel by using (1.90). The limit kernels $K(t)$ and $\mathbb{K}(t)$ are shown in Fig. 1.12.

1.5.5 Behavior of the limit model in small and large time

For small time $t \to 0$ we have $s \to \infty$, the first iteration becomes:

$$\lim_{s\to\infty} \overline{K}(s) \approx \lim_{s\to\infty} \frac{6}{\pi^2} \sum_{k=1}^{\infty} \frac{\theta - 1 + \sqrt{(1-\theta)^2 + 4s\,\theta}}{sk^2 \left(\theta - 1 + \dfrac{2\alpha A \mu_k}{b} + \sqrt{(1-\theta)^2 + 4s\,\theta} \right)} \tag{1.93}$$

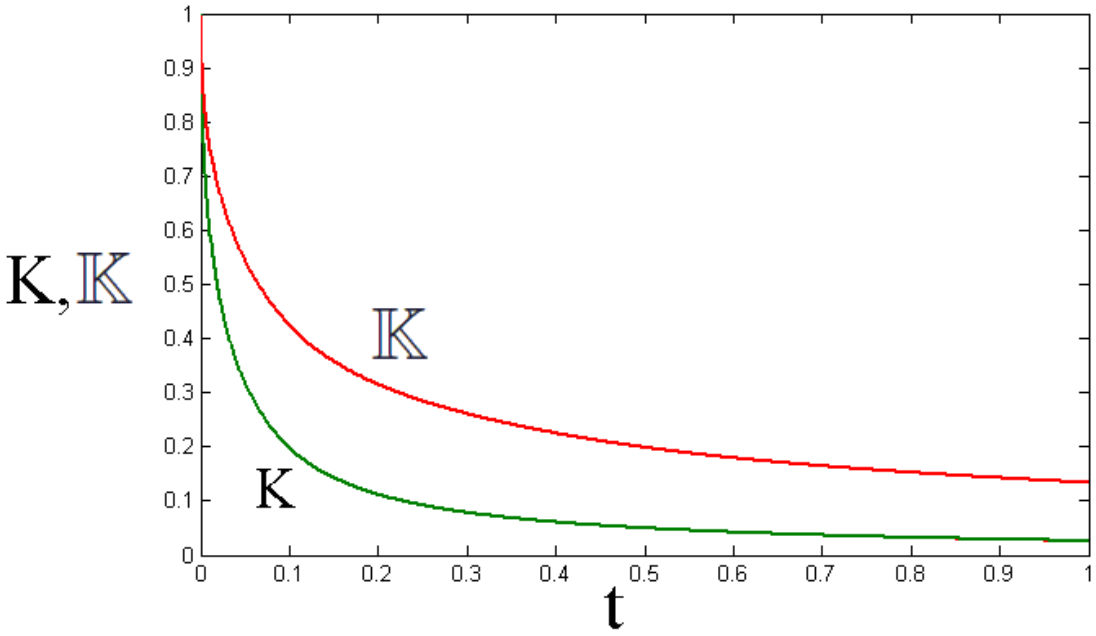

Figure 1.12: Limit local and effective kernels calculated numerically for $\theta = 0.8$

1.5.6 Comparison of the limit model with hierarchical model for finite-scale medium

The kernels calculated by using the recurrent equations (1.82) for a medium having a finite number of scales, should converge to the limit kernels calculated by using (1.91) and (1.90). The comparison of the results obtained if presented in Fig. 1.13 and 1.14.

The hierarchical model converges well to the limit model. For local kernels, four scales are sufficient to reach the result proper to an infinite number of scales. For the efficient kernel, five scales are sufficient.

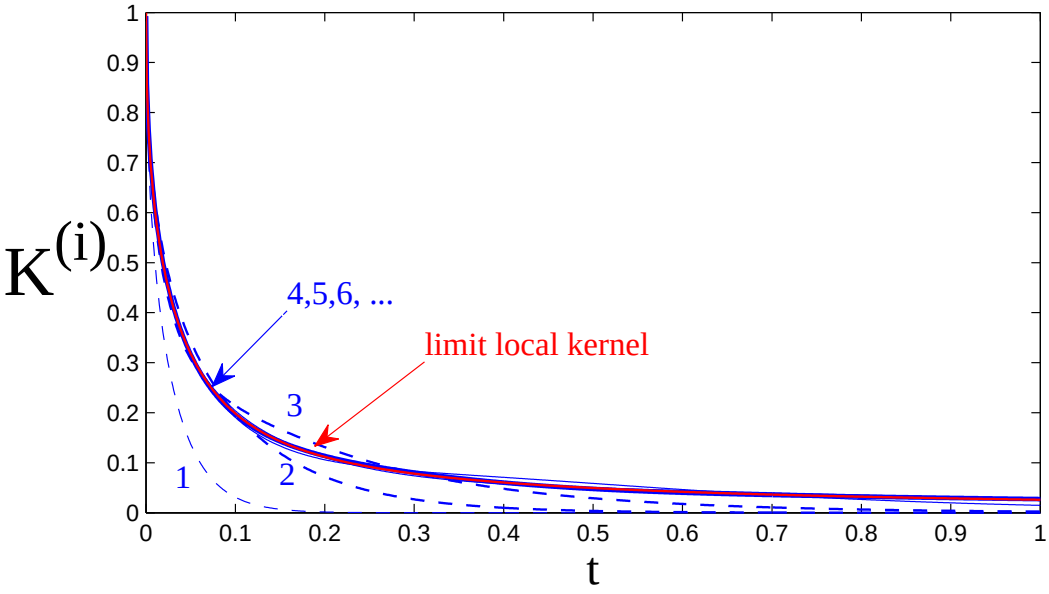

Figure 1.13: Comparison of the hierarchical local kernels (the blue curves) and the limit local kernel (the red curve) for $\theta = 0.8$

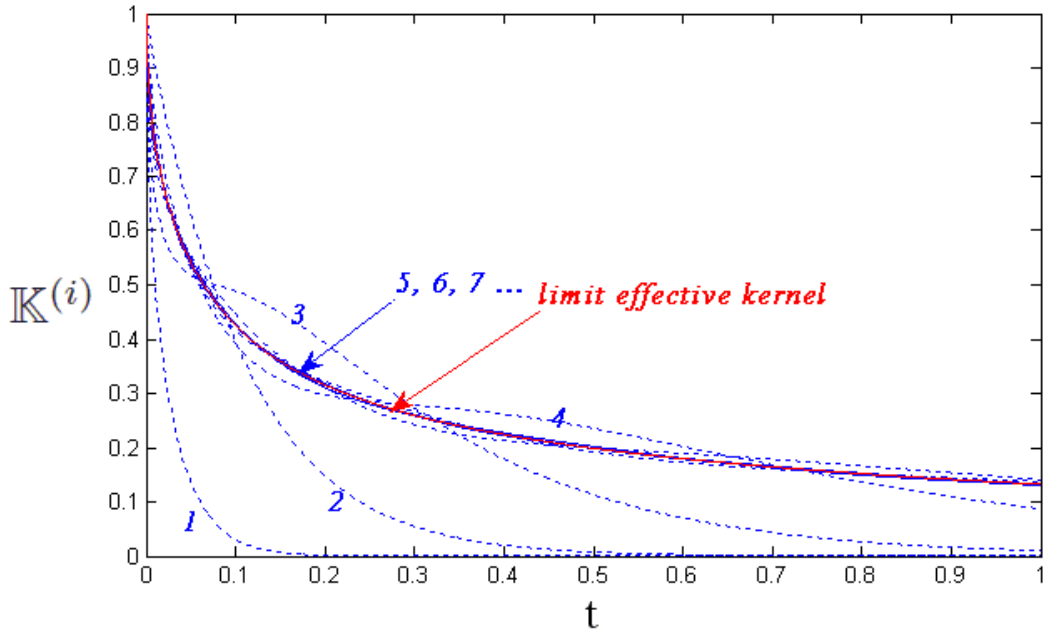

Figure 1.14: Comparison of the hierarchical effective kernels (the blue curves) and the limit effective kernel (the red curve) for $\theta = 0.8$

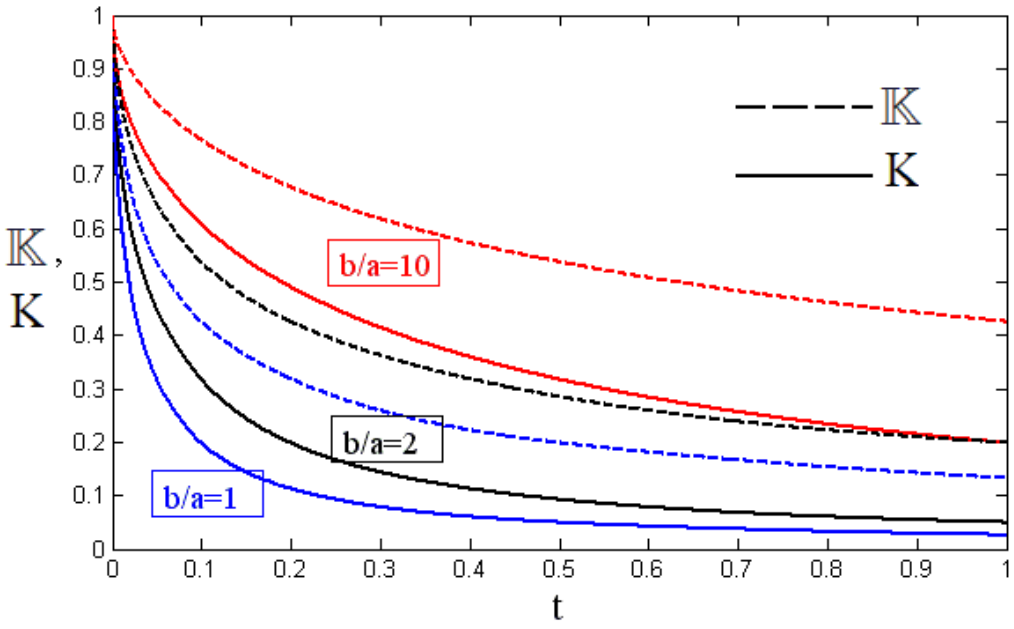

Figure 1.15: Comparison of the local limit kernel K and the limit effective kernel $\mathbb{K}$ for different properties of block, $\theta = 0.8$

Chapter 2

Homogenization of flow in two-scale fractured medium

2.1 Formulation of the problem

2.1.1 Background and objectives

The results obtained in the previous chapter for the limit kernels represent the system of nonlinear integro-differential equations. Its solution may be obtained in terms of the Laplace transform. For fractured media, it is possible to go more in depth and to obtain analytical results for the effective kernels.

The main difference of fractured media from double porosity media consists of the fact that the fractures ar very thin, which means the appearance of a new small parameter. It changes the structure of asymptotic expansions and, consecutively, the macroscale behavior. In particular, the high internal permeability of each fracture does not ensure its dominant role in the transport process. If the fracture aperture is too thin, then its effective permeability can be equal or even lower than the permeability of blocks. In particular, if the local permeability of a fracture and a block is 1 and ω respectively, the fracture aperture is h, then the contribution of fractures and blocks into the transport process will be identical if $\omega \sim h$. In this case the medium behaves as homogeneous one, such a behavior is sufficiently trivial. So the regimes of flow will depend on the ratio between the local permeability of blocks and the effective permeability of fractures: ω/h. Respectively, the appearance of the nonlocal effects, which are the main object of study of this thesis, will correspond to the case $\omega/h \sim \varepsilon^2$. This corresponds to the situation when $\omega \sim \varepsilon^{2+\alpha}$ and $h \sim \varepsilon^{\alpha}$, where $\alpha > 0$.

But in this case, it is easy to show that each block will be perturbed only within a narrow boundary layer just in contact with the fracture. In this boundary layer each block works as a source with respect to the flow in fracture. This changes qualitatively the structure of Green functions of the operators describing flow in a block, and the respective structure of the kernels in macroscopic equations. It will be shown that such class of media corresponds to Abel kernels which allows for analytical solutions of the corresponding integral equations.

The appearance of the boundary layer and the macroscopic model corresponding to this case was obtained in [Pankratov and Rybalko, 2003]. In order to develop the general method of upscaling which will be applied next for three-scale fractured media in chapter 3 and to reveal some non-formal physical aspects related to various aspects of the homogenization of fractured media, we will perform the homogenization in this chapter, by applying the technique of two-scale asymptotic expansions.

2.1.2 Medium geometry

We consider only the case of axis-symmetrical fractures representing the result of subtracting the central parallelepiped ("the block") from the unit cubic cell Fig. 2.1.

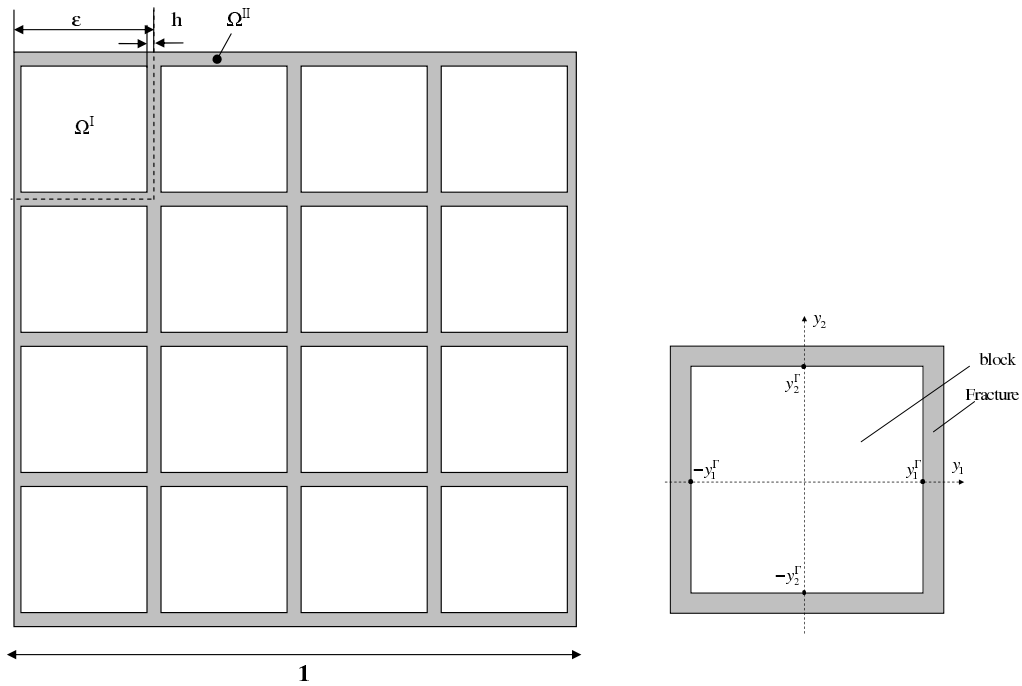

(1) (2)

Figure 2.1: Structure of a two-scale fractured medium (1) and the extended unite cell Y (2)

The flow equations in blocks, fractures and at the interfaces between blocks and fractures are:

$$b^{(1)}\frac{\partial p^1}{\partial t} = \varepsilon^{2+\alpha}\nabla_x \cdot \left(a^{(1)}\nabla_x p^1\right), \qquad x \in \Omega^1 \tag{2.1a}$$

$$b^{(2)}\frac{\partial p^2}{\partial t} = \nabla_x \cdot \left(a^{(2)}\nabla_x p^2\right), \qquad x \in \Omega^2 \tag{2.1b}$$

The following ratios between parameters are assumed:

$$\frac{K^{(1)}}{K^{(2)}} = \varepsilon^{2+\alpha}, \qquad \frac{h}{\varepsilon} = \varepsilon^{\alpha/2}, \qquad \alpha > 1 \tag{2.2}$$

2.1.3 Two-scale formulation

Two-scale formulation through $p(x,y,t)$, $y = x/\varepsilon$ gives:

$$b^{(1)}\frac{\partial p^1}{\partial t} = \varepsilon^{\alpha}\nabla_y \cdot \left(a^{(1)}\nabla_y p^1\right) + \varepsilon^{\alpha+1}\left[\nabla_y \cdot \left(a^{(1)}\nabla_x p^1\right) + \nabla_x \cdot \left(a^{(1)}\nabla_y p^1\right)\right] + \\ +\varepsilon^{\alpha+2}\nabla_x \cdot \left(a^{(1)}\nabla_x p^1\right), \qquad x \in \Omega^1, \quad y \in Y^1 \tag{2.3a}$$

$$b^{(2)}\frac{\partial p^2}{\partial t} = \frac{1}{\varepsilon^2}\nabla_y \cdot \left(a^{(2)}\nabla_y p^2\right) + \frac{1}{\varepsilon}\left[\nabla_y \cdot \left(a^{(2)}\nabla_x p^2\right) + \nabla_x \cdot \left(a^{(2)}\nabla_y p^2\right)\right] + \\ \nabla_x \cdot \left(a^{(2)}\nabla_x p^2\right), \qquad x \in \Omega^2, \quad y \in Y^2 \tag{2.3b}$$

$$p^1, p^2\big|_{t=0} = p^0 \tag{2.3c}$$

$$p^1\big|_{\Gamma} = p^2\big|_{\Gamma} \tag{2.3d}$$

$$\left(\frac{1}{\varepsilon}a^{(2)}\nabla_y p^2 + a^{(2)}\nabla_x p^2\right)\vec{n}\Big|_{\Gamma} = \varepsilon^{\alpha+2}\left(\frac{1}{\varepsilon}a^{(1)}\nabla_y p^1 + a^{(1)}\nabla_x p^1\right)\vec{n}\Big|_{\Gamma} \tag{2.3e}$$

$$p^2 \quad \text{is} \quad y-\text{periodic} \tag{2.3f}$$

2.1.4 Integral relation

If we average equations (2.3) over the entire cell Y, then we will obtain:

$$\left\langle b^{(2)}\frac{\partial p^2}{\partial t}\right\rangle_{Y^2} + \left\langle b^{(1)}\frac{\partial p^1}{\partial t}\right\rangle_{Y^1} = \nabla_x \cdot \left\langle \frac{1}{\varepsilon}a^{(2)}\nabla_y p^2 + a^{(2)}\nabla_x p^2\right\rangle_{Y^2} + \varepsilon^{1+\alpha}... \tag{2.4}$$

Herein we have taken into account for the condition (2.3e) and the condition of a periodic function due to which the integral over the external boundary in zero.

2.1.5 Singular behavior, boundary layer in the blocks

When $\varepsilon \to 0$ the equation (2.3a) loses the second-derivative term w.r.t. y and changes the type. Due to this it is impossible to satisfy the conditions at the block boundary. So for the formal regular asymptotic expansion of p^1, we obtain the problem described by an ordinary differential equation

$$b^{(1)}\frac{\partial p^1}{\partial t} = 0\,, \quad y \in Y^1; \qquad p^1\big|_{t=0} = p^0$$

which has a trivial solution:

$$p^1 \equiv p^0 \tag{2.5}$$

in the block, i.e. the solution remains unperturbed. It is clear that such a situation corresponds to the block center, but to the block boundary. We will call such a solution "external solution". The fact that

the external solution does not satisfy the conditions at the block boundary means that the problem in the block has a thin boundary layer just near the boundary, in which equation (2.3a) keeps the term with the second derivative w.r.t. y, Fig. 2.2. Based on the method of singular perturbations in differential

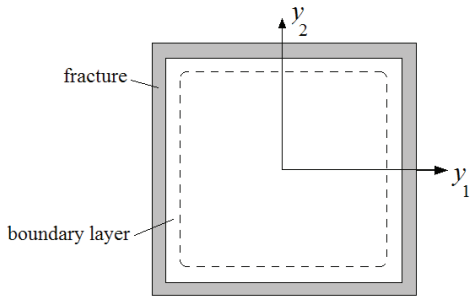

Figure 2.2: Boundary layer in the block Y^1

equations it is easy to find the size of the boundary layer: $\varepsilon^{\alpha/2}$. We introduce M boundary layers which are in contact with M fractures. In particular in 2D case $M = 4$. Since the overlapped areas between two layers are very small (equal to the square or cube of the boundary layer thickness), they may be neglected and then each layer may be considered independently of other ones. For an arbitrary independent part of the boundary layer, for example, the right vertical layer in Fig. 2.2, we introduce new local variable ξ which is of the order of unity within this layer:

$$\xi = \frac{y_1^\Gamma - y_1}{\sqrt{\varepsilon^\alpha}} \tag{2.6}$$

where y_1^Γ is the coordinate of the block boundary, as shown in Fig. 2.3. Axis ξ is oriented to the block center. We will designate this band of the boundary layer as $\mathcal{B} = \left\{0 < \xi < \frac{y_1^\Gamma - y_1^{b-l}}{\sqrt{\varepsilon^\alpha}},\ \ -s < y_2, y_3 < s\right\}$,

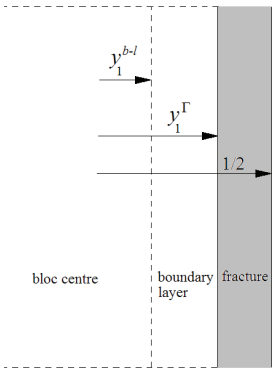

Figure 2.3: One vertical right-hand band of the boundary layer

$s \equiv \frac{1}{2}\left(1 - \frac{h}{\varepsilon}\right) = \frac{1}{2}\left(1 - \varepsilon^\beta\right)$, where $h = \varepsilon^{1+\beta}$ is the thickness of a fracture in coordinates x. We replace the microscale variables (y_1, y_2, y_3) by new variables within the boundary layer (ξ, y_2, y_3). Equation (2.3a)

reformulated through the new variables becomes:

$$b^{(1)}\frac{\partial p^1}{\partial t} = \frac{\partial}{\partial \xi}\left(a^{(1)}\frac{\partial p^1}{\partial \xi}\right) + \varepsilon^{\alpha}\sum_{i=2}^{3}\nabla_y \cdot \left(a^{(1)}\nabla_y p^1\right) + \varepsilon^{1+\alpha/2}... \,, \qquad y, \xi \in B \tag{2.7}$$

2.1.6 About the size of the boundary layer

The exact limit of the boundary layer does not exist, as it continuously transits into the intermediary zone whose size is much higher than $\sim \varepsilon^{\alpha/2}$ (the order of the formal size of the boundary layer), but is much lower than the size of the block ~ 1.

Let y_1^{b-l} be an estimation for the size of the boundary layer Fig. 2.3. So the distance between y_1^{Γ} and y_1^{b-l} is much higher than $\varepsilon^{\alpha/2}$, so that:

$$y_1^{\Gamma} - y_1^{b-l} = \varepsilon^{\alpha/2}a, \qquad \text{where} \quad a >> 1 \tag{2.8}$$

2.2 Homogenization

2.2.1 Asymptotic expansion

The pressure in block and fracture may be presented through the following asymptotic expansions:

$$p^1 = p_0^1\left(\xi, y_2, y_3, x_1, x_2, x_3, t\right) + O\left(\varepsilon^{\alpha} + \varepsilon^{1+\alpha/2}\right) \tag{2.9}$$

$$p^2 = p_0^2\left(x_1, x_2, x_3, t\right) + \varepsilon p_0^2\left(y_1, y_2, y_3, x_1, x_2, x_3, t\right) + O\left(\varepsilon^{1+\alpha/2}\right) \tag{2.10}$$

It is clear that the zero term p_0^1 depends on the local variables and on the boundary-layer variable, while the zero term p_0^2 depends only on the macroscale variables.

Substitution of this expansion into the problems (2.3) gives the following problems for the first terms:

- for p_0^1:

$$\begin{cases} b^{(1)}\dfrac{\partial p_0^1}{\partial t} = \dfrac{\partial}{\partial \xi}\left(a^{(1)}\dfrac{\partial p_0^1}{\partial \xi}\right), \quad \xi \in \mathcal{B} \quad x \in \Omega^1 \\ \\ p^1\big|_{t=0} = p^0, \qquad p_0^1\big|_{\xi=0} = p_0^2 \end{cases} \tag{2.11}$$

- for p_1^2:

$$\begin{cases} \nabla_y \cdot \left(a^{(2)}\nabla_y p_1^2\right) + \nabla_y \cdot \left(a^{(2)}\nabla_x p_1^2\right), \quad y \in Y^2, \quad x \in \Omega^2 \\ \\ \left(a^{(2)}\nabla_y p_1^2 + a^{(2)}\nabla_x p_1^2\right)\vec{n}\Big|_{\Gamma} = 0 \\ p_1^2 \text{ is } \quad y-\text{periodic} \end{cases} \tag{2.12}$$

- for p_0^2 we obtain from the integral relation (2.4):

$$\left\langle b^{(2)}\right\rangle_{Y^2}\frac{\partial p_0^2}{\partial t} + \left\langle b^{(1)}\frac{\partial p_0^1}{\partial t}\right\rangle_{Y^1} = \nabla_x \cdot \left\langle a^{(2)}\nabla_y p_1^2 + a^{(2)}\nabla_x p_0^2\right\rangle_{Y^2} \tag{2.13}$$

2.2.2 Solution of the problem in Y^2

Similar to section 1.3.6, for p_1^2 we obtain the same result:

$$p_1^2\left(x, y, t\right) = \sum_{k=1}^{3}\psi_k\left(y\right)\frac{\partial p_0^2}{\partial y_k} + p_{10}^2\left(x, t\right) \tag{2.14}$$

where the functions $\psi_k(y)$, $k = 1, 2, 3$, are the solution of the cell problem:

$$\begin{cases} \nabla_y \cdot \left(a^{(2)} \nabla_y \psi_k \right) = -\nabla_y a^{(2)} \cdot \vec{e}_k, & y \in Y^2 \\ \psi_k \ \text{ is } y - \text{periodic} \\ \langle \psi_k \rangle_{Y^2} = 0 \end{cases} \tag{2.15}$$

where $\vec{e}_k$ is the unit vector along the axis y_k.

We consider the symmetrical case, so that all functions ψ_k will be identical. It is then sufficient to resolve a single cell problem for a fixed k.

Then the integral relation (2.13) takes the form:

$$\left\langle b^{(2)} \right\rangle_{Y^2} \frac{\partial p_0^2}{\partial t} + \left\langle b^{(1)} \frac{\partial p_0^1}{\partial t} \right\rangle_{Y^1} = \nabla_x \cdot \left(A^2 \nabla_x p_0^2 \right) \tag{2.16}$$

where

$$A^2 = \left\langle a^{(2)} \nabla_y \psi_1 + a^{(2)} \right\rangle_{Y^2} \tag{2.17}$$

is the effective permeability of the medium.

2.2.3 Solution of the local problem in block Y^1

Let us analyze problem (2.11):

$$b^{(1)} \frac{\partial p_0^1}{\partial t} = \frac{\partial}{\partial \xi} \left(a^{(1)} \frac{\partial p_0^1}{\partial \xi} \right), \qquad \xi \in \mathcal{B} \tag{2.18a}$$

$$p^1 \big|_{t=0} = p^0 \tag{2.18b}$$

$$p_0^1 \big|_{\xi=0} = p_0^2 \tag{2.18c}$$

This problem needs an additional condition which determines the smooth matching between the boundary layer expansion and the exterior expansion (2.5). Due to the exponential behaviour of the solutions of (2.18) along ξ, such a condition is:

$$p_0^1 \big|_{\xi \to \infty} = p^0 \tag{2.18d}$$

The solution is obtained through the Duhamel integral as the convolution of the boundary condition (2.18c) with the solution of the auxiliary problem with a constant boundary condition:

$$p_0^1 - p^0 = \int_0^t \frac{\partial \left(p_0^2(\xi, \tau) - p^0 \right)}{\partial \tau} u(\xi, t - \tau) \, d\tau = - \int_0^t \left(p_0^2 - p^0 \right) \frac{\partial u(\xi, t - \tau)}{\partial \tau} d\tau \tag{2.19}$$

where

$$b^{(1)} \frac{\partial u}{\partial t} = \frac{\partial}{\partial \xi} \left(a^{(1)} \frac{\partial u}{\partial \xi} \right), \quad y \in Y^1 \tag{2.20}$$

$$u|_{t=0} = 0, \qquad u|_{\xi=0} = 1, \qquad u|_{\xi\to\infty} = 0 \tag{2.21}$$

The solution of this problem is:

$$u = 1 - \operatorname{erf}\left(\frac{\xi}{2\sqrt{Dt}}\right), \qquad D \equiv \frac{a^{(1)}}{b^{(1)}}, \qquad \operatorname{erf}(s) \equiv \frac{2}{\sqrt{\pi}}\int\limits_0^s e^{-v^2}dv \tag{2.22}$$

Then

$$\frac{\partial u}{\partial t} = \frac{\xi}{2\sqrt{\pi D}}\frac{\mathrm{e}^{-\frac{\xi^2}{4Dt}}}{t^{3/2}} \tag{2.23}$$

So (2.19) yields:

$$p_0^1 - p^0 = -\frac{\xi}{2\sqrt{\pi D}}\int\limits_0^t \left(p_0^2 - p^0\right)\frac{\mathrm{e}^{-\frac{\xi^2}{4D(t-\tau)}}}{(t-\tau)^{3/2}}d\tau \tag{2.24}$$

Thus, the pressure distribution in the block center is (2.5), while in the boundary layer it is (2.24). The transition between them is smooth within an intermediate zone, so the exact limit of the boundary layer does not exist.

2.3 Averaged model

Let us introduce the averaged pressure in blocks and in pressure:

$$P^1 = \frac{1}{\theta}\left\langle p_0^1 \right\rangle_{Y^1} + O\left(\varepsilon^{\alpha/2}\right), \quad P^1 = p_0^2 + O\left(\varepsilon^{1+\alpha/2}\right) \tag{2.25}$$

2.3.1 Average pressure in the block

One can prove that the averaged pressure over a block is determined as:

$$P_0^1 \equiv \frac{1}{\theta}\left\langle p_0^1 \right\rangle_{Y^1} = p^0 + \varepsilon^{\alpha/2}\lambda \int\limits_0^t \frac{\left(p_0^2 - p^0\right)}{\sqrt{t-\tau}} d\tau \tag{2.26}$$

where

$$\lambda = \begin{cases} \dfrac{8\left(y_2^\Gamma y_3^\Gamma + y_3^\Gamma y_1^\Gamma + y_1^\Gamma y_2^\Gamma\right)}{\theta}\sqrt{\dfrac{a^{(1)}}{\pi b^{(1)}}}, & \text{for the case of axis - symmetrical fractures} \\ \dfrac{6}{\theta^{1/3}}\sqrt{\dfrac{a^{(1)}}{\pi b^{(1)}}}, & \text{when all fractures are identical} \end{cases} \tag{2.27}$$

Proof:

1°. For the average pressure we have:

$P_0^1 = \frac{1}{\left|Y^1\right|}\int\limits_{Y^1} p_0^1 dy = \frac{1}{\theta}\left(\int\limits_{\substack{Block\\centre}} p_0^1 dy + \int\limits_{\substack{Bound.\\layer}} p_0^1 dy\right) = \frac{1}{\theta}\left(\int\limits_{\substack{Block\\centre}} p^0 dy + \int\limits_{\substack{Bound.\\layer}} p_0^1 dy\right)$

taking into account equation (2.5). Herein $\left|Y^1\right| = \theta$ is the volume fraction of the blocks. This may be presented in the equivalent form:

$$P_0^1 = \frac{1}{|Y^1|}\int\limits_{Y^1} p_0^1 dy = \frac{1}{\theta}\left(\int\limits_{Y^1} p^0 dy + \int\limits_{\substack{Bound.\\Layer}} \left(p_0^1 - p^0\right) dy\right) = p^0 + \frac{1}{\theta}\int\limits_{\substack{Bound.\\Layer}} \left(p_0^1 - p^0\right) dy \tag{2.28}$$

2°. In turn, the boundary layer consists of thin bands. It is sufficient to determine one vertical right-hand band we have analyzed in the previous section: $\left\{y_1^{b-l} < y_1 < y_1^\Gamma; \quad -y_2^\Gamma < y_2 < y_2^\Gamma, \quad -y_3^\Gamma < y_3 < y_3^\Gamma\right\}$ as shown in Fig. 2.3.

In terms of variable ξ equation (2.6) the considered element of the boundary layer is:

$$\left\{0 < \xi < a, \quad -y_2^\Gamma < y_2 < y_2^\Gamma, \quad -y_3^\Gamma < y_3 < y_3^\Gamma\right\} \tag{2.29}$$

3°. To calculate the average pressure it is sufficient to calculate the last integral in (2.28)along one element of the boundary layer:

$$\int\limits_{\substack{Element\\ of\ Bound.\\ Layer}} \left(p_0^1 - p^0\right) dy = \int\limits_{y_1^{b-l}}^{y_1^\Gamma} \int\limits_{-y_2^\Gamma}^{y_2^\Gamma} \int\limits_{-y_3^\Gamma}^{y_3^\Gamma} \left[p_0^1\left(y_1, y_2, y_3, t\right) - p^0\right] dy_1 dy_2 dy_3 =$$

$$-\varepsilon^{\alpha/2} \int\limits_{a}^{0} \int\limits_{-y_2^\Gamma}^{y_2^\Gamma} \int\limits_{-y_3^\Gamma}^{y_3^\Gamma} \left[p_0^1\left(\xi, y_2, y_3, t\right) - p^0\right] d\xi dy_2 dy_3 = 4\varepsilon^{\alpha/2} y_2^\Gamma y_3^\Gamma \int\limits_{0}^{a} \left[p_0^1\left(\xi, t\right) - p^0\right] d\xi$$

4°. The last integral is easily calculated from (2.24):

$$\int\limits_{0}^{a} \left[p_0^1\left(\xi, t\right) - p^0\right] d\xi = \frac{\sqrt{D}}{\sqrt{\pi}} \int\limits_{0}^{t} \frac{\left(p_0^2 - p^0\right)}{\left(t-\tau\right)^{1/2}} \left(1 - \mathrm{e}^{-\frac{a^{(2)}}{4D(t-\tau)}}\right) d\tau \tag{2.30}$$

because:

$$\int\limits_{0}^{a} \left[p_0^1\left(\xi, t\right) - p^0\right] d\xi = -\frac{1}{2\sqrt{\pi D}} \int\limits_{0}^{t} \frac{\left(p_0^2 - p^0\right)}{\left(t-\tau\right)^{3/2}} \left(\int\limits_{0}^{a} \xi \mathrm{e}^{-\frac{\xi^2}{4D(t-\tau)}} d\xi\right) d\tau$$

and

$$\int\limits_{0}^{a} \xi \mathrm{e}^{-\frac{\xi^2}{4D(t-\tau)}} d\xi = -2D(t-\tau) \int\limits_{0}^{-\frac{a^{(2)}}{4D(t-\tau)}} \mathrm{e}^{-\frac{\xi^2}{4D(t-\tau)}} d\left(-\frac{\xi^2}{4D(t-\tau)}\right) = 2D(t-\tau)\left(1 - \mathrm{e}^{-\frac{a^{(2)}}{4D(t-\tau)}}\right)$$

Taking into account that $a >> 1$ according to (2.8), we obtain:

$$\int\limits_{0}^{a} \left[p_0^1\left(\xi, t\right) - p^0\right] d\xi = \frac{\sqrt{D}}{\sqrt{\pi}} \int\limits_{0}^{t} \frac{\left(p_0^2 - p^0\right)}{\left(t-\tau\right)^{1/2}} d\tau$$

5°. Definitely, the average pressure in the block is according to (2.28):

$$P_0^1 = p^0 + \frac{1}{\theta} \int\limits_{\substack{Bound.\\ Layer}} \left(p_0^1 - p^0\right) dy = p^0 + \frac{8\varepsilon^{\alpha/2}}{\theta} \int\limits_{0}^{a} \left[p_0^1\left(\xi, t\right) - p^0\right] d\xi \sum_{i,j} y_i^\Gamma y_j^\Gamma =$$

$$= p^0 + \frac{8\varepsilon^{\alpha/2} \sum\limits_{i,j} y_i^\Gamma y_j^\Gamma \sqrt{D}}{\sqrt{\pi}\,\theta} \int\limits_{0}^{t} \frac{\left(p_0^2 - p^0\right)}{\left(t-\tau\right)^{1/2}} d\tau$$

Therefore:

$$P_0^1 = p^0 + \frac{8\varepsilon^{\alpha/2}\left(y_2^\Gamma y_3^\Gamma + y_3^\Gamma y_1^\Gamma + y_1^\Gamma y_2^\Gamma\right)}{\theta} \sqrt{\frac{a^{(1)}}{\pi b^{(1)}}} \int\limits_{0}^{t} \frac{\left(p_0^2 - p^0\right)}{\sqrt{t-\tau}} d\tau$$

If $y_1^\Gamma = y_2^\Gamma = y_3^\Gamma \equiv y^\Gamma$, then $\theta = 8\left(y^\Gamma\right)^3$, and we obtain:

$$P_0^1 = p^0 + \frac{6\varepsilon^{\alpha/2}}{\theta^{1/3}}\sqrt{\frac{a^{(1)}}{\pi b^{(1)}}}\int\limits_0^t \frac{\left(p_0^2 - p^0\right)}{\sqrt{t-\tau}}d\tau$$

which proves (2.26) - (2.27).

2.3.2 Other form of the averaged equation in blocks

From (2.25), it is possible to presents equation (2.26) in another form, while taking into account for the zero approximation only: :

$$P^1 = p^0 + \varepsilon^{\alpha/2}\lambda\int\limits_0^t \frac{P^2 - p^0}{\sqrt{t-\tau}}d\tau$$

Integration by parts in (2.26) leads to:

$$P^1 = p^0 + 2\varepsilon^{\alpha/2}\lambda\int\limits_0^t \frac{\partial P^2}{\partial\tau}\sqrt{t-\tau}\,d\tau \tag{2.31}$$

Another form may be obtained from the identity:

$$p^0 = P^2 - \int\limits_0^t \frac{\partial P^2}{\partial\tau}d\tau$$

which gives:

$$P^1 = P^2 - \int\limits_0^t \frac{\partial P^2}{\partial\tau}K\left(t-\tau\right)\,d\tau, \qquad K(t) \equiv 1 - 2\varepsilon^{\alpha/2}\lambda\sqrt{t} \tag{2.32}$$

which is formally identical to double-porosity media but with different kernel $K(t)$.

2.3.3 Averaged equation in fractures

The equation averaged over fractures results from (2.16):

$$\left\langle b^{(2)}\right\rangle_{Y^2}\frac{\partial P^2}{\partial t} + \left\langle b^{(1)}\right\rangle_{Y^1}\frac{\partial P^1}{\partial t} = \operatorname{div}\left(A^{(2)}\operatorname{grad} P^2\right)$$

where $A^{(2)}$ is defined as (2.17) and is the effective permeability of fractures averaged over the entire cell Y.

Let $\widehat{B}^{(2)}$ and $\widehat{A}^{(2)}$ be the porosity and permeability averaged over fractures Y^2 only, and $\widehat{B}^{(1)}$ is the porosity of blocks averaged over blocks:

$$\widehat{B}^{(2)} \equiv \frac{1}{|Y^2|}\int\limits_{Y^2} b^{(2)}dy, \quad \widehat{B}^{(1)} \equiv \frac{1}{|Y^1|}\int\limits_{Y^1} b^{(1)}dy, \quad \text{and so on...}$$

Then we have:

$$\left\langle b^{(2)} \right\rangle_{Y^2} \equiv \int\limits_{Y^2} b^{(2)}\, dy = \left|Y^2\right| \widehat{B}^{(2)}, \qquad A^{(2)} = \left|Y^2\right| \widehat{A}^{(2)}, \quad \left\langle b^{(1)} \right\rangle_{Y^1} = \left|Y^1\right| \widehat{B}^{(1)} \tag{2.33}$$

where $1-\theta = \left|Y^2\right|$ is the volume of the fracture in the cell Y.

Then the averaged equation can be rewritten in the following form:

$$\left|Y^2\right| \widehat{B}^{(2)} \frac{\partial P^2}{\partial t} + \left|Y^1\right| \widehat{B}^{(1)} \frac{\partial P^1}{\partial t} = \operatorname{div}\left(\left|Y^2\right| \widehat{A}^{(2)} \operatorname{grad} P^2\right)$$

The volumes of a block and a fracture are easy to calculate for cubic blocks, i.e. for identical thickness h of all fractures:

$$\begin{gathered} \left|Y^1\right| = \left(1-\tfrac{h}{\varepsilon}\right)^m = \left(1-\varepsilon^{\alpha/2}\right)^m \sim 1 - m\,\varepsilon^{\alpha/2} + ..., \\ \left|Y^2\right| = 1 - \left|Y^1\right| = 1 - \left(1-\varepsilon^{\alpha/2}\right)^m \sim m\,\varepsilon^{\alpha/2} + ... \end{gathered} \tag{2.34}$$

where m is the space dimension ($m = 2$ or 3). Taking into account for (2.34) we get:

$$\frac{\left|Y^1\right|}{\left|Y^2\right|} \sim \frac{1 - m\,\varepsilon^{\alpha/2} + ...}{m\,\varepsilon^{\alpha/2} + ...} = \frac{1}{m}\varepsilon^{-\alpha/2} + ... \tag{2.35}$$

Then the averaged equation in fractures becomes:

$$\widehat{B}^{(2)} \frac{\partial P^2}{\partial t} = \operatorname{div}\left(\widehat{A}^{(2)} \operatorname{grad} P^2\right) - \frac{\widehat{B}^{(1)}}{m} \varepsilon^{-\alpha/2} \frac{\partial P^1}{\partial t} \tag{2.36}$$

Substituting (2.31):

$$\widehat{B}^{(2)} \frac{\partial P^2}{\partial t} = \operatorname{div}\left(\widehat{A}^{(2)} \operatorname{grad} P^2\right) - 2\gamma\lambda \widehat{B}^{(1)} \frac{\partial}{\partial t} \left(\int\limits_0^t \frac{\partial P^2}{\partial \tau} \sqrt{t-\tau}\, d\tau \right)$$

$$\gamma = \frac{1}{m} = \begin{cases} \dfrac{1}{2}, & \text{for 2D case} \\ \dfrac{1}{3}, & \text{for 3D case} \end{cases}$$

Differentiating by parts:

$$\frac{\partial}{\partial t} \left(\int\limits_0^t \frac{\partial P^2}{\partial \tau} \sqrt{t-\tau}\, d\tau \right) = \frac{1}{2} \int\limits_0^t \frac{\partial P^2}{\partial \tau} \frac{1}{\sqrt{t-\tau}}\, d\tau$$

we obtain

$$\widehat{B}^{(2)} \frac{\partial P^2}{\partial t} = \operatorname{div}\left(\widehat{A}^{(2)} \operatorname{grad} P^2\right) - \gamma\lambda \widehat{B}^{(1)} \int\limits_0^t \frac{\partial P^2}{\partial \tau} \frac{1}{\sqrt{t-\tau}}\, d\tau \tag{2.37}$$

All terms of this model are of order 1. Physically this means the following: the very thin fractures stress flow and rend the effective flow to be very difficult (the flow term is small); but despite the large dimension

of a block, its permeability is so low that the exchange flow happens only in a very thin boundary layer. Due to this the flow through fractures and the exchange flow from blocks occurs to be of the same order.

2.3.4 Definite form of the averaged model

The definite form of the averaged equation becomes:

$$\widehat{B}^{(2)}\frac{\partial P^2}{\partial t} = \operatorname{div}\left(\widehat{A}^{(2)}\operatorname{grad} P^2\right) - \gamma\lambda\widehat{B}^{(1)}\int\limits_0^t \frac{\partial P^2}{\partial \tau}\frac{1}{\sqrt{t-\tau}}\,d\tau \tag{2.38}$$

This is the system of integro-differential equations with Abel's kernels.

Another equivalent form is:

$$\widehat{B}^{(2)}\frac{\partial P^2}{\partial t} = \operatorname{div}\left(\widehat{A}^{(2)}\operatorname{grad} P^2\right) - 2\gamma\lambda\widehat{B}^{(1)}\frac{\partial}{\partial t}\left(\int\limits_0^t \frac{\partial P^2}{\partial \tau}\sqrt{t-\tau}\,d\tau\right) \tag{2.39}$$

2.4 Example of using the averaged model

2.4.1 Problem of flow in an oil reservoir

As it has been shown in the previous section, the averaged macroscale equations of flow in a two scale fractured medium can be described through an integro-differential equation with Abel kernel.

Let us examine the problem of 1D flow to a single well in a bounded reservoir ($0 < X < l$). Let X and T_* be the coordinate and time. The well is placed at point $X = l$ and produce fluid at a given volumetric rate Q. The left-hand boundary of the reservoir $X = 0$ is impermeable. The initial state is unperturbed. The problem is formulated as:

$$\widehat{B}^{(2)}\frac{\partial P^2}{\partial T} = \frac{\partial}{\partial X}\left(\widehat{A}^{(2)}\frac{\partial P^2}{\partial X}\right) - \lambda\widehat{B}^{(1)}\int\limits_0^T \frac{\partial P^2}{\partial \tau}K\left(T-\tau\right)d\tau, \quad X \in (0,l),\ T \in (0,T_*) \tag{2.40}$$

$$P^2\Big|_{T=0} = P^0, \qquad \frac{\partial P^2}{\partial X}\Big|_{X=l} = 0, \qquad -DA^{(2)}\frac{\partial P^2}{\partial X}\Big|_{X=0} = -Q(T) \tag{2.41}$$

where D is the cross section, T_* is the time of the complete reservoir depletion which may be determined as $T_* = \dfrac{Dl\widehat{\phi}}{\bar{Q}}$, $\widehat{\phi}$ is the average porosity of the medium; the kernel K is defined as:

$$K(T) \equiv \frac{1}{\sqrt{T}}$$

Let us introduce dimensionless variables:

$$t = \frac{T}{T_*}, \qquad x = \frac{X}{l}, \qquad p = \frac{P^2}{P^0}$$

then the problem takes the form:

$$\begin{cases} \varepsilon\dfrac{\partial p}{\partial t} = \dfrac{\partial^2 p}{\partial x^2} - \varepsilon a\displaystyle\int\limits_0^t \frac{\partial p}{\partial \tau}K\left(t-\tau\right)d\tau \\ \\ p\Big|_{t=0} = 1, \qquad \dfrac{\partial p}{\partial x}\Big|_{x=0} = \varepsilon\gamma q(t), \qquad \dfrac{\partial p}{\partial x}\Big|_{x=1} = 0 \end{cases} \tag{2.42}$$

where

$$\varepsilon = \frac{l^2\widehat{B}^{(2)}}{T_*\widehat{A}^{(2)}} = \frac{T^*}{T_*} = \frac{l\widehat{B}^{(2)}\bar{Q}}{D\widehat{A}^{(2)}\widehat{\phi}}, \qquad a = \frac{\lambda\sqrt{T_*}\widehat{B}^{(1)}}{\widehat{B}^{(2)}}, \qquad \gamma = \frac{\widehat{\phi}}{\widehat{B}^{(2)}P^0}$$

where $T^* = \dfrac{l^2 \widehat{B}^{(2)}}{\widehat{A}^{(2)}}$ is the perturbation propagation time in the reservoir. Parameter γ is the dimensionless compressibility coefficient for liquid.

2.4.2 Asymptotic expansion at $\varepsilon \to 0$

In practice the perturbation propagation time is of order of several hours, while the depletion time constitutes several tens years. Then parameter ε is small.

The problem is singularly perturbed, as the differential equation (2.42) changes the type when $\varepsilon \to 0$ and loses the initial condition.

The asymptotic valid for $t >> \varepsilon$ is obtained in the form of the regular asymptotic series:

$$p = p_0(t) + \varepsilon p_1(x,t) + \varepsilon^2 ...$$

The independence of the zero approximation of x is easy to show by substituting this expansion in the original equations.

As shown in [Panfilov, 1986], the technique of solution includes the introduction of the integral relation (similar to the homogenization technique) which is obtained by integrating Eq. (2.42) over the entire domain:

$$\varepsilon \frac{\partial \bar{p}}{\partial t} = \left.\frac{\partial p}{\partial x}\right|_{x=1} - \left.\frac{\partial p}{\partial x}\right|_{x=0} - \varepsilon a \int\limits_0^t \frac{\partial \bar{p}}{\partial \tau} K(t-\tau)\, d\tau \tag{2.43}$$

where:

$$\bar{p}(t) = \int_0^1 p(x,t) dx \tag{2.44}$$

is the average pressure.

Then we obtain:

$$\frac{d\overline{p}}{dt} + a \int\limits_0^t \frac{d\overline{p}}{d\tau} K(t-\tau)\, d\tau = -\gamma q \tag{2.45}$$

Substituting the asymptotic expansion in (2.42) and (2.45), we obtain:

- for the zero-th approximation:

$$\frac{dp_0}{dt} + a \int\limits_0^t \frac{dp_0}{d\tau} K(t-\tau)\, d\tau = -\gamma q \tag{2.46}$$

- for the first approximation:

$$\begin{cases} \dfrac{\partial^2 p_1}{\partial x^2} = -\gamma q; \\ \\ \left.\dfrac{\partial p_1}{\partial x}\right|_{x=0} = \gamma q, \qquad \left.\dfrac{\partial p_1}{\partial x}\right|_{x=1} = 0 \end{cases} \tag{2.47}$$

The solution of the latter problem is obtained immediately:

$$p_1 = \gamma q(t) \left[1 + x - \frac{x^2}{2} \right] \tag{2.48}$$

2.4.3 Solution of the problem for p_0

Reduction of the problem for p_0 to the Fredholm integral equation with Abel kernel

The integro-differential equation (2.46) with Abel kernel can be solved analytically.

Let us introduce the new variable:

$$z(t) = \frac{dp_0}{dt}$$

Then

$$z(t) + a \int_0^t z(\tau) \frac{d\tau}{\sqrt{t-\tau}} = -\gamma q(t) \tag{2.49}$$

This is the Fredholm integral equation which may be also presented as:

$$z(t) + az(t) * \frac{1}{\sqrt{t}} = -\gamma q(t) \tag{2.50}$$

Solution of the Fredholm equation

The analytical solution of Abel's integral equations is based on the property of the kernel:

$$\frac{1}{\sqrt{t}} * \frac{1}{\sqrt{t}} = \pi \tag{2.51}$$

Let us convolute both sides of (2.50) with $1/\sqrt{t}$ and use (2.51):

$$z(t) * \frac{1}{\sqrt{t}} + az(t) * \pi = -\gamma q(t) * \frac{1}{\sqrt{t}}$$

The first convolution may be removed by using (2.50):

$$-z(t) - \gamma q + \pi a^2 \int_0^t z(\tau) d\tau = -a\gamma q * \frac{1}{\sqrt{t}}, \qquad p^0 = 1$$

Returning to pressure p_0 we obtain:

$$-\frac{dp_0}{dt} - \gamma q + \pi a^2 (p_0 - 1) = -a\gamma q * \frac{1}{\sqrt{t}}$$

or

$$\frac{dp_0}{dt} - \pi a^2 p_0 = -\gamma q + a\gamma q * \frac{1}{\sqrt{t}} - \pi a^2$$

This is the first-order ODE which has the explicit solution, while taking into account the initial

condition:

$$p_0(t) = e^{\pi a^2 t} + \int_0^t R(\tau) e^{\pi a^2 (t-\tau)} d\tau, \qquad R(t) \equiv -\gamma q + a\gamma q * \frac{1}{\sqrt{t}} - \pi a^{(2)} \tag{2.52}$$

In particular case $q(t) = 1 = cte$:

$$p_0(t) = 1 - \frac{\gamma}{\pi a^2} \left[2a\sqrt{t} + e^{\pi a^2 t} \mathrm{erfc}\left(a\sqrt{\pi t}\right) - 1 \right] \tag{2.53}$$

2.4.4 Solution of the flow problem

Assembling (2.52) or (2.53) with (2.48), we obtain the definite solution of the original flow problem:

$$p(t)(x,t) = e^{\pi a^2 t} + \int_0^t \left(-\gamma q + a\gamma q * \frac{1}{\sqrt{\tau}} - \pi a^{(2)} \right) e^{\pi a^2 (t-\tau)} d\tau + \varepsilon \gamma q(t) \left[1 + x - \frac{x^2}{2} \right] \tag{2.54}$$

For constant production rate $q(t) = 1$:

$$p(t)(x,t) = 1 - \frac{\gamma}{\pi a^2} \left[2a\sqrt{t} + e^{\pi a^2 t} \mathrm{erfc}\left(a\sqrt{\pi t}\right) - 1 \right] + \varepsilon \gamma q(t) \left[1 + x - \frac{x^2}{2} \right] \tag{2.55}$$

The behavior of the averaged pressure $p_0(t)$ in time at a fixed point in space is shown in Fig. 2.4.

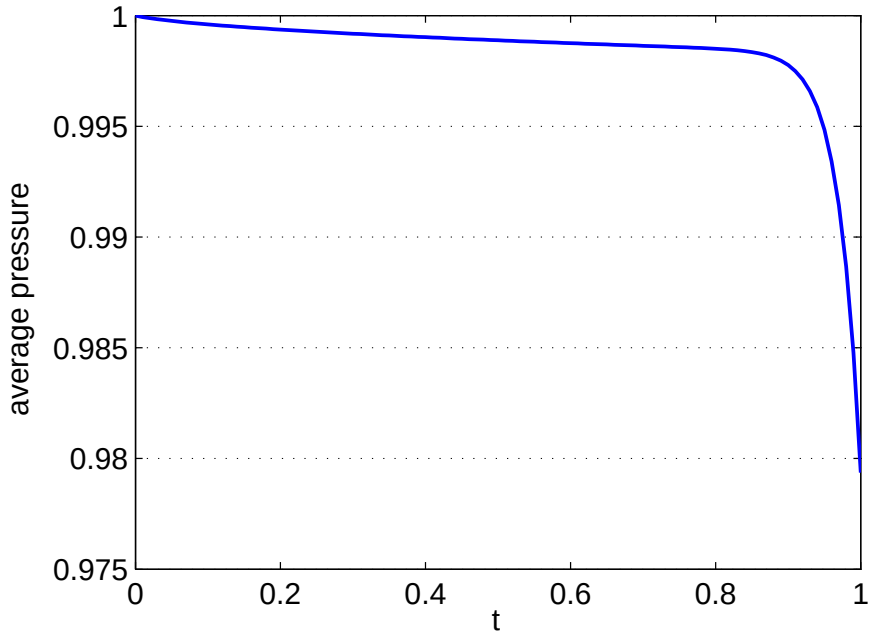

Figure 2.4: Average pressure in one dimensional fractured medium with narrow fractures, block volume fraction $\theta = 0.95$

As seen, during the major part of time, the average pressure (in fractures) remains practically constant due to the intensive mass exchange with blocks.

Chapter 3

Homogenization of three-scale fractured media

3.1 Classes of three-scale fractured media

3.1.1 Medium geometry

Let us consider a multiscale fractured medium similar to the medium determined in section (1.1.1), but having significantly different ratios between parameters. In particular, we assume that each medium Ω^i represents a network of thin fractures, except the lowest medium Ω^1 which is the system of uniform low permeable blocks. The blocks Ω^1 have no internal structure. Such a medium is presented in Fig. 3.1 for the case of three scales.

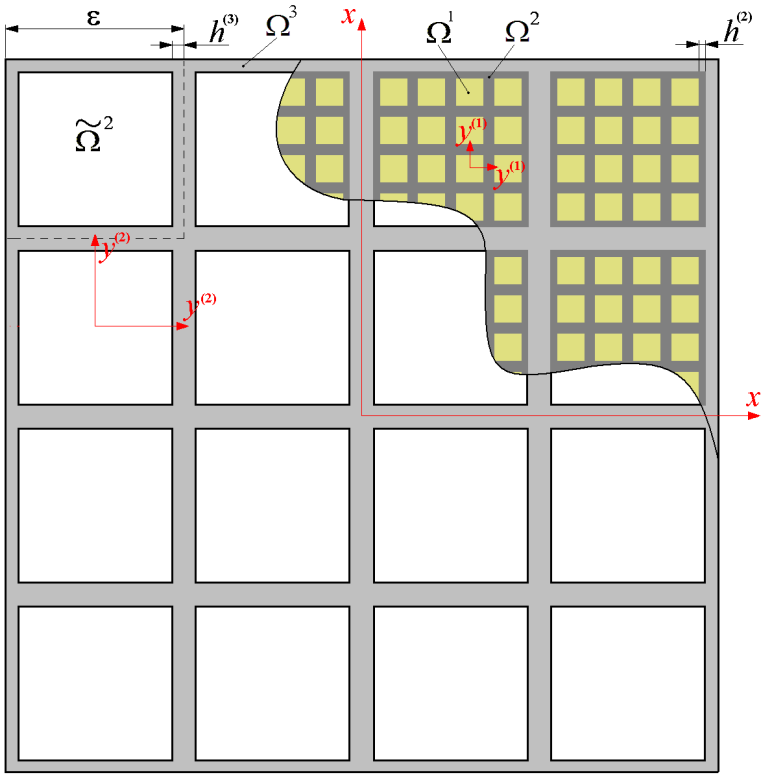

Figure 3.1: Three-scale fractured-porous medium

The term "fracture" is applied to a porous medium having the external form similar to a thin channel

We analyze a not self-similar process, so the infinite number of scales seems to be impossible to analyze. We consider only three-scale medium.

The period of the networks Ω^3 and Ω^2 are $\varepsilon << 1$ and ε^2 respectively.

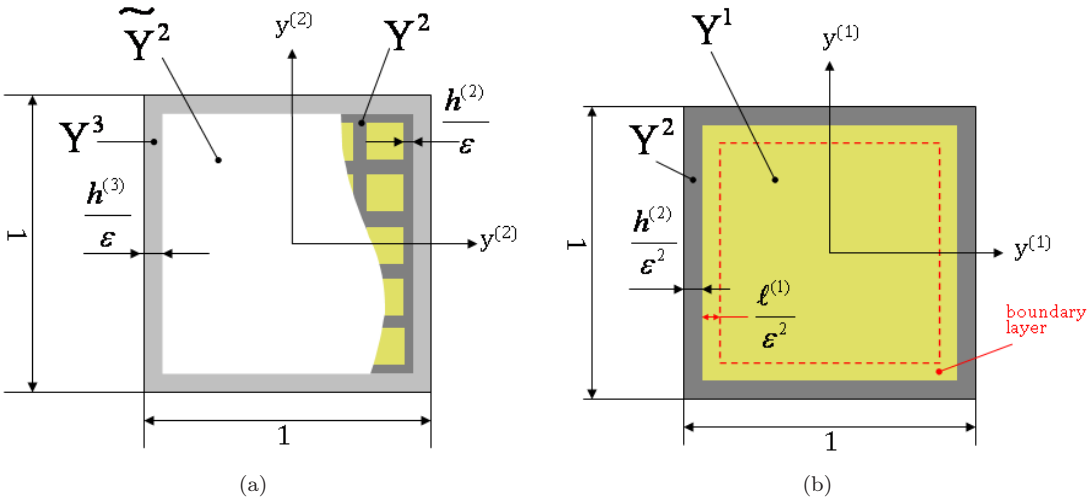

Figure 3.2: Elementary cells

We assume that the permeability of media monotonically increases from medium Ω^1 to medium Ω^3. The permeability of largest fracture is of order 1, the permeability of fractures Ω^2 is $\omega \leq 1$. The ratio between the permeability of fracture Ω^1 and Ω^2 is $\varepsilon^{2+\alpha}$, similar to the case analyzed for two-scale fractured-porous medium (chapter 2).

The half-thickness of a fracture Ω^i, $h^{(i)}$ is much smaller than the period of the same fracture network, so that: $h^{(i)}/\varepsilon^{4-i} = o(1)$, $\quad i = 3, 2$, or

$$h^{(3)} << \varepsilon, \qquad h^{(2)} << \varepsilon^2$$

where h^3 and h^2 are measured in the global coordinate system x shown in Fig. 3.1.

Along with the global system of coordinates x, we introduce two local coordinate frames $y^{(1)}$ and $y^{(2)}$ which correspond to two smallest scales Fig. 3.1 and are defined as:

$$y^{(2)} = \frac{x}{\varepsilon}, \qquad y^{(1)} = \frac{x}{\varepsilon^2}$$

They vary within the elementary cells $Y^3 \cup \widetilde{Y}^2$ and $Y^2 \cup Y^1$ shown in Fig. 3.2(a) and Fig. 3.2(b) and are defined as:

$$Y^3 \cup \widetilde{Y}^2 = \left\{ -\frac{1}{2} < y_i^{(2)} < \frac{1}{2} \right\}, \qquad Y^2 \cup Y^1 = \left\{ -\frac{1}{2} < y_i^{(1)} < \frac{1}{2}, \quad i = 1, 2, 3 \right\}$$

so that $Y^3 \cup \widetilde{Y}^2$ is the image $x \mapsto y^{(2)}$ of the unit period of the domain $\widetilde{\Omega}^3$, while $Y^2 \cup Y^1$ is the image $x \mapsto y^{(1)}$ of the unit period of the domain $\widetilde{\Omega}^2$. The linear size of any domain cell in local coordinates is equal to 1, as shown in Fig. 3.2.

The characteristic scale of medium Ω^3 is 1, and the characteristic time of flow through this medium is

of order 1. The macroscopic coordinate is x.

3.1.2 General flow equations

The flow model formulated through x for three scales is:

$$b^1 \frac{\partial p}{\partial t} = \omega \varepsilon^{2+\alpha} \nabla \cdot \left(a^1 \nabla p \right), \qquad x \in \Omega^1 \tag{3.1a}$$

$$b^2 \frac{\partial p}{\partial t} = \omega \nabla \cdot \left(a^2 \nabla p \right), \qquad x \in \Omega^2 \tag{3.1b}$$

$$b^3 \frac{\partial p}{\partial t} = \nabla \cdot \left(a^3 \nabla p \right), \qquad x \in \Omega^3 \tag{3.1c}$$

with conditions:

$$a^{(n+1)} \frac{\partial p}{\partial \nu}\bigg|_{\Gamma_+^{n+1,n}} = \omega a^{(n)} \frac{\partial p}{\partial \nu}\bigg|_{\Gamma_-^{n+1,n}}, \qquad n = 1, 2 \tag{3.1d}$$

where $\Gamma^{n+1,n}$ is the interface between Ω^{n+1} and Ω^n; ν is the vector normal to $\Gamma^{n+1,n}$; $\Gamma_+^{n+1,n}$ means that side of the interface $\Gamma^{n+1,n}$ which touches the domain Ω^{n+1}; ∇ is the operator of gradient expressed in terms of variable x.

In particular, if $\omega = \varepsilon^2$ and $\alpha = 0$ then we obtain the self-similar three-scale double-porosity model studied in chapter 2.

In this chapter, we assume that $\alpha > 0$, which determines non self-similar behavior on various scales. Moreover, similar to the section 2.1.5, this means that the process in blocks Y^1 are focused within the boundary layer of the size $\ell^{(1)} \sim \varepsilon^{\alpha/2}$.

3.1.3 Parametrization of the model: selection of fracture thickness and permeability

The main parameters of the model, such as fracture aperture $h^{(3)}$ and $h^{(2)}$ and the ratio between the permeability of two fracture families, ω, should be determined according to the following principle: the obtained macroscopic model would contain the contribution of all scales in zero approximation.

Let us assume, the behavior of the system is self-similar at each scale. Then a boundary layer appears in blocks Y^1, and a similar boundary layer appears in blocks $\tilde{Y}^2$. This means that only a thin layer of fractures Y^2 and blocks Y^1 will be active, while the main part of the domain $\tilde{Y}^2$ will remain unperturbed. The only thin layer situated just in the vicinity of Y^3 will contribute to the macroscopic behavior. This is only possible, if the aperture of fractures Y^2 is very high. We obtain an nonrealistic situation with small fractures which have higher aperture that large fractures. Such a medium does not present any interest.

Therefore, the principle enabling us to select well the medium parameters is the following:

- the block Y^1 should have a boundary layer (it is analyzed in chapter 2);
- the block $\tilde{Y}^2$ should work entirely, but not through a boundary layer.

This means that the system of flow equations formulated in local coordinates should have the form:

$$b^{(1)}\frac{\partial p}{\partial t} = \varepsilon^{\alpha}\nabla_1\cdot\left(a^{(1)}\nabla_1 p\right), \qquad y^{(1)} \in Y^1 \cup Y^2$$

$$b^{(2)}\frac{\partial p}{\partial t} = \nabla_2\cdot\left(a^{(2)}\nabla_2 p\right), \qquad y^{(2)} \in \tilde{Y}^2 \cup Y^3$$

$$b^{(3)}\frac{\partial p}{\partial t} = \nabla\cdot\left(a^{(3)}\nabla p\right), \qquad x \in \Omega^3$$

One sees that only the boundary layer in blocks Y^1 exists, while the domain $\tilde{Y}^2$ will be entirely covered by the perturbation. In this case the entire medium is engaged into the process, except the central part of each block Y^1. The size of the boundary layer is :

$$\frac{\ell^{(1)}}{\varepsilon^2} = \varepsilon^{\alpha/2} \tag{3.2}$$

This means that the ratio between permeability of two fractures $\omega \sim \varepsilon^2$ (if we return to macroscopic variable x, then the equation for Y^2 will contain the factor ε^2 in face of the diffusion operator). The ratio between permeability of fractures Y^2 and blocks Y^1 is $\varepsilon^{2+\alpha}$. Such a system is clearly non self-similar. This case should provide a fractured model at the lowest scales combined with the double porosity model at the largest scale.

To determine the contribution of various terms in the averaged equation we will take into account that the averaging procedure means the homogenization over the cell $Y^3 \cup \tilde{Y}^2$ shown in Fig. 3.2-(a):

$$\langle ... \rangle = \int\limits_{Y^3} ...dy^{(2)} + \int\limits_{\tilde{Y}^2} ...dy^{(2)} \tag{3.3}$$

where $dy^{(n)} \equiv dy_1^{(n)} dy_2^{(n)} dy_3^{(n)}$ is 3D space.

The domain $\tilde{Y}^2$ represents a cube of the length 1 which consists of N cells $Y^1 \cup Y^2$ of the length $\varepsilon^{(-1)}$ measured through $y^{(2)}$. Obviously, $N = \varepsilon^{(-3)}$. Then the term $\int\limits_{\tilde{Y}^2} dy^{(2)}$ in the averaging procedure (3.3) becomes:

$$\int\limits_{\tilde{Y}^2} dy^{(2)} = N\left(\int\limits_{Y^2\cup Y^1}\right) dy^{(2)} = \varepsilon^{-3}\left(\int\limits_{Y^2\cup Y^1}\right) dy^{(2)} = \left(\int\limits_{Y^2} + \int\limits_{Y^1}\right) dy^{(1)}$$

Then the averaging of our system (3.1) will give:

$$\underbrace{\int\limits_{Y^3}\left(b^{(3)}\frac{\partial P}{\partial t} + \mathrm{div}(...)\right) dy^{(2)}}_{A} + \underbrace{\int\limits_{Y^2}\left(b^{(2)}\frac{\partial P}{\partial t} + \mathrm{div}(...)\right) dy^{(1)}}_{B} + \underbrace{\int\limits_{Y^1}\left(b^{(1)}\frac{\partial P}{\partial t} + \mathrm{div}(...)\right) dy^{(1)}}_{C} = 0 \tag{3.4}$$

The order of terms measured in coordinate x will be:

$$A \sim h^{(3)}\varepsilon^{-1}, \qquad B \sim h^{(2)}\varepsilon^{-2}, \qquad C \sim \ell^{(1)}\varepsilon^{-2}$$

(because $|Y^3| \sim h^{(3)}$, $|Y^2| \sim h^{(2)}$, $|Y^1| \sim \ell^{(1)}$).

In order to keep all these terms, it is necessary to accept that:

$$h^{(3)} \sim \ell^{(1)}\varepsilon^{-1} = \varepsilon^{1+\frac{\alpha}{2}}, \qquad h^{(2)} \sim \ell^{(1)} = \varepsilon^{2+\frac{\alpha}{2}} \tag{3.5}$$

where we have taken into account for (3.2).

So, the aperture of small-scale fractures Y^2 is lower than that of large-scale fractures Y^3, which corresponds to the real situation.

It is not necessary to consider the case when ω is larger than ε^2 and tends to 1, as in all these cases all fractures function as a unique system of the same scale. So we obtain the two-scale model, but with more complicated geometry of the heterogeneity.

3.2 Homogenization : first step

The homogenization of a multiscale medium represents an iterative process of scaling up from medium $\widetilde{\Omega}^{n-1}$ to medium $\widetilde{\Omega}^{n}$. In the considered case the homogenization will be performed step by step from the scale of the smallest cell $Y^1 \cup Y^2$ to the scale $y^{(2)}$, and after this to the scale x.

3.2.1 Setting of the problem

According to the previous analysis we will analyze the following problem:

$$\begin{aligned} b^{(1)}\frac{\partial p}{\partial t} &= \varepsilon^{4+\alpha}\nabla\cdot\left(a^{(1)}\nabla p\right), \qquad x\in\Omega^1 \\ b^{(2)}\frac{\partial p}{\partial t} &= \varepsilon^{2}\nabla\cdot\left(a^{(2)}\nabla p\right), \qquad x\in\Omega^2 \\ b^{(3)}\frac{\partial p}{\partial t} &= \nabla\cdot\left(a^{(3)}\nabla p\right), \qquad x\in\Omega^3 \end{aligned} \tag{3.6}$$

with conditions:

$$a^{(n+1)}\frac{\partial p}{\partial \nu}\Big|_{\Gamma_+^{n+1,n}} = \varepsilon^2 a^{(n)}\frac{\partial p}{\partial \nu}\Big|_{\Gamma_-^{n+1,n}} \tag{3.7}$$

where operator ∇ is expressed in terms of variable x.

The half-aperture of fracture Ω^2 and Ω^3 correspond to the case (3.5):

$$h^{(3)} \sim \varepsilon^{1+\frac{\alpha}{2}}, \qquad h^{(2)} \sim \varepsilon^{2+\frac{\alpha}{2}} \tag{3.8}$$

As mentioned, under selected parameters we expect the following:

- for blocks Ω^1, only the narrow boundary layer will be perturbed;

- for fractures Ω^2, the process is non-stationary and cover the overall medium;

- for fractures Ω^3, the process is non-stationary in the scale of the entire medium, but quasi-stationary within each unique fracture Y^3.

It is sufficient that the boundary layer in blocks will certainly disappear at large times. This will change qualitatively the flow geometry in each block. Indeed, in the boundary layer the flow is practically linear from the block center to the boundary with fractures Y^2 and happens at a constant pressure in the block center. At large times, the entire block will be covered by perturbation. The flow inside the block will become radial and happens at decreasing pressure at the block center.

So the considered case corresponds only to bounded time:

$$0 < t < \mathcal{T} \leq 1 \tag{3.9}$$

3.2.2 Flow problem at the lowest scales

For the lowest scale, the macroscopic "slow" coordinate is $y^{(2)}$ and the macroscopic domain is $\widetilde{Y}^2$ Fig. 3.3-(a), while the microscopic "fast" variable is $y^{(1)}$ and the microscopic cell is $Y^2 \cup Y^1$ Fig. 3.3-(b). The

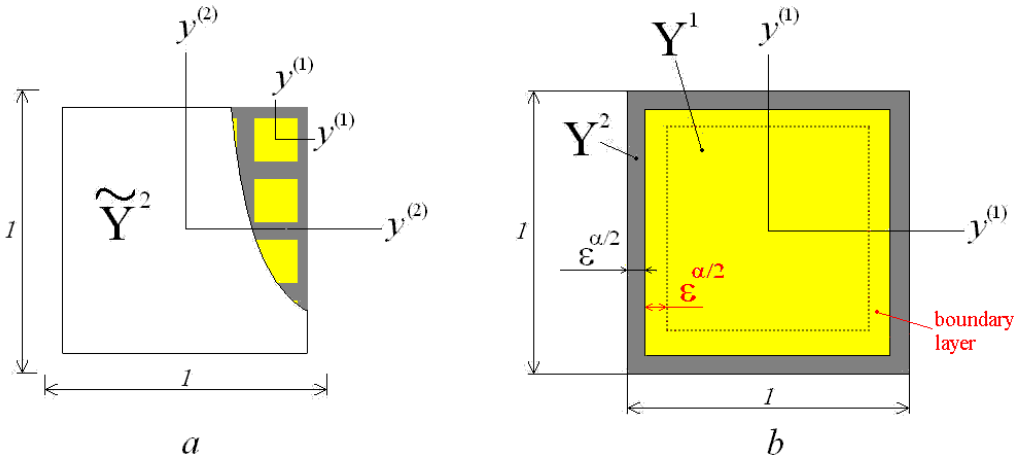

Figure 3.3: First step of homogenization: "macroscopic" domain (a) and the microscopic cell (b)

problem (3.6) formulated through the slow variable becomes:

$$b^{(1)}\frac{\partial p}{\partial t} = \varepsilon^{2+\alpha}\nabla_2\cdot\left(a^{(1)}\nabla_2 p\right), \qquad y^{(2)} \in Y^1 \cap \widetilde{Y}^2 \tag{3.10a}$$

$$b^{(2)}\frac{\partial p}{\partial t} = \nabla_2\cdot\left(a^{(2)}\nabla_2 p\right), \qquad y^{(2)} \in Y^2 \cap \widetilde{Y}^2 \tag{3.10b}$$

$$a^{(2)}\frac{\partial p}{\partial \nu}\Big|_{\Gamma_+^{2,1}} = \varepsilon^{2+\alpha}a^{(1)}\frac{\partial p}{\partial \nu}\Big|_{\Gamma_-^{2,1}}, \qquad p|_{\Gamma_+^{2,1}} = p|_{\Gamma_-^{2,1}} \tag{3.10c}$$

After introducing two-scale functions $p(y^{(2)}, y^{(1)}, t)$ and two-scale operators, we obtain the two-scale formulation of the problem:

$$\begin{aligned} b^{(1)}\frac{\partial p}{\partial t} = {} & \varepsilon^{\alpha}\nabla_1\cdot\left(a^{(1)}\nabla_1 p\right) + \varepsilon^{\alpha+1}\left(\nabla_1\cdot\left(a^{(1)}\nabla_2 p\right) + \nabla_2\cdot\left(a^{(1)}\nabla_1 p\right)\right) + \\ & + \varepsilon^{\alpha+2}\left(\nabla_2\cdot\left(a^{(1)}\nabla_2 p\right)\right), \qquad y^{(1)} \in Y^1, \quad y^{(2)} \in \widetilde{Y}^2; \end{aligned} \tag{3.11}$$

$$\begin{aligned} b^{(2)}\frac{\partial p}{\partial t} = {} & \varepsilon^{-2}\nabla_1\cdot\left(a^{(2)}\nabla_1 p\right) + \varepsilon^{-1}\left(\nabla_1\cdot\left(a^{(2)}\nabla_2 p\right) + \nabla_2\cdot\left(a^{(2)}\nabla_1 p\right)\right) + \\ & \left(\nabla_2\cdot\left(a^{(2)}\nabla_2 p\right)\right), \qquad y^{(2)} \in \widetilde{Y}^2, \quad y^{(1)} \in Y^2 \end{aligned} \tag{3.12}$$

3.2.3 Homogenized model of the first level

The problem of the first-scale is identical to that studied in the preceding chapter. The homogenization of this system of equations leads to the nonlocal model of flow in fractured medium with two pressures

P^1 and P^2, averaged respectively over Y^1 and Y^2 (see (2.38) or (2.36)):

$$P^1 = p^0 + 2\lambda\varepsilon^{\alpha/2} \int_0^t \frac{\partial P^2}{\partial \tau}\sqrt{t-\tau}d\tau \tag{3.13a}$$

$$\widehat{B}^{(2)}\frac{\partial P^2}{\partial t} = \nabla_2 \cdot \left(\widehat{A}^{(2)}\nabla_2 P^2\right) - \gamma\lambda\widehat{B}^{(1)} \int_0^t \frac{\partial P^2}{\partial \tau}\frac{d\tau}{\sqrt{t-\tau}} \tag{3.13b}$$

with:

$$\widehat{B}^{(2)} = \frac{1}{|Y^2|}\int_{Y^2} b^{(2)}dy^{(1)} = b^{(2)}, \qquad \widehat{B}^{(1)} = \frac{1}{|Y^1|}\int_{Y^1} b^{(1)}dy^{(1)} = b^{(1)}, \qquad \lambda = \frac{6}{\theta^{1/3}}\sqrt{\frac{a^{(1)}}{\pi b^{(1)}}}, \qquad \gamma = 1/m$$

where m is the space dimension; $\left|Y^2\right|$ is the volume of medium Y^2 measured through the proper coordinate $y^{(1)}$; symbol $\widehat{A}^{(2)}$ means the effective permeability of the medium Y^2 divided to its volume $\left|Y^2\right|$; θ is the ratio of the volume of medium Y^1 to the volume of the entire cell $Y^2 \cup Y^1$.

The symbols

$$\langle\cdot\rangle_{Y^i} = \int_{Y^i} (\cdot)dy^{(1)}, \quad i = 1, 2 \tag{3.14}$$

Parameter $\gamma\varepsilon^{-\alpha/2}$ is the ratio of the block volumes $\left|Y^1\right|$ to the fracture volume $\left|Y^2\right|$:

$$\gamma = \varepsilon^{\alpha/2}\frac{\left|Y^1\right|}{\left|Y^2\right|} = \frac{1}{m}$$

Note that all the terms in equation (3.13b) are of the order 1.

3.3 Homogenization: second step

3.3.1 Formulation of the flow problem at the second scale

At the second step we consider the passage from medium $\widetilde{\Omega}^{(2)}$ to medium $\widetilde{\Omega}^{(3)} = \widetilde{\Omega}^{(2)} \cup \Omega^{(3)}$. Flow in medium $\widetilde{\Omega}^{(2)}$ will be now considered as already homogenized.

The macroscale coordinate is $x \in \widetilde{\Omega}^{(3)}$ while the microscale coordinate is $y^{(2)} \in \widetilde{Y}^{(3)} = \widetilde{Y}^2 \cup Y^3$.

The couple of equations describing the flow in block $\widetilde{\Omega}^{(2)}$ and in fracture $\Omega^{(3)}$ results from (3.13b) and (3.6) respectively. Being formulated through the macroscale variable x it becomes:

$$\widehat{B}^{(2)} \frac{\partial P^2}{\partial t} = \varepsilon^2 \nabla \cdot \left(\widehat{B}^{(2)} \nabla P^2 \right) - \gamma \lambda \widehat{B}^{(1)} \int_0^t \frac{\partial P^2}{\partial \tau} \frac{d\tau}{\sqrt{t-\tau}}, \quad x \in \widetilde{\Omega}^2 \tag{3.15a}$$

$$b^{(3)} \frac{\partial p}{\partial t} = \nabla \cdot \left(a^{(3)} \nabla p \right), \qquad x \in \Omega^3 \tag{3.15b}$$

$$a^{(3)} \frac{\partial p}{\partial \nu}\Big|_{\Gamma_+^{3,2}} = \varepsilon^2 \left| Y^2 \right| \widehat{A}^{(2)} \frac{\partial P^2}{\partial \nu}\Big|_{\Gamma_-^{3,2}}, \qquad p|_{\Gamma_+^{3,2}} = P^2|_{\Gamma_-^{3,2}} \tag{3.15c}$$

We have taken into account that the effective permeability of the medium Y^2 is $\left| Y^2 \right| \widehat{A}^{(2)}$. The unit local cell is shown in Fig. 3.4.

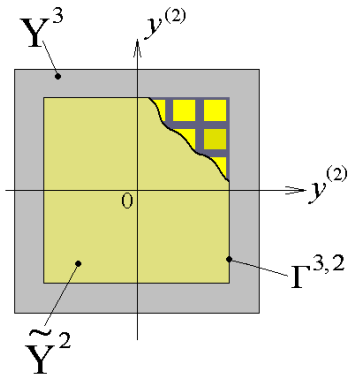

Figure 3.4: Unit cell at the second step of homogenization

After introducing two-scale functions $p\left(x, y^{(2)}, t\right)$ and two-scale operators:

$$\frac{\partial}{\partial x_i} \to \frac{\partial}{\partial x_i} + \frac{1}{\varepsilon} \frac{\partial}{\partial y_i^{(2)}}, \qquad \nabla \to \nabla + \frac{1}{\varepsilon} \nabla_2$$

we obtain the two-scale formulation:

$$\widehat{B}^{(2)}\frac{\partial P^2}{\partial t}+\gamma\lambda\widehat{B}^{(1)}\int\limits_0^t\frac{\partial P^2}{\partial\tau}\frac{d\tau}{\sqrt{t-\tau}}=\nabla_2\cdot\left(\widehat{A}^{(2)}\nabla_2P^2\right)+\varepsilon^2\nabla\cdot\left(\widehat{A}^{(2)}\nabla P^2\right)+$$
$$+\varepsilon\left(\nabla_2\cdot\left(\widehat{A}^{(2)}\nabla P^2\right)+\nabla\cdot\left(\widehat{A}^{(2)}\nabla_2P^2\right)\right),\qquad x\in\widetilde{\Omega}^3,\quad y^{(2)}\in\widetilde{Y}^2 \tag{3.16a}$$

$$b^{(3)}\frac{\partial p}{\partial t}=\frac{1}{\varepsilon^2}\nabla_2\cdot\left(a^{(3)}\nabla_2p\right)+\frac{1}{\varepsilon}\left(\nabla_2\cdot\left(a^{(3)}\nabla p\right)+\nabla\cdot\left(a^{(3)}\nabla_2p\right)\right)+\nabla\cdot\left(a^{(3)}\nabla p\right),$$
$$x\in\widetilde{\Omega}^3,\quad y^{(2)}\in Y^3 \tag{3.16b}$$

$$a^{(3)}\left(\frac{\partial p}{\partial x_i}+\frac{1}{\varepsilon}\frac{\partial p}{\partial y_i^{(2)}}\right)\nu_i\Big|_{\Gamma_+^{3,2}}=\varepsilon^2\left|Y^2\right|\widehat{A}^{(2)}\left(\frac{\partial P^2}{\partial x_i}+\frac{1}{\varepsilon}\frac{\partial P^2}{\partial y_i^{(2)}}\right)\nu_i\Big|_{\Gamma_-^{3,2}}, \tag{3.16c}$$

$$p|_{\Gamma_+^{3,2}}=P^2|_{\Gamma_-^{3,2}} \tag{3.16d}$$

3.3.2 Averaged equation over the cell Y^3

Let us designate:

$$\langle\cdot\rangle_{\widetilde{Y}^2}=\int\limits_{\widetilde{Y}^2}(\cdot)dy^{(2)},\quad\langle\cdot\rangle_{Y^3}=\int\limits_{Y^3}(\cdot)dy^{(2)},\quad\overline{(\cdot)}_{Y^3}=\frac{1}{|Y^3|}\langle\cdot\rangle_{Y^3},\qquad\overline{(\cdot)}_{\widetilde{Y}^2}=\frac{1}{\left|\widetilde{Y}^2\right|}\langle\cdot\rangle_{\widetilde{Y}^2} \tag{3.17}$$

where $\left|Y^3\right|$ and $\left|\widetilde{Y}^2\right|$ are the volumes of subdomains Y^3 and $\widetilde{Y}^2$ respectively measured both through $y^{(2)}$, while $\left|Y^2\right|$ is the volume of medium Y^2 measured through the coordinate $y^{(1)}$:

$$\left|Y^2\right|\sim\frac{h^{(2)}}{\varepsilon^2}=\varepsilon^{\frac{\alpha}{2}},\qquad\left|Y^3\right|\sim\frac{h^{(3)}}{\varepsilon}=\varepsilon^{\frac{\alpha}{2}} \tag{3.18}$$

The averaged equations over Y^3 takes the form:

$$\left|Y^3\right|\left[\left(\overline{b^{(3)}\frac{\partial p}{\partial t}}\right)_{Y^3}-\nabla\cdot\left(\overline{a^{(3)}\nabla p}\right)_{Y^3}-\frac{1}{\varepsilon}\nabla\cdot\left(\overline{a^{(3)}\nabla_2p}\right)_{Y^3}\right]+$$
$$+\left|Y^2\right|\left[\left\langle\widehat{B}^{(2)}\frac{\partial P^2}{\partial t}\right\rangle_{\tilde{Y}^2}+\left\langle\gamma\lambda\widehat{B}^{(1)}\int\limits_0^t\frac{\partial P^2}{\partial\tau}\frac{d\tau}{\sqrt{t-\tau}}\right\rangle_{\tilde{Y}^2}\right]-$$
$$-\varepsilon\left|Y^2\right|\nabla\cdot\left\langle\left(\widehat{A}^{(2)}\nabla_2P^2+\varepsilon\widehat{A}^{(2)}\nabla P^2\right)\right\rangle_{\tilde{Y}^2}=0 \tag{3.19}$$

One sees that, according to (3.18), the first and the second square brackets are of the same order.

Proof:

The integration of (3.16) over Y^3 yields:

$$0=\left\langle b^{(3)}\frac{\partial p}{\partial t}\right\rangle_{Y^3}-\nabla\cdot\left\langle a^{(3)}\nabla p\right\rangle_{Y^3}-\frac{1}{\varepsilon}\left\langle\nabla_2\cdot a^{(3)}\nabla p+\frac{1}{\varepsilon}\nabla_2\cdot a^{(3)}\nabla_2p\right\rangle_{Y^3}-\frac{1}{\varepsilon}\nabla\cdot\left\langle a^{(3)}\nabla_2p\right\rangle_{Y^3} \tag{3.20}$$

The integral

$$I\equiv-\frac{1}{\varepsilon}\left\langle\nabla_2\cdot a^{(3)}\nabla p+\frac{1}{\varepsilon}\nabla_2\cdot a^{(3)}\nabla_2p\right\rangle_{Y^3}$$

may be reduced to the integral over the boundary of the domain Y^3 which consists of the external boundary ∂Y^3 and the internal boundary $\Gamma^{3,2}$ between Y^2 and $\widetilde{Y}^2$:

$$I = -\frac{1}{\varepsilon} \int\limits_{\partial Y^3 \cup \Gamma^{3,2}} a^{(3)} \left(\frac{\partial p}{\partial x_i} + \frac{1}{\varepsilon} \frac{\partial p}{\partial y_i^{(2)}} \right) \nu_i dy^{(2)}$$

Due to periodicity, the external integral over ∂Y^3 will be zero.

Due to condition (3.16c) at the boundary $\Gamma^{3,2}$, we obtain:

$$I = \varepsilon \left| Y^2 \right| \int\limits_{\Gamma^{3,2}} \widehat{A}^{(2)} \left(\frac{\partial P^2}{\partial x_i} + \frac{1}{\varepsilon} \frac{\partial P^2}{\partial y_i^{(2)}} \right) \nu_i dy^{(2)} = \varepsilon \left| Y^2 \right| \int\limits_{\widetilde{Y}^2} \nabla_2 \cdot \left(\widehat{A}^{(2)} \left(\nabla P^2 + \frac{1}{\varepsilon} \nabla_2 P^2 \right) \right) dy^{(2)}$$

From equation (3.16a) it follows:

$$I = \left| Y^2 \right| \int\limits_{\widetilde{Y}^2} \left(\widehat{B}^{(2)} \frac{\partial P^2}{\partial t} + \lambda \gamma \widehat{B}^{(1)} \int\limits_0^t \frac{\partial P^2}{\partial \tau} \frac{d\tau}{\sqrt{t-\tau}} \right) dy^{(2)} -$$

$$-\varepsilon \left| Y^2 \right| \int\limits_{\widetilde{Y}^2} \nabla \cdot \left(\widehat{A}^{(2)} \nabla_2 P^2 + \varepsilon \widehat{A}^{(2)} \nabla P^2 \right) dy^{(2)}$$

Substituting into (3.20), we obtain equation (3.19).

3.3.3 Asymptotic expansion of the averaged equation

Using the asymptotic expansion:

$$p^3 = p_0(x,t) + \varepsilon p_1(x, y^{(2)}, t) + ..., \qquad P^2 = P_0^2(x, y^{(2)}, t) + ...$$

we obtain in the major approximation from (3.19):

$$\left| Y^3 \right| \left[\left(\overline{b^{(3)} \frac{\partial p_0}{\partial t}} \right)_{Y^3} - \nabla \cdot \left(\overline{a^{(3)} \nabla p_0} \right)_{Y^3} - \nabla \cdot \left(\overline{a^{(3)} \nabla_2 p_1} \right)_{Y^3} \right] +$$

$$+ \left| Y^2 \right| \left[\left\langle \widehat{B}^{(2)} \frac{\partial P_0^2}{\partial t} \right\rangle_{\widetilde{Y}^2} + \left\langle \gamma \lambda \widehat{B}^{(1)} \int\limits_0^t \frac{\partial P_0^2}{\partial \tau} \frac{d\tau}{\sqrt{t-\tau}} \right\rangle_{\widetilde{Y}^2} \right] + O\left(\varepsilon \left| Y^2 \right| \right) \tag{3.21}$$

One sees that, according to (3.18), all terms are of the same order.

To close this equation we have to solve the problem in the domain $\widetilde{Y}^2$ for P_0^2.

3.4 Solution of the problem in $\widetilde{Y}^2$

3.4.1 Representation through Green's function

In the block $\widetilde{Y}^2$ we obtain the following problem for the major term:

$$\widehat{B}^{(2)}\frac{\partial P_0^2}{\partial t} = \nabla_2 \cdot \left(\widehat{A}^{(2)}\nabla_2 P_0^2\right) - \gamma\lambda\widehat{B}^{(1)}\int\limits_0^t \frac{\partial P_0^2}{\partial \tau}\frac{d\tau}{\sqrt{t-\tau}},$$

$$y^{(2)} \in \widetilde{Y}^2; \qquad 0 < t < \mathcal{T} \leq 1$$

$$P_0^2\big|_{\Gamma^{3,2}} = p_0^3; \qquad P_0^2\big|_{t=0} = p^0 \tag{3.22}$$

By replacing variables: $U \equiv P_0^2 - p_0^3$ we obtain the problem with homogeneous boundary and initial conditions:

$$\mathcal{L}U \equiv \frac{\partial U}{\partial t} - \frac{\widehat{A}^{(2)}}{\widehat{B}^{(2)}}\nabla_2^2 U + \gamma\lambda\frac{\widehat{B}^{(1)}}{\widehat{B}^{(2)}}\int\limits_0^t \frac{\partial U}{\partial \tau}K\left(t-\tau\right)d\tau =$$

$$= -\frac{\partial p_0^3}{\partial t} - \gamma\lambda\frac{\widehat{B}^{(1)}}{\widehat{B}^{(2)}}\int\limits_0^t \frac{\partial p_0^3}{\partial \tau}K\left(t-\tau\right)d\tau, \quad y^{(2)} \in \widetilde{Y}^2; \tag{3.23}$$

$$U|_{\Gamma^{3,2}} = 0; \qquad U|_{t=0} = 0, \qquad K(t) = \frac{1}{\sqrt{t}} \tag{3.24}$$

The solution of this problem is the convolution of the Green function of the operator $\mathcal{L}$ with the right-hand side of equation (3.23):

$$U = -\int\limits_{\widetilde{Y}^{(2)}}\int\limits_0^t G\left(y^{(2)},\xi,t-\tau\right)\left[\frac{\partial p_0^3}{\partial \tau} + \gamma\lambda\frac{\widehat{B}^{(1)}}{\widehat{B}^{(2)}}\int\limits_0^\tau \frac{\partial p_0^3}{\partial \theta}K\left(\tau-\theta\right)d\theta\right]d\xi d\tau$$

Then the pressure in block $\widetilde{Y}^2$ is:

$$P_0^2 = p_0^3 - \int\limits_{\widetilde{Y}^2}\int\limits_0^t G\left(y^{(2)},\xi,t-\tau\right)\left[\frac{\partial p_0^3}{\partial \tau} + \gamma\lambda\frac{\widehat{B}^{(1)}}{\widehat{B}^{(2)}}\int\limits_0^\tau \frac{\partial p_0^3}{\partial \theta}K\left(\tau-\theta\right)d\theta\right]d\xi d\tau \tag{3.25}$$

where the Green function $G\left(y^{(2)},\xi,t-\tau\right)$ is determined as the solution of the homogeneous equation

(3.24) with homogeneous boundary conditions at $\Gamma^{(3,2)}$ and the initial condition:

$$\frac{\partial G}{\partial t} - \frac{\widehat{A}^{(2)}}{\widehat{B}^{(2)}}\nabla_2^2 G + \gamma\lambda\frac{\widehat{B}^{(1)}}{\widehat{B}^{(2)}}\int\limits_0^t \frac{\partial G}{\partial \tau}K\left(t-\tau\right)d\tau = 0, \tag{3.26a}$$

$$G\left(x^{(2)},\xi,t\right)\Big|_{t=0} = \delta\left(x^{(2)}-\xi\right), \tag{3.26b}$$

$$G\left(x^{(2)},\xi,t\right)\Big|_{x^{(2)},\xi\in\Gamma^{3,2}} = 0 \tag{3.26c}$$

Now we get down to the construction of the Green's function.

3.4.2 Spectral expansion of the Green's function G

The Green function may be presented through the Fourier series with respect to a complete orthogonal system of functions. Such a system may be presented by the eigenfunctions of the Laplace operator.

Let us introduce the Hilbert space of functions $\mathcal{H}$ which have the following properties:

- they are determined in the domain $\widetilde{Y}^2 \times (0 < t < \mathcal{T})$ where $\mathcal{T} < 1$;
- they satisfy the homogeneous Dirichlet boundary condition at $\Gamma^{3,2}$;
- the norm in $\mathcal{H}$ is determined through the scalar product:

$$||f|| = \left(\int_{\widetilde{Y}^2} f^2 dx\right)^{1/2} \tag{3.27}$$

Then the Green's function (3.26) may be presented in the form of the following Fourier series:

$$G\left(y^{(2)},\xi,t\right) = \sum_{k=1}^{\infty}\frac{1}{||R_k||^2}T_k(t)R_k(y^{(2)})R_k(\xi) \tag{3.28}$$

where μ_k and $R_k(x),\ k \geq 1$ are the series of eigenvalues and eigenfunctions of the Laplace operator in $\mathcal{H}$, so that:

$$\nabla_2^2 R_k = -\mu_k R_k, \quad y^{(2)} \in \widetilde{Y}^2; \qquad R_k|_{\Gamma^{(3,2)}} = 0 \tag{3.29}$$

while $T_k(t)$ are determined as the solutions of the problem:

$$T_k' + \gamma\lambda\frac{\widehat{B}^{(1)}}{\widehat{B}^{(2)}}\int\limits_0^t T_k'(\tau)K\left(t-\tau\right)d\tau = -\mu_k\frac{\widehat{A}^{(2)}}{\widehat{B}^{(2)}}T_k, \qquad (0 < t < \mathcal{T}), \tag{3.30a}$$

$$T_k|_{t=0} = 1, \quad \forall k \tag{3.30b}$$

where $T_k'(t) \equiv dT_k/dt$

Proof:

1°. It is known that the system $\{R_k\}$ is complete and orthogonal in $\mathcal{H}$. We will use orthonormal

eigenfunctions. The completeness and orthonormality means that:

$$\sum_{k\geq 1}\frac{1}{||R_k||^2}R_k(y^{(2)})R_k(\xi)=\delta\left(y^{(2)}-\xi\right) \tag{3.31}$$

2°. The form of the expansion (3.28) is determined by the symmetry of the Green function with respect to $y^{(2)}$ and ξ.

3°. Substituting this series and (3.29) in (3.26) we obtain (3.30a) for functions $T_k(t)$.

4°. Using the initial condition (3.26b) we obtain:

$$\sum_{k\geq 0}\frac{1}{||R_k||^2}T_k(0)R_k(y^{(2)})R_k(\xi)=\delta\left(y^{(2)}-\xi\right)$$

Using this relation and the property (3.31) we obtain the initial condition (3.30b) for functions T_k.

Now we should determine the structure of the functions $T_k(t)$.

3.4.3 Reduction from integro-differential equation to the differential one

The integro-differential equation (3.30a) with Abel's kernel $K(t)$ has analytical solution. It can be obtained by reducing this equation to the differential one if we use the following property of the Abel kernels:

$$K(t)*K(t)=\pi \tag{3.32}$$

where $(*)$ is the convolution operator.

Equation (3.30a) may be presented in the form

$$\frac{dT_k}{dt}+M\frac{dT_k}{dt}*K(t)=-NT_k,\qquad M\equiv\gamma\lambda\frac{\widehat{B}^{(1)}}{\widehat{B}^{(2)}},\quad N\equiv\mu_k\frac{\widehat{A}^{(2)}}{\widehat{B}^{(2)}} \tag{3.33}$$

which is:

$$\frac{dT_k}{dt}*[\delta(t)+MK(t)]=-NT_k$$

Let us convolute this equation with $\delta(t)-MK(t)$, then we obtain:

$$T_k'*\left[\delta(t)*\delta(t)-\pi M^2\right]=-NT_k*[\delta(t)-MK(t)]$$

or

$$T_k'-\pi M^2\left(T_k-T_k(0)\right)=-NT_k+NMT_k*K(t)$$

Differentiating this equation we obtain:

$$T_k'' - \pi M^2 T_k' = -NT_k' + NM\left(T_k' * K(t) + T_k(0)K(t)\right)$$

From the equation (3.33): $MT' * K(t) = -T_k' - NT_k$, so one can write:

$$T_k'' + \left(2N - \pi M^2\right) T_k' + N^2 T_k = NMK(t) \tag{3.34}$$

where we have used (3.30b).

The augmentation of the order of the equation implies the necessity to introduce an additional initial condition, which results from the original integro-differential equation (3.30a) at the initial time instant:

$$T_k'\big|_{t=0} + M \lim_{t\to 0} \int_0^t T_k'(t-\tau)K(\tau)d\tau = -\,NT_k|_{t=0} = -N \tag{3.35}$$

Depending on the behaviour of the derivative T_k' the integral operator can converge to zero, to a constant nonzero value, or diverge.

3.4.4 Analytical solution of the integro-differential equation (3.30a)

The solution of the equation (3.34) with conditions (3.30b) and (3.35) is:

$$T_k(t) = \begin{cases} e^{\rho(1-\alpha_k)t}\left[\cos\left(\rho\nu_k\, t\right) - \dfrac{1}{\nu_k}\sin\left(\rho\nu_k\, t\right)\right] + \\ \qquad + \dfrac{\beta_k}{\nu_k}\displaystyle\int_0^t \frac{\sin\left(\rho\nu_k(t-\tau)\right)}{\sqrt{\tau}}\, e^{\rho(1-\alpha_k)(t-\tau)}d\tau, \quad \text{for} \quad k > k_*; \\ \\ e^{\rho t/2}\left(1-\rho t\right) + \beta_k\rho\displaystyle\int_0^t \frac{t-\tau}{\sqrt{\tau}}\, e^{\rho(t-\tau)/2}d\tau, \quad \text{for} \quad k = k_*; \\ \\ \dfrac{\nu_k - 1}{2\nu_k}\, e^{\omega_k^{(1)}t} + \dfrac{\nu_k + 1}{2\nu_k}\, e^{\omega_k^{(2)}t} + \\ \qquad + \dfrac{\beta_k}{2\nu_k}\displaystyle\int_0^t \frac{1}{\sqrt{\tau}}\left(e^{\omega_k^{(1)}(t-\tau)} - e^{\omega_k^{(2)}(t-\tau)}\right)d\tau, \quad \text{for} \quad 1 \le k < k_* \end{cases} \tag{3.36}$$

where

$$\rho = \frac{\pi M^2}{2} = \frac{\pi\left(\gamma\lambda\widehat{B}^{(1)}\right)^2}{2\left(\widehat{B}^{(2)}\right)^2}, \quad \alpha_k \equiv \frac{N}{\rho} = \frac{2\mu_k\widehat{A}^{(2)}\widehat{B}^{(2)}}{\pi\left(\gamma\lambda\widehat{B}^{(1)}\right)^2}, \quad \nu_k = \sqrt{|2\alpha_k - 1|}, \quad \beta_k = \frac{2\mu_k\widehat{A}^{(2)}}{\pi\gamma\lambda\widehat{B}^{(1)}} \tag{3.37}$$

$$\omega_k^{(1,2)} = \rho\left[1 - \alpha_k \pm \nu_k\right] \tag{3.38}$$

where ω_k^1 corresponds to the sign $+$.

The numbers $\mu_k, \quad k = 1, 2, ...$ represent the infinite set of eigenvalues of the Laplace operator in $\mathcal{H}$

defined as the solutions of the problem (3.29). The critical value k_* corresponds to the eigenvalue μ_* defined as:

$$\mu_{k_*} \equiv \mu_* \equiv \frac{\pi \left(\gamma \lambda \widehat{B}^{(1)}\right)^2}{\widehat{A}^{(2)} \widehat{B}^{(2)}} \tag{3.39}$$

which is equivalent to $\alpha_{k_*} = 1/2$.

For the spherical shape of the block $\widetilde{Y}^2$, the eigenvalues are determined as:

$$\mu_k = \left(\frac{\pi k}{l^{(2)}}\right)^2, \qquad l^{(2)} \equiv \left(\frac{3\theta^{(2)}}{4\pi}\right)^{1/3}$$

where $\theta^{(2)}$ is the volume fraction of the block $\widetilde{Y}^2$ in a periodic cell Y^2.

In this case the critical values k_* may be found explicitly:

$$k_* = \frac{\gamma \lambda B^{(1)}}{2\sqrt{\pi \widehat{A}^{(2)} \widehat{B}^{(2)}}} \left(\frac{3\theta^{(2)}}{4\pi}\right)^{1/3} \tag{3.40}$$

3.4.5 Proof of the solution (3.36)

1 . The general solution of the equation (3.34) is the sum of the solution U_k of the homogeneous equation and a particular solution of (3.34).

2 . The homogeneous equation (3.34) takes the form:

$$U_k'' - 2\rho\,(1-\alpha_k)\,U_k' + \rho^2 \alpha_k^2 U_k = 0$$

The solution of its characteristic equations is (3.38).

3 . Depending on the sign of the discriminant we obtain three types of solution:

$$U_k(t) = \begin{cases} e^{\rho(1-\alpha_k)t}\left[C_k \sin\left(\rho\nu_k\, t\right) + D_k \cos\left(\rho\nu_k\, t\right)\right], & \text{for } \alpha_k > 0.5, \text{ i.e. } \mu_k > \mu_*, \text{ i.e. } k > k_* \\ e^{\rho t/2}\left(C_k^* + D_k^* t\right), & \text{for } \alpha_k = 0.5, \text{ i.e. } \mu_k = \mu_*, \text{ i.e. } k = k_* \\ C_k^{**} e^{\omega_k^{(1)} t} + D_k^{**} e^{\omega_k^{(2)} t}, & \text{for } 0 < \alpha_k < 0.5, \text{ i.e. } 0 < \mu_k < \mu_*, \text{ i.e. } 1 < k < k_* \end{cases} \tag{3.41}$$

where $\omega_k^{(1,2)}$ are defined through (3.38).

Several of theses solutions are exponentially growing in time, but this is not prohibited as we work at small times according to (3.22).

4 . The particular solution of the non-homogeneous equation (3.34) is the convolution of a particular homogeneous solution U_* with the right-hand side of (3.34). The homogeneous solution U_* must satisfy

two initial conditions:

$$U_{k*}|_{t=0} = 0, \qquad U'_{k*}\big|_{t=0} = 1$$

The solutions which satisfy these conditions are:

$$U_{k*}(t) = \begin{cases} \dfrac{1}{\rho\nu_k} e^{\rho(1-\alpha_k)t} \sin\left(\rho\nu_k\, t\right), & \text{for} \quad k > k_*, \\ \\ te^{\rho t/2}, & \text{for} \quad k = k_*, \\ \\ \dfrac{1}{2\rho\nu_k}\left(e^{\omega_k^{(1)} t} - e^{\omega_k^{(2)} t}\right), & \text{for} \quad 1 < k < k_* \end{cases}$$

Thus, the general solution of equation (3.34) is:

$$T_k(t) = U_k(t) + \rho\alpha_k M \int\limits_0^t U_{k*}(t-\tau) K(\tau) d\tau \tag{3.42}$$

or

$$T_k(t) = \begin{cases} e^{\rho(1-\alpha_k)t}\left[C_k \sin\left(\rho\nu_k\, t\right) + D_k \cos\left(\rho\nu_k\, t\right)\right] + \\ \qquad + \dfrac{\alpha_k M}{\nu_k} \displaystyle\int_0^t K(\tau) e^{\rho(1-\alpha_k)(t-\tau)} \sin\Big(\rho\nu_k (t-\tau)\Big)\, d\tau, \quad \text{for } k > k_*; \\ \\ e^{\rho t/2}\left(C_k^* + D_k^* t\right) + \alpha_k \rho M \displaystyle\int_0^t K(\tau)(t-\tau) e^{\rho(t-\tau)/2} d\tau, \quad \text{for } k = k_*; \\ \\ C_k^{**} e^{\omega_k^{(1)} t} + D_k^{**} e^{\omega_k^{(2)} t} + \dfrac{\alpha_k M}{2\nu_k} \displaystyle\int_0^t \left(e^{\omega_k^{(1)}(t-\tau)} - e^{\omega_k^{(2)}(t-\tau)}\right) K(\tau) d\tau, \quad \text{for } 1 < k < k_* \end{cases} \tag{3.43}$$

5 . For small times, the solution behaves as:

$$T_k(t) \to \begin{cases} D_k + \dfrac{\alpha_k M}{\nu_k} \displaystyle\int_0^t \frac{\rho\nu_k (t-\tau)}{\sqrt{\tau}} d\tau \to D_k, \qquad t \to 0, \quad \text{for } k > k_*; \\ \\ C_k^* + \alpha_k \rho M \int_0^t \dfrac{t-\tau}{\sqrt{\tau}} d\tau \to C_k^*, \quad \text{for } k = k_*; \\ \\ C_k^{**} + D_k^{**}, \quad \text{for } 1 < k < k_* \end{cases}$$

So from the initial condition (3.30b) it follows: $D_k = 1$, $C_k^* = 1$, $C_k^{**} + D_k^{**} = 1$.

6 . For the derivative we obtain:

For $k > k*$:

$$T_k'(t) = \rho\,(1-\alpha_k)\,e^{\rho(1-\alpha_k)t}\left[C_k \sin(\rho\nu_k\,t) + \cos(\rho\nu_k\,t)\right] + \\ + \rho\nu_k e^{\rho(1-\alpha_k)t}\left[C_k\cos(\rho\nu_k\,t) - \sin(\rho\nu_k\,t)\right] + \\ + \frac{\alpha_k M\rho\,(1-\alpha_k)}{\nu_k}\int_0^t K(\tau)e^{\rho(1-\alpha_k)(t-\tau)}\sin\Big(\rho\nu_k(t-\tau)\Big)\,d\tau + \\ + \alpha_k M\rho\int_0^t K(\tau)e^{\rho(1-\alpha_k)(t-\tau)}\cos\Big(\rho\nu_k(t-\tau)\Big)\,d\tau$$

For $k = k_*$:

$$T_k'(t) = \frac{\rho}{2}e^{\rho t/2}\,(1 + D_k^*\,t) + D_k^* e^{\rho t/2} + \alpha_k\rho M\int_0^t K(\tau)e^{\rho(t-\tau)/2}\left[1 + \frac{\rho}{2}(t-\tau)\right]d\tau,$$

For $1 < k < k_*$:

$$T_k'(t) = \omega_k^{(1)}C_k^{**}e^{\omega_k^{(1)}t} + \omega_k^{(2)}D_k^{**}e^{\omega_k^{(2)}t} + \alpha_k\rho M\int\limits_0^t\left(e^{\omega_k^{(1)}(t-\tau)} - e^{\omega_k^{(2)}(t-\tau)}\right)K(\tau)d\tau$$

7 . At small times we obtain up to small values of order $O(\sqrt{t})$:

$$T_k'(t) \to \begin{cases} \rho\,(1-\alpha_k) + \rho\nu_k C_k, \quad \text{for } k > k_*, \\ \\ \dfrac{\rho}{2} + D_k^*, \quad \text{for } k = k_* \\ \\ \omega_k^{(1)}C_k^{**} + \omega_k^{(2)}\,(1 - C_k^{**})\,, \quad \text{for } 1 < k < k_* \end{cases}$$

So from the initial condition (3.35) and $N = \rho\alpha_k$ it follows

$$\begin{cases} \rho\,(1-\alpha_k) + \rho\nu_k C_k = -\rho\alpha_k, \\ \\ \dfrac{\rho}{2} + D_k^* = -\dfrac{\rho}{2}, \\ \\ \omega_k^{(1)}C_k^{**} + \omega_k^{(2)}\,(1 - C_k^{**}) = -\rho\alpha_k \end{cases} \to \begin{cases} C_k = -\dfrac{1}{\nu_k}, \quad \text{for } k > k_*, \\ \\ D_k^* = -\rho, \quad \text{for } k = k_* \\ \\ C_k^{**} = \dfrac{\nu_k - 1}{2\nu_k}, \quad \text{for } 1 < k < k_* \end{cases}$$

Thus, we obtain (3.36).

3.4.6 Final form of the solution in blocks $\widetilde{Y}^{(2)}$

The Green function has the following structure:

$$
\begin{aligned}
&G(x,\xi,t-\tau)= \\
&\quad=\sum_{k>k_*}^{\infty} R_k(x)R_k(\xi)\left\{e^{\rho(1-\alpha_k)(t-\tau)}\left[\cos\left(\rho\nu_k(t-\tau)\right)-\frac{1}{\nu_k}\sin\left(\rho\nu_k(t-\tau)\right)\right]+\right. \\
&\quad\left.+\frac{\beta_k}{\nu_k}\int_0^{t-\tau}\frac{\sin\left(\rho\nu_k(t-\tau-\theta)\right)}{\sqrt{\theta}}e^{\rho(1-a_k)(t-\tau-\theta)}d\tau\right\}+ \\
&\quad+R_{k_*}(x)R_{k_*}(\xi)e^{\rho(t-\tau)/2}\left(1-\rho(t-\tau)\right)+\beta_{k_*}\rho\int_0^{t-\tau}\frac{t-\tau-\theta}{\sqrt{\theta}}\,e^{\rho(t-\tau-\theta)/2}d\tau+ \\
&\quad+\sum_{1<k<k_*}R_k(x)R_k(\xi)\left\{\frac{\nu_k-1}{2\nu_k}\,e^{\omega_k^{(1)}(t-\tau)}+\frac{\nu_k+1}{2\nu_k}\,e^{\omega_k^{(2)}(t-\tau)}+\right. \\
&\quad\left.+\frac{\beta_k}{2\nu_k}\int_0^{t-\tau}\frac{1}{\sqrt{\theta}}\left(e^{\omega_k^{(1)}(t-\tau-\theta)}-e^{\omega_k^{(2)}(t-\tau-\theta)}\right)d\tau\right\}
\end{aligned}
\tag{3.44}
$$

where $R_k(x)$ are the orthonormal eigenfunctions of the Laplace operator.

If the block $\widetilde{Y}^{(2)}$ may be approximated by a sphere of radius $x^{(2)}=l$ then:

$$
\mu_k=\left(\frac{\pi k}{l}\right)^2,\qquad R_k(x)=\frac{r_k(x)}{||r_k||},\qquad r_k(x)=\frac{\sin\left(l\sqrt{\mu_k}\right)}{l},\qquad l^2\equiv\sum_{i=1}^{3}\left(x_i^{(2)}\right)^2,
$$

$$
||r_k||=\left(\int_{\widetilde{Y}^{(2)}}r_k^2(x)\right)^{1/2}=\left\langle r_k^2\right\rangle_1
$$

The pressure in block $\widetilde{Y}^{(2)}$ is:

$$
P_0^{(2)}\left(x^{(2)},t\right)=p_0^3-\frac{\widehat{B}^{(2)}}{\widehat{A}^{(2)}}\int_0^t\overline{G}\left(x^{(2)},t-\tau\right)\left[\frac{\partial p_0^3}{\partial\tau}-\gamma\lambda\frac{\widehat{B}^{(1)}}{\widehat{B}^{(2)}}\int_0^{\tau}\frac{\partial p_0^3}{\partial\theta}K\left(\tau-\theta\right)d\theta\right]d\tau \tag{3.45}
$$

where

$$
\overline{G}\left(x^{(2)},t-\tau\right)=\int_{\widetilde{Y}^{(2)}}G\left(x^{(2)},\xi,t-\tau\right)d\xi=\langle G\rangle_2
$$

3.5 Averaged model

Let $\mathcal{P}_{\rm b}$ and $\mathcal{P}_{\rm f}$ are the averaged pressures in the blocks $\widetilde{\Omega}^2$ and fractures Ω^3 respectively:

$$\mathcal{P}_{\rm b} = \left(\overline{P_0^2}\right)_{\widetilde{Y}^2}, \qquad \mathcal{P}_{\rm f} = \left(\overline{p_0^3}\right)_{Y^3}$$

The average model results from (3.21) and (3.45):

$$\begin{cases} \mathcal{P}_b = \mathcal{P}_f - \dfrac{\widehat{B}^{(2)}}{\widehat{A}^{(2)}} \dfrac{\partial \mathcal{P}_f}{\partial t} * \mathbb{K}^2, \\ \\ \widehat{B}^{(3)} \dfrac{\partial \mathcal{P}_f}{\partial t} = \nabla \cdot \left(\widehat{A}^{(3)} \nabla \mathcal{P}_f \right) - \widehat{B}^{(2)} \dfrac{\partial \mathcal{P}_b}{\partial t} * \mathbb{L}^{(2)} \end{cases} \tag{3.46}$$

where

$$\mathbb{K}^2 = \mathcal{K} - \gamma\lambda \frac{\widehat{B}^{(1)}}{\widehat{B}^{(2)}} \left(\mathcal{K} * \frac{1}{\sqrt{t}} \right), \tag{3.47}$$

$$\begin{aligned} \mathcal{K}(t) = \langle G(x, t-\tau) \rangle_2 = \frac{1}{\theta^{(2)}} \sum_{k>k_*} \frac{\langle r_k \rangle_2^2}{\langle r_k^2 \rangle_2} \Bigg\{ & e^{\rho(1-\alpha_k)t} \left[\cos(\rho\nu_k\, t) - \frac{1}{\nu_k} \sin(\rho\nu_k\, t) \right] + \\ & + \frac{\beta_k}{\nu_k} \int_0^t \frac{\sin\left(\rho\nu_k(t-\tau)\right)}{\sqrt{\tau}} e^{\rho(1-a_k)(t-\tau)} d\tau \Bigg\} + \\ & + \frac{1}{\theta^{(2)}} \frac{\langle r_{k_*} \rangle_2^2}{\langle r_{k_*}^2 \rangle_2} \left\{ e^{\rho t/2} (1 - \rho\, t) + \beta_{k_*} \rho \int_0^t \frac{t-\tau}{\sqrt{\tau}}\, e^{\rho(t-\tau)/2} d\tau \right\} + \\ & + \frac{1}{\theta^{(2)}} \sum_{1<k<k_*} \frac{\langle r_k \rangle_2^2}{\langle r_k^2 \rangle_2} \Bigg\{ \frac{\nu_k + 1}{2\nu_k}\, e^{\omega_k^{(1)}\, t} + \frac{\nu_k - 1}{2\nu_k}\, e^{\omega_k^{(2)}\, t} + \\ & + \frac{\beta_k}{2\nu_k} \int_0^t \frac{1}{\sqrt{\tau}} \left(e^{\omega_k^{(1)}(t-\tau)} - e^{\omega_k^{(2)}(t-\tau)} \right) d\tau \Bigg\} \end{aligned} \tag{3.48}$$

$$\mathbb{L}^{(2)} = \delta(t) + \gamma\lambda \frac{\widehat{B}^{(1)}}{\widehat{B}^{(2)}} \frac{1}{\sqrt{t}} \tag{3.49}$$

In Fig. 3.5 the equivalent kernel of three level fractured medium $\mathbb{K}^2$ from equation (3.47) is shown.

A numerical finite difference model is established for a two dimensional rectangular shape reservoir with the constant flux on the wellbore, and no flow boundary conditions as it is seen in Fig. 3.6:

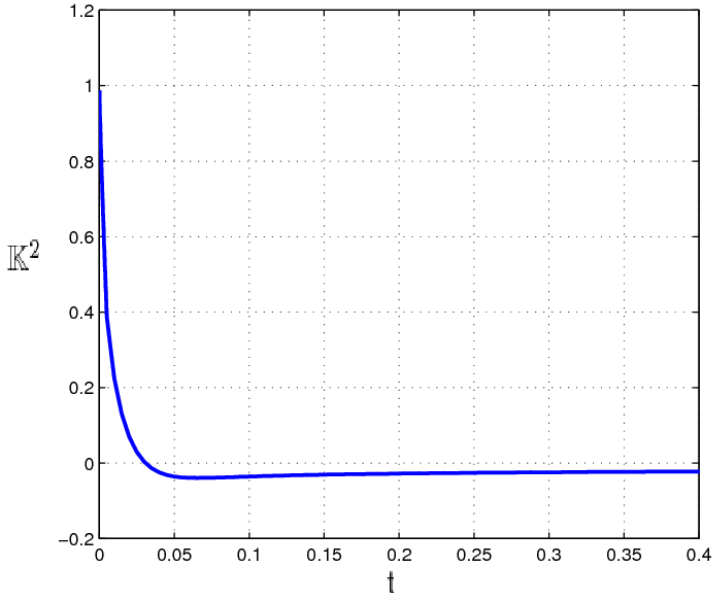

Figure 3.5: Effective kernel $\mathbb{K}^2$ for three level(short time behavior) fractured medium volume fraction of blocks $\theta = 0.99$

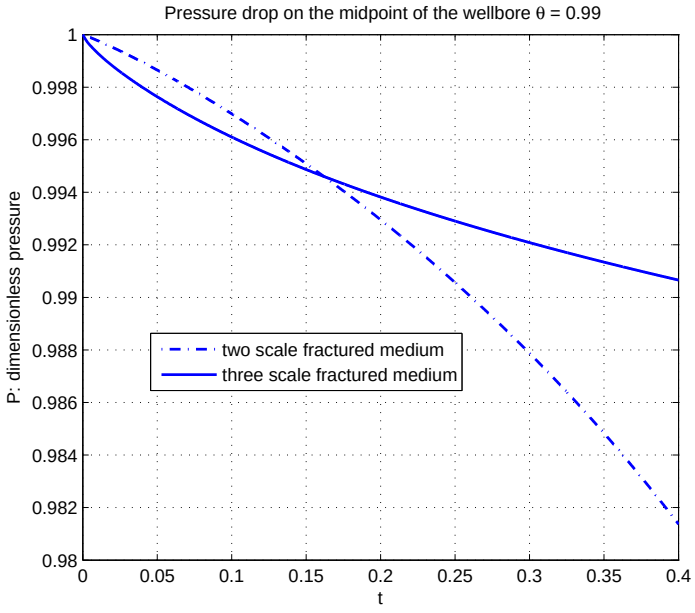

Figure 3.6: Pressure in the middle of the horizontal well for two and three level fractured medium (short time behavior)

Chapter 4

Model of flow in a single fracture

4.1 Problem formulation

4.1.1 Problem setting

Let us consider the fracture symmetric with respect to the axial plane and having wavy walls, as shown in Fig. 4.1. The fracture is surrounded by the porous medium containing fluid (oil). The walls are permeable and authorize the oil to cross them. The thickness of fracture in the direction orthogonal to flow is infinite, so that the problem is 2D. Let the wall oscillations be periodic with period ℓ, the mean fracture aperture

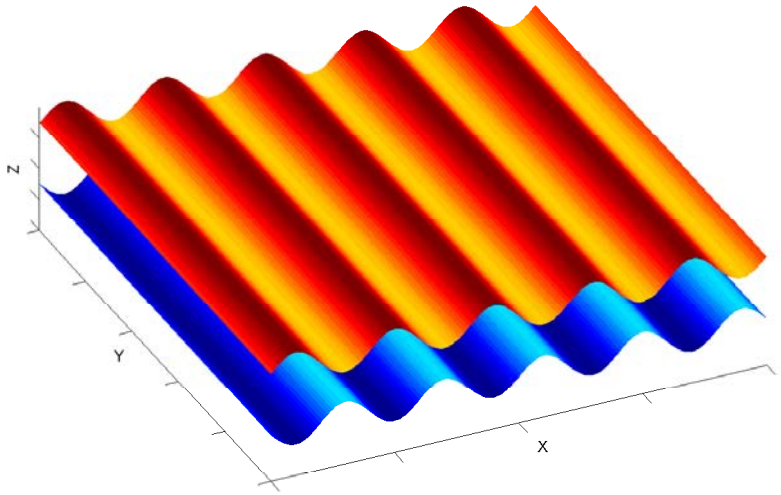

Figure 4.1: 2D fracture with wavy walls

be $2H$, and the characteristic length of the fracture be L. The fluid is incompressible, and the flow is steady-state.

The upper half of the 2D fracture represents the domain: $\{0 < Z < H\phi(X), \quad 0 < X < L\}$, where $\phi(X)$ is the periodic function with period ℓ and the mean value $\frac{1}{2}$. In case when $\phi(X) = \frac{1}{2}$, the fracture walls are non-oscillating.

The flow is described by Navier-Stokes equations.

The boundary condition at the inlet section imposes the given mean velocity U°:

$$U^\circ \equiv \frac{1}{H\phi(0)} \int_0^{H\phi(0)} U_x(0, Z) dZ \tag{4.1}$$

It is sufficient to assume that $\phi(0) = 1/2$.

The upper boundary of the well is penetrable by fluid. We impose the constant inflow velocity (U_x^*, U_z^*).

4.1.2 Formulation through dimensionless variables

Let us introduce dimensionless variables:

$$x = \frac{X}{L}, \quad z = \frac{Z}{H}, \quad u = \frac{U_x}{U^\circ}, \quad v = \frac{U_z}{U^\circ}, \quad p = \frac{P}{p^\circ}$$

with three dimensionless parameters:

$$\omega = \frac{H}{L}, \qquad \varepsilon = \frac{\ell}{L}, \qquad Re = \frac{\rho U^\circ H}{\mu}$$

The characteristic value p° is determined as the pressure drop over the distance L which might be caused by the Poiseuille flow at velocity U°: $p^\circ = \dfrac{\mu U^\circ L}{H^2}$.

In dimensionless variables the flow problem takes the form of Navier-Stokes equations in the domain $\mathcal{W} = \{0 < z < \phi(x), 0 < x < 1\}$:

$$\omega \frac{\partial u}{\partial x} + \frac{\partial v}{\partial z} = 0 \tag{4.2a}$$

$$\mathrm{Re}\left(\omega u \frac{\partial u}{\partial x} + v \frac{\partial u}{\partial z}\right) = -\frac{\partial p}{\partial x} + \omega^2 \frac{\partial^2 u}{\partial x^2} + \frac{\partial^2 u}{\partial z^2} \tag{4.2b}$$

$$\mathrm{Re}\left(\omega u \frac{\partial v}{\partial x} + v \frac{\partial v}{\partial z}\right) = -\frac{1}{\omega}\frac{\partial p}{\partial z} + \omega^2 \frac{\partial^2 v}{\partial x^2} + \frac{\partial^2 v}{\partial z^2} \tag{4.2c}$$

The boundary conditions are:

$$\frac{1}{2} = \int_0^{\phi(0)} u(0, z) dz = \int_0^{1/2} u(0, z) dz \tag{4.3a}$$

$$v|_{z=\phi(x)} = -\omega v^*, \qquad u|_{z=\phi(x)} = \omega u^*, \tag{4.3b}$$

$$\left.\frac{\partial u}{\partial z}\right|_{z=0} = 0, \qquad v|_{z=0} = 0, \tag{4.3c}$$

where $\omega u^* = U_x^*/U^\circ$, $\omega v^* = U_z^*/U^\circ$ are two components of the inflow velocity through the boundary; condition (4.3a) results from (4.1), conditions (4.3c) means the symmetry with respect to the fracture axis.

The presence of the small parameter ω in the relations for the inflow velocity means that it is assumed to be low.

This system possesses an integral relation which represents the mass balance between the external flux

and the internal flow:

$$\int_0^{\phi(x)} u(x,z)dz = F_0(x) + \omega F_1(x), \qquad F_0(x) \equiv \frac{1}{2} + \int_0^x v^* d\bar{x}, \qquad F_1(x) \equiv u^* \left(\phi(x) - \phi(0)\right) \tag{4.4}$$

Proof:

This relation is obtained by integrating the continuity equation (4.2a) over z:

$$0 = \omega \int_0^{\phi(x)} \frac{\partial u}{\partial x} dz + v\Big|_{z=0}^{z=\phi(x)} = \omega \int_0^{\phi(x)} \frac{\partial u}{\partial x} dz - \omega v^* = \omega \frac{\partial}{\partial x} \int_0^{\phi(x)} u dz - \omega^2 \phi' u^* - \omega v^*$$

Integration over x yields:

$$\int_0^{\phi(x)} u dz - \int_0^{\phi(0)} u dz - \omega u^* \Big(\phi(x) - \phi(0)\Big) - \int_0^x v^* dx = 0 \tag{4.5}$$

Taking into account for (4.3a) we obtain (4.4).

Remark: The system of boundary conditions is not sufficient to determine the unique solution, which is not important for our analysis, because the objective is to analyze the behavior of a family of solutions.

For simulations, the uniqueness may be reached by replacing condition (4.3a) imposed on the average velocity by the condition on the velocity at each point of the inlet section.

4.1.3 Parameters of the model

We will assume that parameters ω and ε are small:

$$0 < \omega, \varepsilon << 1$$

The ratio between them determines various regimes of flow. In particular, two limit cases do not represent any interest as reduce to a fracture with straight walls:

- if $\omega/\varepsilon << 1$, then the corrugation period is very large;

- if $\omega/\varepsilon >> 1$, then the fracture aperture is enormous, and the corrugation is neglecting.

Due to this we will consider the non-trivial case when:

$$\omega \sim \varepsilon^\alpha, \quad \text{where } \alpha \text{ is close to 1}$$

In contrast, the Reynolds number Re may take various values, from zero to several hundreds while the flow remains stable.

4.2 Method of solution

The analysis is performed by applying the asymptotic method: the solution is searched in the form of an asymptotic expansions with respect to small parameters ω and ε. In the limit $\varepsilon \to 0$ we will obtain a system that is homogenized along x. The limit $\omega \to 0$ formally means elimination of the transverse variable z, which means the homogenization along z. Thus the zero term of the asymptotic expansion is expected to be equal to the averaged value. Hence the technique of the suggested method is close to those procedures which are applied in the homogenization theory. The flow equations averaged over z represent the main interest of this chapter.

Owing to the particularity of the method used, the solutions obtained do not need to provide an exact detailed flow pattern, but they are expected to exhibit adequate homogenized behavior.

The asymptotic expansion can be constructed in two consecutive steps: first of all, one will develop the asymptotic equations as $\omega \to 0$ while assuming that ε is constant and of order 1; after this the asymptotic expansion $\varepsilon \to 0$ will be developed, i.e. we assume that:

$$\lim_{\varepsilon,\omega\to 0} \mathcal{U} = \lim_{\varepsilon\to 0} \left(\lim_{\omega\to 0} \mathcal{U} \right)$$

where $\mathcal{U} \equiv \{u, v, p\}$ is the solution to the considered problem.

At the first step, the solution is constructed as a regular asymptotic expansion when $\omega \to 0$: the zero term leads to functions averaged over the fracture aperture, or, at least, to functions whose behavior along x corresponds to the exact solution in the average sense only.

4.2.1 Asymptotic expansion - first step

Let us introduce the regular asymptotic expansion of $\mathcal{U} = \{u, v, p\}$ regarding to the small parameter ω:

$$\mathcal{U}(x, z) = \mathcal{U}_0(x, z) + \omega \mathcal{U}_1(x, z) + \omega^2 \mathcal{U}_2(x, z) + \dots \tag{4.6}$$

After substituting it in the problem (4.2) and (4.3) we will obtain for the first terms:

- Zero approximation u_0, v_0, p_0:

$$\frac{\partial v_0}{\partial z} = 0, \qquad \frac{\partial p_0}{\partial z} = 0, \qquad \mathrm{Re}\, v_0 \frac{\partial u_0}{\partial z} = -\frac{\partial p_0}{\partial x} + \frac{\partial^2 u_0}{\partial z^2}$$

$$v_0|_{z=\phi(x)} = 0, \qquad u_0|_{z=\phi(x)} = 0, \qquad \left.\frac{\partial u_0}{\partial z}\right|_{z=0} = 0, \qquad v_0|_{z=0} = 0, \qquad \int_0^{\phi(x)} u_0 dz = F_0(x)$$

where we used the integral relation (4.4).

This directly gives: $v_0 \equiv 0$.

- The first approximation u_1, v_1, p_1:

$$\frac{\partial u_0}{\partial x} + \frac{\partial v_1}{\partial z} = 0, \qquad 0 = \frac{\partial p_1}{\partial z}, \qquad \mathrm{Re}\left(u_0\frac{\partial u_0}{\partial x} + v_1\frac{\partial u_0}{\partial z}\right) = -\frac{\partial p_1}{\partial x} + \frac{\partial^2 u_1}{\partial z^2}$$
$$v_1|_{z=\phi(x)} = -v^*, \qquad u_1|_{z=\phi(x)} = u^*, \qquad \left.\frac{\partial u_1}{\partial z}\right|_{z=0} = 0, \qquad v_1|_{z=0} = 0$$
$$\int_0^{\phi(x)} u_1 dz = F_1(x)$$

The second approximation u_2, v_2, p_2:

$$\frac{\partial u_1}{\partial x} + \frac{\partial v_2}{\partial z} = 0, \qquad 0 = -\frac{\partial p_2}{\partial z} + \frac{\partial^2 v_1}{\partial z^2}$$
$$\mathrm{Re}\left(u_1\frac{\partial u_0}{\partial x} + u_0\frac{\partial u_1}{\partial x} + v_1\frac{\partial u_1}{\partial z} + v_2\frac{\partial u_0}{\partial z}\right) = -\frac{\partial p_2}{\partial x} + \frac{\partial^2 u_0}{\partial x^2} + \frac{\partial^2 u_2}{\partial z^2}$$
$$v_2|_{z=\phi(x)} = 0, \qquad u_2|_{z=\phi(x)} = 0, \qquad \left.\frac{\partial u_2}{\partial z}\right|_{z=0} = 0, \qquad v|_{z=0} = 0 \qquad \int_0^{\phi(x)} u_2 dz = 0$$

Introducing new mapping $(x, z) \to (x, \zeta)$ with $\zeta = \dfrac{z}{\phi}$, we have:

$$\frac{\partial}{\partial x} = \frac{\partial}{\partial x} - \frac{\zeta\phi'}{\phi}\frac{\partial}{\partial \zeta}, \qquad \frac{\partial}{\partial z} = \frac{1}{\phi}\frac{\partial}{\partial \zeta}$$

with $\phi' = \dfrac{d\phi}{dx}$. Now the zero, first and second-order problems would be simply integrable.

4.2.2 Solution of the zero-order problem

The zero-order approximation can be presented in the analytical form:

$$u_0 = -\frac{3F_0}{2\phi}(\zeta^2 - 1), \qquad p_0 = p_0(x), \qquad \frac{dp_0}{dx} = -\frac{3F_0}{\phi^3}$$

Proof: In terms of new variables the zero-order problem can be written as:

$$\begin{cases} \dfrac{\partial p_0}{\partial x} = \dfrac{1}{\phi^2}\dfrac{\partial^2 u_0}{\partial \zeta^2}, \\ \\ u_0|_{\zeta=1} = 0, \qquad \left.\dfrac{\partial u_0}{\partial z}\right|_{\zeta=0} = 0, \qquad \displaystyle\int_0^1 u_0 d\zeta = \frac{F_0}{\phi} \end{cases} \tag{4.7}$$

Separating the variables we obtain:

$$\frac{\partial^2 u_0}{\partial \zeta^2} = \phi^2\frac{dp_0}{dx}$$

The right-hand side of this equation depends only on x, then we obtain:

$$u_0 = \frac{\phi^2}{2}\frac{dp_0}{dx}\left(\zeta^2 - 1\right)$$

where we have used the boundary conditions. Then the integral relation in (4.7) gives:

$$\frac{dp_0}{dx} = -\frac{3F_0}{\phi^3}$$

Then $u_0 = -\frac{3F_0}{2\phi}(\zeta^2 - 1)$.

The solution for other approximations can be found in the annexes (A), (B).

4.2.3 Definite form of the solution

Let the inflow velocity u^*, v^* be constant. In this case, the asymptotic expansion takes the following form:

$$u(x,z) = u_0(x,z) + \omega u_1(x,z) + \omega^2 u_2(x,z) + ..., \tag{4.8}$$

$$v(x,z) = \omega v_1(x,z) + \omega^2 v_2(x,z), + ..., \tag{4.9}$$

$$\frac{\partial p}{\partial x} = \frac{dp_0}{dx}(x) + \omega \frac{\partial p_1}{\partial x} + \omega^2 \frac{\partial p_2}{\partial x} + ..., \tag{4.10}$$

where:

$$u_0(x,\zeta) = -\frac{3}{2}\frac{F_0}{\phi}(\zeta^2 - 1), \tag{4.11a}$$

$$u_1(x,\zeta) = u^* + \frac{\mathrm{Re}\, F_0 v^*}{280}\left(7\zeta^6 - 9\zeta^2 + 2\right) - \frac{3\mathrm{Re}\, F_0^2 \phi'}{280\phi}\left(7\zeta^6 - 35\zeta^4 + 33\zeta^2 - 5\right) + \\ + \frac{3u^*\phi(0)}{2\phi}\left(\zeta^2 - 1\right); \tag{4.11b}$$

$$u_2(x,\zeta) = \frac{1}{20}\left(-3F_0\phi'' - 5v^*\phi' + \frac{9F_0\phi'^2}{\phi}\right)\left(5\zeta^4 - 6\zeta^2 + 1\right) + \\ + \frac{\mathrm{Re}\, u^*\phi' F_0}{280}\left(105\zeta^4 - 126\zeta^2 + 21\right) - \frac{\mathrm{Re}\, u^* v^* \phi(0)}{280}\left(7\zeta^6 - 9\zeta^2 + 2\right) + \\ + \frac{3\mathrm{Re}\, u^*\phi(0)\phi' F_0}{140\,\phi}\left(7\zeta^6 - 35\zeta^4 + 33\zeta^2 - 5\right) - \frac{\mathrm{Re}\, u^* v^* \phi}{40}\left(5\zeta^4 - 6\zeta^2 + 1\right) + \\ + \frac{\mathrm{Re}^2 F_0^3 \phi''}{1120}\left(\zeta^{10} - 9\zeta^8 + \frac{138}{5}\zeta^6 - 42\zeta^4 + \frac{9837}{385}\zeta^2 - \frac{1213}{385}\right) - \\ - \frac{\mathrm{Re}^2 F_0^3 \phi'^2}{280\,\phi}\left(\frac{7}{10}\zeta^{10} - \frac{27}{4}\zeta^8 + \frac{102}{5}\zeta^6 - \frac{57}{2}\zeta^4 + \frac{12333}{770}\zeta^2 - \frac{575}{313}\right) + \\ + \frac{\mathrm{Re}^2 v^{*2} F_0 \phi}{2800}\left(\frac{\zeta^{10}}{3} - \frac{15}{2}\zeta^8 + 3\zeta^6 + \frac{438}{77}\zeta^2 - \frac{703}{462}\right) + \\ + \frac{\mathrm{Re}^2 v^* F_0^2 \phi'}{5600}\left(6\zeta^{10} - \frac{75}{4}\zeta^8 - 21\zeta^6 - 1725\zeta^4 + \frac{2759}{11}\zeta^2 - \frac{1961}{44}\right) \tag{4.11c}$$

$$v_1(x,\zeta) = -\frac{3F_0\phi'}{2\phi}\left(\zeta^3-\zeta\right) + \frac{3v^*}{2}\left(\frac{\zeta^3}{3}-\zeta\right), \tag{4.11d}$$

$$\begin{aligned} v_2(x,\zeta) = {} & \frac{3u^*\phi'\phi(0)}{2\phi}\left(\zeta^3-\zeta\right) - \frac{\mathrm{Re}\,\phi {v^*}^2}{280}\left(\zeta^7-3\zeta^3+2\zeta\right) - \\ & -\frac{3\mathrm{Re}\,\phi'^2F_0^2}{280\phi}\left(7\zeta^7-35\zeta^5+33\zeta^3-5\zeta\right) + \frac{3\mathrm{Re}\,v^*\phi'F_0}{140}\left(2\zeta^7-7\zeta^5+10\zeta^3-5\zeta\right) + \\ & +\frac{3\mathrm{Re}\,\phi''F_0^2}{280}\left(\zeta^7-7\zeta^5+11\zeta^3-5\zeta\right) \end{aligned} \tag{4.11e}$$

$$\frac{dp_0}{dx}(x) = -\frac{3F_0}{\phi^3}, \tag{4.11f}$$

$$\frac{dp_1}{dx}(x) = \frac{3u^*\phi(0)}{\phi^3} - \frac{81\mathrm{Re}\,v^*F_0}{35\phi^2} + \frac{54\mathrm{Re}\,F_0^2\phi'}{35\phi^3}, \tag{4.11g}$$

$$\begin{aligned} \frac{\partial p_2}{\partial x}(x,\zeta) = {} & \left(\frac{9F_0\phi'^2}{\phi^3} - \frac{9F_0\phi''}{2\phi^2} - \frac{6v^*\phi'}{\phi^2}\right)\zeta^2 + \frac{3F_0\phi''}{10\phi^2} - \frac{12F_0\phi'^2}{5\phi^3} - \frac{6\,\mathrm{Re}\,u^*v^*}{5\phi} + \\ & +\frac{81\,\mathrm{Re}\,u^*v^*\phi(0)}{35\phi^2} + \frac{3\,\mathrm{Re}\,u^*F_0\phi'}{5\phi^2} + \frac{156\,\mathrm{Re}^2F_0^3}{13475}\left(\frac{4\phi'^2}{\phi^3} - \frac{3\phi''}{\phi^2}\right) - \\ & -\frac{234\,\mathrm{Re}^2F_0{v^*}^2}{13475\,\phi} - \frac{271\,\mathrm{Re}^2F_0^2v^*\phi'}{1925\,\phi^2} - \frac{108\,\mathrm{Re}\,u^*\phi(0)F_0\phi'}{35\,\phi^3} \end{aligned} \tag{4.11h}$$

4.2.4 Two-scale form of the obtained solution

In order to average over the fluctuations caused by the wavy walls, we can use the fact that the scale of the oscillations is small with respect to the high length of the well. Due to the high difference between two scales, the behavior at two scales may be assumed to be independent of one another. This means that we can introduce the small-scale ("fast") variable $y = x/\varepsilon$ and consider it as independent of the slow variable x. Then we introduce the extended functions $\tilde{f}(x,y)$ which are equal to $f(x)$ when $y = x/\varepsilon$. The derivative becomes also two-scale and if defined as:

$$\frac{\partial f}{\partial x} = \frac{\partial \tilde{f}}{\partial x} + \frac{1}{\varepsilon}\frac{\partial \tilde{f}}{\partial y}$$

Noting : $\frac{1}{\varepsilon}\phi'_y = \frac{d\phi}{dx} = \phi'$, $\qquad \zeta = z/\phi$, then the two-scale form of the solution (4.11) becomes:

$$
\begin{aligned}
u = &-\frac{3}{2}\frac{F_0}{\phi}(\zeta^2-1) + \frac{\omega}{\varepsilon}\Bigg\{ - \frac{3\mathrm{Re}\,F_0^2\phi'_y}{280\phi}\left(7\zeta^6 - 35\zeta^4 + 33\zeta^2 - 5\right) + \\
&+\varepsilon\left[\frac{\mathrm{Re}\,F_0 v^*}{280}\left(7\zeta^6 - 9\zeta^2 + 2\right) + \frac{3u^*\phi(0)}{2\phi}\left(\zeta^2-1\right) + u^*\right] + \varepsilon^2 ...\Bigg\} + \\
&+\frac{\omega^2}{\varepsilon^2}\Bigg\{ \frac{1}{20}\left(-3F_0\phi''_{yy} + \frac{9F_0\phi'^2_y}{\phi}\right)\left(5\zeta^4 - 6\zeta^2 + 1\right) + \\
&\quad +\frac{\mathrm{Re}^2F_0^3\phi''_{yy}}{1120}\left(\zeta^{10} - 9\zeta^8 + \frac{138}{5}\zeta^6 - 42\zeta^4 + \frac{9837}{385}\zeta^2 - \frac{1213}{385}\right) - \\
&\quad -\frac{\mathrm{Re}^2F_0^3\phi'^2_y}{280\,\phi}\left(\frac{7}{10}\zeta^{10} - \frac{27}{4}\zeta^8 + \frac{102}{5}\zeta^6 - \frac{57}{2}\zeta^4 + \frac{12333}{770}\zeta^2 - \frac{575}{313}\right) + \\
&\quad +\varepsilon\Bigg[-\frac{1}{4}\left(v^*\phi'_y\right)\left(5\zeta^4 - 6\zeta^2 + 1\right) + \frac{\mathrm{Re}\,u^*\phi'_yF_0}{280}\left(105\zeta^4 - 126\zeta^2 + 21\right) + \\
&\quad\quad +\frac{3\mathrm{Re}\,u^*\phi(0)\phi'_yF_0}{140\,\phi}\left(7\zeta^6 - 35\zeta^4 + 33\zeta^2 - 5\right) + \\
&\quad\quad +\frac{\mathrm{Re}^2v^*F_0^2\phi'_y}{5600}\left(6\zeta^{10} - \frac{75}{4}\zeta^8 - 21\zeta^6 - 1725\zeta^4 + \frac{2759}{11}\zeta^2 - \frac{1961}{44}\right)\Bigg] + \\
&\quad +\varepsilon^2\Bigg[-\frac{\mathrm{Re}\,u^*v^*\phi(0)}{280}\left(7\zeta^6 - 9\zeta^2 + 2\right) - \frac{\mathrm{Re}\,u^*v^*\phi}{40}\left(5\zeta^4 - 6\zeta^2 + 1\right) + \\
&\quad\quad +\frac{\mathrm{Re}^2v^{*2}F_0\phi}{2800}\left(\frac{\zeta^{10}}{3} - \frac{15}{2}\zeta^8 + 3\zeta^6 + \frac{438}{77}\zeta^2 - \frac{703}{462}\right)\Bigg] + \varepsilon^3 ...\Bigg\} + O(\frac{\omega^3}{\varepsilon^3} + \omega\varepsilon)
\end{aligned}
\tag{4.12}
$$

$$
\begin{aligned}
v = &\frac{\omega}{\varepsilon}\Bigg\{ -\frac{3F_0\phi'_y}{2\phi}\left(\zeta^3 - \zeta\right) + \varepsilon\frac{3v^*}{2}\left(\frac{\zeta^3}{3} - \zeta\right) + \varepsilon^2 ...\Bigg\} + \\
&+\frac{\omega^2}{\varepsilon^2}\Bigg\{ -\frac{3\mathrm{Re}\,\phi'^2_yF_0^2}{280\phi}\left(7\zeta^7 - 35\zeta^5 + 33\zeta^3 - 5\zeta\right) + \frac{3\mathrm{Re}\,\phi''_{yy}F_0^2}{280}\left(\zeta^7 - 7\zeta^5 + 11\zeta^3 - 5\zeta\right) + \\
&\quad +\varepsilon\left[\frac{3u^*\phi'_y\phi(0)}{2\phi}\left(\zeta^3 - \zeta\right) + \frac{3\mathrm{Re}\,v^*\phi'_yF_0}{140}\left(2\zeta^7 - 7\zeta^5 + 10\zeta^3 - 5\zeta\right)\right] + \\
&\quad +\varepsilon^2\left[\frac{\mathrm{Re}\,\phi v^{*2}}{280}\left(-\zeta^7 + 3\zeta^3 - 2\zeta\right)\right] + \varepsilon^3 ...\Bigg\} + O(\frac{\omega^3}{\varepsilon^3} + \omega\varepsilon)
\end{aligned}
\tag{4.13}
$$

$$
\begin{aligned}
\frac{\partial p}{\partial x} = &-\frac{3F_0}{\phi^3} + \frac{\omega}{\varepsilon}\left\{\frac{54\mathrm{Re}\,\phi'_yF_0^2}{35\phi^3} + \varepsilon\left[\frac{3u^*\phi(0)}{\phi^3} - \frac{81\mathrm{Re}\,v^*F_0}{35\phi^2}\right] + \varepsilon^2 ...\right\} + \\
&+\frac{\omega^2}{\varepsilon^2}\Bigg\{ \left(\frac{9\phi'^2_yF_0}{\phi^3} - \frac{9\phi''_{yy}F_0}{2\phi^2}\right)\zeta^2 + \frac{3\phi''_{yy}F_0}{10\phi^2} - \frac{12\phi'^2_yF_0}{5\phi^3} + \frac{156\,\mathrm{Re}^2F_0^3}{13475}\left(\frac{4\phi'^2_y}{\phi^3} - \frac{3\phi''_{yy}}{\phi^2}\right) + \\
&\quad +\varepsilon\left[-\frac{6v^*\phi'}{\phi^2}\zeta^2 + \frac{3\,\mathrm{Re}\,u^*\phi'_yF_0}{5\phi^2} - \frac{271\,\mathrm{Re}^2v^*\phi'_yF_0^2}{1925\,\phi^2} - \frac{108\,\mathrm{Re}\,u^*\phi(0)\phi'_yF_0}{35\,\phi^3}\right] + \\
&\quad +\varepsilon^2\left[\frac{81\,\mathrm{Re}\,u^*v^*\phi(0)}{35\phi^2} - \frac{6\,\mathrm{Re}\,u^*v^*}{5\phi} - \frac{234\,\mathrm{Re}^2v^{*2}F_0}{13475\,\phi}\right] + \varepsilon^3 ...\Bigg\} + O(\frac{\omega^3}{\varepsilon^3} + \omega\varepsilon)
\end{aligned}
\tag{4.14}
$$

4.2.5 Calculation of the stream function

The streamlines are defined through the following relations:

$$u = \frac{\partial \psi}{\partial z}, \qquad v = -\frac{\partial \psi}{\partial x}$$

Integration of the first relation gives:

$$\begin{aligned}\psi = \int u\phi d\zeta = -\frac{3}{2}F_0\left(\frac{\zeta^3}{3}-\zeta\right) + \omega\Bigg\{ -\frac{3}{280}\mathrm{Re}\, F_0^2\phi'\left(\zeta^7 - 7\zeta^5 + 11\zeta^3 - 5\zeta\right)\Bigg\} + \\ +\omega^2\Bigg\{\left(-3F_0\phi\phi'' + 9F_0\phi'^2\right)\left(\frac{\zeta^5}{20} - \frac{\zeta^3}{10} + \frac{\zeta}{20}\right) + \\ +\frac{1}{280}\mathrm{Re}^2F_0^3\phi\phi''\left(\frac{\zeta^{11}}{44} - \frac{\zeta^9}{4} + \frac{69}{70}\zeta^7 - \frac{21}{10}\zeta^5 + \frac{3279}{154}\zeta^3 - \frac{1213}{154}\zeta\right) - \\ -\frac{1}{280}\mathrm{Re}^2F_0^3\phi'^2\left(\frac{7\zeta^{11}}{110} - \frac{3}{4}\zeta^9 + \frac{204}{70}\zeta^7 - \frac{57}{10}\zeta^5 + \frac{4111}{770}\zeta^3 - \frac{575}{313}\zeta\right)\Bigg\} + C + O(\omega^3)\end{aligned} \tag{4.15}$$

where C is an arbitrary constant.

4.2.6 Results obtained

The solution obtained can be used to examine the microscale flow pattern. For a sinusoidal corrugation given by:

$$\phi(x) = 0.5\,(1 + a\sin(2\pi x/\varepsilon)) \tag{4.16}$$

where a is new dimensionless parameter equal to the ratio of the corrugation amplitude at half of the mean aperture.

The calculations based on the obtained asymptotic solutions performed for $\omega = 0.01$, $\varepsilon = 0.01^{0,75} = 0.0316$ and $a = 0.3$, are shown in Fig. 4.2, for $\mathrm{Re} = 12$.

It is seen that at small Re the inflow through the walls Fig. 4.2(b) influences the flow streamlines in the vicinity of walls, but weakly influences the velocity field.

For high Re ($\mathrm{Re} = 55$), the results of solution are shown in Fig. 4.3.

For high Re, the impact of the inflow through the walls on the flow structure in the fracture is significant, both in terms of the streamlines, but also in terms of the velocity. In the presence of inflow the flow in the well is no longer periodic.

The behavior of pressure gradient along the fracture axis at $\mathrm{Re} = 12$ and $\mathrm{Re} = 20$ is presented in Fig. 4.4.

The pressure drop along the fracture is periodic when there is no inflow. In the case with inflow the amplitude of oscillations of the pressure gradient increases along the flow direction. At high Reynolds, starting around $\mathrm{Re} = 20$, the pressure gradient becomes locally positive which means the appearance of a local reverse flow. This counter-current flow might result in the appearance of the instability.

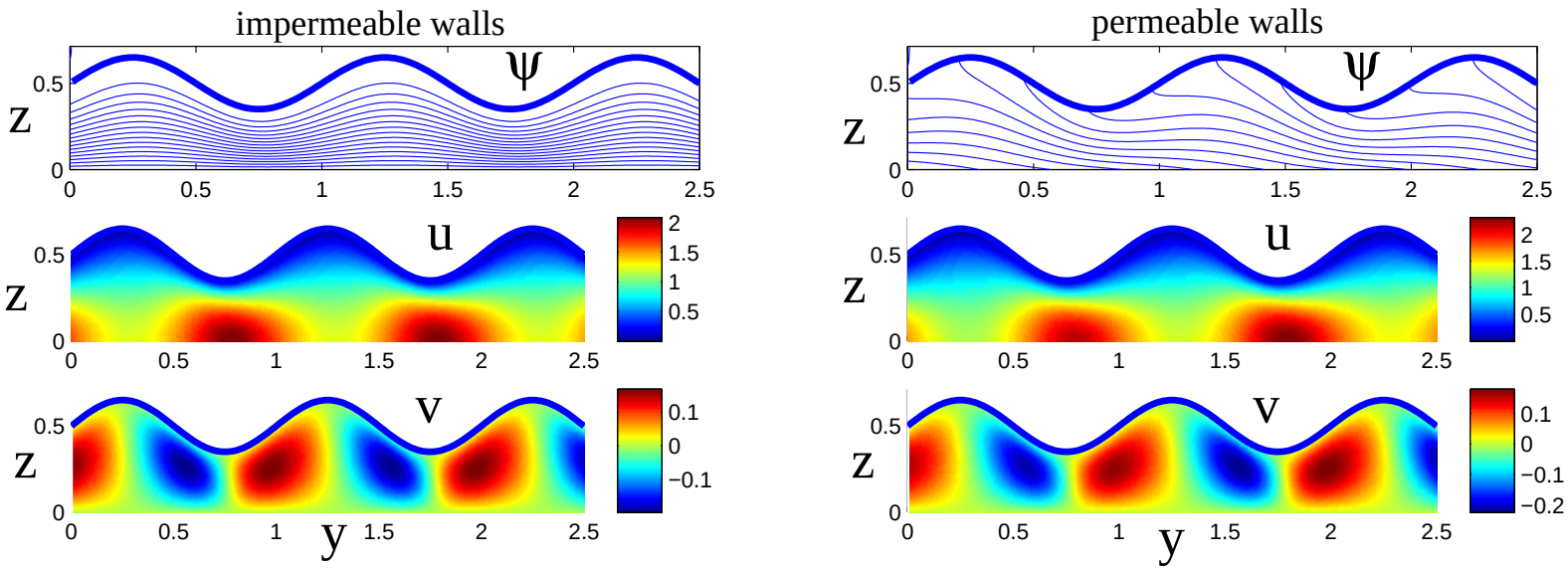

(a) (b)

Figure 4.2: Stream function (ψ), and isolines of longitudinal velocity (u) and transversal velocity (v) for Re $= 12$

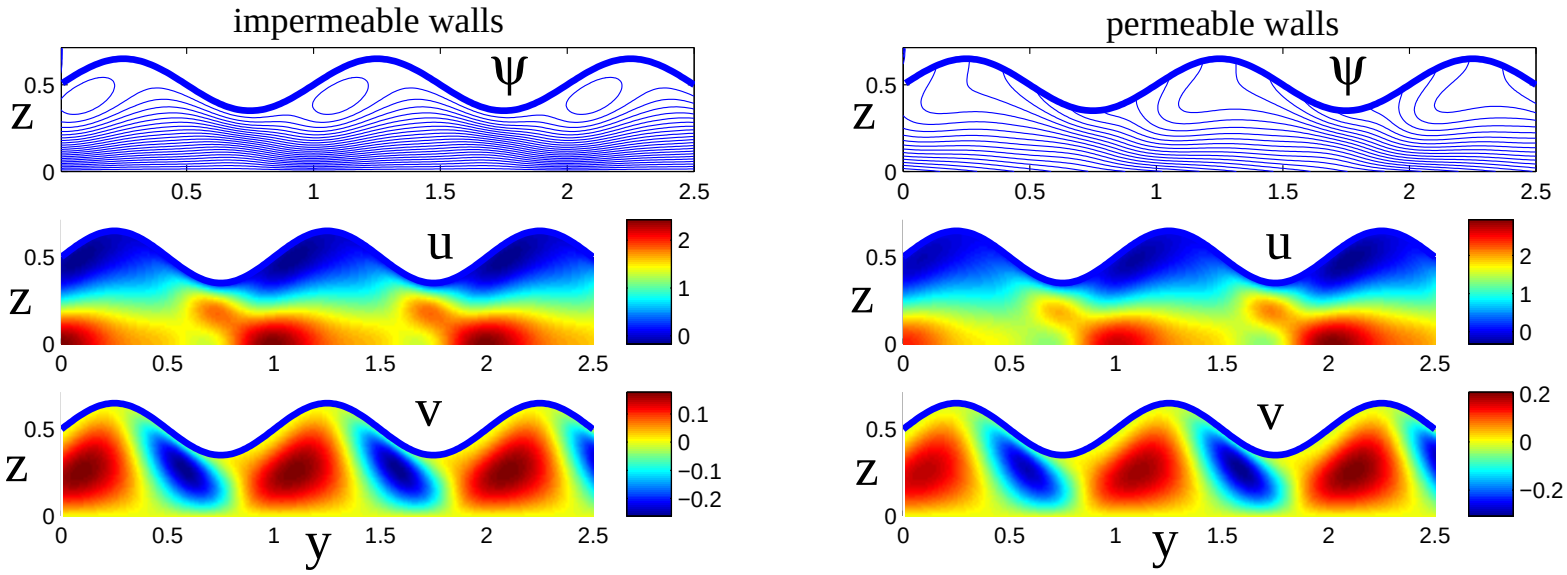

(a) (b)

Figure 4.3: Stream function (ψ), and isolines of longitudinal velocity (u) and transversal velocity (v) for Re = 55

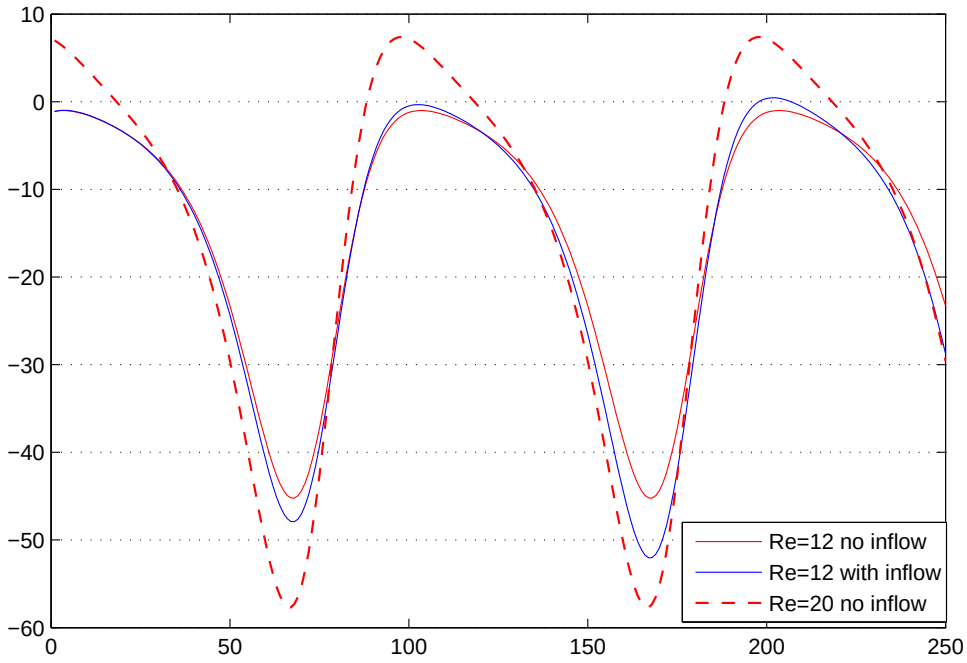

Figure 4.4: Pressure drop dp/dx averaged on axis of fracture aperture, $\omega = 0.01, \quad \varepsilon = 0.0316$

4.3 Model averaged over the wall oscillations

The practical interest represents the momentum equation averaged twice: (1) over the fracture aperture and (2) over the fluctuations caused by the wavy walls. The technique of second averaging is presented in this section. It consists of separating the scales and averaging over the lowest scale.

4.3.1 Averaged equation of flow

Let us introduce the single and twice averaging for an arbitrary two-scale function $\tilde{f}(x, yz)$:

$$\langle f\rangle = \int_0^1 \tilde{f}(x,y,z)dy, \qquad \langle\langle f\rangle\rangle = \int_0^1 \left(\frac{1}{\phi(y)}\int_0^{\phi(y)} \tilde{f}(x,y,z)dz\right)dy \tag{4.17}$$

The twice averaged equations (4.12), (4.13), and (4.14) become:

$$\langle\langle u\rangle\rangle = F_0\left\langle\frac{1}{\phi}\right\rangle + \omega\, u^*\left(1-\phi(0)\left\langle\frac{1}{\phi}\right\rangle\right) \tag{4.18}$$

$$\langle\langle v\rangle\rangle = 0 \tag{4.19}$$

$$\begin{aligned}\left\langle\left\langle\frac{\partial p}{\partial x}\right\rangle\right\rangle = &-3F_0\left\langle\frac{1}{\phi^3}\right\rangle + 3\omega\, u^*\phi(0)\left\langle\frac{1}{\phi^3}\right\rangle + \frac{\omega^2}{\varepsilon^2}\frac{3}{5}F_0\left(\left\langle\frac{(\phi_y')^2}{\phi^3}\right\rangle - 2\left\langle\frac{\phi_{yy}''}{\phi^2}\right\rangle\right) + \\ &+\mathrm{Re}\, v^*\left\{-\omega\frac{81}{35}F_0\left\langle\frac{1}{\phi^2}\right\rangle + \omega^2\left[-\frac{6}{5}u^*\left\langle\frac{1}{\phi}\right\rangle + \frac{81}{35}u^*\phi(0)\left\langle\frac{1}{\phi^2}\right\rangle\right]\right\} + \\ &+\mathrm{Re}^2\frac{3}{13475}\left\{\frac{\omega^2}{\varepsilon^2}4F_0^3\left(-39\left\langle\frac{\phi_{yy}''}{\phi^2}\right\rangle + 52\left\langle\frac{\phi_y'^{\,2}}{\phi^3}\right\rangle\right) - \omega^2 78F_0 v^{*2}\left\langle\frac{1}{\phi}\right\rangle\right\}\end{aligned} \tag{4.20}$$

Returning back to the dimensional variables, and denoting $\mathcal{U} \equiv \langle\langle U\rangle\rangle$, $\mathcal{P} \equiv \langle\langle P\rangle\rangle$, we obtain:

$$\mathcal{U} = U^0\left(F_0\left\langle\frac{1}{\phi}\right\rangle + \omega\, u^*\left(1-\phi(0)\left\langle\frac{1}{\phi}\right\rangle\right)\right) \tag{4.21}$$

$$\begin{aligned}\frac{d\mathcal{P}}{dX} = &\frac{\mu U^0}{H^2}\left\{-3F_0\left\langle\frac{1}{\phi^3}\right\rangle + \omega\, 3u^*\phi(0)\left\langle\frac{1}{\phi^3}\right\rangle + \frac{\omega^2}{\varepsilon^2}\frac{3}{5}F_0\left(\left\langle\frac{(\phi_y')^2}{\phi^3}\right\rangle - 2\left\langle\frac{\phi_{yy}''}{\phi^2}\right\rangle\right)\right\} + \\ &+\frac{\rho U^{0\,2}\, v^*}{H}\left\{-\omega\frac{81}{35}F_0\left\langle\frac{1}{\phi^2}\right\rangle + \omega^2\left[-\frac{6}{5}u^*\left\langle\frac{1}{\phi}\right\rangle + \frac{81}{35}u^*\phi(0)\left\langle\frac{1}{\phi^2}\right\rangle\right]\right\} + \\ &+\frac{\rho^2 U^{0\,3}}{\mu}\frac{3}{13475}\left\{\frac{\omega^2}{\varepsilon^2}4F_0^3\left(-39\left\langle\frac{\phi_{yy}''}{\phi^2}\right\rangle + 52\left\langle\frac{\phi_y'^{\,2}}{\phi^3}\right\rangle\right) - \omega^2 78F_0 v^{*2}\left\langle\frac{1}{\phi}\right\rangle\right\}\end{aligned}$$

Replacing U^0 by $\mathcal{U}$ by using (4.21), we obtain the averaged momentum balance equation in the form of a cubic law:

$$-\frac{d\mathcal{P}}{dX} = \frac{\mu\mathcal{U}}{K^{\text{ef}}} + \beta^{\text{ef}}\rho\mathcal{U}^2 + \frac{\gamma^{\text{ef}}\rho^2\mathcal{U}^3}{\mu} \tag{4.22}$$

$$K^{\text{ef}} \equiv \frac{H^2}{12}\lambda; \qquad \lambda = \frac{4\left[F_0\left\langle\frac{1}{\phi}\right\rangle + \omega\, u^*\left(1-\phi(0)\left\langle\frac{1}{\phi}\right\rangle\right)\right]}{F_0\left\langle\frac{1}{\phi^3}\right\rangle - \omega\, u^*\phi(0)\left\langle\frac{1}{\phi^3}\right\rangle - \frac{\omega^2}{\varepsilon^2}\frac{F_0}{5}\left(\left\langle\frac{(\phi_y')^2}{\phi^3}\right\rangle - 2\left\langle\frac{\phi_{yy}''}{\phi^2}\right\rangle\right)} \tag{4.23a}$$

$$\beta^{\text{ef}} \equiv \frac{v^*\omega}{35H}\cdot\frac{81F_0\left\langle\frac{1}{\phi^2}\right\rangle + \omega u^*\left[42\left\langle\frac{1}{\phi}\right\rangle - 81\phi(0)\left\langle\frac{1}{\phi^2}\right\rangle\right]}{\left(F_0\left\langle\frac{1}{\phi}\right\rangle + \omega\, u^*\left(1-\phi(0)\left\langle\frac{1}{\phi}\right\rangle\right)\right)^2} \tag{4.23b}$$

$$\gamma^{\text{ef}} \equiv \frac{6}{13475}\frac{\frac{\omega^2}{\varepsilon^2}2F_0^3\left(39\left\langle\frac{\phi_{yy}''}{\phi^2}\right\rangle - 52\left\langle\frac{\phi_y'^{\,2}}{\phi^3}\right\rangle\right) + \omega^2 39F_0v^{*2}\left\langle\frac{1}{\phi}\right\rangle}{\left(F_0\left\langle\frac{1}{\phi}\right\rangle + \omega\, u^*\left(1-\phi(0)\left\langle\frac{1}{\phi}\right\rangle\right)\right)^3} \tag{4.23c}$$

4.3.2 Effective parameters of flow

Three effective parameters determine the averaged behavior of the system:

- K^{ef} is the fracture permeability [m^2], the parameter responsible for the pure viscous dissipation (the firction) which corresponds to the Stokes flow. According to [Panfilov and Fourar, 2006] we will use the term "zero-order field" to describe the case of Re $\to 0$.

- β^{ef} is the inertia parameter having the dimension [m^{-1}]. It is responsible for the integral losses of the kinetic energy within a period caused by the that component of the inflow velocity which is orthogonal to the fracture axis, v^*. The orthogonal component of inflow deviates fluid from the axial direction of flow, which reduces the fluid axial velocity. The energy transferred with the inflow plays the role of a decelerator, which means the appearance of a negative acceleration, or the inertia losses of energy.

- γ^{ef} is the dimensionless parameter responsible for the inertia-viscous cross-effect which was described first in [Panfilov and Bues, 2004] and [Panfilov and Fourar, 2006]. It represents a supplementary viscous dissipation produced by the deviation of the streamlines from the zero-order field. As the streamline deformation is caused by the inertia forces, this term depends on Re.

Two limit cases helps to analyze the behavior of these parameters: the non-corrugated fracture, and the impermeable walls.

For the case of non-corrugated walls, when $\phi = 1/2$, we obtain:

$$K^{\text{ef}} \equiv \frac{H^2}{12}\lambda; \qquad \lambda = \frac{2F_0}{2F_0 - \omega\, u^*} \tag{4.24a}$$

$$\beta^{\text{ef}} \equiv \frac{v^*\omega}{35H} \cdot \frac{81F_0 - 19.5\omega u^*}{F_0^2} \tag{4.24b}$$

$$\gamma^{\text{ef}} \equiv \frac{117\omega^2 v^{*2}}{26950F_0^2} \tag{4.24c}$$

For the case of zero inflow through the walls $u^* = v^* = 0$, we obtain:

$$K^{\text{ef}} \equiv \frac{H^2}{12}\lambda; \qquad \lambda = \frac{4\left\langle \frac{1}{\phi} \right\rangle}{\left\langle \frac{1}{\phi^3} \right\rangle - \frac{\omega^2}{\varepsilon^2}\frac{1}{5}\left(\left\langle \frac{(\phi_y')^2}{\phi^3} \right\rangle - 2\left\langle \frac{\phi_{yy}''}{\phi^2} \right\rangle \right)} \tag{4.25a}$$

$$\beta^{\text{ef}} \equiv 0 \tag{4.25b}$$

$$\gamma^{\text{ef}} \equiv \frac{12\,\omega^2}{13475\,\varepsilon^2} \frac{\left(39\left\langle \frac{\phi_{yy}''}{\phi^2} \right\rangle - 52\left\langle \frac{\phi_y'^{\,2}}{\phi^3} \right\rangle \right)}{\left\langle \frac{1}{\phi} \right\rangle^3} \tag{4.25c}$$

The dependence of these parameters, taken in dimensionless form, on the dimensionless amplitude of wall oscillations a (the amplitude divided by the fracture aperture H), is shown in Fig. 4.5, 4.6 and 4.7. It was assumed that $\omega = 0.01$, $\varepsilon = 0.01^{0.75}$.

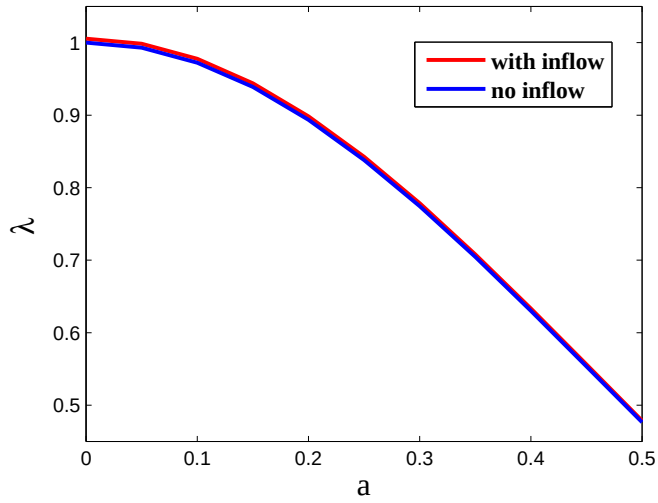

Figure 4.5: Dimensionless fracture permeability λ vs. wall oscillation amplitude a

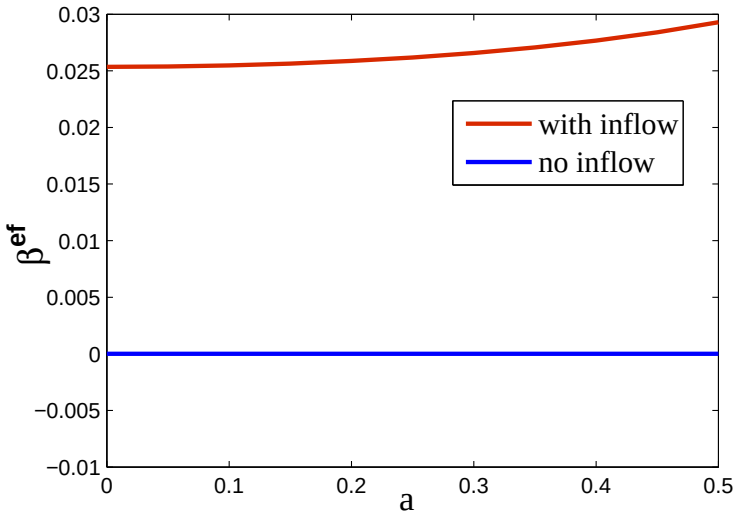

Figure 4.6: Dimensionless pure inertia coefficient $\beta^{\text{ef}} \cdot H$ vs. wall oscillation amplitude a

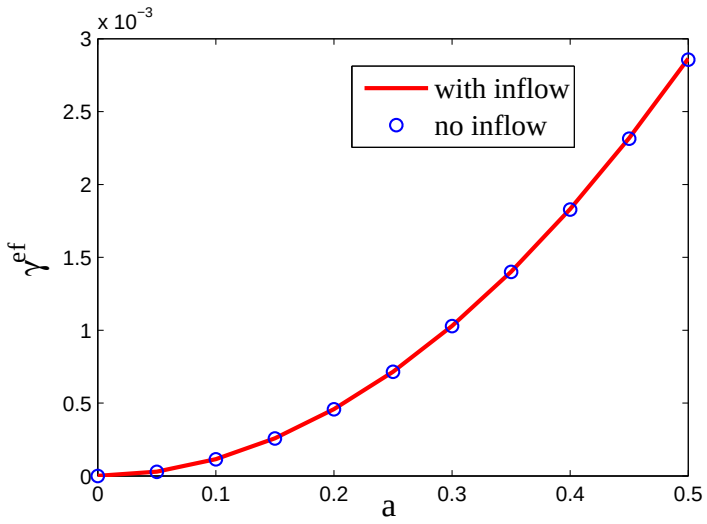

Figure 4.7: Dimensionless viscous-inertia cross parameter γ^{ef} vs. wall oscillation amplitude a

As seen, the inertia-viscous parameter is practically independent of the inflow. The inflow increases the permeability but this influence is low. The pure inertia parameter β^{ef} is the most sensible with respect to the inflow, and increases when the inflow velocity augments.

4.4 Comparison of analytic model and numerical simulations

A COMSOL©model was also developed to study the qualitative behavior of streamlines in the case of flow between two wavy planes, when there is no inflow through them. The simulations are based on the finite element method with triangular discretization of the domain, and the implicit method of discretization in time.

The results of simulations prove the same qualitative behavior as in analytical solutions. The maximum longitudinal velocity is close to what obtained analytically. The streamlines and the velocity field plotted for $Re = 12$ without and with inflow in Fig. 4.8.

The qualitative behavior of the solutions is similar to that obtained by the asymptotic method. In Fig. 4.9 for a rather higher Reynolds we can see the appearance of vorticties.

Other characteristics of flow calculated numerically are presented in Fig. 4.10(a) and Fig. 4.10(b). They also are in good correspondence with the asymptotic model.

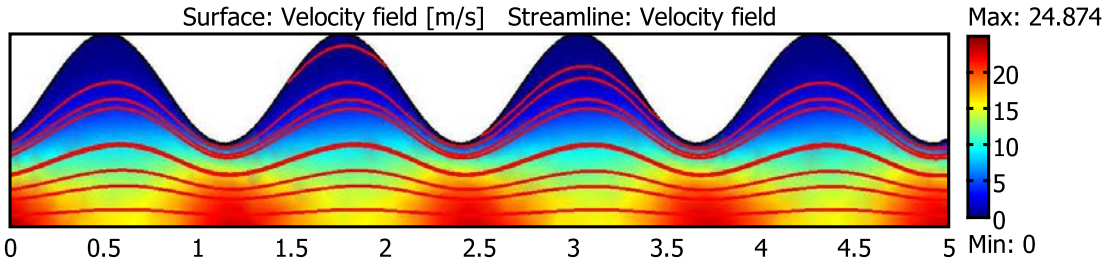

(a) without inflow

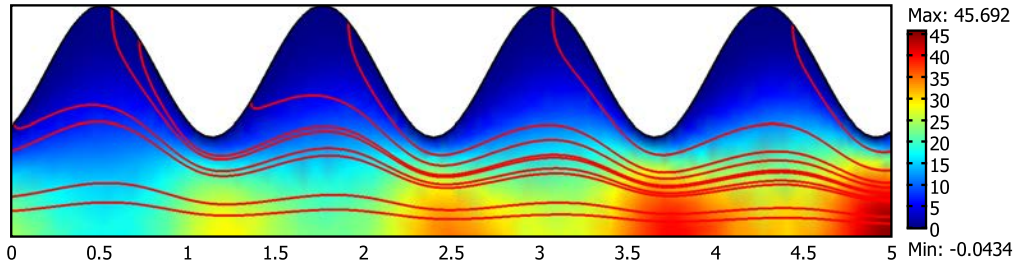

(b) with inflow

Figure 4.8: Numerical simulation: streamlines and longitudinal velocity U for Re = 12:

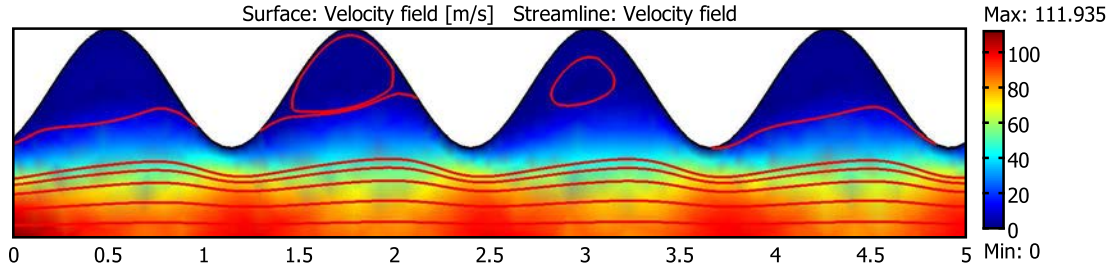

Figure 4.9: Numerical simulation: streamlines and longitudinal velocity U for Re = 55; without inflow

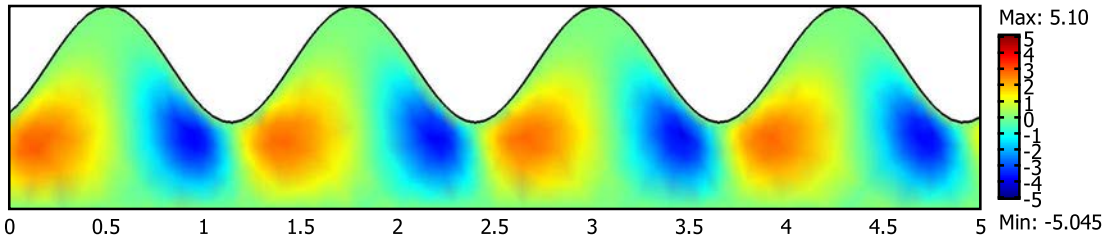

(a) Re = 12

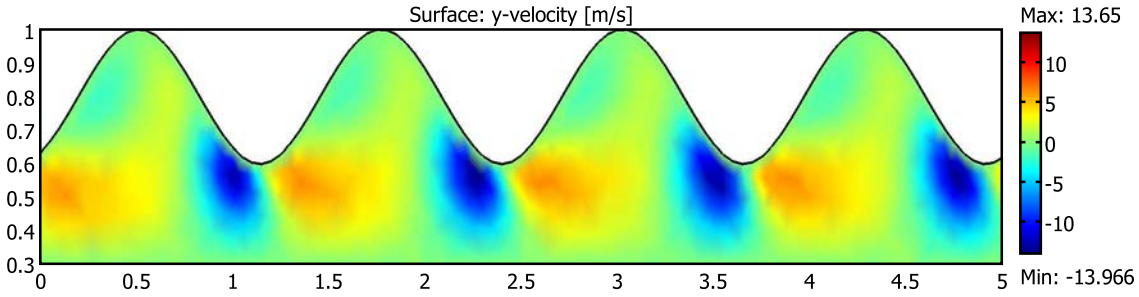

(b) Re = 55

Figure 4.10: Numerical simulation: transverse velocity V; without inflow

Chapter 5

Flow in circular channel with corrugated walls

5.1 Problem Formulation

5.1.1 Problem setting

The similar problem may be solved for another geometry of the channel, in particular for an axis-symmetric horizontal channel having wavy walls, as shown in Fig. 5.1.

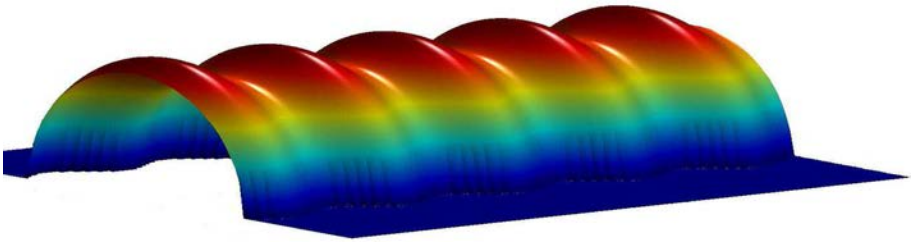

Figure 5.1: The upper half of a horizontal channel with wavy walls

The channel is surrounded by porous medium saturated with liquid (oil). Another fluid (water) is injected through the left-hand section at a given flow rate Q°. In applications such a channel represents a horizontal well drilled in an oil reservoir. The walls are permeable and authorize water of oil to cross them. Depending on the type of drilling, the fluid can flow from the channel to the surrounding rock (case of classical drilling), as well as the fluid can arrive to the channel through the walls from the oil reservoir (corresponds to the underbalanced drilling, when the pressure inside the well is maintained to be lower than that in reservoir). In the first approximation we assume that the physical properties of oil and water are close, so the fluid may be considered as the almost single-phase liquid of density ρ and dynamic viscosity μ. The fluid is incompressible, the flow is steady-state. The flow is axis-symmetric, so the angular component is zero.

Let the wall oscillations be periodic with period ℓ, the mean radius of the well be R_w, the characteristic length of the well be L.

In cylindrical coordinates (R, θ, X) with the origin at the well axis, the upper half of the well represents the domain: $\{0 < R < R_w\phi(X), \quad 0 < X < L, \quad 0 < \theta < 2\pi\}$, where $\phi(X)$ is the periodic function with period ℓ and the mean value 1. In case when $\phi = 1$, the well is the regular infinite cylinder.

The flow is described by Navier-Stokes equations.

The boundary condition at the inlet section imposes the given mean velocity U° (or flow rate Q°):

$$U^\circ \equiv \frac{2}{(R_w\phi(0))^2} \int_0^{R_w\phi(0)} RU_x(0,r)dR \tag{5.1}$$

It is sufficient to assume that $\phi(0) = 1$.

The upper boundary of the well is penetrable by fluid. We impose the constant inflow velocity (U_x^*, U_z^*).

5.1.2 Formulation through dimensionless variables

Let us introduce the following dimensionless variables:

$$x = \frac{X}{L}, \quad r = \frac{R}{R_w}, \quad p = \frac{p}{p^\circ}, \quad u = \frac{U_x}{U^\circ}, \quad v = \frac{U_r}{U^\circ} \tag{5.2}$$

with three dimensionless parameters:

$$\omega = \frac{R_w}{L}, \qquad \varepsilon = \frac{\ell}{L}, \qquad Re = \frac{\rho U^\circ R_w}{\mu}$$

The characteristic pressure p° is determined as the pressure drop along the length L caused by a Poiseuille flow at velocity U°: $p^\circ = \dfrac{\mu U^\circ L}{R_w^2}$.

In dimensionless variables the flow problem takes the form of Navier-Stokes equations in the domain $\mathcal{W} = \{0 < r < \phi(x), \quad 0 < x < 1\}$:

$$\omega\frac{\partial u}{\partial x} + \frac{1}{r}\frac{\partial (rv)}{\partial r} = 0 \tag{5.3a}$$

$$\mathrm{Re}\left(\omega u\frac{\partial u}{\partial x} + v\frac{\partial u}{\partial r}\right) = -\frac{\partial p}{\partial x} + \left[\omega^2\frac{\partial^2 u}{\partial x^2} + \frac{1}{r}\frac{\partial}{\partial r}\left(r\frac{\partial u}{\partial r}\right)\right] \tag{5.3b}$$

$$\mathrm{Re}\left(\omega u\frac{\partial v}{\partial x} + v\frac{\partial v}{\partial r}\right) = -\frac{1}{\omega}\frac{\partial p}{\partial r} + \left[\omega^2\frac{\partial^2 v}{\partial x^2} + \frac{1}{r}\frac{\partial}{\partial r}\left(r\frac{\partial v}{\partial r}\right) - \frac{v}{r^2}\right] \tag{5.3c}$$

where $\phi(x)$ is the periodic function with period ε and the mean value 1.

The boundary conditions are:

$$1 = 2\int_0^{\phi(0)} r\,u(0,r)\,dr = 2\int_0^1 r\,u(0,r)\,dr \tag{5.4a}$$

$$\left.\frac{\partial u}{\partial r}\right|_{r=0} = 0, \qquad v|_{r=0} = 0 \tag{5.4b}$$

$$u|_{r=\phi(x)} = \omega u^*, \quad v|_{r=\phi(x)} = -\omega v^* \tag{5.4c}$$

where $\omega u^* = U_x^*/U^\circ$, $\omega v^* = U_r^*/U^\circ$ are two components of the inflow velocity through the boundary;

condition (5.4a) results from (5.1), conditions (5.4b) means the symmetry with respect to the fracture axis.

The presence of the small parameter ω in the relations for the inflow velocity means that it is assumed to be low.

This system possesses an integral relation which represents the mass balance between the external flux and the internal flow:

$$\int_0^{\phi(x)} r\,u(x,r)\,dr = F_0(x) + \omega F_1(x), \tag{5.5}$$

$$F_0(x) \equiv \frac{1}{2} + v^* \int_0^x \phi(\bar{x})d\bar{x}, \quad F_1(x) \equiv \frac{u^*}{2}\left(\phi^2(x) - \phi^2(0)\right)$$

This relation is the average mass conservation, which says that the mass is not conserved due to the cross-flow through the walls.

Proof:

This relation is obtained by integrating the continuity equation (5.3a) over the cross-section:

$$0 = \omega \int_0^{\phi(x)} r\frac{\partial u}{\partial x}dr + r\,v|_{r=0}^{r=\phi(x)} = \omega\frac{\partial}{\partial x}\left(\int_0^{\phi(x)} rudr\right) - \frac{d\phi}{dx}\phi(x)\omega^2 u^* - \phi\omega v^*$$

Integrating over x, we obtain:

$$0 = \int_0^{\phi(x)} r\,u\,dr - \int_0^{\phi(0)} r\,u\,dr - \omega\frac{u^*}{2}\left(\phi^2(x) - \phi^2(0)\right) - \int_0^x v^*\,\phi(\bar{x})\,d\bar{x}$$

Using (5.4a) we obtain definitely (5.5).

This means that the flow as a function of x at each point on the length of well results from the sum of inlet flow and inflow through the walls.

Remark: The system of boundary conditions is not sufficient to determine the unique solution, which is not important for our analysis, because the objective is to analyze the behavior of a family of solutions.

For simulations, the uniqueness may be reached by replacing condition (5.4a) imposed on the average velocity by the condition on the velocity at each point of the inlet section.

5.1.3 Parameters of the model

We will assume that parameters ω and ε are small:

$$0 < \omega, \varepsilon << 1$$

As in the preceding chapter, we will analyze the non-trivial case when:

$$\omega \sim \varepsilon^{\alpha}, \quad \text{where } \alpha \text{ is close to 1}$$

In contrast, the Reynolds number Re may by variable.

5.2 Method of solution

We will apply the same method as in the previous chapter.

5.2.1 Asymptotic expansion

Let us introduce the regular asymptotical expansion of $\mathcal{U} = \{u, v, p\}$ with respect to the small parameter ω:

$$\mathcal{U}(r,z) = \mathcal{U}_0(r,z) + \omega\mathcal{U}_1(r,z) + \omega^2\mathcal{U}_2(r,z) + \dots \tag{5.6}$$

In zero approximation, for u_0, v_0, p_0 we have:

$$\frac{1}{r}\frac{\partial(rv_0)}{\partial r} = 0, \qquad \frac{\partial p_0}{\partial r} = 0, \qquad \mathrm{Re}\, v_0\frac{\partial u_0}{\partial r} = -\frac{\partial p_0}{\partial x} + \frac{1}{r}\frac{\partial}{\partial r}\left(r\frac{\partial u_0}{\partial r}\right)$$

$$v_0|_{r=\phi} = 0, \quad u_0|_{r=\phi} = 0, \quad v_0|_{r=0} = 0, \quad \left.\frac{\partial u_0}{\partial r}\right|_{r=0} = 0, \quad \int\limits_0^{\phi} ru_0(x,r)dr = F_0(x)$$

which directly gives: $v_0 \equiv 0$.

In the first approximation, for u_1, v_1, p_1:

$$\frac{1}{r}\frac{\partial(rv_1)}{\partial r} + \frac{\partial u_0}{\partial x} = 0, \quad \mathrm{Re}\left(u_0\frac{\partial u_0}{\partial x} + v_1\frac{\partial u_0}{\partial r}\right) = -\frac{\partial p_1}{\partial x} + \frac{1}{r}\frac{\partial}{\partial r}\left(r\frac{\partial u_1}{\partial r}\right), \quad \frac{\partial p_1}{\partial r} = 0,$$

$$\left.\frac{\partial u_1}{\partial r}\right|_{r=0} = 0, \qquad v_1|_{r=0} = 0, \quad u_1|_{r=\phi(x)} = u^*, \quad v_1|_{r=\phi(x)} = -v^*, \quad \int\limits_0^{\phi(x)} ru_1(x,r)dr = F_1(x)$$

In the second approximation, for u_2, v_2, p_2:

$$\frac{1}{r}\frac{\partial(rv_2)}{\partial r} + \frac{\partial u_1}{\partial x} = 0, \qquad 0 = -\frac{\partial p_2}{\partial r} + \frac{1}{r}\frac{\partial}{\partial r}\left(r\frac{\partial v_1}{\partial r}\right) - \frac{v_1}{r^2},$$

$$\mathrm{Re}\left(u_1\frac{\partial u_0}{\partial x} + u_0\frac{\partial u_1}{\partial x} + v_2\frac{\partial u_0}{\partial r} + v_1\frac{\partial u_1}{\partial r}\right) = -\frac{\partial p_2}{\partial x} + \frac{\partial^2 u_0}{\partial x^2} + \frac{1}{r}\frac{\partial}{\partial r}\left(r\frac{\partial u_2}{\partial r}\right),$$

$$\left.\frac{\partial u_2}{\partial r}\right|_{r=0} = 0, \qquad v_2|_{r=0} = 0, \quad u_2|_{r=\phi(x)} = 0, \quad v_2|_{r=\phi(x)} = 0, \quad \int\limits_0^{\phi(x)} ru_2(x,r)dr = 0$$

5.2.2 Example of solution of the zero-order problem

The obtained problems may be solved by introducing new variables: $(x,r) \to (x,\zeta)$, $\zeta \equiv \dfrac{r}{\phi(x)}$. Then $\dfrac{\partial}{\partial x} = \dfrac{\partial}{\partial x} - \dfrac{\zeta\phi'}{\phi}\dfrac{\partial}{\partial \zeta}$, $\dfrac{\partial}{\partial r} = \dfrac{1}{\phi}\dfrac{\partial}{\partial \zeta}$, where $\phi' = \dfrac{d\phi}{dx}$.

Then the zero-order problem of the asymptotic series becomes:

$$\frac{\partial p_0}{\partial \zeta} = 0, \qquad 0 = -\frac{dp_0}{dx} + \frac{1}{\zeta\phi^2}\frac{\partial}{\partial \zeta}\left(\zeta \frac{\partial u_0}{\partial \zeta}\right)$$

$$u_0|_{\zeta=1} = 0, \qquad \left.\frac{\partial u_0}{\partial \zeta}\right|_{\zeta=0} = 0, \qquad \phi^2 \int_0^1 \zeta u_0(x,\zeta) d\zeta = F_0(x) \tag{5.7}$$

In the second equation the variables x and ζ may be split:

$$\phi^2(x)\frac{dp_0}{dx} = \frac{1}{\zeta}\frac{\partial}{\partial \zeta}\left(\zeta \frac{\partial u_0}{\partial \zeta}\right)$$

The left-hand side depends on x only, then this equation is easy to integrate while taking into account the boundary conditions: $u_0 = \dfrac{A(x)}{4}\left(\zeta^2 - 1\right), \qquad A(x) \equiv \phi^2(x)\dfrac{dp_0}{dx}.$

From the last integral relation in (5.7) we obtain: $\dfrac{A}{4}\phi^2 \displaystyle\int_0^1 \left(\zeta^3 - \zeta\right) d\zeta = F_0.$

Then $A(x) \equiv \phi^2 \dfrac{dp_0}{dx} = -16\dfrac{F_0}{\phi^2}.$

The solution takes the form:

$$u_0 = -4\frac{F_0}{\phi^2}\left(\zeta^2 - 1\right), \qquad \frac{dp_0}{dx} = -16\frac{F_0}{\phi^4}$$

In the similar way one can solve other problems of the preceding paragraph. The corresponding developments are placed in the annexes (C) and (D).

5.2.3 Definite form of the solution

$$u = u_0(x,r) + \omega u_1(x,r) + \omega^2 u_2(x,r) + ..., \tag{5.8}$$

$$v = \omega v_1(x,r) + \omega^2 v_2(x,r) + ..., \tag{5.9}$$

$$\frac{\partial p}{\partial x} = \frac{dp_0}{dx}(x) + \omega\frac{dp_1}{dx}(x) + \omega^2\frac{\partial p_2}{\partial x}(x,r) + ..., \tag{5.10}$$

$$\tag{5.11}$$

where:

$$u_0(x,\zeta) = -4\frac{F_0}{\phi^2}\left(\zeta^2-1\right), \tag{5.12a}$$

$$u_1 = u^*\left(1+\frac{2\phi^2(0)}{\phi^2}\left(\zeta^2-1\right)\right) + \frac{\mathrm{Re}F_0v^*}{\phi}\left(\frac{2\zeta^6}{9}-\zeta^4+\zeta^2-\frac{2}{9}\right) - \frac{\mathrm{Re}\phi' F_0^2}{\phi^3}\left(\frac{8\zeta^6}{9}-4\zeta^4+4\zeta^2-\frac{8}{9}\right) \tag{5.12b}$$

$$\begin{aligned} u_2 = {} & \left(8\left(\frac{\phi'}{\phi}\right)^2 F_0 - 2\frac{\phi'' F_0}{\phi} + \frac{\mathrm{Re}\phi' F_0 u^*}{\phi} - 3v^*\phi' - \mathrm{Re}\frac{u^*v^*\phi}{4}\right)\left(\zeta^4-\frac{4}{3}\zeta^2+\frac{1}{3}\right) + \\ & + \left(\frac{8\mathrm{Re}\,\phi' F_0 u^*}{\phi^3} - \frac{\mathrm{Re}\,u^*v^*}{\phi}\right)\left(\frac{\zeta^6}{9}-\frac{\zeta^4}{2}+\frac{\zeta^2}{2}-\frac{1}{9}\right) - \\ & -\mathrm{Re}^2 v^{*2} F_0\left(\frac{\zeta^{10}}{450}-\frac{\zeta^8}{36}+\frac{\zeta^6}{9}-\frac{11}{36}\zeta^4+\frac{38}{135}\zeta^2-\frac{83}{1350}\right) + \\ & + \frac{\mathrm{Re}^2\phi' F_0^2 v^*}{\phi^2}\left(\frac{29}{450}\zeta^{10}-\frac{7}{12}\zeta^8+\frac{11}{6}\zeta^6-\frac{115}{36}\zeta^4+\frac{1261}{540}\zeta^2-\frac{1229}{2700}\right) + \\ & + \frac{\mathrm{Re}^2\phi'' F_0^3}{\phi^3}\left(\frac{2}{75}\zeta^{10}-\frac{2}{9}\zeta^8+\frac{2}{3}\zeta^6-\zeta^4+\frac{29}{45}\zeta^2-\frac{26}{225}\right) - \\ & - \frac{\mathrm{Re}^2\phi'^2 F_0^3}{\phi^4}\left(\frac{38}{225}\zeta^{10}-\frac{13}{9}\zeta^8+\frac{38}{9}\zeta^6-\frac{53}{9}\zeta^4+\frac{479}{135}\zeta^2-\frac{409}{675}\right) \end{aligned} \tag{5.12c}$$

$$v_1 = v^*\left(\zeta^3-2\zeta\right) - \frac{4\phi' F_0}{\phi^2}\left(\zeta^3-\zeta\right) \tag{5.12d}$$

$$\begin{aligned} v_2 = {} & \frac{2u^*\phi'\phi^2(0)}{\phi^2}\left(\zeta^3-\zeta\right) + \\ & + \left(\frac{\mathrm{Re}\,\phi'' F_0^2}{\phi^2} - \frac{\mathrm{Re}\,v^{*2}\phi}{4}\right)\left(\frac{\zeta^7}{9}-\frac{2\zeta^5}{3}+\zeta^3-\frac{4\zeta}{9}\right) - \\ & - \frac{\mathrm{Re}\,\phi'^2 F_0^2}{\phi^3}\left(\zeta^7-\frac{14\zeta^5}{3}+5\zeta^3-\frac{4\zeta}{3}\right) + \\ & + \frac{\mathrm{Re}F_0\phi' v^*}{\phi}\left(\frac{5\zeta^7}{12}-\frac{13\zeta^5}{6}+\frac{11\zeta^3}{4}-\zeta\right) \end{aligned} \tag{5.12e}$$

$$\frac{dp_0}{dx} = -16\frac{F_0}{\phi^4}, \tag{5.12f}$$

$$\frac{\partial p_1}{\partial x} = \frac{8u^*\phi^2(0)}{\phi^4} - \frac{12\mathrm{Re}F_0v^*}{\phi^3} + \frac{16\mathrm{Re}\phi' F_0^2}{\phi^5}, \tag{5.12g}$$

$$\begin{aligned} \frac{\partial p_2}{\partial x} = {} & 16\left(-\frac{5\phi' v^*}{4\phi^2} - \frac{\phi'' F_0}{\phi^3} + 3\frac{\phi'^2 F_0}{\phi^4}\right)\zeta^2 + \\ & + \frac{8}{3}\frac{\phi'' F_0}{\phi^3} - \frac{56}{3}\frac{\phi'^2 F_0}{\phi^4} + \frac{4v^*\phi'}{\phi^2} + \\ & + \frac{8\mathrm{Re}u^*\phi' F_0}{3\phi^3} + \frac{6\mathrm{Re}u^*v^*}{\phi^3} - \frac{16\mathrm{Re}u^*\phi' F_0}{\phi^5} - \frac{8\mathrm{Re}u^*v^*}{3\phi} - \\ & - \frac{44\mathrm{Re}^2\phi''}{45\phi^5}(F_0^3-1) + \frac{484\mathrm{Re}^2\phi'^2 F_0^3}{135\phi^6} + \frac{88\mathrm{Re}^2 v^{*2} F_0}{135\phi^2} - \frac{539\mathrm{Re}^2\phi' v^*}{135\phi^4}(F_0^2-1) \end{aligned} \tag{5.12h}$$

5.3 Two-scale form of the obtained solutions

Similar to the previous chapter, we will introduce the small-scale variable $y = x/\varepsilon$ and consider it as independent of the slow variable x. Then the two-scale form of the solution (5.12) becomes:

$$
\begin{aligned}
u = &-\frac{4F_0}{\phi^2}\left(\zeta^2-1\right)+\\
&\frac{\omega}{\varepsilon}\Bigg\{-\frac{8\mathrm{Re}\,\phi_y' F_0^2}{\phi^3}\left(\frac{\zeta^6}{9}-\frac{\zeta^4}{2}+\frac{\zeta^2}{2}-\frac{1}{9}\right)+\\
&\quad+\varepsilon\left[\frac{2\mathrm{Re}\,v^* F_0}{\phi}\left(\frac{\zeta^6}{9}-\frac{\zeta^4}{2}+\frac{\zeta^2}{2}-\frac{1}{9}\right)+u^*\left(1+\frac{2\phi^2(0)}{\phi^2}\left(\zeta^2-1\right)\right)\right]+\varepsilon^2\ldots\Bigg\}+\\
&+\frac{\omega^2}{\varepsilon^2}\Bigg\{\left(8\left(\frac{\phi_y'}{\phi}\right)^2 F_0-2\frac{\phi_{yy}'' F_0}{\phi}\right)\left(\zeta^4-\frac{4}{3}\zeta^2+\frac{1}{3}\right)+\\
&\qquad+\frac{\mathrm{Re}^2\phi_{yy}'' F_0^3}{\phi^3}\left(\frac{2}{75}\zeta^{10}-\frac{2}{9}\zeta^8+\frac{2}{3}\zeta^6-\zeta^4+\frac{29}{45}\zeta^2-\frac{26}{225}\right)-\\
&\qquad-\frac{\mathrm{Re}^2{\phi_y'}^2 F_0^3}{\phi^4}\left(\frac{38}{225}\zeta^{10}-\frac{13}{9}\zeta^8+\frac{38}{9}\zeta^6-\frac{53}{9}\zeta^4+\frac{479}{135}\zeta^2-\frac{409}{675}\right)+\\
&\quad+\varepsilon\Bigg[\left(\frac{\mathrm{Re}\phi_y' F_0 u^*}{\phi}-3v^*\phi_y'\right)\left(\zeta^4-\frac{4}{3}\zeta^2+\frac{1}{3}\right)+\\
&\qquad+\frac{8\mathrm{Re}\,\phi_y' F_0 u^*}{\phi^3}\left(\frac{\zeta^6}{9}-\frac{\zeta^4}{2}+\frac{\zeta^2}{2}-\frac{1}{9}\right)+\\
&\qquad+\frac{\mathrm{Re}^2\phi_y' F_0^2 v^*}{\phi^2}\left(\frac{29}{450}\zeta^{10}-\frac{7}{12}\zeta^8+\frac{11}{6}\zeta^6-\frac{115}{36}\zeta^4+\frac{1261}{540}\zeta^2-\frac{1229}{2700}\right)\Bigg]+\\
&\quad+\varepsilon^2\Bigg[-\mathrm{Re}\frac{u^* v^*\phi}{4}\left(\zeta^4-\frac{4}{3}\zeta^2+\frac{1}{3}\right)-\frac{\mathrm{Re}\,u^* v^*}{\phi}\left(\frac{\zeta^6}{9}-\frac{\zeta^4}{2}+\frac{\zeta^2}{2}-\frac{1}{9}\right)-\\
&\qquad-\mathrm{Re}^2{v^*}^2 F_0\left(\frac{\zeta^{10}}{450}-\frac{\zeta^8}{36}+\frac{\zeta^6}{9}-\frac{11}{36}\zeta^4+\frac{38}{135}\zeta^2-\frac{83}{1350}\right)\Bigg]+\varepsilon^3\ldots\Bigg\}+O(\frac{\omega^3}{\varepsilon^3}+\omega\varepsilon)
\end{aligned}
\tag{5.13}
$$

$$
\begin{aligned}
v = &\frac{\omega}{\varepsilon}\left\{-\frac{4\phi_y' F_0}{\phi^2}\left(\zeta^3-\zeta\right)+\varepsilon v^*\left(\zeta^3-2\zeta\right)+\varepsilon^2\ldots\right\}+\\
&+\frac{\omega^2}{\varepsilon^2}\Bigg\{\frac{\mathrm{Re}\,\phi_y'' F_0^2}{\phi^2}\left(\frac{\zeta^7}{9}-\frac{2\zeta^5}{3}+\zeta^3-\frac{4\zeta}{9}\right)-\frac{\mathrm{Re}\,\phi_y'^2 F_0^2}{\phi^3}\left(\zeta^7-\frac{14\zeta^5}{3}+5\zeta^3-\frac{4\zeta}{3}\right)+\\
&\quad+\varepsilon\left[\frac{2u^*\phi_y'\phi^2(0)}{\phi^2}\left(\zeta^3-\zeta\right)+\frac{\mathrm{Re}F_0\phi_y' v^*}{\phi}\left(\frac{5\zeta^7}{12}-\frac{13\zeta^5}{6}+\frac{11\zeta^3}{4}-\zeta\right)\right]+\\
&\quad+\varepsilon^2\left[-\frac{\mathrm{Re}\,{v^*}^2\phi}{4}\left(\frac{\zeta^7}{9}-\frac{2\zeta^5}{3}+\zeta^3-\frac{4\zeta}{9}\right)\right]+\varepsilon^3\ldots+O(\frac{\omega^3}{\varepsilon^3}+\omega\varepsilon)\Bigg\}
\end{aligned}
\tag{5.14}
$$

$$\frac{\partial p}{\partial x} = -16\frac{F_0}{\phi^4} + \frac{\omega}{\varepsilon}\left\{\frac{16\mathrm{Re}\phi' F_0^2}{\phi^5} + \varepsilon\left[8u^*\frac{\phi^2(0)}{\phi^4} - \frac{12\mathrm{Re}F_0 v^*}{\phi^3}\right] + \varepsilon^2 ...\right\} +$$
$$\frac{\omega^2}{\varepsilon^2}\left\{16\left(-\frac{\phi'' F_0}{\phi^3} + 3\frac{\phi'^2 F_0}{\phi^4}\right)\zeta^2 + \frac{8}{3}\frac{\phi'' F_0}{\phi^3} - \mathrm{Re}^2\frac{44}{45}\frac{\phi''}{\phi^5}(F_0^3 - 1) - \frac{56}{3}\frac{\phi'^2 F_0}{\phi^4} + \mathrm{Re}^2\frac{484}{135}\frac{\phi'^2 F_0^3}{\phi^6} +\right.$$
$$+\varepsilon\left[-20\frac{\phi' v^*}{\phi^2}\zeta^2 + 4\frac{v^*\phi'}{\phi^2} - \mathrm{Re}^2\frac{539}{135}\frac{\phi' v^*}{\phi^4}(F_0^2 - 1) + \mathrm{Re}\frac{8}{3}\frac{u^*\phi' F_0}{\phi^3} - 16\mathrm{Re}\frac{u^*\phi' F_0}{\phi^5}\right] +$$
$$\left.+\varepsilon^2\left[-\mathrm{Re}\frac{8}{3}\frac{u^* v^*}{\phi} + 6\mathrm{Re}\frac{u^* v^*}{\phi^3} + \mathrm{Re}^2\frac{88}{135}\frac{v^{*2} F_0}{\phi^2}\right] + \varepsilon^3 ...\right\} + O(\frac{\omega^3}{\varepsilon^3} + \omega\varepsilon) \tag{5.15}$$

5.4 Stream functions

In cylindrical coordinating system considering the symmetry w.r.t. the angular coordinate the streamlines in terms of radial and longitudinal velocity components respectively u, v can be written as:

$$u = -\frac{1}{r}\frac{\partial\psi}{\partial r}, \qquad v = \frac{1}{r}\frac{\partial\psi}{\partial x} \tag{5.16}$$

This is:

$$\psi = F_0\left(\zeta^4 - 2\zeta^2\right) +$$
$$+\frac{\omega}{\varepsilon}\frac{8\mathrm{Re}\,\phi' F_0^2}{\phi}\left(\frac{\zeta^8}{9} - \frac{2\zeta^6}{3} + \zeta^4 - \frac{4\zeta^2}{9}\right)$$
$$+\frac{\omega^2}{\varepsilon^2}\left\{\left(-4\phi'^2 F_0 + \phi''\phi F_0\right)\left(\frac{\zeta^6}{3} - \frac{2}{3}\zeta^4 + \frac{\zeta^2}{3}\right) -\right.$$
$$-\frac{\mathrm{Re}^2\phi'' F_0^3}{\phi}\left(\frac{\zeta^{12}}{450} - \frac{\zeta^{10}}{45} + \frac{\zeta^8}{12} - \frac{\zeta^6}{6} + \frac{29}{180}\zeta^4 - \frac{13}{225}\zeta^2\right) +$$
$$\left.+\frac{\mathrm{Re}^2\phi'^2 F_0^3}{\phi^2}\left(\frac{38}{2700}\zeta^{12} - \frac{13\zeta^{10}}{90} + \frac{38\zeta^8}{72} - \frac{53\zeta^6}{54} + \frac{479\zeta^4}{540} - \frac{409\zeta^2}{1350}\right)\right\} + C + O(\omega^3) \tag{5.17}$$

where C is an arbitrary constant, representing different streamline sets.

5.5 Results obtained

5.5.1 Microscale flow behavior in a regular channel

The results obtained for regular pipe ($\phi = 1, \quad \phi' = 0$) either without or with inflow, have the objective to validate correctness of the solutions obtained. For this case we obtain:

$$u = -4F_0\ \left(\zeta^2 - 1\right) + \omega\left[u^*\left(2\zeta^2 - 1\right) + 2\mathrm{Re}\, v^* F_0\left(\frac{\zeta^6}{9} - \frac{\zeta^4}{2} + \frac{\zeta^2}{2} - \frac{1}{9}\right)\right] - \\ -\omega^2\left[\frac{\mathrm{Re}\, u^* v^*}{4}\left(\zeta^4 - \frac{4}{3}\zeta^2 + \frac{1}{3}\right) + \mathrm{Re}\, u^* v^*\left(\frac{\zeta^6}{9} - \frac{\zeta^4}{2} + \frac{\zeta^2}{2} - \frac{1}{9}\right) + \right. \\ \left. + \mathrm{Re}^2 v^{*2} F_0\left(\frac{\zeta^{10}}{450} - \frac{\zeta^8}{36} + \frac{\zeta^6}{9} - \frac{11}{36}\zeta^4 + \frac{38}{135}\zeta^2 - \frac{83}{1350}\right)\right] \tag{5.18}$$

$$v = \omega v^*\left(\zeta^3 - 2\zeta\right) - \frac{\mathrm{Re}\, v^{*2}}{4}\left(\frac{\zeta^7}{9} - \frac{2\zeta^5}{3} + \zeta^3 - \frac{4\zeta}{9}\right) \tag{5.19}$$

$$\frac{\partial p}{\partial x} = -16F_0 + \omega\left(8u^* - 12v^* F_0\right) + \omega^2\left(\frac{10\mathrm{Re}\, u^* v^*}{3} + \frac{88\mathrm{Re}^2 v^{*2} F_0}{135}\right) \tag{5.20}$$

When there is no inflow, $u^* = v^* = 0$, the velocity profile is parabolic, Fig. 5.2, and the pressure gradient is constant.

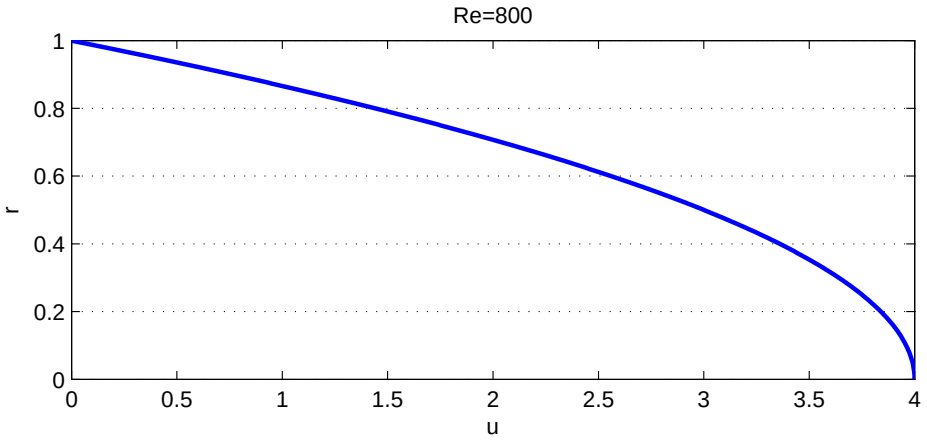

Figure 5.2: Longitudinal velocity in a regular pipe with no inflow, Re=800

The inflow influences the streamlines as shown in Fig. 5.3 and Fig. 5.4.

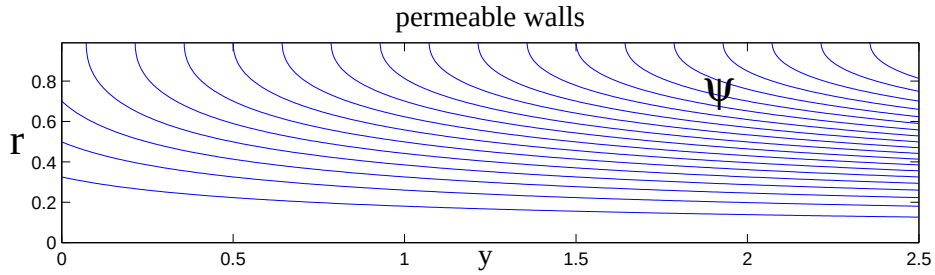

Figure 5.3: Regular pipe with inflow, Re=25

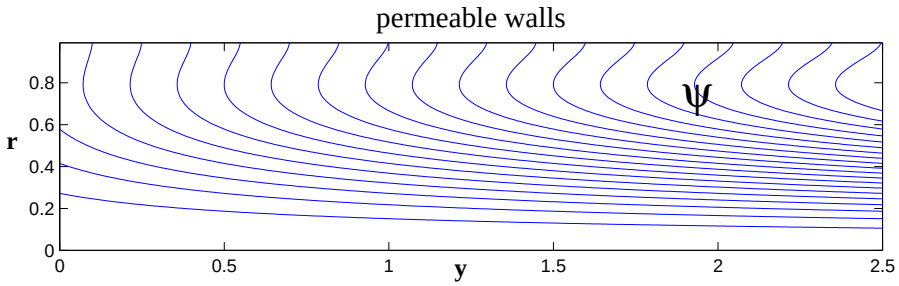

Figure 5.4: Reverse flow in regular pipe with inflow, Re=35

5.5.2 Microscale flow behavior in a wavy pipe: secondary flows

Let us analyze the sinusoidal corrugation given by the relation:

$$\phi(x) = 1 + a\sin(2\pi x/\varepsilon) \tag{5.21}$$

where a is new dimensionless parameter equal to the ratio of the corrugation amplitude to the mean radius.

In this section the results for $\omega = 0.01$, $\varepsilon = 0.01^{0,75} = 0.0316$ and $a = 0.3$ are presented in the form of stream-function isolines and pressure and velocity field.

The flow travels from left to right, the upper half-domain is presented.

Secondary flows are not visible up to some certain Reynolds, as it is seen in Fig. 5.5-a no secondary flow appears. In Fig. 5.6 a relatively high Reynolds number is chosen in order to ensure the formation of secondary flow. In Fig. 5.7, the stream function has been plotted using the zeroth, first and second approximations. The most exact correspondence with the true flow pattern is obtained in the second approximation.

5.5.3 Microscale flow behavior in a wavy pipe: influence of the inflow on pressure

It can be seen that when there is no inflow through the walls the gradient of pressure along the well is periodic. In the presence of inflow the streamlines change, and the pressure gradient increases along the channel axis Fig. 5.5, Fig. 5.8 which results in arising the instability.

The raise of instability can be noted through the appearance of the positive pressure drop which determines the reverse flow.

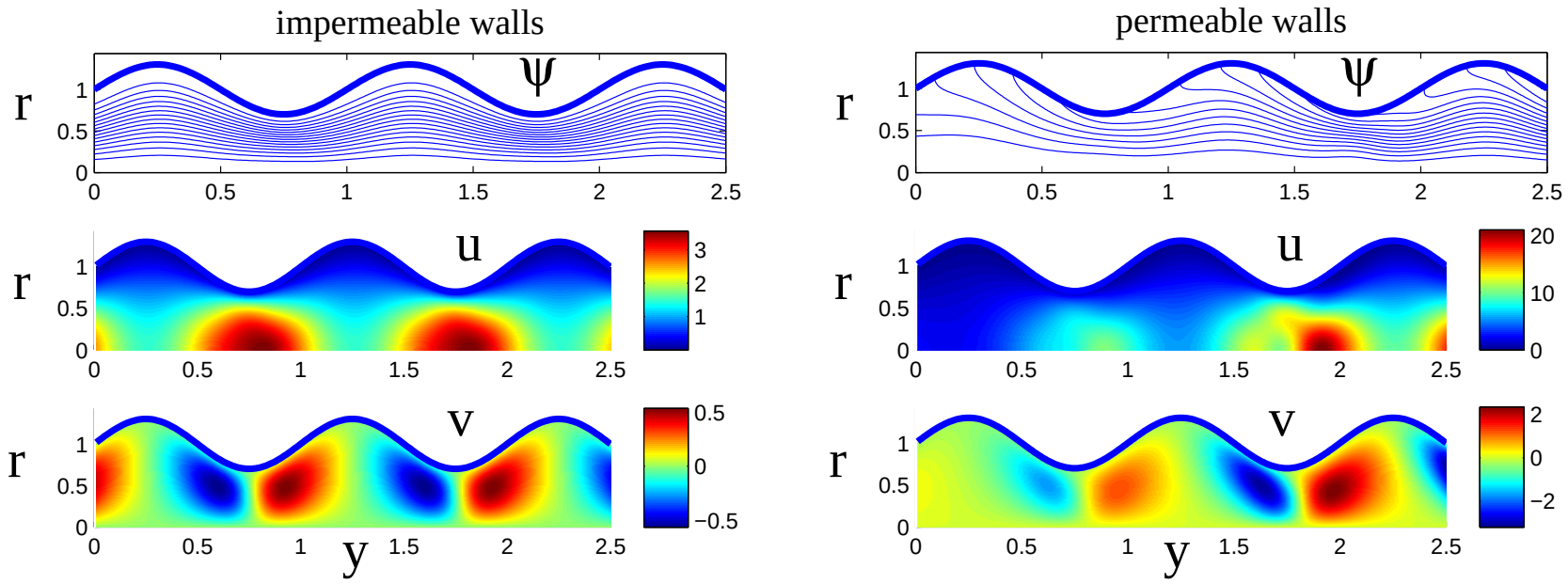

(a) (b)

Figure 5.5: Flow in corrugated pipe with/without inflow through the walls, Re=1

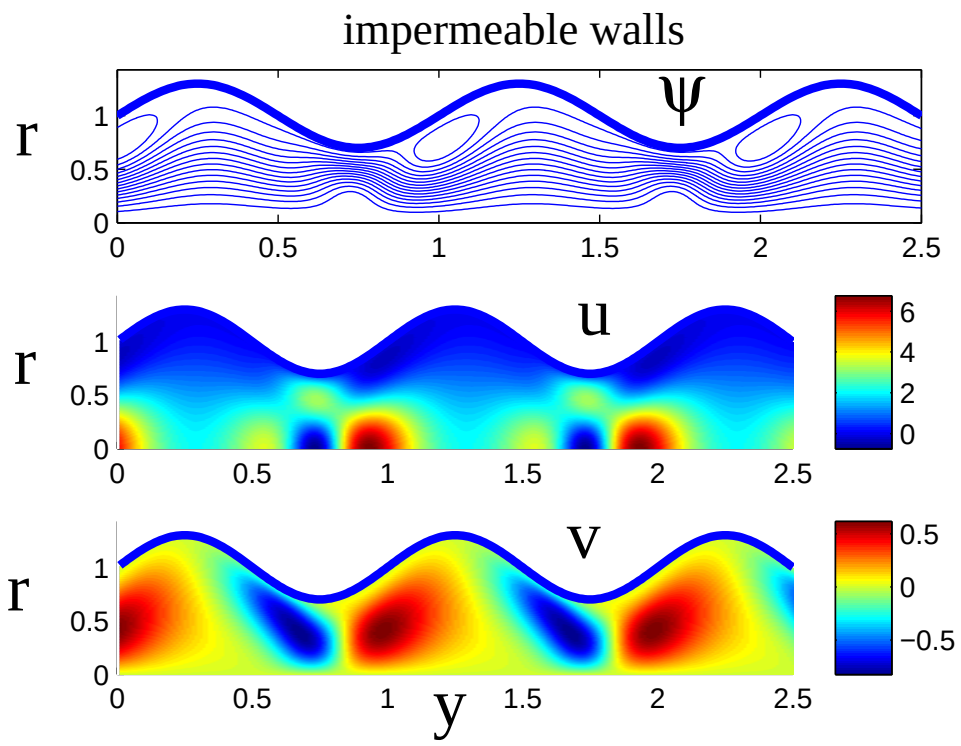

Figure 5.6: Appearance of secondary flow in higher Reynolds, Re=5

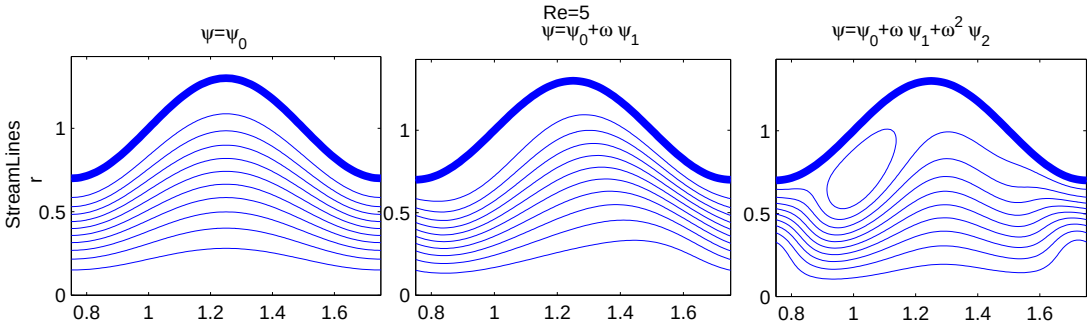

Figure 5.7: Streamlines in the zero , first and second approximations .

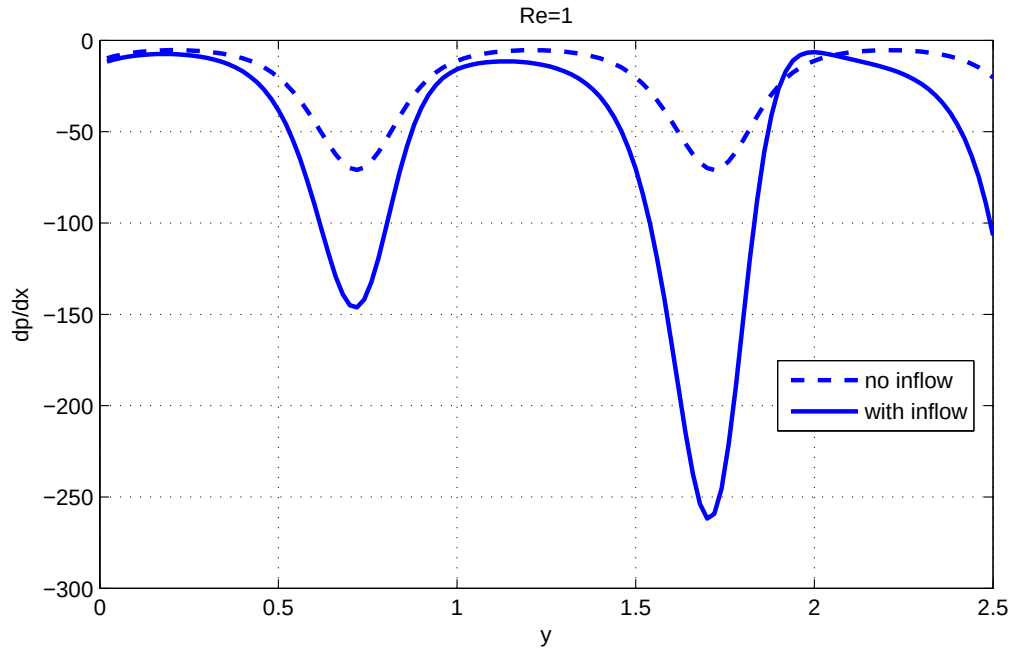

(a) no instability in pressure in low Reynolds

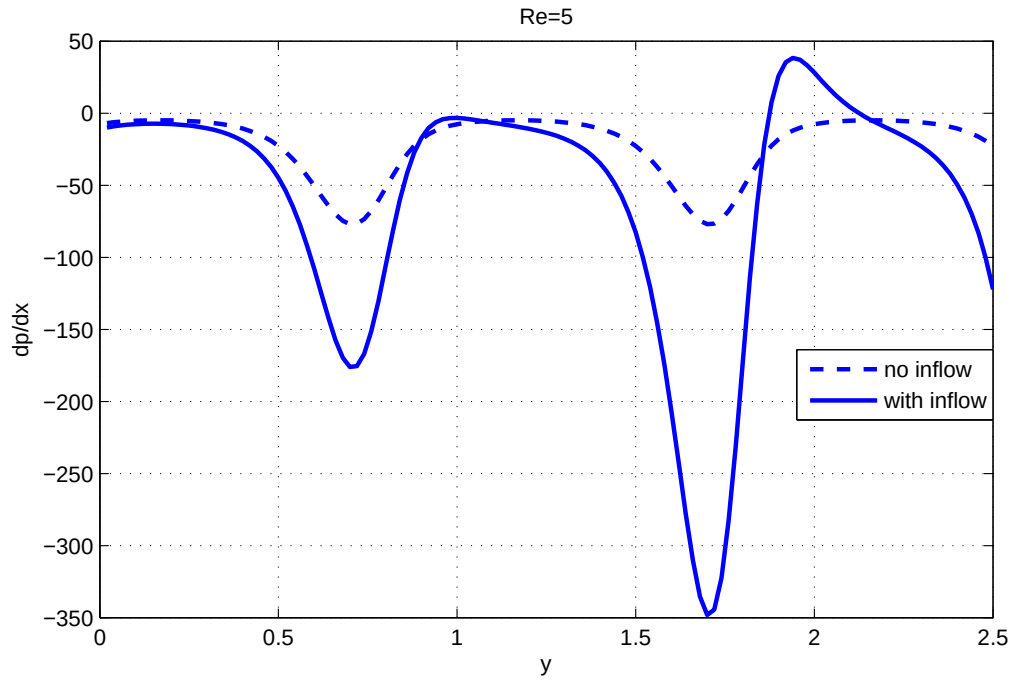

(b) high Reynolds pressure instability

Figure 5.8: The micro scale pressure drop in a perforated pipe with and without inflow

5.6 Model averaged over the wall oscillations

5.6.1 Averaged equations of flow

Let us define the single and double averaging for a two scale function $f(r,z,y)$:

$$\langle f\rangle = \int_0^1 f(r,y,z)dy, \qquad \langle\langle f\rangle\rangle = \int_0^1 \left(\frac{2}{\phi^2}\int_0^\phi rf(r,y,z)dr\right)dy \tag{5.22}$$

Then the two-scale form of the solution becomes:

$$\langle\langle u\rangle\rangle = 2F_0\left\langle\frac{1}{\phi^2}\right\rangle + \omega u^*\left(1-\phi(0)\left\langle\frac{1}{\phi^2}\right\rangle\right) \tag{5.23}$$

$$\langle\langle v\rangle\rangle = 0 \tag{5.24}$$

$$\begin{aligned}\left\langle\left\langle\frac{\partial p}{\partial x}\right\rangle\right\rangle = -16F_0\left\langle\frac{1}{\phi^4}\right\rangle + \omega\left[8u^*\phi^2(0)\left\langle\frac{1}{\phi^4}\right\rangle - 12\mathrm{Re}\,F_0v^*\left\langle\frac{1}{\phi^3}\right\rangle\right] + \\ \frac{\omega^2}{\varepsilon^2}\left[8F_0\left\langle-\frac{\phi''}{\phi^3}+3\frac{\phi'^2}{\phi^4}\right\rangle + \frac{8}{3}F_0\left\langle\frac{\phi''}{\phi^3}-\frac{7\phi'^2}{\phi^4}\right\rangle - \right. \\ \left. -\mathrm{Re}^2\frac{44}{45}(F_0^3-1)\left\langle\frac{\phi''}{\phi^5}\right\rangle + \mathrm{Re}^2\frac{484}{135}F_0^3\left\langle\frac{\phi'^2}{\phi^6}\right\rangle\right] + \\ +\omega^2\left[\mathrm{Re}\,u^*v^*\left\langle-\frac{8}{3\phi}+\frac{6}{\phi^3}\right\rangle + \mathrm{Re}^2\frac{88}{135}v^{*2}F_0\left\langle\frac{1}{\phi^2}\right\rangle\right]\end{aligned}$$

Returning back to the dimensional variables, and denoting $\mathcal{U}\equiv\langle\langle U\rangle\rangle$, $\mathcal{P}\equiv\langle\langle P\rangle\rangle$, we obtain:

$$\mathcal{U} = U^0\left(2F_0\left\langle\frac{1}{\phi^2}\right\rangle + \omega\,u^*\left(1-\phi(0)\left\langle\frac{1}{\phi^2}\right\rangle\right)\right) \tag{5.25}$$

In dimensional form the pressure drop along the wellbore length can be said:

$$\begin{aligned}\frac{d\mathcal{P}}{dX} = \frac{\mu U^0}{R_w^2}\left\{-16F_0\left\langle\frac{1}{\phi^4}\right\rangle + 8\omega u^*\phi^2(0)\left\langle\frac{1}{\phi^4}\right\rangle + \right. \\ \left. +\frac{\omega^2}{\varepsilon^2}\left(8F_0\left\langle-\frac{\phi''}{\phi^3}+3\frac{\phi'^2}{\phi^4}\right\rangle + \frac{8}{3}F_0\left\langle\frac{\phi''}{\phi^3}-\frac{7\phi'^2}{\phi^4}\right\rangle\right)\right\} + \\ +\frac{\rho U^{0\,2}}{R_w}\left\{-12\omega F_0v^*\left\langle\frac{1}{\phi^3}\right\rangle + \omega^2u^*v^*\left\langle\frac{6}{\phi^3}-\frac{8}{3\phi}\right\rangle\right\} + \\ +\frac{\rho^2U^{0\,2}}{\mu}\frac{44}{45}\left\{\omega^2\frac{2}{3}F_0v^{*2}\left\langle\frac{1}{\phi^2}\right\rangle + \frac{\omega^2}{\varepsilon^2}\left(-\left\langle\frac{\phi''}{\phi^5}\right\rangle(1-F_0^3) + \frac{11}{3}F_0^3\left\langle\frac{\phi'^2}{\phi^6}\right\rangle\right)\right\}\end{aligned}$$

Replacing U^0 by $\mathcal{U}$ by using (5.25), we obtain the averaged momentum balance equation in the form of a

cubic law:

$$-\frac{d\mathcal{P}}{dX}=\frac{\mu\mathcal{U}}{K^{\mathrm{ef}}}+\beta^{\mathrm{ef}}\rho\mathcal{U}^2+\frac{\gamma^{\mathrm{ef}}\rho^2\mathcal{U}^3}{\mu} \tag{5.26}$$

where:

$$\begin{aligned}
K^{ef}&=\frac{R_w^2}{8}\lambda,\\
\lambda&=\frac{2F_0\left\langle\frac{1}{\phi^2}\right\rangle+\omega\,u^*\left(1-\phi(0)\left\langle\frac{1}{\phi^2}\right\rangle\right)}{2F_0\left\langle\frac{1}{\phi^4}\right\rangle-\omega u^*\phi^2(0)\left\langle\frac{1}{\phi^4}\right\rangle+\frac{2}{3}\frac{\omega^2}{\varepsilon^2}F_0\left\langle\frac{\phi''}{\phi^3}-\frac{\phi'^2}{\phi^4}\right\rangle}\\
\beta^{ef}&=\frac{v^*\omega}{R_w}\frac{12F_0\left\langle\frac{1}{\phi^3}\right\rangle+\omega u^*\left\langle\frac{8}{3\phi}-\frac{6}{\phi^3}\right\rangle}{\left(2F_0\left\langle\frac{1}{\phi^2}\right\rangle+\omega\,u^*\left(1-\phi(0)\left\langle\frac{1}{\phi^2}\right\rangle\right)\right)^2}\\
\gamma^{ef}&=-\frac{44\omega^2}{135}\frac{2F_0v^{*2}\left\langle\frac{1}{\phi^2}\right\rangle+\frac{1}{\varepsilon^2}\left(-3\left\langle\frac{\phi''}{\phi^5}\right\rangle(1-F_0^3)+11F_0^3\left\langle\frac{\phi'^2}{\phi^6}\right\rangle\right)}{\left(2F_0\left\langle\frac{1}{\phi^2}\right\rangle+\omega\,u^*\left(1-\phi(0)\left\langle\frac{1}{\phi^2}\right\rangle\right)\right)^3}\\
\gamma^{ef}&=-\frac{44\omega^2}{135\varepsilon^2}\frac{-3\left\langle\frac{\phi''}{\phi^5}\right\rangle(1-F_0^3)+11F_0^3\left\langle\frac{\phi'^2}{\phi^6}\right\rangle+\varepsilon^2 2F_0v^{*2}\left\langle\frac{1}{\phi^2}\right\rangle}{\left(2F_0\left\langle\frac{1}{\phi^2}\right\rangle+\omega\,u^*\left(1-\phi(0)\left\langle\frac{1}{\phi^2}\right\rangle\right)\right)^3}
\end{aligned} \tag{5.27}$$

Three effective parameters determine the averaged behavior of the system:

- K^{ef} is the effective permeability [m^2], the parameter responsible for the pure viscous dissipation (the firction) which corresponds to the Stokes flow. According to [Panfilov and Fourar, 2006] we will use the term "zero-order field" to describe the case of $\mathrm{Re}\to 0$.

The effective permeability also includes the consequences of irregular boundaries as the local Darcy like term. These effects are assumed as a correction to the effective permeability, here determined in terms of coefficients of ω^2/ε^2 in parameter λ, the corrugation parameter. In Fig. 5.9 the corrugation parameter is plotted vs. the oscillation amplitude either with or without inflow. It can be seen that the presence of irregularities in the geometry of the boundaries decreases the effective permeability of the wellbore significantly, while presence or absence of inflow has not a significant role on the effective permeability.

- β^{ef} is the inertia parameter having the dimension [m^{-1}]. It is responsible for the integral losses of the kinetic energy within a period caused by the that component of the inflow velocity which is orthogonal to the fracture axis, v^*. The orthogonal component of inflow deviates fluid from the axial direction of flow, which reduces the fluid axial velocity. The energy transferred with the inflow plays the role of a decelerator, which means the appearance of a negative acceleration, or the inertia losses of energy. β^{ef} vanishes in the absence of inflow through the walls Fig. 5.10.

- γ^{ef} is the dimensionless parameter responsible for the inertia-viscous cross-effect which was described first in [Panfilov and Bues, 2004] and [Panfilov and Fourar, 2006]. It represents a supplementary viscous dissipation produced by the deviation of the streamlines from the zero-order field. As the streamline deformation is caused by the inertia forces, this term depends on Re. This term represents the global and local cross visco-intertia effect. The global effect is zero in the absence of inflow.
As it is shown in Fig. 5.11, this term vanishes for a regular pipe.

5.6.2 Average behavior of pressure drop in a regular pipe

In the special case the average pressure drop in a regular pipe with inflow would be of our interest; where $F_0 = \frac{1}{2} + v^* x$

$$
\begin{aligned}
K^{eff} &= \frac{R_w^2}{8}\lambda, \qquad \lambda = \frac{2F_0}{2F_0 - u^*\omega} \\
\beta^{eff} &= \frac{3\omega F_0 v^* - \frac{5}{6}\omega^2 u^* v^*}{F_0^2} \\
\gamma^{eff} &= -\frac{11}{135}\omega^2 \frac{v^{*2}}{F_0^2}
\end{aligned}
\tag{5.28}
$$

It is seen that for a pipe with inflow through the walls the pure inertia effects and cross visco-inertia effects enters the averaged pressure drop. For a regular pipe with no inflow we reduce to Hagen-Poiseuille equation for pressure drop in pipes, with $\lambda = 1$. Also in the presence of inflow through the walls the effective permeability increases for a regular pipe, Fig. 5.12. As a result of $\omega << 1$, the limit value of the effective permeability reduces to the one for the pipe with no inflow through the walls.

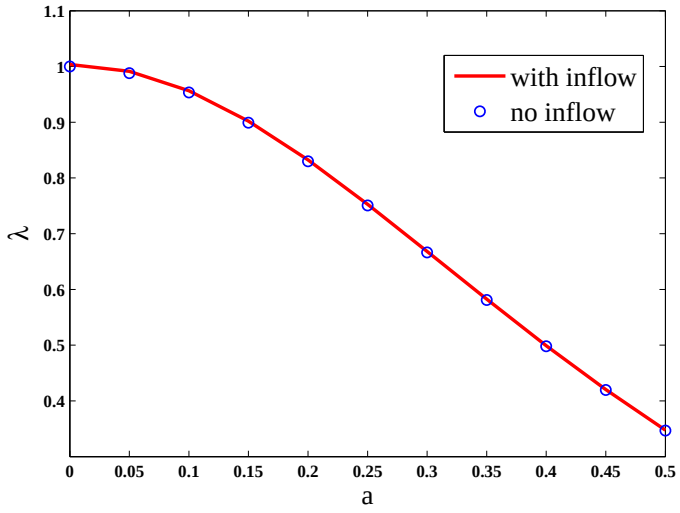

Figure 5.9: Pure viscous effects coefficient(Effective permeability) vs. different corrugation amplitudes a, $\omega = 0.01, \varepsilon = 0.01^{0.75}$

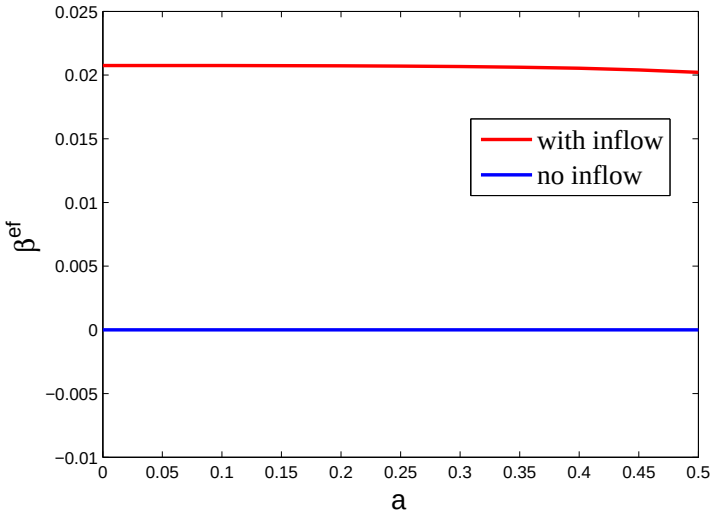

Figure 5.10: Pure inertial effect coefficient vs. different corrugation amplitudes a, $\omega = 0.01, \varepsilon = 0.01^{0.75}$

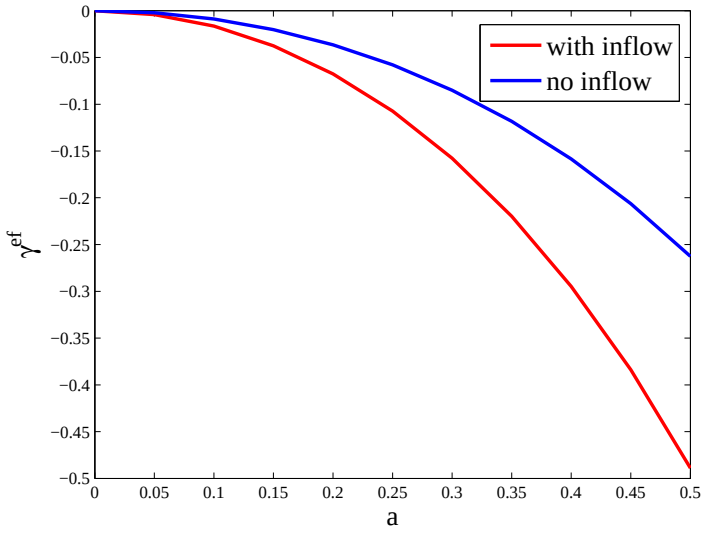

Figure 5.11: Cross visco-inertial effect coefficient vs. different corrugation amplitudes a, $\omega = 0.01, \varepsilon = 0.01^{0.75}$

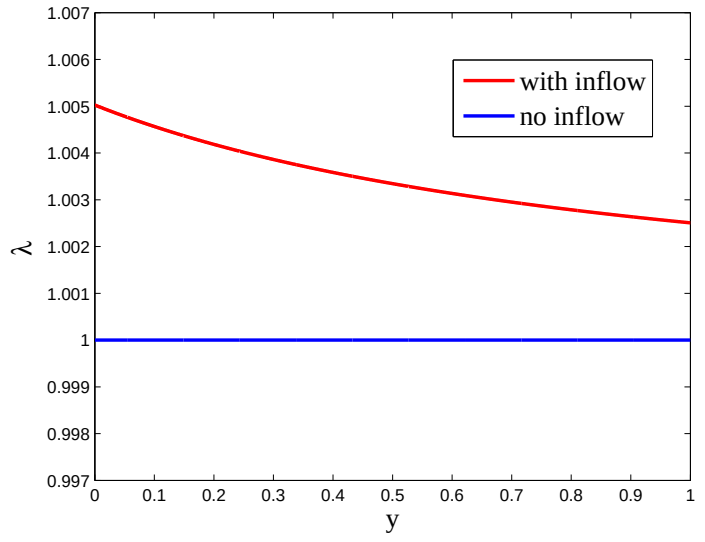

Figure 5.12: Effective permeability of a regular pipe with/without inflow through the walls

Chapter 6

Two-phase flow in a channel with wavy walls

6.1 Analytico-numerical method: levelset method

6.1.1 Engineering applications of two-phase flow in a channel imbedded in porous medium: underbalanced drilling

The description of two-phase flow may be based on two approaches:

- the fluids can be considered as separated from one another by a macroscale interface, which may be mobile. The interface divides the entire flow domain on two mobile sub-domains each of them contains single-phase fluid.

- the phases may be considered as highly dispersed in porous medium, due to which they are described as two interpenetrating continua each of them is present at any space points. The presence of each fluid at a point is defined by its volumetric fraction called "the saturation".

Both approaches lead to nonlinear models, due to which the analytical solutions of flow problems are low probable.

In order to develop an iterative method based on the analytical solutions obtained in the previous section, we will apply the first approach.

The asymptotic method developed in two previous chapters can be applied to two-phase flow with the macroscale interface in a fracture or a cylindrical hole, but the presence of the mobile interface imposes such difficulties that analytical solution may be obtained only for fluids of different "colors" (i.e. the physical parameters of both fluids are identical, except their colors).

At the same time the two-phase flow represents high engineering interest. In particular it concerns the technology known as the underbalanced drilling (UBD). It consists of injecting water ("the drilling mud") in the well at a pressure slightly lower than the reservoir pressure. Due to this oil can enter in the well which causes countercurrent flow inside the well. In contrast, the drilling mud no longer enters the formation, which reduces the formation damage. Increased penetration rate, minimized circulation loss especially in naturally fractured or depleted reservoirs, prolonged bit life, improved formation evaluation, reduced formation damage are some of the advantages of UBD in front of the classical drilling technique. As a result of these advantages the number of wells drilled using this technology is increasing.

The objective of our analysis is to develop the effective model of two-phase flow applicable for large variations of the Reynolds number.

We suggest the iterative approach which consists of a combination between the asymptotic analytical approach and the level-set method. In zero approximation two fluids are considered as those having only

different colors.

6.1.2 Levelset method

The level-set method was developed for incompressible two-phase flow. A levelset function is an indicator function which is positive in one phase, negative in another one, and zero just at the interface between fluids:

$$\varphi(x,t) = \begin{cases} > 0, & x \in \text{ phase 1;} \\ 0, & \text{at the interface;} \\ < 0, & x \in \text{ phase 2} \end{cases} \tag{6.1}$$

The evolution of such a function is governed by the Eulerian formulation as a simple convection equation at the velocity equal to the true velocity of fluid at each point:

$$\phi \frac{\partial \varphi}{\partial t} + \overrightarrow{V}.\nabla\varphi = 0 \tag{6.2}$$

where $\overrightarrow{V}$ is the Darcy flow velocity.

This function has a clear geometrical meaning of a minimal distance between any spatial position and the interface.

In terms of our geometry, we obtain:

$$\omega \frac{\partial \varphi}{\partial t} + \omega u \frac{\partial \varphi}{\partial z} + v \frac{\partial \varphi}{\partial r} = 0 \tag{6.3}$$

where ω is a small parameter representing the ratio of the radius of pipe vs. its length. u, v are the velocity components in r, z direction respectively.

In the equations of mass and conservation for each of fluids fluids, we can introduce the uniform equations for the entire fluid with coefficients depending on the levelset function:

$$\rho(\varphi) = \lambda + (1-\lambda)H(\varphi), \qquad \mu(\varphi) = \eta + (1-\eta)H(\varphi) \tag{6.4}$$

where: $\lambda = \rho_1/\rho_2, (\rho_1 < \rho_2)$ and $\eta = \mu_1/\mu_2$, H is the Heaviside function.

6.1.3 Introduction of the capillary pressure

When the capillary force is significant, the pressure at the interface is discontinuous. The pressure jump is defined through the surface tension σ and the surface curvature κ

$$[p] = \sigma\kappa$$

Instead of working with discontinuous pressure, it is possible to introduce an additional term (applied

to the interface) to the momentum equations. In this case we may consider the continuous function of pressure. This new term has the form

$$\frac{Re}{We}\frac{\delta(\varphi)\sigma\kappa\overrightarrow{N}}{\rho} \tag{6.5}$$

$We = \dfrac{\rho_1 L V^2}{\sigma}$ is the Weber number, and $\delta(\varphi)$ is the delta function.

The orthonormal vector $\overrightarrow{N}$ at the interface and the interface curvature are defined as:

$$\overrightarrow{N} = \frac{\nabla\varphi}{|\nabla\varphi|}|_{\varphi=0}, \qquad \kappa = \nabla.\overrightarrow{N}|_{\varphi=0} = \nabla.\left(\frac{\nabla\varphi}{|\nabla\varphi|}\right)|_{\varphi=0} \tag{6.6}$$

One of the properties of the levelset function is: $|\nabla\varphi| = 1$, which simplifies the last relations.

6.1.4 Essence of the method

In zero approximation, let us assume the fluids have the same densities and viscosities. The capillary pressure is nil. Using analytical solutions obtained in the preceding chapter, we obtain the velocity field at any point of the domain.

Using the equation for φ, (6.3), we can calculate the level-set function. Its zero level determines the placing of the interface.

For the fixed position of the interface, we can recalculate the velocity field by using the same analytical solutions but used with the true physical properties of both fluids in corresponding domains. Using the new velocity field we can recalculate the levelset function, etc.

The defect of this method is that at each step the two velocity fields in two domains do not correspond necessarily to the contact conditions at the interface. This is why we recommend to apply this method only for fluids with close physical properties.

As the velocity field in (6.3) is defined in the form of the asymptotic series, we should consider the levelset function in terms of the asymptotic expansion:

$$\varphi(r,z) = \varphi_0(r,z) + \omega\varphi_1(r,z) + \omega^2\varphi_2(r,z) + ...$$

Substituting in (6.3) we obtain for two first terms:

$$\frac{\partial\varphi_0}{\partial t} + v_1\frac{\partial\varphi_0}{\partial r} + u_0\frac{\partial\varphi_0}{\partial z} = 0 \tag{6.7}$$

$$\frac{\partial\varphi_1}{\partial t} + v_1\frac{\partial\varphi_1}{\partial r} + u_0\frac{\partial\varphi_1}{\partial z} = -v_2\frac{\partial\varphi_0}{\partial r} - u_1\frac{\partial\varphi_0}{\partial z} \tag{6.8}$$

when we taken into account that $v_0 \equiv 0$.

Eqs. (6.7), (6.8) may be solved numerically.

6.2 Numerical procedure

6.2.1 Numerical redistancing process

During simulations, the evolution the initially signed distance function can deviate its properties. A redistancing process [Sussman and Fatemi, 1999] is applied after each evolution:

$$\frac{\partial d}{\partial \tau} = \mathsf{sgn}(\varphi)(1 - |\nabla d|), \qquad d(x,0) = \varphi(x) \tag{6.9}$$

where sgn determines the smeared out sign function of φ:

$$\mathsf{sgn}(\varphi) = \frac{\varphi}{\sqrt{\varphi^2 + \epsilon^2}} \tag{6.10}$$

and τ is an artificial time. The steady state solutions of (6.9) are distance functions. Besides as $\mathsf{sgn}(0) = 0$ the zero levelsets of d and φ coincides.

The above equation could be solved for the entire domain; however to save time, one may reinitialize φ only at cells close to the interface. The re-initialization is performed for the cells within $10 \triangle x$ of the interface. The solution often reaches the steady state after approximately 10 iteration.

6.2.2 Discretization of the Heaviside and delta-function

In numerical model the Heaviside function in (6.4) is defined as:

$$H(\varphi) = \begin{cases} 0, & \varphi < -\epsilon; \\ \frac{1}{2} + \frac{\varphi}{2\epsilon} + \frac{1}{2\pi}\sin(\frac{\pi\varphi}{\epsilon}), & -\epsilon \le \varphi \le \epsilon \\ 1, & \varphi > \epsilon. \end{cases} \tag{6.11}$$

ϵ is chosen $\epsilon = 1.5\triangle x$ so that ensures definitely two nodes are in the interval.

For delta function one uses:

$$\delta(\varphi) = \frac{dH}{d\varphi} = \begin{cases} 0, & \varphi < -\epsilon; \\ \frac{1}{2\epsilon} + \frac{1}{2\epsilon}\cos(\frac{\pi\varphi}{\epsilon}), & -\epsilon \le \varphi \le \epsilon \\ 0, & \varphi > \epsilon. \end{cases} \tag{6.12}$$

6.2.3 Domain discretization

We consider a rectangular mesh including all the wavy geometry. To specify the corrugations we apply the condition of zero velocities wherever the spatial radius coordinate is more than the corrugation radius:

$$u, v = 0, \qquad r > \varphi(z) \tag{6.13}$$

A structured MAC grid is used. The scalar values , here φ, is determined in the center of the cells and the vectorial values are defined on the edges.

A high order Essentially non-oscillating (ENO) scheme is used for the convective derivative discretization and a Total Vairational Diminishing (TVD) Runge-Kutta scheme is used for the temporal terms.

6.2.4 Discretization of the convection term

High order essentially non-oscillating scheme (ENO) is used to determine the spatial derivatives appearing in $\overrightarrow{V}.\nabla\varphi$.

The idea of ENO polynomial interpolation of data for the numerical solution of conservation laws is based on computing the numerical flux functions using the smoothest possible polynomial interpolants. The zeroth divided differences of φ are defined at the grid nodes i by:

$$D_i^0\varphi = \varphi_i \tag{6.14}$$

The first divided differences of φ, in a uniformly spaced grid are defined midway between the grid nodes as:

$$D_{i+1/2}^1\varphi = \frac{D_{i+1}^0\varphi - D_i^0\varphi}{\triangle x} \tag{6.15}$$

Defining backward divided difference $D_{i-1/2}^1 = (D^-\varphi)_i$, and forward divided difference $D_{i+1/2}^1 = (D^+\varphi)_i$, we have for **first order upwind scheme** at each grid point "i":

$$\varphi_x(x_i) = \begin{cases} D^-\varphi, & u_i > 0 \\ D^+\varphi, & u_i < 0 \end{cases} \tag{6.16}$$

The second divided difference at grid nodes is:

$$D_i^2\varphi = \frac{D_{i+1/2}^1\varphi - D_{i-1/2}^1\varphi}{2\triangle x} \tag{6.17}$$

and

$$D_{i+1/2}^3\varphi = \frac{D_{i+1}^2\varphi - D_i^1\varphi}{3\triangle x} \tag{6.18}$$

Now we introduce first, second and third order upwind scheme, the accuracies are reached by adding corrections: $Q'_1(x_i)$, $Q'_2(x_i)$, $Q'_3(x_i)$ to $\varphi_x(x_i)$, which results in first, second and third order accurate differencing schemes:

$$\varphi_x(x_i) = Q'_1(x_i) + Q'_2(x_i) + Q'_3(x_i) \tag{6.19}$$

As we have seen for the first order upwind scheme depending on $u_i > 0$ we choose $k = i - 1$ and $u_i < 0$, we choose $k = i$:

$$\begin{aligned} Q'_1(x_i) = \quad & D^1_{k+\frac{1}{2}}\varphi & (6.20)\\ & if \quad |D^2_k\varphi| \leq |D^2_{k+1}\varphi| : \qquad c = D^2_k\varphi \qquad k^* = k-1 \\ & else \quad c = D^2_{k+1}\varphi \qquad k^* = k \\ Q'_2(x_i) = \quad & c(2(i-k)-1)\triangle x & (6.21)\\ & if \quad |D^3_{k^*+\frac{1}{2}}\varphi| \leq |D^3_{k^*+\frac{3}{2}}\varphi| : \qquad c^* = D^3_{k^*+\frac{1}{2}}\varphi \\ & else \quad c^* = D^3_{k^*+\frac{3}{2}}\varphi \\ Q'_3(x_i) = \quad & c^*\left(3(i-k^*)^2 - 6(i-k^*) + 2\right)\triangle x^2 & (6.22) \end{aligned}$$

6.2.5 Time derivative

The time derivative is is done by the use of second or third order TVD Runge-Kutta method. Discretization is:

$$\frac{\varphi^{n+1} - \varphi^n}{\triangle t} + \overrightarrow{V}^n.\nabla\varphi^n = 0 \tag{6.23}$$

followed by a second Euler step to advance the solution to time $t + 2\triangle t$, then averaging we have second-order accurate TVD:

$$\varphi^{n+1} = \frac{1}{2}\varphi^n + \frac{1}{2}\varphi^{n+2} \tag{6.24}$$

The third-order accurate TVD RK scheme:

$$\varphi^{n+1} = \quad \frac{1}{3}\varphi^n + \frac{2}{3}\varphi^{n+\frac{3}{2}} \tag{6.25}$$

with

$$\varphi^{n+\frac{1}{2}} = \frac{3}{4}\varphi^n + \frac{1}{4}\varphi^{n+2} \tag{6.26}$$

Then another Euler step is taken to advance the solution to time $t + \frac{3}{2}\triangle t$.

6.2.6 Time step

The time step is determined by CFL condition, viscous and surface tension constraints.

$$\begin{aligned} \triangle t = \quad & \frac{1}{2} min\Big(\triangle t_v, \triangle t_c\Big) \\ & \triangle t_v = min\Big(\frac{3}{14}\frac{\rho \triangle x^2}{\mu}\Big) \\ & \triangle t_c = min\Big(\frac{\triangle x}{|u|}\Big) \end{aligned} \tag{6.27}$$

6.2.7 Results of simulation

In this section we present some results of numerical simulation of two-phase annular flow in a horizontal hole perforated in a porous medium.

The pipe is initially filled with oil. Water is injected from the left-hand section. Due to permeability of the wall, oil can enter in the channel from the exterior medium. The velocity of oil flux is rather small, resulted from low pressure difference between the wellbore and the reservoir. The drilling fluid has density and viscosity very close to those of oil. Parameters of fluids are:

$$\lambda = \frac{\rho_{oil}}{\rho_{fluid}} = 0.8, \qquad \eta = \frac{\mu_{oil}}{\mu_{fluid}} = 1.1 \tag{6.28}$$

The direction of injection is from left to write. In the figures below the red curve is the interface between water (on the left) and oil. We see that water never reaches the channel walls. So the suggested method allows for simulating to-phase flow in a very efficient analytico-numerical way.

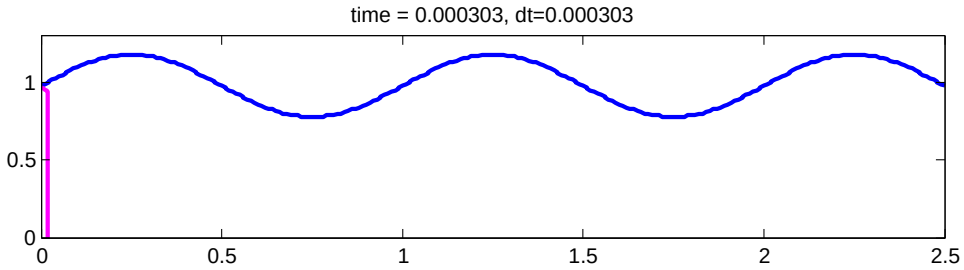

(a)

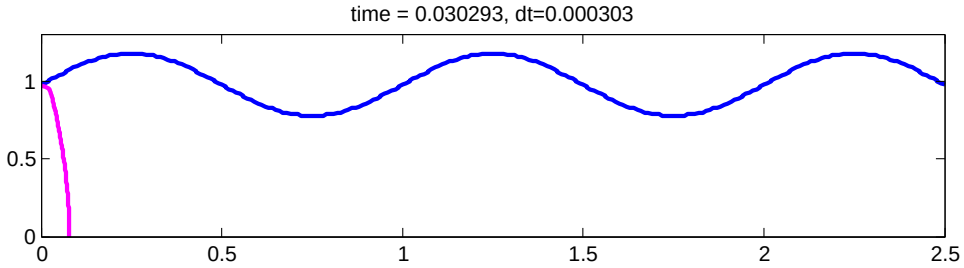

(b)

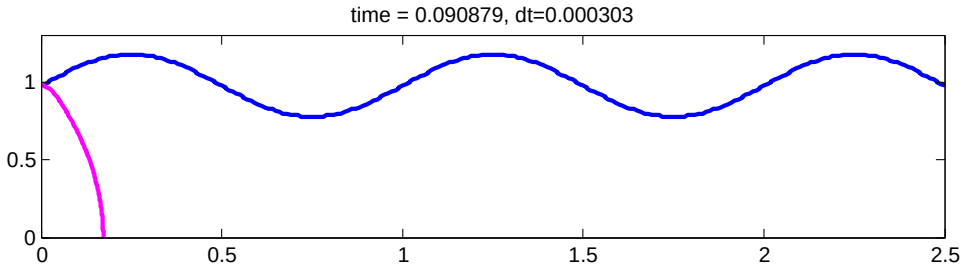

(c)

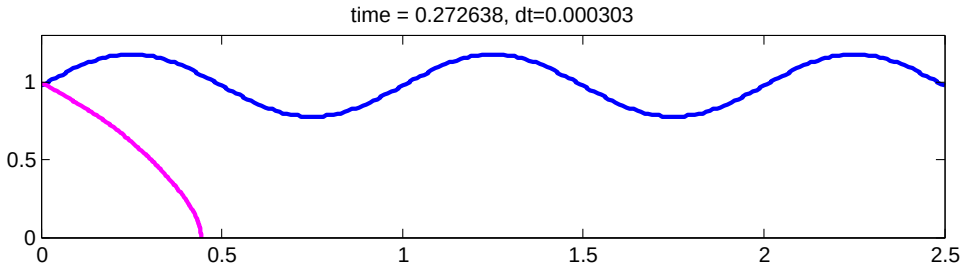

(d)

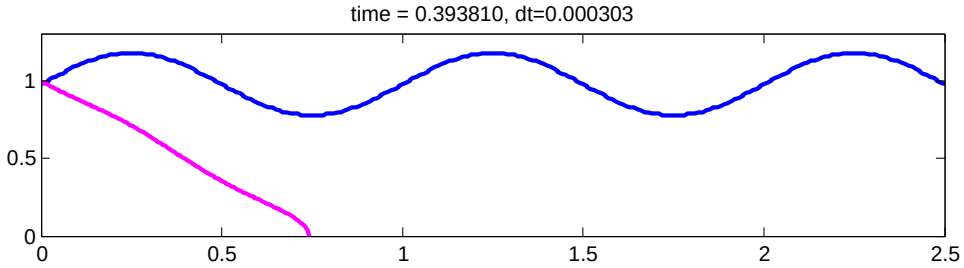

(e)

Figure 6.1: Interface of two phase annular flow in a corrugated pipe with inflow through the walls

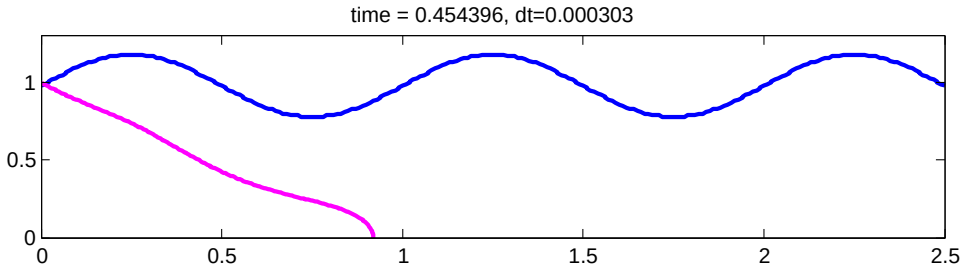

(a)

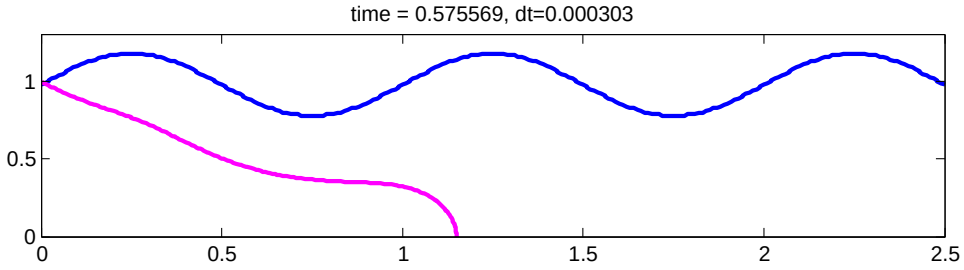

(b)

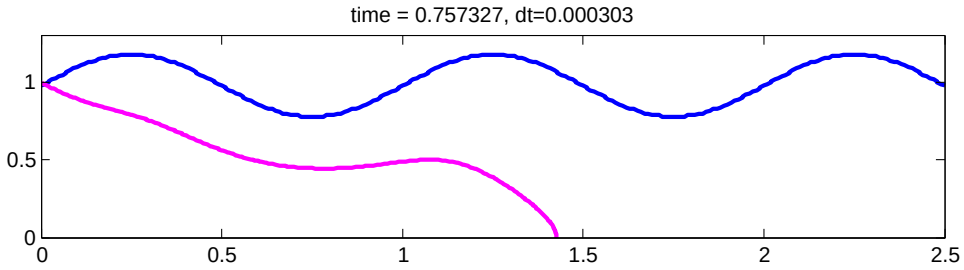

(c)

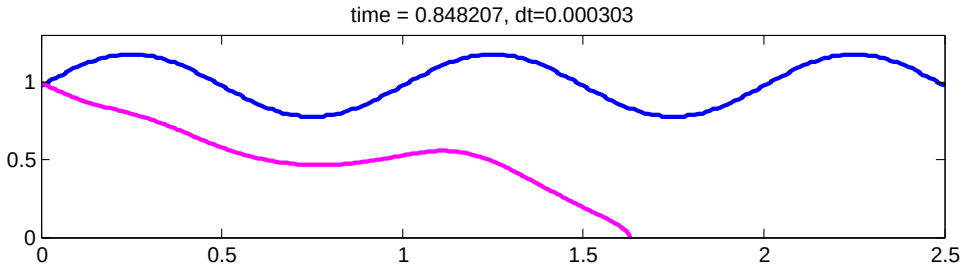

(d)

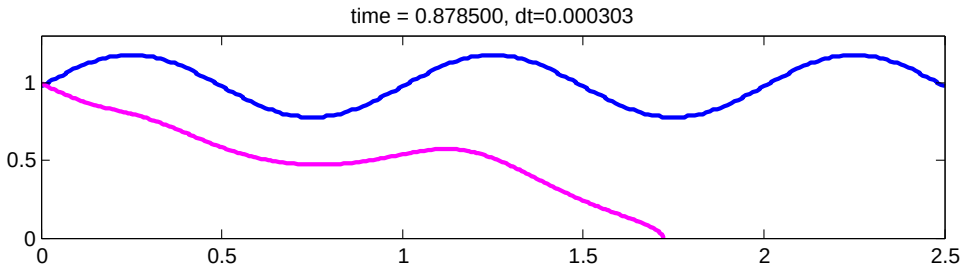

(e)

Figure 6.2: ...Interface of two phase annular flow in a corrugated pipe with inflow through the walls

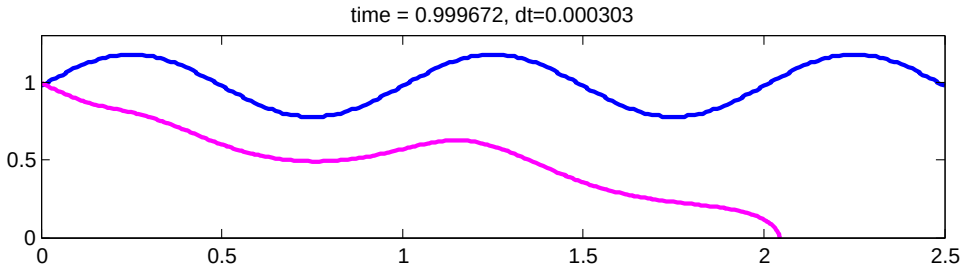

(a)

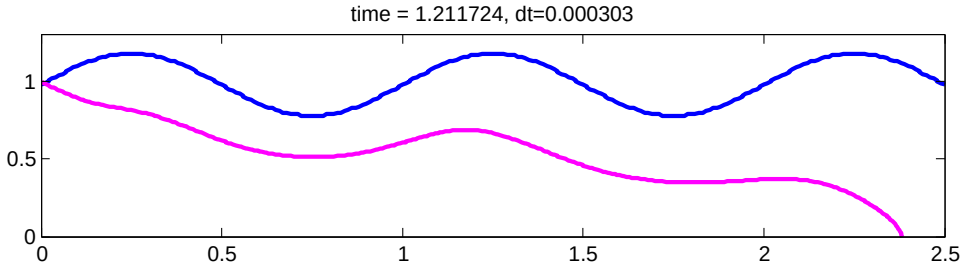

(b)

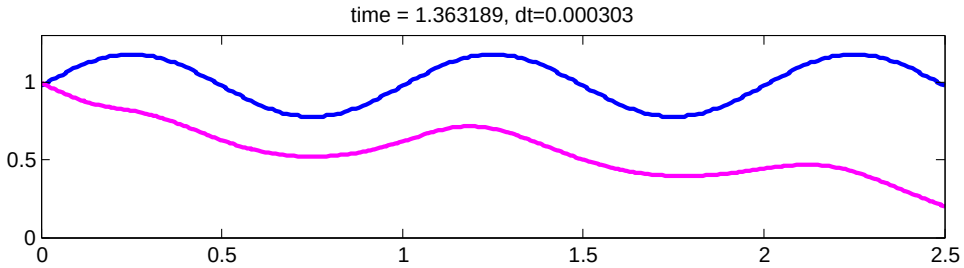

(c)

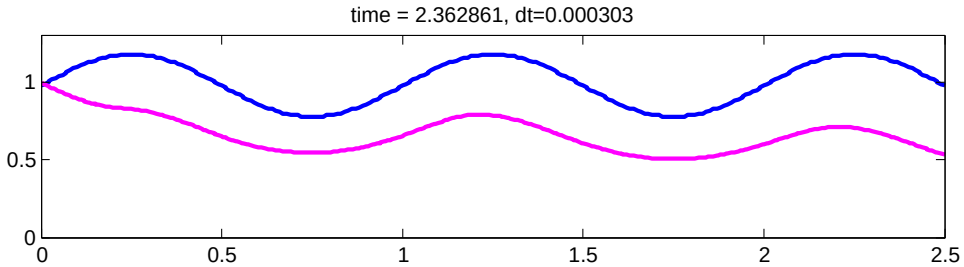

(d)

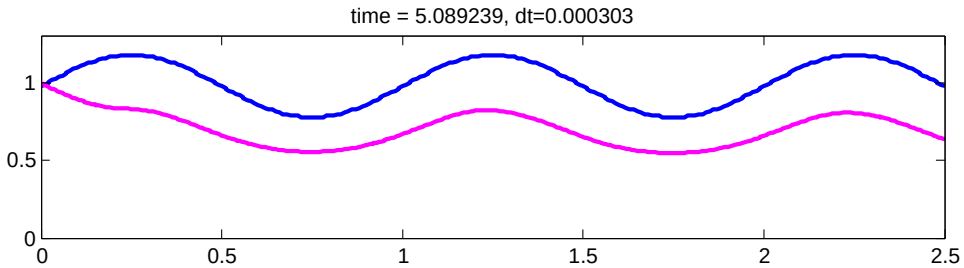

(e)

Figure 6.3: ...Interface of two phase annular flow in a corrugated pipe with inflow through the walls

Conclusion

The research consists of two parts: in the first one (chapters 1,2, and 3) we developed the models of flow in multiscale media which prove the memory effect at each scale; in the second one (chapters 4,5, and 6) we analyzed the flow in a single fracture and circular channel immersed in porous reservoir at various Reynolds numbers. In the first part we analyzed the diffusion equation at each scale and applied the asymptotic homogenization method with the objective to construct the macroscopic model averaged over all scales of heterogeneity. In the second part we studied the Navier-Stokes equations and applied the two-scale asymptotic method with the objective to obtain the flow equation averaged over the fracture aperture.

Models of flow in multiscale ε^2 media

First of all, we analyzed the double-porosity media (chapter 1) which are ε^2 as each scale, which means that the ratio of the permeability of two neighboring media is ε^2, where ε is the small period of heterogeneity at each scale. The two-scale media of such kind were studied: the obtained model proved the appearance of the non-locality in time. Physically, the nonlocal term describes the mass exchange between two media, which is highly non-stationary and depends on the direction of the process in time. For a two-scale medium, the homogenization model consists of two equations for two average pressures. Each of these equation contains the "exchange terms" : they are responsible for the interaction between two pressures.

The main problems which concern these media consist in the following:

(i) a unique homogenization for two scales causes the appearance of the nonlocality, i.e. changes the type of the equations. If we have three-scale medium and more, what will be the type of the averaged model ?

(ii) The multiple homogenization will lead to the memory accumulation. How happens this process ?

(iii) Is it possible to obtain the closed limit model for the infinite number of scales ?

(iv) How is it possible to calculate the effective parameters of the multiscale medium ?

For media with moderate heterogeneity, the diffusion equation keeps the form at each step of homogenization. Due to this the macroscopic model may be obtained by the method of direct ascension: at the first step one homogenizes the couple of media 1 and 2. At the next step, one considers the couple of medium 3 and the averaged medium 2 which already keeps the interaction with the preceding medium. This operation is repeated at each scale. In this way it is possible to reveal the structure of the effective parameters of the macroscopic equation. What is important in this case, it is the fact that the averaged equation at each scale is known a priori.

This is not the case of the media with memory. Indeed, at each step of homogenization the average equation changes the type, so the form of the average equation is unknown for any scale. Due to this, it is impossible to apply the direct iterative hierarchical method described above.

We applied another method. For an arbitrary number of scales, we applied the **method of mathematical induction** which consists in the following:

1) one postulates the general form of the averaged equation for any scale i;

2) one proves that this form is valid for $i = 1$ (the induction basis);

3) one proves that, if this form is valid for any i, then it will be also valid for $i + 1$.

The main point of this method is **to postulate the general form of the macroscale model**. In order to suggest an idea about this question, we analyzed the common features in two models obtained for $i = 1$ (a two-scale medium) and $i = 2$ (a three-scale medium). For this we performed homogenization of a three-scale ε^2 medium. The obtained results for $i = 1$ and $i = 2$ have revealed that the macroscopic model may be presented in the form of two equations for two "conjugated" pressures. One of these pressures is averaged over the medium i and is designated as P^i, while the second one is averaged over all preceding hierarchical media starting from $i - 1$. Each equation contains the exchange terms. According to these results we assumed that the exchange terms may be presented as the convolution with the derivative of the conjugate pressure. So the problem was reduced to determine the kernels of these convolution operators, and other effective parameters (permeability, porosity,...).

Based on the postulated form of the average equations, we applied the induction method: assuming that this form is valid for $i - 1$ we proved that it is also valid for i. To do it, we performed the two-scale homogenization of the flow in the couple of media i and $i - 1$, which gave us the model for the average pressure P^i related with the pressure averaged over all preceding media $\tilde{P}^{i-1}$. The result obtained confirmed that the average model for the scale i has the same form as it was postulated for the scale $i - 1$.

The homogenization at each scale was based on the technique of singular asymptotic expansions.

This applied method gave us the system of closed recurrent equations for the effective exchange kernels. The procedure of analytico-numerical solution of this system was developed, based on the Laplace

transform. We showed a convergence of the results obtained for various number of scales to a stable limit behavior.

The analyzed process in these media is self-similar, which was shown in this chapter. The necessary and sufficient condition of self-similarity has been proposed so that at each scale the homogenized model becomes self-similar. The advantage of a self-similar medium is the possibility to analyze its behavior for any number of scales, even for the infinite number.

Limit model of flow in medium with infinite number of scales

The next problem we solved was the transition to the limit $i \to \infty$. As said, the analytico-numerical simulations have revealed a fast convergence to a stable limit behavior. Assuming that the process stabilizes when $i \to \infty$, we conclude that the iterative hierarchical functions (pressure and effective kernels) tend to a limit. This enabled us to obtain the limit macroscale model of flow, and the limit problem for the effective kernels from the recurrent equations obtained for any scale i.

The limit model is nonlocal, and the effective kernel of this equation is the solution of the nonlinear integro-differential equation. Other parameters are also solution of the integro-differential equations. This system was reduced to a closed nonlinear system for the "local" kernel K in the form of the Fourier series with Fourier-components depending on the function K itself.

Using Laplace transform we developed a numerical code which resolves this equation numerically.

The solution was obtained by an iterative method: in zero approximation one assumes that the kernel is the delta-function, which gives the explicit equation for the kernel. This approximation is next substituted to the right-hand side of the analyzed equation, and so on.

The obtained solutions are exactly the same as those obtained as the numerical limit of the iterative solutions for any i, which proves the convergence of the results obtained.

The main qualitative result following from this study consist in the following: we have shown that the nonlocality may generate the nonlinearity, which is a fundamental result.

Two-scale fractured media

The case of fractured medium has a significant advantage, and a significant defect. The advantage is that this case leads to the analytical relations for the effective kernels, due to a simple, mono-dimensional strucrure of flow in a thin fracture. The defect consists of that the fractured medium which keeps the nonlocality at each scale, is not self-similar. So it is impossible to obtain the limit model for the infinite number of scales. Due to this we analyzed only the two-scale and three-scale media.

In chapter 2, we obtained the averaged model for two-scales fractured medium, in which the ratio between block and fracture permeability is $\omega = \varepsilon^{2+\alpha}, \quad \alpha > 0$. The appearance of a new small parameter, the fracture aperture, changes the structure of the asymptotic expansions and, consecutively, the

macroscale behavior. The results obtained in this chapter are not new (the model of the same type was obtained first by L. Pankratov), but are needed to develop next the model for three-scale medium, using the same methodology.

A very significant feature of fractured media is the appearance of the boundary layer in the tight block which is only perturbed by flow in the fracture. Within this boundary layer each block works as a source with respect to the flow in fracture. The internal part of each block remains unperturbed. Due to such a special (simplified) geometry of the exchange flow between fractures and blocks, the exchange kernel in the memory operator of the averaged model is the Abel kernel. The Integral equations with Abel's kernels frequently have analytical solutions or can be reduced to differential equations. This provides the effective tool to analyze multiscale fractured media, up to obtaining the structure of the effective kernels in completely analytical form. Some examples of application of this model were analyzed.

Three-scale fractured media

In chapter 3 a non self-similar three scales fractured medium was studied. It consists of the tight small blocks surrounded by highly permeable but thin fractures which are surrounded, in turn, by the second system of even more permeable and larger fractures. In the smallest scale the nonlocal behavior results only if the boundary layer in blocks, described above, exists. This gives the rule to determine the aperture of the small fractures and the permeability ratio between them and blocks. In the next level, in contrast, the appearance of the boundary layer in the superposition of two preceding media is prohibited, otherwise the major part of medium will be entirely excluded from the process. This determines the optimal parameters for the aperture and the permeability of the large fractures. As the result, we have shown that he permeability ratio between the blocks and small fractures should be lower than ε^2, while the permeability ratio between two nets of fractures should be ε^2. The fracture apertures do not follow the same scaling law as heterogeneity periods.

Than at the first (small) scale the medium behave as the fractured model with Abel's kernels described above, while at the second scale the medium behaves as a double porosity medium. The effective model averaged over all scales is the integro-differential equation whose kernel is determined analytically.

We compared the results which provide the two-scale and a three-scale model, which are in good correspondence with physical meaning. In particular, during the oil recovery from reservoir the pressure in three-scale medium should be higher than that in two-scale medium (due to a double system of sources which aliment the large fractures), which was exactly obtained by the obtained models.

Flow in a single fracture and a circular channel

To complete the study of fractured media, we also analyzed the flow in a single fracture (chapter 4).

We have studied the problem of flow in a single fracture immersed in a porous reservoir. The fracture

walls was assumed to be corrugated. The objective was to develop the flow model averaged over the fracture aperture while taking into account the inflow into the fracture from the reservoir. The inflow constituted the main new element of this study. The flow in the fracture was described by the Navier-Stokes equations at various Re. The solution of the flow problem in a very long and thin fracture was obtained in the analytical form by the method of asymptotic expansions with respect to the fracture aperture and the period of wall oscillations. .

We have obtained the averaged momentum equation which determines the mean pressure gradient at the cubic function of the mean flow velocity. The linear term corresponds to the Darcy's law, the quadratic term is caused by the inflow which reduces the kinetic energy, and the cubic term is the inertia-viscous cross-effect. For the effective parameters we have obtained analytical relationships.

The quadratic term may be neglected in all situations.

The inflow which was assumed to be low, due to this it influences weakly the viscous and the inertia-viscous terms. So the inflow influences more the averaged mass balance, but not the momentum balance.

The results were compared with numerical simulations based on Comsol Multiphysics.

We have shown that even when there is no flow entry through the walls after a critical Reynolds, a kind of instability arises. The instability is characterized as local reverse flow.

Applying the same technique, we also obtained the analytical solution of the flow problem in a circular horizontal channel (chapter 5). The obtained results are qualitatively similar to those obtained in chapter 4.

Two-phase flow in channel

Two phase flow in fractures and horizontal holes in the presence of inflow through the walls was studied in chapter 6, with a look to the application in the problem of under-balanced drilling of horizontal wells.

We developed an analytico-numerical method of solving the problem for fluids with close physical properties. One calculates analytically the velocity field by using the results obtained in chapter 5. After this one can calculate the indicator function (levelset function) which is transported at the true fluid velocity. The zero level of this function is the macroscopic interface between fluids. These operations may be repeated, which leads to an iterative method of solution. The equation for the levelset function is solved numerically.

The example of solution is shown for the case of underbalanced drilling, when water is injected into the channel (the horizontal well), and oil enters through the channel walls from the reservoir, as the pressure in water is maintained to be lower that that in the reservoir. The evolution of the interface in time is demonstrated.

Open problems

- Nonlocal diffusion-convection in multiscale media; diffusion-reaction, etc.
- Non-Darcy flow in multiscale media (cubic law).
- Problems of nonlocal flow in multiscale media to producing wells. Application to well testing.
- Approximations for the exchange kernels of multiscale models.

Appendix A

Flow in a fracture with wavy surface: solution of the first-order problem

Formulation of the first-order problem

Through the introduced variables (x, ζ) we have for the first order problem:

$$\begin{aligned}
&\frac{1}{\phi}\frac{\partial v_1}{\partial \zeta} = \frac{\zeta\phi'}{\phi}\frac{\partial u_0}{\partial \zeta} - \frac{\partial u_0}{\partial x}, \qquad \frac{\partial p_1}{\partial \zeta} = 0,\\
&\frac{1}{\phi^2}\frac{\partial^2 u_1}{\partial \zeta^2} = \mathrm{Re}\left(u_0\frac{\partial u_0}{\partial x} - u_0\frac{\zeta\phi'}{\phi}\frac{\partial u_0}{\partial \zeta} + \frac{1}{\phi}v_1\frac{\partial u_0}{\partial \zeta}\right) + \frac{\partial p_1}{\partial x},\\
&v_1|_{\zeta=1} = -v^*, \qquad u_1|_{\zeta=1} = u^*, \qquad \left.\frac{\partial u_1}{\partial z}\right|_{\zeta=0} = 0, \qquad v_1|_{\zeta=0} = 0, \qquad \int_0^1 u_1 d\zeta = \frac{F_1}{\phi} \quad \text{(A.1)}
\end{aligned}$$

Solution for v_1

Having solutions for $u_0, \dfrac{dp_0}{dx}$ we can say:

$$\frac{\partial v_1}{\partial \zeta} = -\frac{3F_0}{\phi}\zeta^2\phi' + \frac{3}{2}\phi\left(\frac{F_0}{\phi}\right)'(\zeta^2 - 1)$$

now taking into account that: $\left(\dfrac{F_0}{\phi}\right)' = \dfrac{v^*}{\phi} - \dfrac{\phi' F_0}{\phi^2}$

$$\frac{\partial v_1}{\partial \zeta} = -\frac{3}{2}\frac{\phi' F_0}{\phi}\left(3\zeta^2 - 1\right) + \frac{3}{2}v^*(\zeta^2 - 1)$$

So regarding to the boundary condition $v_1|_{\zeta=0} = 0$ we have:

$$v_1 = -\frac{3}{2}\frac{\phi' F_0}{\phi}\left(\zeta^3 - \zeta\right) + \frac{3}{2}v^*(\frac{\zeta^3}{3} - \zeta)$$

Note that this function automatically satisfies the condition :$v_1|_{\zeta=1} = -v^*$

Determination of u_1

For u_1 we obtain:

$$u_0 = -\frac{3F_0}{2\phi}(\zeta^2 - 1), \qquad \frac{dp_0}{dx} = -\frac{3F_0}{\phi^3}$$

$$\begin{aligned}
\frac{\partial^2 u_1}{\partial \zeta^2} &= \mathrm{Re}\left(\phi^2 u_0\frac{\partial u_0}{\partial x} - \left(\phi v_1 - u_0\zeta\phi'\phi\right)\frac{3F_0}{\phi}\zeta\right) + \frac{dp_1}{dx}\phi^2 =\\
&= \mathrm{Re}\left(v^* F_0\frac{9}{4}(\zeta^4 - 2\zeta^2 + 1) - \frac{\phi' F_0^2}{\phi}\frac{9}{4}(\zeta^4 - 2\zeta^2 + 1) + \right.\\
&\qquad \left. + \frac{\phi' F_0^2}{\phi}\frac{9}{2}\left(\zeta^4 - \zeta^2\right) - v^* F_0\frac{9}{2}(\frac{\zeta^4}{3} - \zeta^2) - \frac{\phi' F_0^2}{\phi}\frac{9}{2}(\zeta^4 - \zeta^2)\right) + \frac{dp_1}{dx}\phi^2 =\\
&= \frac{9}{4}\mathrm{Re}\left(v^* F_0(\frac{\zeta^4}{3} + 1) - \frac{\phi' F_0^2}{\phi}\left(\zeta^4 - 2\zeta^2 + 1\right)\right) + \frac{dp_1}{dx}\phi^2
\end{aligned}$$

Then the first integration yields:

$$\frac{\partial u_1}{\partial \zeta} = \frac{9}{4}\mathrm{Re}\left(v^* F_0(\frac{\zeta^5}{15}+\zeta) - \frac{\phi' F_0^2}{\phi}\left(\frac{\zeta^5}{5} - \frac{2\zeta^3}{3} + \zeta\right)\right) + \frac{dp_1}{dx}\phi^2\zeta$$

where we have taken into account that the longitudinal velocity is maximum on the axis of fracture.

The second integration gives:

$$u_1 = \frac{9}{4}\mathrm{Re}\left(v^* F_0(\frac{\zeta^6}{90}+\frac{\zeta^2}{2}) - \frac{\phi' F_0^2}{\phi}\left(\frac{\zeta^6}{30} - \frac{\zeta^4}{6} + \frac{\zeta^2}{2}\right)\right) + \frac{dp_1}{dx}\phi^2\frac{\zeta^2}{2} + \\ +u^* - \frac{9}{4}\mathrm{Re}\left(v^* F_0\frac{23}{45} - \frac{\phi' F_0^2}{\phi}\frac{11}{30}\right) - \frac{dp_1}{dx}\frac{\phi^2}{2}$$

Solution for p_1

For p_1 we obtain by substituting the last relation in the integral relation in (A.1)

$$u^*\left(1-\frac{\phi(0)}{\phi}\right) = \int_0^1 u_1 d\zeta \\ = \left[\frac{9}{4}\mathrm{Re}\left(v^* F_0(\frac{\zeta^7}{630}+\frac{\zeta^3}{6}) - \frac{\phi' F_0^2}{\phi}\left(\frac{\zeta^7}{210} - \frac{\zeta^5}{30} + \frac{\zeta^3}{6}\right)\right) + \frac{dp_1}{dx}\frac{\phi^2}{6}\zeta^3 + \right. \\ \left. +u^*\zeta - \frac{9}{4}\mathrm{Re}\left(v^* F_0\frac{23}{45} - \frac{\phi' F_0^2}{\phi}\frac{11}{30}\right)\zeta - \frac{dp_1}{dx}\frac{\phi^2}{2}\zeta\right]\Big|_0^1 = \\ = \frac{9}{4}\mathrm{Re}\left(v^* F_0\frac{53}{315} - \frac{\phi' F_0^2}{\phi}\frac{13}{84}\right) - \frac{1}{3}\frac{dp_1}{dx}\phi^2 + u^* - \frac{9}{4}\mathrm{Re}\left(v^* F_0\frac{23}{45} - \frac{\phi' F_0^2}{\phi}\frac{11}{30}\right)$$

or:

$$\frac{dp_1}{dx} = \mathrm{Re}\left(\frac{54}{35}\frac{\phi' F_0^2}{\phi^3} - \frac{81 v^* F_0}{35\phi^2}\right) + \frac{3u^*\phi(0)}{\phi^3} \tag{A.2}$$

Solution for u_1

For u_1

$$u_1 = \frac{9}{4}\mathrm{Re}\left(v^* F_0(\frac{\zeta^6}{90}+\frac{\zeta^2}{2}) - \frac{\phi' F_0^2}{\phi}\left(\frac{\zeta^6}{30} - \frac{\zeta^4}{6} + \frac{\zeta^2}{2}\right)\right) + \\ +u^* - \frac{9}{4}\mathrm{Re}\left(v^* F_0\frac{23}{45} - \frac{\phi' F_0^2}{\phi}\frac{11}{30}\right) + \mathrm{Re}\left(\frac{27}{35}\frac{\phi' F_0^2}{\phi}(\zeta^2-1) - \frac{81 v^* F_0}{70}(\zeta^2-1)\right) + \\ +\frac{3u^*\phi(0)}{2\phi}(\zeta^2-1)$$

$$u_1 = \frac{9}{4}\mathrm{Re}\left(v^* F_0(\frac{\zeta^6}{90}+\frac{\zeta^2}{2}-\frac{23}{45}) - \frac{\phi' F_0^2}{\phi}\left(\frac{\zeta^6}{30} - \frac{\zeta^4}{6} + \frac{\zeta^2}{2} - \frac{11}{30}\right)\right) + \\ +u^* + \frac{9}{4}\mathrm{Re}\left(\frac{12}{35}\frac{\phi' F_0^2}{\phi}(\zeta^2-1) - \frac{18 v^* F_0}{35}(\zeta^2-1)\right) + \frac{3u^*\phi(0)}{2\phi}(\zeta^2-1)$$

So:

$$u_1 = \frac{9}{4}\mathrm{Re}\left(v^* F_0\left(\frac{\zeta^6}{90}+\frac{\zeta^2}{2}-\frac{23}{45}-\frac{18}{35}(\zeta^2-1)\right)-\frac{\phi' F_0^2}{\phi}\left(\frac{\zeta^6}{30}-\frac{\zeta^4}{6}+\frac{\zeta^2}{2}-\frac{11}{30}-\frac{12}{35}(\zeta^2-1)\right)\right)+$$
$$+u^*+\frac{3u^*\phi(0)}{2\phi}(\zeta^2-1)$$

Gives:

$$u_1 = \frac{\mathrm{Re}\, v^* F_0}{280}\left(7\zeta^6-9\zeta^2+2\right)-\frac{3\mathrm{Re}\,\phi' F_0^2}{280\phi}\left(7\zeta^6-35\zeta^4+33\zeta^2-5\right)+u^*\left(1+\frac{3\phi(0)}{2\phi}(\zeta^2-1)\right)$$

Appendix B

Flow in a fracture with wavy surface: solution of the second-order problem

Formulation of the second-order problem

Through the introduced variables (x, ζ) we have for the second order problem:

$$\frac{1}{\phi}\frac{\partial v_2}{\partial \zeta} = \frac{\zeta\phi'}{\phi}\frac{\partial u_1}{\partial \zeta} - \frac{\partial u_1}{\partial x}, \qquad \frac{\partial p_2}{\partial \zeta} = \frac{1}{\phi}\frac{\partial^2 v_1}{\partial \zeta^2},$$
$$\frac{1}{\phi^2}\frac{\partial^2 u_2}{\partial \zeta^2} = \mathrm{Re}\left(u_1\frac{\partial u_0}{\partial x} - u_1\frac{\zeta\phi'}{\phi}\frac{\partial u_0}{\partial \zeta} + u_0\frac{\partial u_1}{\partial x} - u_0\frac{\zeta\phi'}{\phi}\frac{\partial u_1}{\partial \zeta} + v_1\frac{1}{\phi}\frac{\partial u_1}{\partial \zeta} + v_2\frac{1}{\phi}\frac{\partial u_0}{\partial \zeta}\right) + \frac{\partial p_2}{\partial x} - \frac{\zeta\phi'}{\phi}\frac{\partial p_2}{\partial \zeta} -$$
$$-\frac{\partial^2 u_0}{\partial x^2} + \zeta\left(\frac{\phi'}{\phi}\right)'\frac{\partial u_0}{\partial \zeta} + 2\frac{\zeta\phi'}{\phi}\frac{\partial^2 u_0}{\partial x \partial \zeta} - \frac{\zeta\phi'^2}{\phi^2}\frac{\partial u_0}{\partial \zeta} - \frac{\zeta^2\phi'^2}{\phi^2}\frac{\partial^2 u_0}{\partial \zeta^2}$$
$$v_2|_{\zeta=1} = 0, \qquad u_2|_{\zeta=1} = 0, \qquad \left.\frac{\partial u_2}{\partial z}\right|_{\zeta=0} = 0, \qquad v|_{\zeta=0} = 0 \qquad \int_0^1 u_2 d\zeta = 0 \tag{B.1}$$

Solution for v_2

The second approximation v_2 can be found by simply integrating the following equation:

$$\frac{\partial v_2}{\partial \zeta} = \zeta\phi'\frac{\partial u_1}{\partial \zeta} - \phi\frac{\partial u_1}{\partial x} \tag{B.2}$$

Noting that:

$$\frac{\partial u_1}{\partial x} = \frac{\mathrm{Re}\, v^{*2}}{280}\left(7\zeta^6 - 9\zeta^2 + 2\right) - \left(\frac{3\mathrm{Re}\, v^*\phi' F_0}{140\phi} - \frac{3\mathrm{Re}\,\phi'^2 F_0^2}{280\phi^2}\right)\left(7\zeta^6 - 35\zeta^4 + 33\zeta^2 - 5\right) -$$
$$-\frac{3\mathrm{Re}\,\phi'' F_0^2}{280\phi}\left(7\zeta^6 - 35\zeta^4 + 33\zeta^2 - 5\right) - u^*\frac{3\phi(0)\phi'}{2\phi^2}(\zeta^2 - 1)$$
$$\frac{\partial u_1}{\partial \zeta} = \frac{\mathrm{Re}\, v^* F_0}{280}\left(42\zeta^5 - 18\zeta\right) - \frac{3\mathrm{Re}\,\phi' F_0^2}{280\phi}\left(42\zeta^5 - 140\zeta^3 + 66\zeta\right) + u^*\frac{3\phi(0)}{\phi}\zeta$$

we have:

$$\frac{\partial v_2}{\partial \zeta} = \frac{\mathrm{Re}\, v^*\phi' F_0}{280}\left(42\zeta^6 - 18\zeta^2\right) - \frac{3\mathrm{Re}\,\phi'^2 F_0^2}{280\phi}\left(42\zeta^6 - 140\zeta^4 + 66\zeta^2\right) + u^*\frac{3\phi(0)\phi'}{\phi}\zeta^2 -$$
$$-\frac{\mathrm{Re}\, v^{*2}\phi}{280}\left(7\zeta^6 - 9\zeta^2 + 2\right) +$$
$$+\left(\frac{6\mathrm{Re}\, v^*\phi' F_0}{280} - \frac{3\mathrm{Re}\,\phi'^2 F_0^2}{280\phi}\right)\left(7\zeta^6 - 35\zeta^4 + 33\zeta^2 - 5\right) +$$
$$+\frac{3\mathrm{Re}\,\phi'' F_0^2}{280}\left(7\zeta^6 - 35\zeta^4 + 33\zeta^2 - 5\right) + u^*\frac{3\phi(0)\phi'}{2\phi}(\zeta^2 - 1) =$$
$$= \frac{6\mathrm{Re}\, v^*\phi' F_0}{280}\left(14\zeta^6 - 35\zeta^4 + 30\zeta^2 - 5\right) -$$
$$-\frac{3\mathrm{Re}\,\phi'^2 F_0^2}{280\phi}\left(49\zeta^6 - 175\zeta^4 + 99\zeta^2 - 5\right) + u^*\frac{3\phi(0)\phi'}{\phi}\zeta^2 -$$
$$-\frac{\mathrm{Re}\, v^{*2}\phi}{280}\left(7\zeta^6 - 9\zeta^2 + 2\right) + +\frac{3\mathrm{Re}\,\phi'' F_0^2}{280}\left(7\zeta^6 - 35\zeta^4 + 33\zeta^2 - 5\right) + u^*\frac{3\phi(0)\phi'}{2\phi}(\zeta^2 - 1)$$

Integration gives:

$$v_2 = \frac{6\mathrm{Re}\, v^* \phi' F_0}{280}\left(2\zeta^7 - 7\zeta^5 + 10\zeta^3 - 5\zeta\right) - \\ -\frac{3\mathrm{Re}\, \phi'^2 F_0^2}{280\phi}\left(7\zeta^7 - 35\zeta^5 + 33\zeta^3 - 5\zeta\right) + u^* \frac{\phi(0)\phi'}{\phi}\zeta^3 - \\ -\frac{\mathrm{Re}\, v^{*2}\phi}{280}\left(\zeta^7 - 3\zeta^3 + 2\zeta\right) + \frac{3\mathrm{Re}\, \phi'' F_0^2}{280}\left(\zeta^7 - 7\zeta^5 + 11\zeta^3 - 5\zeta\right) + u^* \frac{\phi(0)\phi'}{2\phi}(\zeta^3 - 3\zeta)$$

where we have taken into account the condition of zero value on the fracture axis. This simplifies to:

$$v_2 = \frac{3u^*\phi(0)\phi'}{2\phi}(\zeta^3 - \zeta) + \frac{\mathrm{Re}\, v^{*2}\phi}{280}\left(-\zeta^7 + 3\zeta^3 - 2\zeta\right) + \frac{3\mathrm{Re}\, \phi'^2 F_0^2}{280\phi}\left(-7\zeta^7 + 35\zeta^5 - 33\zeta^3 + 5\zeta\right) + \\ + \frac{3\mathrm{Re}\, v^* \phi' F_0}{140}\left(2\zeta^7 - 7\zeta^5 + 10\zeta^3 - 5\zeta\right) + \frac{3\mathrm{Re}\, \phi'' F_0^2}{280}\left(\zeta^7 - 7\zeta^5 + 11\zeta^3 - 5\zeta\right)$$

Automatically we have $v_2|_{\zeta=1} = 0$.

Determination of p_2

p_2 can be found through v_1:

$$\frac{\partial p_2}{\partial \zeta} = \left(\frac{3v^*}{\phi} - 9\frac{\phi' F_0}{\phi^2}\right)\zeta$$

Integrating gives:

$$p_2 = \left(\frac{v^*}{\phi} - 3\frac{\phi' F_0}{\phi^2}\right)\frac{3\zeta^2}{2} + M(x)$$

$M(x)$ should be determined later.

Then we can say:

$$\frac{\partial p_2}{\partial x} = \left(-\frac{v^*\phi'}{\phi^2} - 3\frac{\phi'' F_0}{\phi^2} - 3\frac{v^*\phi'}{\phi^2} + 6\frac{\phi' F_0}{\phi^3}\right)\frac{3\zeta^2}{2} + M'(x)$$

Finally:

$$\frac{\partial p_2}{\partial x} = \left(\frac{9F_0\phi'^2}{\phi^3} - \frac{9F_0\phi''}{2\phi^2} - \frac{6v^*\phi'}{\phi^2}\right)\zeta^2 + M'(x)$$

Determination of u_2

The second order approximation:

$$\frac{1}{\phi^2}\frac{\partial^2 u_2}{\partial \zeta^2} = \mathrm{Re}\left(u_1\frac{\partial u_0}{\partial x} - u_1\frac{\zeta\phi'}{\phi}\frac{\partial u_0}{\partial \zeta} + u_0\frac{\partial u_1}{\partial x} - u_0\frac{\zeta\phi'}{\phi}\frac{\partial u_1}{\partial \zeta} + v_1\frac{1}{\phi}\frac{\partial u_1}{\partial \zeta} + v_2\frac{1}{\phi}\frac{\partial u_0}{\partial \zeta}\right) + \frac{\partial p_2}{\partial x} - \frac{\zeta\phi'}{\phi}\frac{\partial p_2}{\partial \zeta} - \\ -\frac{\partial^2 u_0}{\partial x^2} + \zeta\left(\frac{\phi'}{\phi}\right)'\frac{\partial u_0}{\partial \zeta} + 2\frac{\zeta\phi'}{\phi}\frac{\partial^2 u_0}{\partial x \partial \zeta} - \frac{\zeta\phi'^2}{\phi^2}\frac{\partial u_0}{\partial \zeta} - \frac{\zeta^2\phi'^2}{\phi^2}\frac{\partial^2 u_0}{\partial \zeta^2}$$

after applying $u_0, v_1, u_1, v_2, \frac{\partial p_2}{\partial x}$ gives:

$$M'(x) = \frac{3F_0\phi''}{10\phi^2} - \frac{12F_0\phi'^2}{5\phi^3} - \frac{6\,\mathrm{Re}\,u^*v^*}{5\phi} + \frac{81\,\mathrm{Re}\,u^*v^*\phi(0)}{35\phi^2} + \frac{3\,\mathrm{Re}\,u^*F_0\phi'}{5\phi^2} + \\ + \frac{156\,\mathrm{Re}^2F_0^3}{13475}\left(\frac{4\phi'^2}{\phi^3} - \frac{3\phi''}{\phi^2}\right) - \frac{234\,\mathrm{Re}^2F_0v^{*2}}{13475\,\phi} - \\ - \frac{271\,\mathrm{Re}^2F_0^2v^*\phi'}{1925\,\phi^2} - \frac{108\,\mathrm{Re}\,u^*\phi(0)F_0\phi'}{35\,\phi^3}$$

Solution for p_2

Definitely for p_2 we have:

$$\frac{\partial p_2}{\partial x} = \left(\frac{9F_0\phi'^2}{\phi^3} - \frac{9F_0\phi''}{2\phi^2} - \frac{6v^*\phi'}{\phi^2}\right)\zeta^2 + \\ + \frac{3F_0\phi''}{10\phi^2} - \frac{12F_0\phi'^2}{5\phi^3} - \frac{6\,\mathrm{Re}\,u^*v^*}{5\phi} + \frac{81\,\mathrm{Re}\,u^*v^*\phi(0)}{35\phi^2} + \frac{3\,\mathrm{Re}\,u^*F_0\phi'}{5\phi^2} + \\ + \frac{156\,\mathrm{Re}^2F_0^3}{13475}\left(\frac{4\phi'^2}{\phi^3} - \frac{3\phi''}{\phi^2}\right) - \frac{234\,\mathrm{Re}^2F_0v^{*2}}{13475\,\phi} - \\ - \frac{271\,\mathrm{Re}^2F_0^2v^*\phi'}{1925\,\phi^2} - \frac{108\,\mathrm{Re}\,u^*\phi(0)F_0\phi'}{35\,\phi^3}$$

Solution for u_2

We have for u_2:

$$u_2 = \frac{1}{20}\left(-3F_0\phi'' - 5v^*\phi' + \frac{9F_0\phi'^2}{\phi}\right)\left(5\zeta^4 - 6\zeta^2 + 1\right) + \\ + \frac{\mathrm{Re}\,u^*\phi'F_0}{280}\left(105\zeta^4 - 126\zeta^2 + 21\right) - \\ - \frac{\mathrm{Re}\,u^*v^*\phi(0)}{280}\left(7\zeta^6 - 9\zeta^2 + 2\right) - \\ - \frac{3\mathrm{Re}\,u^*\phi(0)\phi'F_0}{140\,\phi}\left(-7\zeta^6 + 35\zeta^4 - 33\zeta^2 + 5\right) - \\ - \frac{\mathrm{Re}\,u^*v^*\phi}{40}\left(5\zeta^4 - 6\zeta^2 + 1\right) + \\ + \frac{\mathrm{Re}^2F_0^3\phi''}{1120}\left(\zeta^{10} - 9\zeta^8 + \frac{138}{5}\zeta^6 - 42\zeta^4 + \frac{9837}{385}\zeta^2 - \frac{1213}{385}\right) + \\ + \frac{\mathrm{Re}^2F_0^3\phi'^2}{280\,\phi}\left(-\frac{7}{10}\zeta^{10} + \frac{27}{4}\zeta^8 - \frac{102}{5}\zeta^6 + \frac{57}{2}\zeta^4 - \frac{12333}{770}\zeta^2 + \frac{575}{313}\right) + \\ + \frac{\mathrm{Re}^2v^{*2}F_0\phi}{2800}\left(\frac{\zeta^{10}}{3} - \frac{15}{2}\zeta^8 + 3\zeta^6 + \frac{438}{77}\zeta^2 - \frac{703}{462}\right) + \\ + \frac{\mathrm{Re}^2v^*F_0^2\phi'}{5600}\left(6\zeta^{10} - \frac{75}{4}\zeta^8 - 21\zeta^6 - 1725\zeta^4 + \frac{2759}{11}\zeta^2 - \frac{1961}{44}\right)$$

Appendix C

Flow in a pipe with wavy surface: solution of the first-order problem

Formulation of the first-order problem

From the first-order problem, we obtain by replacing the variables:

$$\frac{1}{\phi\zeta}\frac{\partial\left(\zeta v_1\right)}{\partial\zeta} = -\frac{\partial u_0}{\partial x} + \frac{\zeta\phi'}{\phi}\frac{\partial u_0}{\partial\zeta},$$
$$\frac{1}{\phi^2\zeta}\frac{\partial}{\partial\zeta}\left(\zeta\frac{\partial u_1}{\partial\zeta}\right) = \frac{dp_1}{dx} + \frac{\mathrm{Re}}{2}\left(\frac{\partial u_0^2}{\partial x} - \frac{\zeta\phi'}{\phi}\frac{\partial u_0^2}{\partial\zeta}\right) + \frac{\mathrm{Re}}{\phi}v_1\frac{\partial u_0}{\partial\zeta},$$
$$\left.\frac{\partial u_1}{\partial\zeta}\right|_{\zeta=0} = 0, \qquad v_1|_{\zeta=0} = 0, \quad u_1|_{\zeta=1} = u^*, \quad v_1|_{\zeta=1} = -v^*, \quad \int_0^1 \zeta u_1(x,\zeta)d\zeta = \frac{F_1}{\phi^2}$$

Taking into account the solution for u_0, v_0, p_0:

$$\frac{1}{\phi\zeta}\frac{\partial\left(\zeta v_1\right)}{\partial\zeta} = 4\left(\zeta^2-1\right)\left(\frac{F_0}{\phi^2}\right)' - \frac{8\zeta^2\phi' F_0}{\phi^3},$$
$$\frac{1}{\phi^2\zeta}\frac{\partial}{\partial\zeta}\left(\zeta\frac{\partial u_1}{\partial\zeta}\right) = \frac{dp_1}{dx} + 8\mathrm{Re}\left(\zeta^2-1\right)^2\left(\frac{F_0^2}{\phi^4}\right)' - \frac{32\mathrm{Re}\,\zeta\phi' F_0^2}{\phi^5}\zeta\left(\zeta^2-1\right) - \frac{8\mathrm{Re}F_0\zeta v_1}{\phi^3},$$
$$\left.\frac{\partial u_1}{\partial\zeta}\right|_{\zeta=0} = 0, \quad v_1|_{\zeta=0} = 0, \quad u_1|_{\zeta=1} = u^*, \quad v_1|_{\zeta=1} = -v^*, \quad \int_0^1 \zeta u_1(x,\zeta)d\zeta = \frac{F_1}{\phi^2}$$

Taking into account that:

$$\left(\frac{F_0}{\phi^2}\right)' = \frac{F_0'}{\phi^2} - \frac{2F_0\phi'}{\phi^3} = \frac{v^*}{\phi} - \frac{2F_0\phi'}{\phi^3}, \tag{C.1a}$$
$$\left(\frac{F_0^2}{\phi^4}\right)' = \frac{2F_0F_0'}{\phi^4} - \frac{4F_0^2\phi'}{\phi^5} = \frac{2F_0v^*}{\phi^3} - \frac{4F_0^2\phi'}{\phi^5} \tag{C.1b}$$
$$\frac{F_1}{\phi^2} = \frac{u^*}{2}\left(1 - \frac{\phi^2(0)}{\phi^2}\right) \tag{C.1c}$$

the problem can be reformulated as:

$$\frac{\partial\left(\zeta v_1\right)}{\partial\zeta} = 4v^*\left(\zeta^3-\zeta\right) - \frac{8\phi' F_0}{\phi^2}\left(2\zeta^3-\zeta\right),$$
$$\frac{\partial}{\partial\zeta}\left(\zeta\frac{\partial u_1}{\partial\zeta}\right) = \phi^2\zeta\frac{dp_1}{dx} + \frac{16\mathrm{Re}\,F_0v^*}{\phi}\left(\zeta^5-2\zeta^3+\zeta\right) - \frac{32\mathrm{Re}\,\phi' F_0^2}{\phi^3}\left(2\zeta^5-3\zeta^3+\zeta\right) - \frac{8\mathrm{Re}\,F_0v_1}{\phi}\zeta^2,$$
$$\left.\frac{\partial u_1}{\partial\zeta}\right|_{\zeta=0} = 0, \quad v_1|_{\zeta=0} = 0, \quad u_1|_{\zeta=1} = u^*, \quad v_1|_{\zeta=1} = -v^*,$$
$$\int_0^1 \zeta u_1(x,\zeta)d\zeta = \frac{u^*}{2}\left(1 - \frac{\phi^2(0)}{\phi^2}\right) \tag{C.2}$$

Solution for v_1

For v_1, we obtain by integrating the first equation:

$$v_1 = v^*\left(\zeta^3-2\zeta\right) - \frac{4\phi' F_0}{\phi^2}\left(\zeta^3-\zeta\right)$$

Note that this function automatically satisfies the condition at the well boundary, indeed for $\zeta = 1$: $v_1 = -v^*$.

Solution for u_1

For u_1, we obtain:

$$\begin{aligned}\frac{\partial}{\partial\zeta}\left(\zeta\frac{\partial u_1}{\partial\zeta}\right) &= \phi^2\frac{\partial p_1}{\partial x}\zeta + \frac{16\mathrm{Re}F_0v^*}{\phi}\left(\zeta^5 - 2\zeta^3 + \zeta\right) - \frac{32\mathrm{Re}\phi' F_0^2}{\phi^3}\left(2\zeta^5 - 3\zeta^3 + \zeta\right) - \\ &- \frac{8\mathrm{Re}F_0}{\phi}\zeta^2\left(v^*\left(\zeta^3 - 2\zeta\right) - \frac{4\phi' F_0}{\phi^2}\left(\zeta^3 - \zeta\right)\right) = \\ &= \phi^2\frac{\partial p_1}{\partial x}\zeta + \frac{8\mathrm{Re}F_0v^*}{\phi}\left(2\zeta^5 - 4\zeta^3 + 2\zeta - \zeta^5 + 2\zeta^3\right) - \frac{32\mathrm{Re}\phi' F_0^2}{\phi^3}\left(2\zeta^5 - 3\zeta^3 + \zeta - \zeta^5 + \zeta^3\right) = \\ &= \phi^2\frac{\partial p_1}{\partial x}\zeta + \frac{8\mathrm{Re}F_0v^*}{\phi}\left(\zeta^5 - 2\zeta^3 + 2\zeta\right) - \frac{32\mathrm{Re}\phi' F_0^2}{\phi^3}\left(\zeta^5 - 2\zeta^3 + \zeta\right)\end{aligned}$$

The first integration yields:

$$\frac{\partial u_1}{\partial\zeta} = \phi^2\frac{\partial p_1}{\partial x}\frac{\zeta}{2} + \frac{8\mathrm{Re}F_0v^*}{\phi}\left(\frac{\zeta^5}{6} - \frac{\zeta^3}{2} + \zeta\right) - \frac{32\mathrm{Re}\phi' F_0^2}{\phi^3}\left(\frac{\zeta^5}{6} - \frac{\zeta^3}{2} + \frac{\zeta}{2}\right)$$

where we taken into account the condition at the well axis.

The second integration gives while taking into account the condition at the wall boundary:

$$u_1 = u^* + \phi^2\frac{\partial p_1}{\partial x}\frac{\zeta^2 - 1}{4} + \frac{8\mathrm{Re}F_0v^*}{\phi}\left(\frac{\zeta^6 - 1}{36} - \frac{\zeta^4 - 1}{8} + \frac{\zeta^2 - 1}{2}\right) - \frac{32\mathrm{Re}\phi' F_0^2}{\phi^3}\left(\frac{\zeta^6 - 1}{36} - \frac{\zeta^4 - 1}{8} + \frac{\zeta^2 - 1}{4}\right)$$

or

$$u_1 = u^* + \frac{\phi^2}{4}\frac{\partial p_1}{\partial x}\left(\zeta^2 - 1\right) + \frac{\mathrm{Re}F_0v^*}{\phi}\left(\frac{2\zeta^6}{9} - \zeta^4 + 4\zeta^2 - \frac{29}{9}\right) - \frac{\mathrm{Re}\phi' F_0^2}{\phi^3}\left(\frac{8\zeta^6}{9} - 4\zeta^4 + 8\zeta^2 - \frac{44}{9}\right)$$

Solution for p_1

For p_1 we obtain by substituting the last relation in the integral relation in (C.2):

$$\begin{aligned}\frac{u^*}{2}\left(1 - \frac{\phi^2(0)}{\phi^2}\right) &= \int_0^1 \zeta\left[u^* + \frac{\phi^2}{4}\frac{\partial p_1}{\partial x}\left(\zeta^2 - 1\right) + \frac{\mathrm{Re}F_0v^*}{\phi}\left(\frac{2\zeta^6}{9} - \zeta^4 + 4\zeta^2 - \frac{29}{9}\right) - \right. \\ &\qquad \left. \frac{\mathrm{Re}\phi' F_0^2}{\phi^3}\left(\frac{8\zeta^6}{9} - 4\zeta^4 + 8\zeta^2 - \frac{44}{9}\right)\right] d\zeta = \\ &= \frac{u^*}{2} + \frac{\phi^2}{4}\frac{\partial p_1}{\partial x}\left(\frac{1}{4} - \frac{1}{2}\right) + \frac{\mathrm{Re}F_0v^*}{\phi}\left(\frac{1}{36} - \frac{1}{6} + 1 - \frac{29}{18}\right) - \frac{\mathrm{Re}\phi' F_0^2}{\phi^3}\left(\frac{1}{9} - \frac{2}{3} + 2 - \frac{22}{9}\right)\end{aligned}$$

or

$$-\frac{u^*}{2}\frac{\phi^2(0)}{\phi^2} = -\frac{\phi^2}{16}\frac{\partial p_1}{\partial x} - \frac{3\mathrm{Re}F_0v^*}{4\phi} + \frac{\mathrm{Re}\phi' F_0^2}{\phi^3}$$

Then

$$\frac{\partial p_1}{\partial x} = 8u^* \frac{\phi^2(0)}{\phi^4} - \frac{12\mathrm{Re}F_0 v^*}{\phi^3} + \frac{16\mathrm{Re}\phi' F_0^2}{\phi^5}$$

Closing the relation for u_1

Then for u_1 :

$$u_1 = u^* \left(1 + \frac{2\phi^2(0)}{\phi^2}\left(\zeta^2 - 1\right)\right) + \frac{\mathrm{Re}\, F_0 v^*}{\phi}\left(\frac{2\zeta^6}{9} - \zeta^4 + 4\zeta^2 - \frac{29}{9} - 3\zeta^2 + 3\right) - \\ - \frac{\mathrm{Re}\phi' F_0^2}{\phi^3}\left(\frac{8\zeta^6}{9} - 4\zeta^4 + 8\zeta^2 - \frac{44}{9} - 4\zeta^2 + 4\right)$$

or

$$u_1 = u^* \left(1 + \frac{2\phi^2(0)}{\phi^2}\left(\zeta^2 - 1\right)\right) + \frac{\mathrm{Re}F_0 v^*}{\phi}\left(\frac{2\zeta^6}{9} - \zeta^4 + \zeta^2 - \frac{2}{9}\right) - \frac{\mathrm{Re}\phi' F_0^2}{\phi^3}\left(\frac{8\zeta^6}{9} - 4\zeta^4 + 4\zeta^2 - \frac{8}{9}\right)$$

Appendix D

Flow in a pipe with wavy surface: solution of the second-order problem

Formulation of the second-order problem

The second-order problem is:

$$\frac{1}{r}\frac{\partial\left(rv_2\right)}{\partial r}+\frac{\partial u_1}{\partial x}=0,\qquad 0=-\frac{\partial p_2}{\partial r}+\frac{1}{r}\frac{\partial}{\partial r}\left(r\frac{\partial v_1}{\partial r}\right)-\frac{v_1}{r^2},$$
$$\mathrm{Re}\left(u_1\frac{\partial u_0}{\partial x}+u_0\frac{\partial u_1}{\partial x}+v_2\frac{\partial u_0}{\partial r}+v_1\frac{\partial u_1}{\partial r}\right)=-\frac{\partial p_2}{\partial x}+\frac{\partial^2 u_0}{\partial x^2}+\frac{1}{r}\frac{\partial}{\partial r}\left(r\frac{\partial u_2}{\partial r}\right),$$
$$\left.\frac{\partial u_2}{\partial r}\right|_{r=0}=0,\qquad v_2|_{r=0}=0,\quad u_2|_{r=\phi(x)}=0,\quad v_2|_{r=\phi(x)}=0,\quad \int_0^{\phi(x)} ru_2(x,r)dr=0$$

Through variables $x,\zeta{=}r/\phi(x)$:

$$\frac{\partial p_2}{\partial\zeta}=\frac{1}{\phi\zeta}\frac{\partial}{\partial\zeta}\left(\zeta\frac{\partial v_1}{\partial\zeta}\right)-\frac{v_1}{\phi\zeta^2}, \tag{D.1}$$
$$\frac{1}{\zeta\phi}\frac{\partial\left(\zeta v_2\right)}{\partial\zeta}+\frac{\partial u_1}{\partial x}-\frac{\phi'\zeta}{\phi}\frac{\partial u_1}{\partial\zeta}=0, \tag{D.2}$$
$$\begin{aligned}\mathrm{Re}\left(u_1\frac{\partial u_0}{\partial x}-\frac{u_1\phi'\zeta}{\phi}\frac{\partial u_0}{\partial\zeta}+u_0\frac{\partial u_1}{\partial x}-\frac{u_0\phi'\zeta}{\phi}\frac{\partial u_1}{\partial\zeta}+\frac{v_2}{\phi}\frac{\partial u_0}{\partial\zeta}+\frac{v_1}{\phi}\frac{\partial u_1}{\partial\zeta}\right)=\\ =-\frac{\partial p_2}{\partial x}+\frac{\phi'\zeta}{\phi}\frac{\partial p_2}{\partial\zeta}+\left(\frac{\partial}{\partial x}-\frac{\phi'\zeta}{\phi}\frac{\partial}{\partial\zeta}\right)\left(\frac{\partial u_0}{\partial x}-\frac{\phi'\zeta}{\phi}\frac{\partial u_0}{\partial\zeta}\right)+\frac{1}{\phi^2\zeta}\frac{\partial}{\partial\zeta}\left(\zeta\frac{\partial u_2}{\partial\zeta}\right)\end{aligned} \tag{D.3}$$
$$\left.\frac{\partial u_2}{\partial r}\right|_{\zeta=0}=0,\qquad v_2|_{\zeta=0}=0,\quad u_2|_{\zeta=1}=0,\quad v_2|_{\zeta=1}=0,\quad \int_0^1 \zeta u_2(x,\zeta)d\zeta=0 \tag{D.4}$$

Determination of p_2

As

$$\zeta\frac{\partial v_1}{\partial\zeta}=v^*\left(3\zeta^3-2\zeta\right)-\frac{4\phi' F_0}{\phi^2}\left(3\zeta^3-\zeta\right)$$
$$\frac{1}{\zeta}\frac{\partial}{\partial\zeta}\left(\zeta\frac{\partial v_1}{\partial\zeta}\right)=v^*\left(9\zeta-\frac{2}{\zeta}\right)-\frac{4\phi' F_0}{\phi^2}\left(9\zeta-\frac{1}{\zeta}\right)$$

then we obtain from (D.1):

$$\frac{\partial p_2}{\partial\zeta}=\frac{v^*}{\phi}\left(9\zeta-\frac{2}{\zeta}\right)-\frac{4\phi' F_0}{\phi^3}\left(9\zeta-\frac{1}{\zeta}\right)-\frac{v^*}{\phi}\left(\zeta-\frac{2}{\zeta}\right)+\frac{4\phi' F_0}{\phi^3}\left(\zeta-\frac{1}{\zeta}\right)=8\left(\frac{v^*}{\phi}-\frac{4\phi' F_0}{\phi^3}\right)\zeta$$

and by integration:

$$p_2=4\left(\frac{v^*}{\phi}-\frac{4\phi' F_0}{\phi^3}\right)\zeta^2+J(x)$$

where function $J(x)$ is not determined yet. Note that we have:

$$\frac{\partial p_2}{\partial x}=4\left(-\frac{\phi' v^*}{\phi^2}-\frac{4\phi'' F_0}{\phi^3}-\frac{4\phi' v^*}{\phi^2}+12\frac{\phi'^2 F_0}{\phi^4}\right)\zeta^2+J'(x)$$

Or:

$$\frac{\partial p_2}{\partial x} = 16\left(-\frac{5\phi' v^*}{4\phi^2} - \frac{\phi'' F_0}{\phi^3} + 3\frac{\phi'^2 F_0}{\phi^4}\right)\zeta^2 + J'(x)$$

Determination of v_2

From (D.2) we obtain:

$$\begin{aligned}\frac{\partial(\zeta v_2)}{\partial\zeta} = {} & \frac{4u^*\phi'\phi^2(0)}{\phi^2}\left(\zeta^3-\zeta\right) - \operatorname{Re} v^*\phi\left(\frac{F_0}{\phi}\right)'\left(\frac{2\zeta^7}{9}-\zeta^5+\zeta^3-\frac{2\zeta}{9}\right)+\\ & +\operatorname{Re}\phi\left(\frac{\phi' F_0^2}{\phi^3}\right)'\left(\frac{8\zeta^7}{9}-4\zeta^5+4\zeta^3-\frac{8\zeta}{9}\right)+\frac{4u^*\phi'\phi^2(0)}{\phi^2}\zeta^3+\frac{\operatorname{Re}F_0\phi' v^*}{\phi}\left(\frac{4\zeta^7}{3}-4\zeta^5+2\zeta^3\right)-\\ & -\frac{\operatorname{Re}\phi'^2 F_0^2}{\phi^3}\left(\frac{16\zeta^7}{3}-16\zeta^5+8\zeta^3\right)\end{aligned}$$

Considering the condition $v_2|_{\zeta=0} = 0$, we have:

$$\begin{aligned}v_2 = {} & \frac{4u^*\phi'\phi^2(0)}{\phi^2}\left(\frac{\zeta^3}{4}-\frac{\zeta}{2}\right) - \operatorname{Re} v^*\phi\left(\frac{F_0}{\phi}\right)'\left(\frac{\zeta^7}{36}-\frac{\zeta^5}{6}+\frac{\zeta^3}{4}-\frac{\zeta}{9}\right)+\\ & +\operatorname{Re}\phi\left(\frac{\phi' F_0^2}{\phi^3}\right)'\left(\frac{\zeta^7}{9}-\frac{2\zeta^5}{3}+\zeta^3-\frac{4\zeta}{9}\right)+\frac{u^*\phi'\phi^2(0)}{\phi^2}\zeta^3+\frac{\operatorname{Re}F_0\phi' v^*}{\phi}\left(\frac{\zeta^7}{6}-\frac{2\zeta^5}{3}+\frac{\zeta^3}{2}\right)-\\ & -\frac{\operatorname{Re}\phi'^2 F_0^2}{\phi^3}\left(\frac{2\zeta^7}{3}-\frac{8\zeta^5}{3}+2\zeta^3\right)\end{aligned}$$

As

$$\begin{aligned}&\left(\frac{F_0}{\phi}\right)' = \frac{F_0'}{\phi} - \frac{F_0\phi'}{\phi^2} = v^* - \frac{F_0\phi'}{\phi^2},\\ &\left(\frac{\phi' F_0^2}{\phi^3}\right)' = \frac{2\phi' F_0 F_0'}{\phi^3} + \frac{\phi'' F_0^2}{\phi^3} - \frac{3\phi'^2 F_0^2}{\phi^4} = \frac{2\phi' F_0 v^*}{\phi^2} + \frac{\phi'' F_0^2}{\phi^3} - \frac{3\phi'^2 F_0^2}{\phi^4}\end{aligned}$$

Considering the condition $v_2|_{\zeta=0} = 0$, we have:

$$\begin{aligned}v_2 = {} & \frac{2u^*\phi'\phi^2(0)}{\phi^2}\left(\zeta^3-\zeta\right)+\\ & +\left(\frac{\operatorname{Re}\phi'' F_0^2}{\phi^2}-\frac{\operatorname{Re} v^{*2}\phi}{4}\right)\left(\frac{\zeta^7}{9}-\frac{2\zeta^5}{3}+\zeta^3-\frac{4\zeta}{9}\right)-\\ & -\frac{\operatorname{Re}\phi'^2 F_0^2}{\phi^3}\left(\zeta^7-\frac{14\zeta^5}{3}+5\zeta^3-\frac{4\zeta}{3}\right)+\\ & +\frac{\operatorname{Re}F_0\phi' v^*}{\phi}\left(\frac{5\zeta^7}{12}-\frac{13\zeta^5}{6}+\frac{11\zeta^3}{4}-\zeta\right)\end{aligned}$$

As seen, the boundary condition at $\zeta = 1$ is automatically satisfied.

Determination of u_2

To find u_2, we can write:

$$\frac{1}{\phi^2\zeta}\frac{\partial}{\partial\zeta}\left(\zeta\frac{\partial u_2}{\partial\zeta}\right) = \\ \mathrm{Re}\,u_1\frac{\partial u_0}{\partial x}+\left(\mathrm{Re}\,\frac{v_2}{\phi}-\mathrm{Re}\,u_1\frac{\zeta\phi'}{\phi}-\frac{\zeta\phi'^2}{\phi^2}+\zeta\left(\frac{\phi'}{\phi}\right)'\right)\frac{\partial u_0}{\partial\zeta}+ \\ +\mathrm{Re}\,u_0\frac{\partial u_1}{\partial x}+\left(\mathrm{Re}\,\frac{v_1}{\phi}-\mathrm{Re}\,u_0\frac{\zeta\phi'}{\phi}\right)\frac{\partial u_1}{\partial\zeta}+ \\ +\frac{\partial p_2}{\partial x}-\frac{\zeta\phi'}{\phi}\frac{\partial p_2}{\partial\zeta}-\frac{\partial^2 u_0}{\partial x^2}+2\frac{\zeta\phi'}{\phi}\frac{\partial^2 u_0}{\partial x\partial\zeta}-\frac{\zeta^2\phi'^2}{\phi^2}\frac{\partial^2 u_0}{\partial\zeta^2}$$

Knowing $u_0, u_1, v_1, v_2, \dfrac{\partial p_2}{\partial x}$:

$$\begin{aligned} u_2 = \quad & \left[\mathrm{Re}\left(\frac{\phi'}{\phi}u^*F_0-\frac{u^*v^*\phi}{4}\right)+8(\frac{\phi'}{\phi})^2F_0-2\frac{\phi''}{\phi}F_0-3v^*\phi'\right]\left(\zeta^4-\frac{4}{3}\zeta^2+\frac{1}{3}\right)+ \\ & +\mathrm{Re}\left(8\frac{\phi'}{\phi^3}u^*F_0-\frac{u^*v^*}{\phi}\right)\left(\frac{\zeta^6}{9}-\frac{\zeta^4}{2}+\frac{\zeta^2}{2}-\frac{1}{9}\right)- \\ & -\mathrm{Re}^2v^{*2}F_0\left(\frac{\zeta^{10}}{450}-\frac{\zeta^8}{36}+\frac{\zeta^6}{9}-\frac{11}{36}\zeta^4+\frac{38}{135}\zeta^2-\frac{83}{1350}\right)+ \\ & +\mathrm{Re}^2\frac{\phi'}{\phi^2}v^*F_0^2\left(\frac{29}{450}\zeta^{10}-\frac{7}{12}\zeta^8+\frac{11}{6}\zeta^6-\frac{115}{36}\zeta^4+\frac{1261}{540}\zeta^2-\frac{1229}{2700}\right)+ \\ & +\mathrm{Re}^2\frac{\phi''}{\phi^3}F_0^3\left(\frac{2}{75}\zeta^{10}-\frac{2}{9}\zeta^8+\frac{2}{3}\zeta^6-\zeta^4+\frac{29}{45}\zeta^2-\frac{26}{225}\right)- \\ & -\mathrm{Re}^2\frac{\phi'^2}{\phi^4}F_0^3\left(\frac{38}{225}\zeta^{10}-\frac{13}{9}\zeta^8+\frac{38}{9}\zeta^6-\frac{53}{9}\zeta^4+\frac{479}{135}\zeta^2-\frac{409}{675}\right) \end{aligned}$$

Regarding to the problem conditions we have:

$$\begin{aligned} J'(x) = & \frac{8}{3}\frac{\phi''F_0}{\phi^3}-\frac{56}{3}\frac{\phi'^2F_0}{\phi^4}+4\frac{v^*\phi'}{\phi^2}+ \\ & +\mathrm{Re}\frac{8}{3}\frac{u^*\phi'F_0}{\phi^3}+6\mathrm{Re}\frac{u^*v^*}{\phi^3}-16\mathrm{Re}\frac{u^*\phi'F_0}{\phi^5}-\mathrm{Re}\frac{8}{3}\frac{u^*v^*}{\phi}- \\ & -\mathrm{Re}^2\frac{44}{45}\frac{\phi''}{\phi^5}(F_0^3-1)+\mathrm{Re}^2\frac{484}{135}\frac{\phi'^2F_0^3}{\phi^6}+\mathrm{Re}^2\frac{88}{135}\frac{v^{*2}F_0}{\phi^2}-\mathrm{Re}^2\frac{539}{135}\frac{\phi'v^*}{\phi^4}(F_0^2-1) \end{aligned}$$

Bibliography

[Adler, 1992] P.M. Adler. *Porous media: Geometry and transports*. Butterworth-Heinemann, N.Y., USA, 1992.

[Adler and Thovert, 1999] P.M. Adler, and J. F. Thovert. *Fractures and Fracture Network*, Kluwer Academic Publishers, Dordrecht, 1999.

[Allaire 1992] G. Allaire. Homogenization and two scale convergence. *SIAM J. Math. Anal.*, **28**, 1992, pp 1482–1518.

[Arbogast, Douglas and Hornung, 1990] T. Arbogast, J. Douglas, and U. Hornung. Derivation of the double porosity model of single phase flow via homogenization theory. *SIAM J. Math. Anal.*, **21**, 1990, pp 823–826.

[Amaziane, Goncharenko and Pankratov, 2005] B. Amaziane, M. Goncharenko, and L. Pankratov. *Homogenization of a Degenerated Triple Porosity Model with Thin Fissures. European Journal of Applied Mathematics*, **16** , 2005, pp 335–359.

[Amaziane, Pankratov and Piatnitski, 2007] B. Amaziane, L. Pankratov and A.L. Piatnitski. Homogenization of a single phase flow in a porous medium containing a thin layer, *Math. Models Methods Appl. Sci.* no. 17, 2007, pp 1317–1349.

[Amaziane, Pankratov and Rybalko, 2005] B. Amaziane, L. Pankratov, and V. Rybalko. On the homogenization of some double-porosity models with periodic thin structures. *Appl. Anal.*, no. 88, 10-11 2009, pp 1469–1492.

[Bakhvalov, 1977] N.S. Bakhvalov. *Averaging PDE With Fast Oscillating Coefficients*. Nauka, Moscow, 1977.

[Bakhvalov and Panasenko, 1989] N. S. Bakhvalov and G. P. Panasenko. *Homogenization: Averaging Processes in Periodic Media*. Kluwer Academic Publishers, Dordrecht, 1989.

[Barenblatt, Zheltov and Kochina, 1960] G.I. Barenblatt, Yu.P. Zheltov, and I.N. Kochina. On main representations in the theory of flow of homogeneous liquids in fractured rocks. *Prikladnaya Mathematika i Mechanika*, **24**, no. 5, 1960, pp 852–864.

[Barenblatt, Entov and Ryzhik, 1972] G.I. Barenblatt, V.M. Entov, and V.M. Ryzhik. *Theory of Non-Stationary Flow of Liquids and Gases Through Porous Media*, Nedra, Moscow, 1972.

[Barenblatt, Entov and Ryzhik, 1990] G.I. Barenblatt, V. M. Entov, and V. M. Ryzhik . *Theory of Fluid Flows Through natural Rocks*, Kluwer Academic Publishers, Dordrecht, 1990.

[Barker, 1985] J.A. Barker. Block-geometry functions characterizing transport in densely fissured media. *J. Hydrol.*, **77**, 1985, pp 263–279.

[Barker, 1985] J.A. Barker. Modelling the effects of matrix diffusion on transport in densely fissured media. *Mem. of XVIII Congr. of the Intern. Assoc. of Hydrogeol.* , Cambridge, 1985, pp 250–269.

[Beavers and Joseph, 1971] G.S. Beavers, and D.D. Joseph. Boundary conditions at a naturally permeable wall. *J. Fluid Mech.*, **30**, 1971, pp 197–207.

[Bennett and Myres, 1962] C. O.Bennett, and J.E. Myers. *Momentum, Heat, and Mass Transfer*, McGraw-Hill, 1962.

[Bensoussan, Lions and Papnicolaou, 1978] A. Bensoussan, J.L. Lions, and G. Papanicolaou. *Asymptotic analysis for periodic structures*, Amsterdam: North-Holland, 1978.

[Berman, 1953] A.S. Berman. Laminar flow in channels with porous walls. *J. Appl. Phys.* **24**, 1953, pp 1232–1235.

[Berman, 1958] A.S. Berman. Effects of porous boundaries on the flow of fluids in systems of various geometries. *Proceedings of the Second United Nations international Conference on the Peacefid Uses of Atomic Energy*, United Nations, Geneva. Vol. **4**, 1958, pp 351–358.

[Bourgat, 1978] J.F. Bourgat. Numerical experiments of the homogenization method for operators with periodic coefficients. *Rapport de Recherche IRI, Rocquencourt*, no. 277, 1978, pp 212–245.

[Bourgeat et. al, 1999] A. Bourgeat, M. Goncharenko, M. Panfilov and L. Pankratov. A general double porosity model, *C. R. Acad. Sci. Paris,. Sér. IIb 327* 1999, pp 1245-Ũ1250

[Bourgeat, Milelić and Piatnitski, 1998] A. Bourgeat, A. Mikelić, and A. Piatnitski. Modè le de double porosité aléatoire. *C.R. Acad. Sci. Paris, Sér. 1*, **327**, 1998, pp 99–104.

[Böhm and Showalter, 1985] M. Böhm, and R.E. Showalter. Diffusion in fissured media. *SIAM J. Math. Anal.*, **16** , no. 3, 1985, pp 500–509.

[Burns and Parkes, 1967] J.C. Burns, T. Parkes. Peristaltic motion. *J. Fluid Mech.* **29**, 1967, pp 731–743 .

[Charlaix, Hulin and Plona, 1987] E. Charlaix, J.P. Hulin, and T.J. Plona, Experimental study of tracer dispersion in sintered glass porous materials of variable compaction. *Phys. Fluids*, **30**, 1987, pp 1690–1698.

[Chen, 1966] C. Chen. Contribution à l'étude expérimentale de l'écoulement radial d'un fluide visqueux incompressible entre deux disques parallèles. *J. Mec.*, **5**, 1966, pp 245–259.

[Clemo, 2006] T. Clemo. Flow in Perforated Pipes: A Comparison of models and experiments. *SPE Prod and Oper21* **2** 2006: pp 302–311. SPE-89036-PA

[Coats and Smith, 1964] K.H. Coats, and B.D. Smith. Dead-end pore volume and dispersion in porous media. *Trans. Soc. Petol. Eng.*, **231**, no. 3, 1964, pp 73–84.

[Crapiste, Rotstein and Whitaker, 1986] G.H. Crapiste, E. Rotstein, and S. Whitaker. A general closure scheme for the method of volume averaging. *Chem. Eng. Sci.*, **41**, 1986, pp 227–235.

[Cronsnier, Chevalier and Buès, 2000] S. Crosnier, S. Chevalier, and M. Buès. Comparison between numerical simulations and experimental investigations of radial flows in rough fracture. *Advances in Fluid Mechanics III*, Ed. M. Ralman, C. A. Brebbia, WIT Press, 2000, pp 43–52.

[Carslaw and Jaeger, 1959] H.S. Carslaw, and J.C. Jaeger. *Conduction of Heat in Solids*, Oxford Univ Press, 1959.

[De Swaan, 1976] A.O. De Swaan. Analytic solutions for determining naturally fractured reservoir properties by well testing. *SPE J.*, no. 6, 1976, pp 117–122.

[Deiber and Schowalter, 1979] J.A. Deiber, W.R. Schowalter. Flow through tubes with sinusoidal axial variations in diameter. *AIChE* **25**, 638Ũ644 (1979).

[Douglas *et al*, 1998] J.Douglas , M.Kischinhevsky, P.J. Paes-leme, and A.M. Spagnuolo. A Multiple-Porosity Model for A Single-Phase Flow Through Naturally-Fractured Porous Media. *Computational and Applied Mathematics*, **17**, 1998, pp 19–48.

[Dreier, Ozkan and Kazemi, 2004] J. Dreier, E. Ozkan, and H. Kazemi. New Analytical Pressure-Transient Models to Detect and Characterize Reservoir with Multiple Fracture System. *SPE 92039, SPE International Petroleum Conference in Mexico*, Puebla Pue, Mexico, 7-9 November 2004.

[Duguid and Lee, 1977] I.O. Duguid, and P.C. Lee. Flow in fractured porous media. *Water Resour. Res.*, **13**, no. 3, 1977, pp 558–566.

[Evans, 1983] R.D. Evans. A proposed model for multiphase flow through naturally fractured reservoir. *Sos. Petr. Eng. J.*, **22**, no. 5, 1983, pp 669–680.

[Fletcher, 1991] C.A.J. Fletcher. *Computational Techniques for Fluid Dynamics, Volume 2, Specific Techniques for Different Flow Categories*, 2nd Edition, Springer Verlag, New York, 1991.

[Gringarten and Ramey, 1973] A.C. Gringarten, and H.J. Ramey. The Use of Source and GreenŠs Functions in Solving Unsteady-Flow Problems in Reservoirs. *SPE 3818*, October 1973, pp 285–296.

[Gringarten and Ramey, 1974] A.C. Gringarten, and H.J. Ramey. Unsteady-state Pressure Distributions Created by a Well with a Single Infinite-Conductivity Vertical Fracture. *SPE 4051*, August 1974, pp 347–360.

[Hasan and Kabir, 1988] A.R. Hasan, and C.S. Kabir. A Study of multiphase flow behavior in vertical wells. *SPE 15138*, 1988.

[Hasan and Kabir, 1992] A.R. Hasan, and C.S. Kabir. Two-phase flow in vertical and inclined annuli. *International Journal of Multiphase Flow*, **18**, no. 2 , 1992, pp 279–293.

[Hasan and Kabir, 1994] A.R. Hasan, and C.S. Kabir. A Simplified Model for Oil/Water Flow in Vertical and Deviated Wellbores. *SPEPF*, **143**, May 1994, Trans. AIME, 297.

[Hornug and Showalter, 1990] U. Hornung, R.E. Showalter. Diffusion models for fractured media. *J. Math. Anal. and Appl.*, **147**, no. 1, 1990, pp 69–80.

[Hornug, 1997] *Homogenization and porous media*, Ed. U. Hornung, Newyork Springer-Verlag, 1997.

[Ihara, Kikuyama and Mizugushi, 1994] M. Ihara, K. Kikuyama, K. Mizugushi. Flow in Horizontal Wellbore with Influx Through Porous Wells. *SPE 28485* , 1994

[Iwai, 1976] K. Iwai. *Fundamental studies of fluid flow through a single fracture*. PhD thesis, University of California, Berkeley, 1976.

[Kazemi and Thomas, 1969] H. Kazemi, and G.W. Thomas. The interpretation of interference tests in naturally fractured reservoirs with uniform fracture distribution. *SPE J.*, no. 12, 1969, pp 463–472.

[G. Korn and T. Korn, 1968] G. Korn , T. Korn. *Mathematical Handbook for Scientists and Engineers*, McGraw-Hill, 1968.

[Kozlov, 1978a] S.M. Kozlov. (1978) Homogenization of differential operators with closely periodic quickly oscillating coefficients. *Mathematicheskii Sbornik. Novaya Seriia*, **107(149)**, 1978, no. 2(10), pp 199–217.

[Kozlov, 1978b] S.M. Kozlov. Homogenization of random structures. *Doklady Academii Nauk SSSR*, **241**,1978 , no 5, pp 1016–1019.

[Kozlov, 1979a] S.M. Kozlov. Homogenization of random operators. *Mathematicheskii Sbornik. Novaya Seriia*, **109(151)**, 1979, no 2(6), pp 188–202.

[Kozlov, 1979b] S.M. Kozlov. Conductivity of two-dimentional random media. *Uspekhi Mathematicheskikh Nauk*, **34**, 1979, no.4(208), pp 193–194.

[Kozlov, 1985] S.M. Kozlov. Homogenization method and random walk in heterogeneous media. *Uspekhi Mathematicheskikh Nauk*,**40**, 1985, no. 2(242), pp 61–120.

[Kozlov, 1989] S.M. Kozlov. Geometric aspects of homogenization. *Uspekhi Mathematicheskikh Nauk*, **44**, 1989, no. 2, pp. 79–120.

[Kuchuk and Habusky, 1994] F.J. Kuchuk, and T.M. Habusky. Pressure Behavior of Horizontal Wells with Multiple Fractures. *SPE Journal 27971*, August 1994, pp 347–360.

[Kuchuk, Habashy and Torres-Verdin, 1996] F.J. Kuchuk, T.M. Habashy, and C. Torres-Verdin. A Non-linear Approximation for the Pressure Behavior of Heterogeneous Reservoirs. *SPE 26456*, September 1996, pp 229–241.

[Kuchuk and Habashy, 1997] F.J. Kuchuk, and T. Habashy. Pressure Behavior of Laterally Composite Reservoirs. *SPE 24678*, March 1997, pp 47–56.

[Landau and Lifshitz, 1986] L.D. Landau, and E.M. Lifshitz. *Hydrodynamics*, Nauka, Moscow,1986.

[Lions, 1978] J.L. Lions. Notes on somes computational aspects of homogenization in composite materials. *Numerical methods in mathematical physics and optimal control*, Ed. Marchuk G.N. and J.-L.Lions, Nauka, Novosibirsk, 1978, pp 5 – 19.

[Malevich, Mityushev and Adler, 2006] A.E. Malevich, V.V. Mityushev, P.M. Adler. Stokes flow through a channel with wavy walls. *Acta Mechanica*, **182**, 2006, pp 151–182

[Marchenko and Khrouslov, 1974] V.A. Marchenko and E.J. Khrouslov. Boundary problems in domains with finely granulated boundaries (in Russian). *Naukova Dumka*, Kiev, 1974

[Odeh, 1965] A.S. Odeh. Unsteady-state behaviour of fractured reservoirs. *SPE J.*, no. 1, 1965, pp 60–66.

[Osher and Sethian, 1988] S. Osher, and J.A. Sethian. Fronts propagating with curvature-dependent speed: Algorithms based on Hamilton-Jacobi formulations. *J. Comput. Phys.*, **79**, 1988, pp 12–49.

[Osher, Fedkiw and Ronald, 2002] S. Osher, J. Fedkiw, and P. Ronald. *Level Set Methods and Dynamic Implicit Surfaces*. Springer-Verlag, 2002.

[Ouyang, Arbabi and Aziz, 1998] L. Ouyang, S. Arbabi, and K. Aziz. General Wellbore Flow Model for Horizontal, Vertical, and Slanted Well Completions. *SPE 36608*, June 1998, pp 124–133.

[Ouyang, 1998] L.B. Ouyang. *Single phase and multiphase fluid flow in horizontal wells*. PhD Thesis, Stanford University, CA 1998.

[Ouyang and Aziz, 2000] L. Ouyang, and K. Aziz. A Homogeneous Model for Gas–Liquid Flow in Horizontal Wells. *Journal of Petroleum Science and Engineering*, no. 27, March, 2000, pp 119–128.

[Panasenko and Sysuev, 1986] G.P. Panasenko, and V.V. Sysuev. Averaging the parameters of mathematic models of heat, water and mass transport in an aggregated random-periodic porous medium. *Mathematical methods of rock description and calculation of their effective propeties*, Moscow, Ed. MOIP, 1986, pp 33 – 42.

[Panasenko, 1988] G.P. Panasenko. Averaging the carcas constructions with random structures. *Doklady AN SSSR*, **244**, no. 2, 1988, pp 335 – 337 (translated in: Soviet Phys. Dokl., 1988.

[Panfilov, 1986] M. Panfilov. Phenomenon of Transient Boundary Layer in Underground Oil and Gas Reservoir Depletion Processes. *Fluid Dynamics*, no. 3, 1986, pp 895–900.

[Panfilov, 1990] M. Panfilov. Main Mode of Porous Flow in Highly Inhomogeneous Media. *Soviet Physics Doclady*, **35**, no. 3, March, 1990, p. 225-227.

[Panfilov, 1993] M. Panfilov. Structural Averaging of Porous Flow Processes in Heterogeneous Media. *Fluid Dynamics*, no. 3, 1993, pp 112–120.

[Panfilov, 1994] M. Panfilov. Averaged Model-Type Transition In Flows Through Multiple Heterogeneous Porous Media. *C.R. Acad. Sci. Paris, Ser.II*, **318**, 1994, pp 1437–1444.

[Panfilov, 2000] M.B. Panfilov. *Macroscale models of flow through highly heterogeneous porous media*, Kluwer Academic Publishers, 2000.

[Panfilov *et al*, 2003] M. Panfilov, C. Oltean, I. Panfilova, and M. Buès. Singular nature of nonlinear macroscale effects in high-rate flow through porous media. *C. R. Acad. Sci. Paris IIb*, **331**, 2003, pp 41 – 48.

[Panfilov and Bues, 2004] M. Bues, M. Panfilov, S. Crosnier, and C. Oltean. Macroscale model and viscous-inertia effects for Navier-Stokes flow in a radial fracture with corrugated walls. *Journal of Fluid Mechanics*, **504**, 2004, pp 41–60.

[Panfilov and Fourar, 2006] M. Panfilov, and M. Fourar. Physical splitting of nonlinear effects in high-velocity stable flow through porous media. *Advances in Water Ressources*, 2006, **29**, pp 30–41.

[Panfilova, Buès, and Panfilov, 2002] I. Panfilova, M. Buès, and M. Panfilov. High-Rate Navier-Stokes Flow in porous media: D'Alembert paradox and its solution. In: *Poromechanics II, Proc. 2nd Biot Conference on Poromechanics*, Grenoble, France, August 26-28, 2002, Eds. J-L. Auriault et al, A.A. Balkema Publishers, The Netherlands, 2002, pp 521 – 526.

[Pankratov and Rybalko, 2002] L.S. Pankratov, and V.A. Rybalko. Asymptotic analysis of the double porosity model with thin fractures. *Mathematicheskii Sbornik*, **194**, no. 1, 2003, pp 121 - 146 (in Russian)

[Pankratov and Rybalko, 2003] L.Pankratov, V. Rybalko. Asymptotic analysis of a double porosity model with thin fissures. *Mat. Sbornik*, 2003,v.194, no. 1, pp 121–146 (in russian); English translation : *Sbornik: Mathematics*,**194**, no. 1,pp 123–150.

[Peszynska 2007] M.L. Peszynska, and R.E. Showalter. Multiscale Elliptic-Parabolic systems for Flow and Transport. *Electronic Journal of Differential Equations*, no. 147, 2007, pp 1–30.

[Peube, 1963] J.L. Peube. Sur l'écoulement radial permanent d'un fluide visqueux incompressible entre deux plans parallèles fixes. *J. Mec.*, **11**, 1963, pp 377–395.

[Pfitzner, 1976] J. Pfitzner. Poiseuille and his law. *Anaesthesia*, **31**, no 2, 1976, pp 273–5, Mar, PMID:779509.

[Polyanin, 2002] A. D.Polyanin. *Handbook of Linear Partial Differential Equations for Engineers and Scientists.* , Chapman Hall/CRC Press, Boca Raton-London, 2002.

[Polyanin and Manzhirov, 1998] A. D.Polyanin, A.V. Manzhirov *Handbook of Integral Equations*. Second Edition, Chapman Hall/CRC Press, Boca Raton-London, 1998.

[Proudman, 1960] I.Proudman. An Example of Steady Laminar. Flow at Large Reynolds Number. *J. Fluid Mech.* **9**, 1960, pp 593–602.

[Renshaw, 1995] C.E. Renshaw. On the relationship between mechanical and hydraulic apertures in rough-walled fractures. *J. Geophys. Res.*, **100**, B12, 1995, pp 629–636.

[Robinson, 1987] W. A. Robinson. The existence of multiple solutions for the laminar flow in a uniformly porous channel with suction at both walls. *SIAM J. Appl. Math.* **10**, 1987, pp 526–533.

[Saffman, 1971] P.G. Saffman. On the boundary condition at the interface of a porous medium. *Stud. Appl. Math.*, **1**, 1971, pp 93–101.

[Sanchez-Palensia, 1980] E. Sanchez-Palensia. *Non-homogeneous media and vibration theory*. **129** of Lecture Notes in Physics, Springer Verlag, Berlin, 1980.

[Savage, 1963] S.B. Savage. Laminar radial flow betwen parallel plates. *J. Appl. Mech.*, 1963, pp 594–596.

[Schlichting, 1968] H. Schlichting. *Boundary-layer Theory*, McGraw-Hill, 1968.

[Sellars, 1955] J. R.Sellars. Laminar flow in channels with porous walls at high suction Reynolds number. *J. Appl. Phys.* **26**, 1955, pp 489–490.

[Sethian 1999] J.A. Sethian. *Level Set Methods and Fast Marching Methods : Evolving Interfaces in Computational Geometry*. Fluid Mechanics, Computer Vision, and Materials Science, Cambridge University Press, 1999.

[Skjetne, Hansen 1999] E. Skjetne, A. Hansen, and J.S. Gudmundsson. High velocity flow in a rough fracture. *J. Fluid Mech.*, **383**, 1999, pp 1–28.

[Sussman and Fatemi, 1999] M.Sussman, and E. Fatemi. An efficient interface-preserving level set redistancing algorithm and its application to interfacial incompressible fluid flow. *SIAM J. Sci. Comput*, **20**, 1999, pp 1165–1191.

[Sutera and Skalak, 1993] S.P. Sutera, R. Skalak. The history of Poiseuille's law. *Annual Review of Fluid Mechanics*, **25**, 1993, pp 1–19.

[Terrill, 1964] R. M. Terrill. Laminar flow in a uniformly porous channel. *Aeronaut. Quart.* **15**, 1964, pp 299–310.

[Unverdi and Tryggvason, 1992] S.O. Unverdi, and G. Tryggvason. A Front-Tracking Method for Viscous, Incompressible, Multi-Fluid Flows. *Journal of Computationa Physics*. **100**, 1992, pp 25–37.

[Vatistas, Ghila, and Zitouni, 1995] G. H. Vatistas, A. Ghila, and G. Zitouni. Radial inflow between two flat disks. *Acta Mechanica*, **113**, 1995, pp 109–118.

[Warren and Root, 1963] J.E. Warren, and P.J. Root, The behavior of Naturally Fractured Reservoirs. *SPE Journal*, September, 1963, pp 245–255.

[White, Barfield and Goglia, 1958] F.M White Jr., B.F Barfield and M.J Goglia. Laminar flow in a uniformly porous channel. *J. Appl. Mech.* 25, 1958, pp 613–617.

[Yuan and Finkelstein, 1956] S.W. Yuan, and A.B. Finkelstein. Laminar Pipe Flow With Injection and Suction Through a Porous Wall. *Trans. ASME*, **78**, 1956, p. 719.

[Yuan, 1956] S.W.Yuan. Further investigation of laminar flow in channels with porous walls. *J. Appl. Phys.*, **27**, 1956, pp 267–269.

[Zaturska, Drazin and Banks, 1988] M.B. Zaturska, P.G. Drazin and W. H.Banks. On the flow of a viscous fluid driven along a channel by suction at porous walls. *Fluid Dyn. Res.* **4**, 1988, pp 151–178.

[Zimmerman and Bodvarsson1996] R. W. Zimmerman, and G. S. Bodvarsson. Effective transmissivity of two-dimensional fracture networks. *Intl J. Rock Mech. Min. Sci. Geomech. Abstr.*, **33**, 1996, pp 433–438.

[Zitouni and Vatistas, 1997] G. Zitouni, and G.H. Vatistas. Purely accelerating flows within two flat disks. *Acta Mechanica*, **123**, 1997, pp 151–161.

[Zuber and Findlay, 1969] N. Zuber, and J. Findlay. Average Volumetric Concentration in Two-Phase Systems. *Trans ASME Journal of Heat Transfer*, **87**, 1969, p 453.

INSTITUT NATIONAL
POLYTECHNIQUE
DE LORRAINE

AUTORISATION DE SOUTENANCE DE THESE
DU DOCTORAT DE L'INSTITUT NATIONAL
POLYTECHNIQUE DE LORRAINE

o0o

VU LES RAPPORTS ETABLIS PAR :
Monsieur Christophe JOSSERAND, Directeur de Recherche, Université Pierre et Marie Curie

Monsieur Brahim AMAZIANE, Maître de Conférences, LMA, Université de Pau

Le Président de l'Institut National Polytechnique de Lorraine, autorise :

Madame RASOULZADEH Mojdeh

NANCY BRABOIS
2, AVENUE DE LA
FORET-DE-HAYE
BOITE POSTALE 3
F - 54501
VANDŒUVRE CEDEX

à soutenir devant un jury de l'INSTITUT NATIONAL POLYTECHNIQUE DE LORRAINE, une thèse intitulée :

"Modèles non locaux des écoulements en milieux poreux et fracturés multi-échelles. "

en vue de l'obtention du titre de :

DOCTEUR DE L'INSTITUT NATIONAL POLYTECHNIQUE DE LORRAINE

Spécialité : « **Mécanique et énergétique** »

Fait à Vandoeuvre, le 7 avril 2011
Le Président de l'I.N.P.L.,
F. LAURENT

INSTITUT NATIONAL POLYTECHNIQUE DE LORRAINE – NANCY

TEL. 33/03.83.59.59.59
FAX. 33/03.83.59.59.55

Modèles non locaux des écoulements en milieux poreux et fracturés multi-échelles

Mots clés : milieu poreux multi échelles, les effets non-locaux, homogénéisation à deux échelles, milieux fracturés

La thèse concerne les modèles de l'écoulement dans les milieux fracturés multi-échelles qui prouvent l'effet de mémoire à chaque échelle. Les processus analysés dans ces milieux est auto-similaire. Nous avons analysé l'équation de diffusion à toutes les échelles et appliqué la méthode d'homogénéisation asymptotique avec l'objectif de construire le modèle macroscopique moyenne sur toutes les échelles d'hétérogénéité. Un système fermé des équations récursives pour les noyaux d'échange effectif est obtenu. La solution analytico-numérique de ce système est développé. Nous avons montré une convergence des résultats obtenus pour le nombre des différentes échelles d'un comportement limite stable. Le problème limite pour les noyaux est obtenus pour un nombre relativement élevé d'échelles. En plus, nous avons analysé l'écoulement dans une immergée dans le réservoir poreux à différents nombres de Reynolds. Les équations de Navier-Stokes sont résolu par la méthode asymptotique à deux échelles avec l'objectif d'obtenir l'équation de la moyenne sur l'ouverture de fracture en présence d'afflux à travers les limites et pour la géométrie irrégulière des murs.

Nonlocal models of flow in multi-scale porous and fractured media

Key words: multiscale medium, nonlocal effects, memory accumulation, two-scales homogenization

The thesis concerns the models of flow in multiscale fractured media which prove the memory effect at each scale. The analyzed process in these media is self-similar. The necessary and sufficient condition of self-similarity has been proposed so that it is possible to analyze the behavior of media for any number of scales. We analyzed the diffusion equation at each scale and applied the asymptotic homogenization method with the objective to construct the macroscopic model averaged over all scales of heterogeneity. A system of closed recurrent equations for the effective exchange kernels was obtained. The procedure of analytico-numerical solution of this system was developed. We showed a convergence of the results obtained for various number of scales to a stable limit behavior. The limit problem for the effective kernels from the recurrent equations obtained for a relatively large number of scales. In addition we analyzed the flow in a single fracture and circular channel immersed in porous reservoir at various Reynolds numbers. The Navier-Stokes equations was solved by the method of two-scale asymptotic method with the objective to obtain the flow equation averaged over the fracture aperture in the presence of inflow through the limits and irregular geometry of walls.